# Synthesis and characterization of biochar from waste biomass: An application for the removal of Arsenic from contaminated water

**THESIS**

SUBMITTED TO

BABASAHEB BHIMRAO AMBEDKAR UNIVERSITY

FOR THE DEGREE OF

**Doctor of Philosophy**

IN

**ENVIRONMENTAL SCIENCE**


Submitted by

*Lata Verma*

Enrolment No. 147/13

Under the Supervision of

*Dr. Jiwan Singh*

Assistant Professor

DEPARTMENT OF ENVIRONMENTAL SCIENCE
SCHOOL FOR ENVIRONMENTAL SCIENCES
BABASAHEB BHIMRAO AMBEDKAR UNIVERSITY
(A Central University)
LUCKNOW-226 025


2022

*Dedicated to*
*My Beloved Mother*

# Declaration

I **Lata Verma,** declare that the research work personified in this thesis entitled "**Synthesis and characterization of biochar from waste biomass: An application for the removal of Arsenic from contaminated water**" which is being submitted to the **Department of Environmental Science, School for Environmental Sciences, Babasaheb Bhimrao Ambedkar University, Lucknow** is based on original research carried out by me. This thesis has not been submitted in part or full form for any degree or diploma in any university. I further proclaim that the thesis is essentially free from all kind of plagiarism.

Lata Verma

**Date:** 11/05/2022

**Lata Verma**

Department of Environmental Science

# Certificate

This is to certify that the thesis entitled **"Synthesis and characterization of biochar from waste biomass: An application for the removal of Arsenic from contaminated water"** submitted by **Mrs. Lata Verma** is an original research work and has not been previously submitted in part or full for the award of any other degree or diploma to this or any other university.

The thesis submitted to Babasaheb Bhimrao Ambedkar University, Lucknow satisfies all the requirements as stipulated in the Doctor of Philosophy (Ph.D.) regulations-1999 as amended in 2008/2010/2013 and it is fit for the submission and evaluation for the award of degree of Doctor of Philosophy of the University.

11/05/2022

**Supervisor**

**Date:** 11/05/2022

11/05/2022

**Head of Department**

# Acknowledgment

I am proud to present my thesis, which is not the outcome of a single person's efforts. Many people have contributed to its development. At the moment, I am really thankful to the universe and all those who helped me to finish my thesis in some form. First and foremost, I thank to "the Almighty," who has blessed me with great willpower, confidence and patience, all of which have aided me in completing the present work.

I extend my profound thanks to my supervisor **Dr. Jiwan Singh, Assistant Professor, Department of Environmental Science, School of Earth & Environmental Sciences, Babasaheb Bhimrao Ambedkar University, Lucknow,** for his invaluable assistance and enlightened supervision during my research work. This thesis submission would not have been possible without his support and encouragement. His timeliness, discipline, and behavior have always boosted my confidence. I could never have gone forward and begun all of this without his help. I feel so richly blessed to have him as my supervisor.

I would like to express my deepest thanks to all the faculty members of the Department of Environmental Science, Babasaheb Bhimrao Ambedkar University, **Late Prof. D.P. Singh, Prof. R.P. Singh, Prof. S.K. Dwivedi, Prof. N.K. Arora, Prof. Shikha, Prof. V. Datta, Dr. Narendra Kumar and Mr. N.K.S. More** for their support, and valuable suggestions which helped me a lot to carry out this research work. I wish to express my profound gratitude and sincere thanks to **Dr. Puja Khare**, Scientist, CSIR-Central Institute of Medicinal and Aromatic Plants, Lucknow, for her encouragement and moral support.

I am highly thankful to my seniors Dr. Vineet Yadav, Dr. Namita Gupta, Dr. S. Shankar, Dr. Disha Mishra, Dr. Priyanka Chaudhary, Dr. Utkarsh Kumar, Dr. S. Ahmad, Dr. Ratindra Gautam, Mr. Har Mohan Singh for their full support and co-operation.

I am also very grateful to my labmates Ms. Shalu Rawat, Mr. Chandrabhan and Ms. Nikita Kanaujia and to my colleagues and friends Mrs. Garima Singh, Mr. Vinay Kumar, Mr. Adil Siddiqui, Ms. Anupriya Verma, Mr. Amar Kumar, Mrs. Shaija Singh, Mr. Suresh, Mr. Ankit Kumar, Ms. Anita and my juniors Mrs. Deepa Kanoujia, Mr. Devesh Kumar, Mr. Arpit, Mr Ajeet, Mr. Aneet Yadav, Mr. Monu Kumar, Ms. Versha Pandey, Late. Raghvendra Pratap Singh, Ms. Akanksha Azad, Ms. Shipra Shukla, Ms. Alka Verma, Ms. Shakshi Singh and Ms. Mansi Mondal for their availability in accordance with my requirements throughout the period of my research.

I sincerely thank staff members Mr. A.K. Jain, Mr. Ranjeet, Mr. Aviral Dixit, Mr. Mukesh Kumar, Mr. Manish Kumar and Mr. Vijay for their co-operation.

Above all, I express my deep sense of gratitude and my unwavering thanks and love to my mother **Mrs. Sanju Verma**, my father **Mr. Karan Singh Verma,** my elder brother **Mr. Amit Verma**, my younger brother **Mr. Sachin Verma** and the entire family members for their selfless support and encouragement throughout my journey of research. I wish to thank my loving and supportive husband **Mr. Ranjeet Kumar Verma**, who provides unending inspiration and understanding of my goals and ambitions. I would like to thank my mother-in-law **Mrs. Nirmala Verma** and Father-in-law **Mr. S.K. Verma** for their love and support.

Finally, I feel my sincere gratitude to all the people and organizations that helped me overcome the challenges I faced during my research work, whether directly or indirectly.

***Lata Verma***

# Preface

Water pollution has become one of the most problematic issues in recent decades as a result of human activities. Water pollution is increasing at an alarming rate, endangering both human health and the environment. Due to the urbanization and intensification of industrial and agricultural operations, chemical pollution has been turned out to be a severe environmental concern. The most extensively dispersed freshwater on the earth is groundwater. Groundwater contamination due to several organic and inorganic contaminants causes various health effects. Arsenic (As) is well known toxic groundwater contaminants and widely dispersed metalloids come from a variety of natural and anthropogenic sources. Arsenic is geogenic in origin and enters into groundwater through the dissolution of the natural minerals containing As. Anthropogenic sources include mining processes and the use of As containing pesticides etc. Consumption of As contaminated drinking water can cause different health problems such as skin lesions, gastrointestinal disorders, impairment of mental activity, and cancer (lung, skin, etc).

Several physicochemical techniques are used for the treatment of As from contaminated water but their principal drawbacks include poor treatment efficacy high related cost, the formation of a large amount of sludge, requires high energy and specialized manpower. Adsorption is considered one of the most successful techniques since it is inexpensive and ecofriendly and discovered to be a sustainable approach to removing As from contaminated water by destructing the drawbacks of other physicochemical processes. Biochar is one of the most effective adsorbents and an

emerging method for removing pollutants from the water in a cost-effective way and can be used to remediate water contaminated with heavy metals.

The current study entitled "**Synthesis and characterization of biochar from waste biomass: An application for the removal of Arsenic from contaminated water"** aims to synthesize the biochar by utilizing waste biomass available locally in bulk amounts and give scientific knowledge about the As adsorption efficacy and mechanism of arsenic adsorption on to the surface of biochar and metal-infused biochar materials and their potential application on As removal from an aqueous solution as well as from groundwater. In this study, dry waste leaves and vegetable waste were used for the development of biochar/modified biochar and was investigated for their potential to remove As. The synthesized biochar materials were characterized using SEM, EDX, FTIR, PSA, $pH_{ZPC}$ and zeta potential. For the adsorption process, an optimization of batch adsorption study was performed with different parameters such as dose of biochar, pH of the solution, initial concentration and operating temperature. Isotherm, kinetics, thermodynamics, regeneration and adsorption mechanism were also studied for a better understanding of As removal using biochar. The goal of this study was to remove As from an aqueous solution as well as from groundwater using biochar in an environmentally acceptable and cost-effective manner. The present thesis is categorized into 6 chapters.

**Chapter 1** is **"Introduction"** which provides context for the current study and highlights the need for the treatment of arsenic (As(III) and As(V)) from the contaminated water.

**Chapter 2** is accomplished with the five foremost objectives of the present work.

**Chapter 3** is **"Review of Literature".** This covers the problem of As worldwide and treatment technologies (Ion-exchange, chemical precipitation, oxidation, membrane filtration and adsorption). Method of biochar synthesis and application of biochar for removal of As are also discussed.

**Chapter 4** is the **"Material and Methods"** which contains the details of the methods and methodology used during the study's journey.

**Chapter 5** is the **"Result and Discussion".** This chapter is divided into four different phases. Firstly the initial characterization of waste biomass and Physico-chemical parameters of collected groundwater samples has been discussed. **Phase-I** describes the synthesis of biochar from waste biomass of plant litter (*Tectona sp.* (TB 800) *and Lagerstroemia speciosa* (LB 800)) and was characterized and applied for the removal of As(III) and As(V) from aqueous solution as well as from groundwater. **Phase-II** is on the synthesis of magnetic biochar from waste leaves (*Tectona sp.* (MTB-800) *and Lagerstroemia speciosa* (MLB-800)) biomass and its effect on adsorption of trivalent and pentavalent As from contaminated water. In **Phase III,** removal of both species of As from contaminated water was performed using iron-infused biochar synthesized from vegetable waste (*Raphanus sativus* (MRB-800) *and Artocarpus heterophyllus* (MJB-800). **Phase IV** deals with the adsorption of As(III) from an aqueous solution and groundwater using monometallic (Fe-TB) and bimetallic biochar (Fe/Mn-TB) synthesized from *Tectona sp.* plant leaves litter.

**Chapter 6** is a **"Summary"** that emphasizes the key findings and conclusion of the present investigation.

**Chapter 7** is the **"Conclusion'**

A list of publications **(Appendix I)** and conferences and workshops attended **(Appendix II)** have been applauded at the end of the thesis.

**Date** **Lata Verma**

# Abbreviation

| | |
|---|---|
| As(III) | Trivalent arsenic |
| As(V) | Pentavalent arsenic |
| DI | Deionized water |
| VOCs | Volatile organic content |
| MC | Moisture content |
| AC | Ash content |
| VM | Volatile matter |
| SEM | Scanning electron microscope |
| EDS/EDX | Energy dispersive x-ray spectrophotometer |
| FTIR | Fourier transform infrared spectroscopy |
| XRD | X-ray diffraction |
| $pH_{ZPC}$ | Point of zero charge |
| PSA | Particle size analysis |
| BET | Brunner Emmet Teller |
| XPS | X-ray photoelectron spectroscopy |
| VSM | Vibrating sample magnetometer |
| MRB | Magnetic Radish Biochar |
| MJB | Magnetic Jackfruit Biochar |
| LB | *Lagerstroemia* Biochar |
| TB | *Tectona* Biochar |

| | |
|---|---|
| MLB | Magnetic *Lagerstroemia* biochar |
| MTB | Magnetic *Tectona* biochar |
| rpm | rotation per minute |
| amu | atomic mass unit |
| TDS | Total dissolve solids |

## General symbols

| | |
|---|---|
| mg | milligram |
| kg | kilogram |
| L | litter |
| g | gram |
| nm | nanometer |
| µM | micromole |
| mm | millimole |
| mL | milliliter |
| °C | degree celsius |
| V | volume |
| m | mass |

# Content

# List of Figures

# List of Tables

# *Chapter-1*
# *Introduction*

# Chapter-1 Introduction

All living being, including humans, necessitates water for their existence. Consequently, it is indispensable to ensure the availability of adequate water supplies for the well-being of humans. A major part of drinking water is stored in glaciers in form of ice and deep aquifers i.e., groundwater, only a lesser quantity of water is accessible (Oki and Kanae, 2006). But in the past few years, the depletion of groundwater has been increased with the increasing population, environmental pollution, poor management of resources due to this the source of clean drinking water diminishing continuously (Siddique et al., 2020). Almost, 1/3$^{rd}$ of the world's population is totally dependent on groundwater for drinking water. In those areas where the precipitation and surface water resources are limited like arid and semiarid regions of the world, groundwater is particularly the primary resource especially for drinking purposes (Li et al., 2020a). Possibly, the fast-growing industrialization, urbanization, agricultural practices, and climate change are the biggest reason and causes of groundwater pollution. Various environmental pollutants entering the water bodies also reduce the availability of clean and safe drinking water and for the sustainable development of any nation fortifying renewable and safe drinking water supply is one of the most essential necessities (Saravanan et al., 2021). The major source of water pollution is various organic and inorganic pollutants like dyes, phenolic compounds, pesticides, pharmaceutical products, heavy metals (Cr, Ni, Pb, As, Zn, Cd, Cu, etc.), etc. Some of the organic pollutants are water-soluble and are easily removed from the environment through adsorption or microbial degradation (Megharaj et al., 2011). Whereas, the heavy metals are inorganic therefore they are non-biodegradable and due to

their high toxicity and persistent nature, they cause numerous threats to living organisms after entering the food chain (Neyaz et al., 2014). Chemical contamination of groundwater seems to be a major subject reported in various recent studies (Li et al., 2021a). The presence of various contaminants in groundwater is due to the dissolution of natural minerals and are of geogenic origins found in the Earth's crust. Though, because of the fast growth of the world's population, industrialization, global economy, urbanization, etc., we are now encountering the drastic impacts of contaminants that originate from anthropogenic activities (Rao et al., 2020).

As is one of the highly toxic metalloids and its contamination in ground groundwater is recognized as a very big problem as it causes various harmful effects on humans and the ecological services of the environment. Over the last two or three decade's presence of high arsenic concentration in drinking water has been identified as a major public-health-related concern in many parts of the world (Nwankwo et al., 2020). Some regions of South America and several countries in South Asia are highly affected by As contamination in groundwater. It has been reported that about thirty-three Asian countries are severely contaminated with As such as Afghanistan, Pakistan, Iraq, Nepal, Japan, Russia, Sri-Lanka, Tajikistan, Thailand, Korea, etc. and the most affected countries are India, China, Pakistan and Bangladesh (Hashim et al., 2019; Shaji et al., 2021). At present, in India, about 50 million population is at high risk of consuming As contaminated groundwater. More than 10 µg/L of As concentration has been reported in many states of India in shallow as well as in deeper aquifers having depths more than 100 m. some of the most As-contaminated states of India are West Bengal, Uttar Pradesh, Bihar, Jharkhand, Assam, Chhattisgarh, etc. (Chakraborti et al., 2018). The main source of groundwater As

contamination in India was alluvial aquifers i.e., ~90% whereas, the remaining 10% source of As contamination was contributed by hard rock terrane (Shaji et al., 2021).

About 3.5 mg/L concentration of As has been reported in the groundwater which is the primary source of drinking water in developing countries (Shakoor et al., 2019). In oxidized water, arsenic mostly occurs in the form of arsenate (As V), whereas in reduced conditions, this species is present in the form of arsenite (As III). As per the available report, arsenite is approximately 25–60 times highly toxic than arsenate. Arsenic is the 20$^{th}$ most abundant metalloid mainly found in two forms Arsenite and Arsenate, both these inorganic species of Arsenic are considered hazardous toxicants to the environment, but the As(III) in comparison with As(V) is more toxic (Wongrod et al., 2018; Alka et al. 2021). Arsenic pollution in water arises from anthropogenic and natural sources (Fig.1.1.). Anthropogenic sources include disposal of residual solid by-products derived from combustion (paper mills, coal plants, cement plants), use of arsenic-containing pesticides in the agricultural field. For medicinal and agricultural uses, arsenic has also been used in antibiotics and pesticide production, consequently, in various ways, it gets into the water bodies, especially in aquifers (Zhang et al., 2013; Mondal and Garg, 2017). As arsenic is present in a less amount in Earth's crust naturally and reaches the groundwater through weathering of rocks comprising arsenic minerals (Pintor et al., 2018; Guo et al., 2019). It was found that ~1.8 mg/Kg of arsenic was present in Earth's crust. The concentration of As in the environment has been exceeded due the human involvement (Srivastav et al., 2021).

Arsenic contamination leads to numerous health-related issues to humans, and about two hundred million peoples worldwide are at high possibility of arsenic

contamination because of consumption of drinking water contaminated with the arsenic, specifically in unindustrialized countries due to its carcinogenic properties (Amen et al., 2020). A 10 µg/L standard arsenic level has been set in the drinking water by US Environmental Protection Agency. Arsenic is noted as the catastrophe of the twenty-first century by researchers, globally because of its various detrimental health-related issues that occur in human beings due to intake of As contaminated water, common diseases are pulmonary disease (arsenicosis, lung cancer, interstitial fibrosis, pulmonary capillary occlusion, etc.), cardiovascular disease (coronary heart disease, heart attack, and hypertension), nervous system dysfunction (impairment of mental activity, neuropathy), dermal diseases (skin cancer, pigmentation, and lesions) and also increases the risk of cancer in humans and animals (Rana et al., 2018; Hare et al., 2019; Alchouron et al., 2020). Consumption of As in the majority of the impacted parts of the world via groundwater sources manifests as chronic health problems. The negative effects of As contaminated groundwater on crops used for irrigation purposes and for aquatic habitats are also a major problem. In addition to causing several human health effects from ingestion of As contaminated food, As contamination also have the potential to reduce agricultural yields. Decreased quality of crops and reduced annual yield due to the As is also major points of concern (Bhattacharya et al., 2007). So, when the concentration of As is above its permissible limits in water that is to be utilized for drinking purposes requires proper treatment systems (Ran et al., 2021).

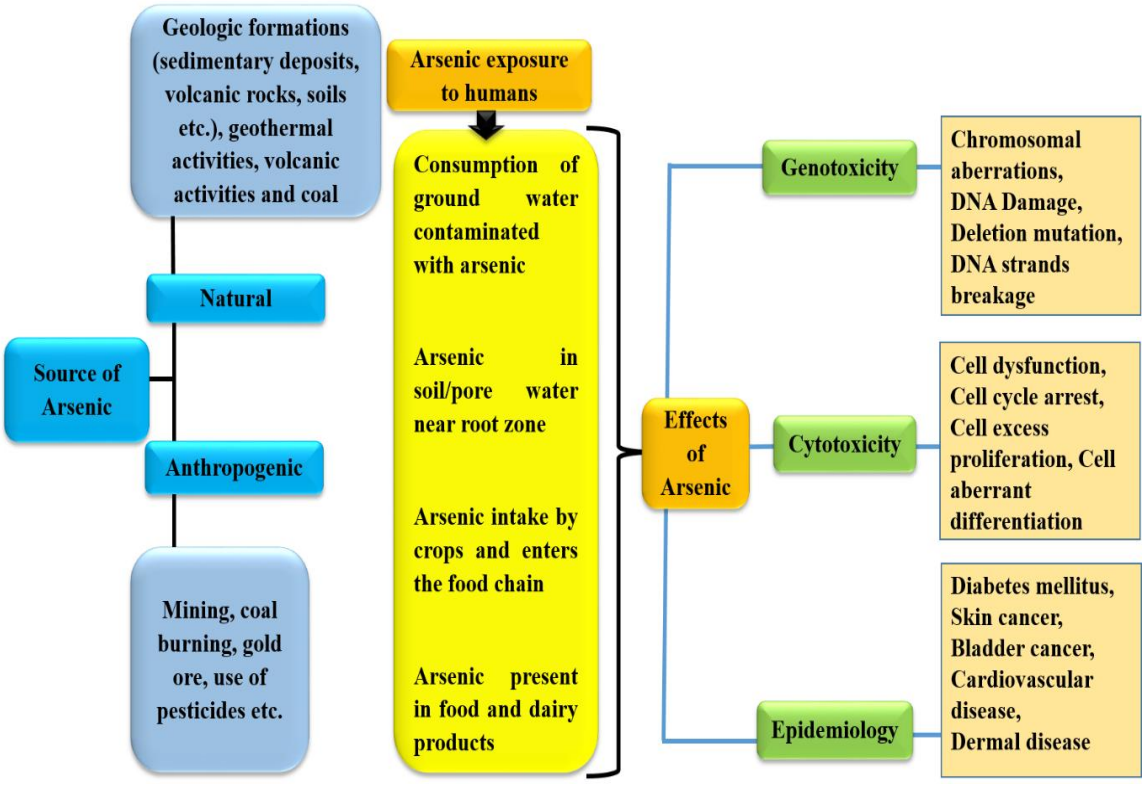


**Fig.1.1. Sources and effects of Arsenic on human health.**

From the last few decades, various research has been focusing to control the hazardous pollutants from groundwater, especially the most toxic As. In the present scenario, there is an urgent need to develop an economically efficient and eco-friendly technique for the treatment of As contaminated groundwater (Premkumar et al., 2018). Several techniques have already been employed for arsenic removal from the water like ion exchange, chemical precipitation, adsorption, membrane separation, permeable reactive barriers, and coagulation (Bakshi et al., 2018). Most of these mentioned techniques were ineffective in removing As from contaminated water and also generates secondary pollutants (Rathi and Kumar, 2021). In contrast to the traditional or common techniques for As removal, adsorption has developed as a simple, cost-effective, environmentally friendly and time-saving method that potentially removes water contaminants including As

without forming toxic end products (Sun et al., 2017; Patra et al., 2020). The adsorption process does not require the addition of any chemical and it is one of the most suitable techniques of As removal and in many developing countries is the most used technique of water treatment because it requires fewer skilled personnel. Many sorbents like commercially available activated carbon, fly ash, iron-coated nano-adsorbents, zeolites, natural materials, biochar, etc. have been utilized for As sorption from water. Currently, researchers focusing on the synthesis of low-cost sorbents from waste material that are efficiently used to remove As from the water, thus, offering a cost-effective and environmentally friendly solution for pollutant removal from the water. Utilization of waste materials that are cheap, and are available in bulk amounts for environmental remediation, it is one of the sustainable approaches. Surface modification of the sorbent is also a topic of interest that makes sorbent more efficient (Nizamuddin et al., 2017; Thines et al., 2017a; Ruthiraan et al., 2017).

Biochar has emerged as the most popular adsorbent and is an emerging technology effectively used for the removal of contaminants from water in a cost-effective way (Liu et al., 2019a). Biochar is a carbonaceous compound produced under oxygen-deficient conditions through the process of thermal decomposition (Yu et al., 2015). Biochar approaches are potentially an innovative technology for As removal from the water or aqueous solution having some unique properties like high porosity, large specific surface area, high cation exchange capacity, consists various oxygen-containing surface functional groups that make it an efficient means for decontaminating water (organic and inorganic pollutants) (Agrafioti et al., 2014a). Availability of abundantly present feedstock is highly economical and was generally obtained from plants and animal waste such as cow dung,

leaf litter, fruit peel, nutshells, bagasse, straw of crops, etc. (Samoraj et al., 2022). Various research has been conducted to assess biochar as a promising adsorbent for removing different organic and inorganic pollutants from water (Mohan et al., 2014). Biochar is a cost-effective and efficient substitute for commercially available activated carbon. A wide range of raw waste biomass was available for the production of biochar at a comparatively low cost, which advances the development of various new technological approaches for the adsorption of As from water (Jiao et al., 2021). The synthesis of biochar using waste biomass is the most promising solution of waste biomass utilization and is the best way of managing organic waste (Yadav et al., 2013).

Considerable up-gradation to the biochar performance as a biosorbent for contaminated water treatment has been reported using different kinds of methods including physical and chemical treatments (Hong et al. 2020). Physical method of modification includes ball milling, the use of steam while, chemical modification involves the activation with bases, acids, organic compounds, metal oxides, metals, or carbon-based substances (Akhil et al., 2021). An increase in the biochar specific surface area was observed with the physical activation method whereas, chemical treatment increases the fraction of oxygen-containing surface functional groups that introduce more active adsorption sites to the biochar. Recently, biochar is developed using metallic and nonmetallic treatment of different feedstock to increase its productivity and capacity to remove various contaminants from aqueous solutions (Ambaye et al. 2020). Magnetic sorbents are extensively used for the removal of As because they are easily separated from water by applying an external magnetic field (Noraini et al., 2016; Thines et al., 2017b). Many studies reported that there is a negative charge on pristine biochar but several modifications

of the biochar material can develop a positive charge or add more functional groups on it that enhance the potential of the biochar to adsorb various adsorbates (Bakshi et al., 2018).

In the present study, dried leaves of *Tectona* and *Lagerstroemia speciosa* were used for the preparation of biochar and these waste along with the two different vegetable waste (*Raphanus stivus and Artocarpus heterophyllus*) further utilized for synthesizing modified biochar by the process of pyrolysis at 800 °C temperature and then applied for As removal from an aqueous solution as well as from groundwater. These waste material were easily available feedstock's present in a large amount and these waste materials are not managed properly. This study is a small initiative to solve the big problem of As contamination as well as the proper management of lignocellulosic waste biomass. Surface modification using metal salts ($FeCl_3$/$MnO_2$/$FeSO_4$) was done to enhance the adsorption capacity of the biochar as the adsorption. It is anticipated that this method of synthesis of biochar treated with metal salts can be protracted to encourage the building of multifunctional metal-induced biochar and other composite material for the removal of As with greater efficiency.

# *Chapter-2*
# *Objectives*

# Chapter-2 Objectives

**2.1.** Collection and selection of waste biomass for the preparation of biochar.

**2.2.** Synthesis of biochar from plant waste biomass.

**2.3.** Pretreatment of biomass for the synthesis of modified biochar.

**2.4.** To characterize biochar/modified biochar using Scanning Electron Microscope (SEM), Energy Dispersive Spectroscopy (EDS), X-ray diffraction (XRD), Fourier Transform Infra-red spectroscopy (FTIR), Particle Size Analysis (PSA), Zeta Potential, Point of Zero Charge ($pH_{ZPC}$).

**2.5.** Application of prepared biochar/modified biochar for the removal of Arsenic from the aqueous solution and groundwater.

# *Chapter-3*
# *Review of Literature*

# Chapter-3 Review of Literature

### 3.1. Arsenic Speciation and chemistry in Water

Arsenic is the 20$^{th}$ most prevalent element found 33 in the earth's crust (atomic number 33) with a predictable abundance of 1.8 parts per million by weight and it is documented for its toxicity on the human and marine world. Elemental As appears as a silver-grey breakable crystalline solid with an atomic weight of 79.4 amu (atomic mass unit); specific gravity (5.73); melting and boiling temperatures of 817 °C (at 28 atm) and 614 °C, correspondingly and its vapor pressure at 372 °C is 1 mm Hg (Yin et al., 2017; Zakhar et al., 2018). Arsenic is ranked 12$^{th}$ in the human body, 14$^{th}$ rank in seawater and it also accounts for around 0.00005 percent of the earth's crust. As content in most of the rocks varies from ~0.5-2.5 mg/kg, however, fine-grain sediments of argillaceous and phosphorites have greater quantities of As (Saha et al., 2021). As was first discovered in the year 1250 A.D. by Albertus Magnus (Mohan and Pittman Jr., 2007). Since its discovery, it is a source of debate because of its toxicity and carcinogenic effects. It is regarded as the 'king of poison' because it is extremely lethal and ranks first in the primacy list of hazardous substances in 2001 as defined by WHO (Shaji et al., 2021).

Arsenic exists in oxidation states of -3, 0, +5 and +3. Arsenic acids ($H_3AsO_4^{2-}$, $H_3AsO_4^-$ and $H_4AsO$), arsenic acids ($H_3AsO_3^{2-}$ and $H_3AsO_3$), methyl-arsenic acid, arsine, dimethyl-arsenic acid, arsenate and arsenite are the different forms of As present in the environment. Among all these forms of arsenic species, the most predominant form that is commonly found in water, are inorganic arsenate ($AsO_4^{3-}$) and arsenite ($AsO_3^{3-}$) signified as arsenic(V) and arsenic(III), respectively, (Pous et al., 2015; Navarathna et al., 2020).

Usually, the arsenic oxidation states are largely determined by redox and pH conditions and in groundwater, the oxidation condition of As is determined by the air exposure and water chemistry. As(III) is a strong acid that prefers to combine with nitrogen and oxides to form complexes, it occurs as $As(OH)_3$, $AsO_3^{3-}$ and $As(OH)_4^-$ whereas, As(V) on the other hand, act like soft-acid and forms compounds with sulfides and it is exiting as $H_2AsO_4^-$, $HAsO_4^{2-}$ and $AsO_4^{3-}$ species. Inorganic As forms are most commonly found in water supplies (Carter et al., 2003; Baig et al., 2015; Weerasundara et al., 2021). Arsenate and arsenite both are present in oxidized and reduced nature due to the delayed conversion rate of redox reaction. Arsenic appears largely as arsenite in anoxic reduced conditions for example; reduced sediments or subterranean water, though arsenate is abundant in oxidizing aerobic habitats like surface water (Liu et al., 2020a). Both the As species (As(III) and As(V)) are exposed to microbial and chemically driven methylation and redox processes in water. Including heavy metalloids, arsenic is particularly susceptible to mobilization at pH 6.5-8.5 under reducing and oxidizing conditions. Trivalent As prevails intemperately reducing anaerobic conditions such as deep groundwater (Litter et al., 2010; Kumar et al., 2019). As speciation is governed by pH and redox potential (Eh). H2AsO4- predominates at low pH (pH<6.9) in oxidizing circumstances. At elevated pH $HAsO_4^{2-}$ is the dominant species (under hard acid and basic conditions As possibly present as $H_3AsO_4^0$ and $AsO_4^{3-}$, correspondingly). At pH less than ~9.2, in reducing environments the predominant species is uncharged $H_3AsO_4^0$. Because of its polarizability, electronic structure, sorption affinity and poisonous characteristics the pentavalent As (hydroxyl anions) and trivalent As (neutral molecule) exhibit noteworthy differences in natural settings (Zouboulis, 2005; Shakya and Ghosh, 2018; Maliva, 2020).

### 3.2. Sources of arsenic

#### 3.2.1. Natural sources of Arsenic

The process of rock weathering containing As, emissions from volcanos and some biological activities are the natural sources of As in water. Arsenic is found in about 200 different forms of minerals as a primary constituent, of which approximately 60 % are arsenates, sulfosalts and sulfide constitute 20 %, arsenide, oxides, sulfides, arsenites, elemental arsenic, and just a handful of which usually contains considerable levels of As. The majority are ore minerals or their byproducts and their mineral components are quite uncommon in the natural world (Garelick et al., 2009; Wang et al., 2019a; Uddin and Jeong, 2020). Alkaline desorption, reductive dissolution, sulfide oxidation and geothermal activities are the four different natural geological processes that are responsible for As release in the environment. Arsenopyrite ($(FeAs, S)_2$) is possibly the very important arsenic-containing mineral in the zone of ore found mainly in the environment with no oxygen where the As is released in groundwater via the process of desorption (Mondal et al., 2013; Hong et al., 2018; Wu et al., 2020). As is commonly adsorbed on the iron-oxyhydroxides surface in sediments and released into the environment by microbial decomposition. Natural sources also comprise FeOOH desorption and oxidation of sulfide minerals having As (Faust et al., 2021).

As is found everywhere, although in varying amounts in soils, unconsolidated sediments and rocks. Igneous rocks contain about 5 mg/kg or less As concentration while volcanic glasses contain roughly 6 mg/kg and metamorphic rocks have a concentration similar to those of sedimentary and igneous ancestors (Tabelin et al., 2018; Moeck et al., 2020). Pelitic rocks that include slates, and phyllites exhibit the highest As concentration

averaging approximately 18 mg/kg (Aghdam et al., 2021). Sedimentary rocks constitute around 5-10 mg/kg of As. The sediments of Canadian soil have a very high concentration of As i.e., 0.9-44 mg/kg and about 1.9-170 mg/g concentration has been reported in glacial till and in the area of high mineralized area and through sedimentary rocks, minerals and soil the As reaches to the water and contaminate it.

### 3.2.2. Anthropogenic source of Arsenic

Anthropogenic sources of As have been raised from human activities like metal ore processing (Copper, gold, zinc tin, etc.), mining, and smelting which cause As release in the environment. These human activities also accelerate the processes of As released into the environment at a high level of magnitude by altering or disturbing the natural mechanism of As. The As dissolution in the aquifers is the result of excessive extraction of groundwater (Sarkar et al., 2012; Basu et al., 2014). Furthermore, these sources of As i.e., anthropogenic in origin affect resources of water as well as the other environments and it includes swine and poultry feed condiments, herbicides (methlarsonic acid), paints, cosmetics, vitamin supplements, electronic production, pesticides (disodium salts, methyl arsenate, etc.), wood preservation (chromate copper arsenate), pharmaceuticals, metallurgical emission, coal combustion, petroleum refining and other industrial activities (Kumar et al., 2019; Ali et al., 2019). About 60 % of As released due to anthropogenic activities globally originates from the smelting process of copper (Cu) and combustion of coal (Ochedi et al., 2020; Li et al., 2022). Coal-burning can also add the As in the air and enhance its quantity in different matrices of the environment because of the presence of a small amount of pyrite in sulfide abundant coals. The anthropogenic sources also include

the disposal of industrial, municipal and domestic waste in the water bodies (Neumann et al., 2010; Madhav et al., 2020). The overall As release pathway in the environment is portrayed in Fig. 3.1.

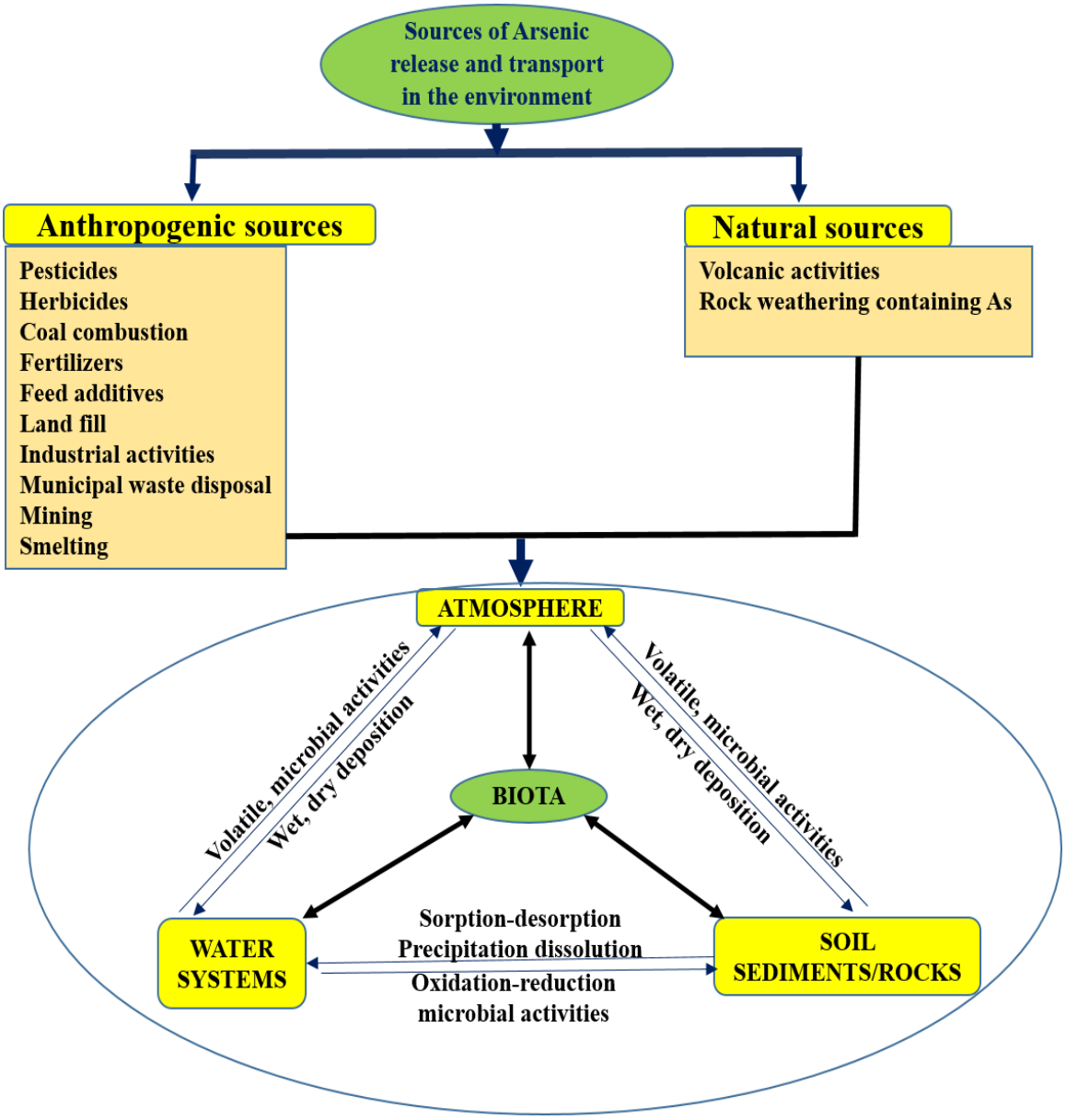


**Fig. 3.1. Arsenic cycle showing source, fate and transport between environmental components (source: Zakhar et al., 2018).**

### 3.3. Arsenic toxicity on humans and the environment

#### 3.3.1. As in the food chain

Food contamination is mostly determined by the amount of As present in the soil and water in which these food or grains are grown (Cai et al., 2019; Kanwar et al., 2020). Consumption of animals as food by a population may be subjected to As exposure by ingesting polluted food and water which was followed by the bioaccumulation of As in their fatty tissues. In chickens, which is one of the most consumed animals by humans, the chronic effect of As contamination is still unknown (Giuliani et al., 2020). In several studies, it was reported that organs, particularly the liver and dermal cells consist of higher As contamination than that of muscles (Ghosh et al., 2012; Hu et al., 2017). In poultry farms, organoarsenic stimulants are used which are commonly employed for their antibacterial properties, help in enhancing and developing the flesh color. Regardless of their modest toxicity, these stimulants can be converted into inorganic As, posing a danger of human exposure (Nachman et al., 2013; Mazhar et al., 2021). The As accumulation in the aquatic ecosystem is favored by invertebrates and algae and it was observed that as per the dietary patterns, detritivorous fishes are highly exposed to As and the liver is the target organ where maximum As accumulation was found (Panel, 2014). There are many sources of oceanic As that contribute to inorganic As viz. arsenite (As(III)), arsenates (As(V)), monomethylarsonic acid (MMA) and dimethylarsinic acid (DMA), these are inorganic and organic forms of As. Arsenobetaine is an organic form of As with minimal toxic effects and marine fishes play a very significant role in its accumulation (Chen et al., 2019; Xiong et al., 2021).

### 3.3.2. Health effects of As on humans

As comes under Group 1 toxicant and human carcinogen and consumption of drinking water contaminated with As regularly has both chronic and acute health consequences (Ahmad et al., 2018; Engwa et al., 2019). As is a metalloid and considered one of the most toxic toxicants, and its exposure upsurges health-related risks. The negative health-related consequences of As exposure are determined by several parameters including the amount of exposure (dose), chemical form, route of exposure (ingestion, direct contact, inhalation, etc.) (Sinha and Prasad, 2020). Chronic exposure to As raises the chance of health problems such as cardiovascular problems, respiratory diseases, failure of the reproductive system (childbirth, pregnancy, fertility), neurotoxicity, disorders in the bladder and kidney, gastrointestinal complications, skin lesions (keratosis, leukomelanosis, and melanosis), lung, bladder, dermal cancer, genotoxicity, endocrine problems, in case of severe exposure it may cause death, etc. (Bozack et al., 2018; Rahman and Singh et al., 2019). Some of the As related effects on humans have been discussed in detail below:

#### *3.3.2.1. Skin disorder*

Skin, nails and hairs altogether form the integumentary system and it is often referred to as the biggest body's organ. Skin is thought to be more vulnerable to arsenicosis and emphasizes the early stage of the disease (Sanyal et al., 2020; Mood et al., 2021). The most prevalent characteristic of arsenic exposure are skin lesions including hypopigmentation, hyperpigmentation, Bowen's disease and keratosis, these all together constitute general symptoms of arsenicosis. Skin lesions, on the other hand, frequently appear within 5 to 10 years of contact (Rahman et al., 2018; Palaniappan and Karthikeyan,

2022). Furthermore, in comparison to women, men are more prone to acquire arsenic stimulated skin problems. According to Hsu et al. (2013), persons with hyperkeratosis or skin cancer exhibited a greater risk of urothelial and lung malignancies and these similar hazards were seen in populations exposed to high, medium and low As concentrations. In a study, conducted by Mazumder et al. (2010) in West Bengal, India, it was observed that about 66 % of patients are suffering from palm thickening and skin pigmentation because of As exposure through consumption of drinking water (As concentration ~0.05-3.2 mg $L^{-1}$). The research done in Bangladesh found a clear link between skin lesion development and exposure to As. It showed that keratosis and melanosis were found in about 36 patients out of 167 and those were encountered with low amounts of As i.e., about ≤10 µg $L^{-1}$ (Abdul et al., 2015).

***3.3.2.2. Cardiovascular disorder***

The incidence of high blood pressure and other cardiovascular diseases has increased at a high rate which is associated with chronic As exposure (Iob and Steptoe, 2019). Long-term consumption of As contaminated drinking water causes cardiovascular dysfunctions as well as hypertension, diabetes, atherosclerosis, arrhythmia, etc. (Ahangarpour et al., 2018). The effects associated with the high exposure to As also depends on the dose and duration of exposure. Inhalation of inorganic As over an extended period might harm the cardiovascular system, especially the heart (Argos et al., 2012; Lipshultz et al., 2019). Several epidemiological research shows that exposure to a higher amount of As via inhalation results in an increased rate of diseases in the population and death owing due to cardiovascular consequences. Exposure to a high level of As through drinking water leads to an elevated risk of cardiovascular disease and death in the

Southwest region of Taiwan, the United States, and Bangladesh disclosed in a cohort study (Chen and Karagas, 2013). The increased death rate was also observed due to cardiovascular disease is linked with exposure to high As concentrations (100 µg/L to 300 µg/L) in the last several years (Abdul et al., 2015).

#### *3.3.2.3. Neurological effect*

Arsenic can quickly pass the blood-brain barrier, the main target of As poisoning in the brain that causes impairing concentration and learning and it is found in almost every part of the brain (Mundey et al., 2013). Though, the pituitary gland had the most accumulation than other parts of the brain. The onset of neurological problems as a result of acute and chronic exposure to As is rapid and manifested as symmetrical sensory neuropathy (Matta and Gjyli, 2016; Nayak, 2017). Numbness and pain in the foot sole, discomfort, paraesthesia, etc. are some of the most prevalent clinical symptoms caused by neurons' reduced ability to cleanse Reactive Oxygen Species and the synthesis of glutathione (Srivastava and Flora, 2020). As exposure can also cause substantial impairment in language learning, memory, etc. according to neuropsychological research (Sinha and Prasad, 2020). In a cohort study on pregnant women, it was reported that in the third to sixth trimester of their pregnancy they suffer from depression with exposure to low As levels (Valdes et al., 2017). Furthermore, over a certain duration, acute exposure to As causes encephalopathy, which results in a progressive decrease in brain activity and function and also leads to headaches, coma, convulsions and hallucinations. Peripheral neuropathy was the predominant nervous consequence among individuals exposed to groundwater contaminated with As in West Bengal, India, according to the latest study

conducted by Mukherjee et al. (2003). It was reported that Alzheimer's disease and its related illness, are also associated with long-term exposure to low-level As (O'Bryant et al., 2011).

#### *3.3.2.4. Effect on the respiratory system*

As poisoning either from drinking water or other sources can cause respiratory problems over a long duration. In the population of Bangladesh (Argos et al., 2010), a high death rate was associated with a higher level of As exposure via drinking water consumption. The link between As exposure and higher mortality rates owing to respiratory disorders including lungs dysfunction has proven devastating (Chatterjee et al., 2018; Chikkanna et al., 2019). Inhaling As fumes or dust all through mining or processing ores can lead to respiratory problems like laryngitis, rhinitis and persistent cough. Chest noises, blood in the sputum, breath shorten, chronic cough are some of the most prevalent respiratory symptoms seen in a cohort study (Parvez et al., 2010). Lungs dysfunction and disease like tuberculosis has been observed in various regions of Bangladesh due to moderate As exposure, reported in a cohort study (Parvez et al., 2013). In another study, it was found that those who were exposed to As in their childhood via consumption of drinking water contaminated with As had a higher risk of death due to bronchiectasis and lung cancer in young peoples (Smith et al., 2006).

#### *3.3.2.5. Effect on the endocrine system*

As is one of the well-distinguished heavy metals, disrupts the endocrine system, including the thyroid, pancreas, thyroid hormone, gonads, as well as hypothalamic-

pituitary glands (Kibenge and Strange, 2021). Prenatal exposure resulted in impaired thymic functioning, presumably due to As-induced apoptosis and oxidative stress. There is limited information about the definite impact of As on the pituitary and adrenal gland (Sabir et al., 2019; Jovanovic et al., 2021). In a study conducted in West Texas counties and it was found that people living in a rural region have been suffering from hypothyroidism which was linked with low As levels for a long duration via drinking water tinted with As (Gong et al., 2015). As build-up in the pancreas lowers insulin secretion and cell survival. In the human body, insulin and glucagon are generated by the pancreas, which also regulates glucose levels in the blood. Diabetes due to As in the population residing in the US has been reported by Gribble et al. (2012). Furthermore, the latest study conducted in Bangladesh shows that even low levels of As exposure raises the risk of Type 2 Diabetes Mellitus (T2DM) (Pan et al., 2013; Moreno et al., 2022).

#### *3.3.2.6. Effect on liver*

Due to the repeated exposure to As, it accumulates in the liver at a greater rate, increasing the risk of hepatic dysfunctions (Muthumani and Prabu, 2012; Mershiba et al., 2013). To detoxify, inorganic As are broken down in the liver and then expelled via urine (Watanabe and Hirano, 2013). Ascites, liver enlargement, and esophageal variceal bleeding are some of the clinical symptoms of liver disease that appear in the early stage of exposure to As. Intensified amount of enzymes secreted from the liver has also been witnessed in blood tests (Jomova et al., 2011). As after instant exposure directly enters the systematic circulation and binds to haemoglobin and leads to hemolysis after accumulating in erythrocytes. Liver lesions as well as some additional problems like cirrhosis, hepatic

fibrosis and increased chance of liver failure in posterior phases of toxicity (Zheng et al., 2021). In West Bengal, India, it was seen that people who come in contact with As, suffer from liver enlargement, increased levels of globulin, alanine aminotransferase, alkaline phosphatase, etc. Poisoning and liver cell damage may also occur as a result of As exposure (Sankar et al., 2015).

### 3.4. Worldwide scenario of arsenic contamination

The natural As contamination in groundwater has been documented throughout the world, with the bulk of cases occurring in South America and South Asian regions. Millions of groundwater aquifers with modest contamination of As (<50 µg/L) exist in several nations. The highly contaminated countries where high concentrations of As have been discovered include India, Bangladesh, USA, Nepal, Cambodia, Vietnam, Myanmar, Laos, Indonesia, China (Dhillon, 2020; Yang et al., 2014; VanDerwerker et al., 2018; Bhattacharya et al., 2019; He et al., 2020a; Medunic et al., 2020). Some countries such as Mexico, Hungary, Pakistan, Chile, Argentina, South Africa, and Canada are also affected by As contamination in groundwater (Rasool et al., 2015; Ali et al., 2019).

The Southeast and South Asian Belt, which includes most developing countries like Bangladesh, India, Nepal, China, and Vietnam, is contemplated as the most polluted regions with As contamination (Fig. 3.2.) (Kim et al., 2011). As pollution in groundwater is also frequent in affluent nations such as US and Canada, while the concentrations are typically lower than those found in Asian countries. High concentrations of As have been discovered worldwide since the largest sources of geogenic As in groundwater were identified in the Bengal delta in the year 1993 (Chakraborty et al., 2015; Raessler, 2018). Australia is the world's most As-polluted country, where about 300 mg/L As concentration

was documented, volcanic eruption, mining and sulfide-bearing minerals oxidation were identified as important sources of As discharge in groundwater (Ali et al., 2019). The majority of As contamination-prone areas are in sedimentary basins and near deltaic and contemporary mountain belts. Tropical climates are especially susceptible to As pollution because the weather encourages the As release from As compounds (Raju, 2012).

### 3.5. As contamination in India

In India, groundwater plays a significant role in meeting the water demands of numerous sectors, including household, irrigational and industrial needs (Mukherjee et al., 2006). Groundwater As in India occurs in two different categories: (i) hard rocks terrane and (ii) alluvial terrane (Pradhan et al., 2021). Alluvial aquifers are the primary source of As pollution and 90 % of As pollution is accounted for by these aquifers whereas, 10 % source is accounted for by hard rock terrane. The Ganga and Brahmaputra rivers' alluvial stretches are India's wealthiest groundwater provinces (MacDonald et al., 2016; Suhag, 2019). Approximately 26 % of India's total area is encompassed by the Ganga river basin and about 50 million population is at high risk of groundwater As poisoning (Chakraborti et al., 2018). The Ganga river basin is one of the world's highest inhabited and most fertile places and currently it is one of the most polluted rivers in the world, with high levels of lead, copper, chromium, cadmium, mercury, arsenic, pathogenic bacteria, pesticides etc. about 3000 times higher than the recommended limits set by World Health Organization (Duttagupta et al., 2021). In shallow aquifers, groundwater with high levels of As i.e., more than 10 µg/L has been reported in different states of India. Jharkhand, West Bengal, Uttar Pradesh, Bihar, Assam, Haryana, Gujarat, Madhya Pradesh, Arunachal Pradesh,

Punjab, Tamil Nadu, Chhattisgarh, Karnataka, Himachal Pradesh, Andhra Pradesh, Telangana, Nagaland, Orissa, Manipur, Tripura are the Indian states and Daman and Diu, Delhi, Jammu and Kashmir, Pondicherry is the 4 Union territories affected by As contamination (Fig. 3.2.) (Mazumder et al., 2010; Verma and Sinha, 2022; Wu et al., 2021). These states were highly affected by the consequence of consumption of As contaminated drinking water. Various health-related issues have been reported in various states of India due to the As contamination (Yadav et al., 2021; Kumar et al., 2021).

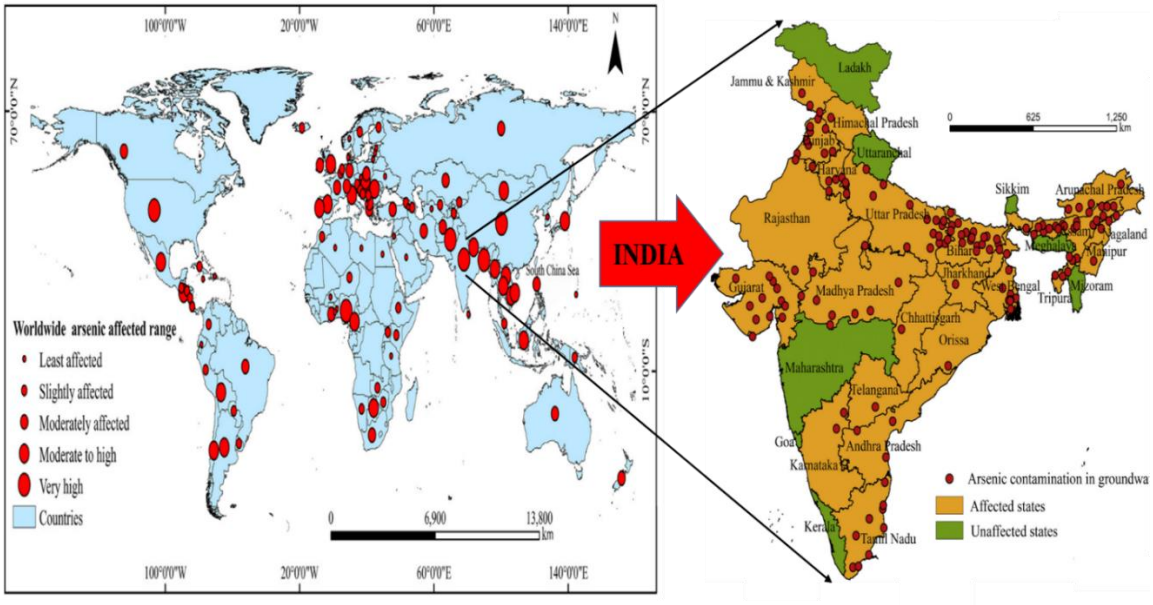


**Fig. 3.2. Arsenic contamination in different parts of the world and arsenic-affected states in India (Source: Shaji et al., 2021).**

### 3.6. Different techniques of As removal from water

#### 3.6.1. Chemical precipitation

The technique of chemical precipitation is used for removing various heavy metals like As, which employs reagents including aluminum alum, aluminium sulfate ($Al_2$

$(SO_4)_3.18H_2O$), ferric sulfate ($Fe_2(SO_4)_3$), ferric chloride ($FeCl_3$), calcium and magnesium salts, etc. (Azimi et al., 2017; Alka et al., 2021). These coagulants are very effective for the As removal from water by transforming dissolved As into a low-solubility compound and they can also utilize in stabilizing solid waste (Sullivan et al., 2010). Based on weight, ferric salts were shown to be more efficient than alum in eliminating As and it is also very effective across a wider pH range. Pentavalent As (As(V)) can be more successfully removed than trivalent As (As(III) in both cases (Chiavola et al., 2019). In this technique, positively charged coagulants such as aluminium sulfate, ferric chloride, etc., lower the colloids' negative charge, thus causing the particles to collide and get larger in coagulation. The addition of an anionic flocculant, on the other hand, produces bridging or neutralization of the charge between the larger particles that were formed in coagulation leading to flocs development (Ferasat et al., 2020). The addition of chemicals during these processes converts dissolved As into an insoluble solid, which later precipitates, and soluble species of As can be co-precipitated after incorporation with a metal hydroxide phase. Solids can be separated or removed subsequently by using sedimentation and filtration processes and these flocs also adsorb As. As(III) occurs mainly in non-ionized form, it is not easily removed thus, as a pretreatment, oxidation of both As(III) and As(V) is required for effective removal (Senn et al., 2018). As demonstrated in Equations 3.1 and 3.2, this can be accomplished by adding chlorine (bleaching powder)/potassium permanganate (Ahmed, 2001):

$$H_3AsO_3 + HClO = HAsO_4^{2-} + Cl^- + 3H^+ \quad (3.1)$$

$$H_3AsO_3 + 2KMnO_4^{2-} = 3HAsO_4 + 2MnO_2^+ + 2K^+ + 4H^+ + H_2O \quad (3.2)$$

The alum coagulation chemical formulae include:

*Alum dissolution:*

$$Al_2(SO_4)_3.18H_2O = 2Al^{3+} + 3SO_4^{2+} + 18H_2O \quad (3.3)$$

*Aluminium precipitation:*

$$2Al^{3+} + 6H_2O = 2Al(OH)_3 + 6H^+ \quad (3.4)$$

*Co-precipitation:*

$$H_2AsO_4^- + Al(OH)_3 = Al - As\ (complex) + other\ compounds/products \quad (3.5)$$

Sedimentation removes As adsorbed on $Al(OH)_3$ flocs as aluminium-As complex and the filtration may be necessary to confirm all flocs are removed completely. Similarly, the same reactions occur with $FeCl_3$ and $FeSO_4$, resulting in the development of the iron-As complex as an end product, which is eliminated using filtration and sedimentation. The interactions of iron oxide (hydrous) with arsenate are depicted here and $_{=}FeOH°$ signifies the surface site of the oxide (Ahmed, 2001).

$$Fe(OH)_3\ (s) + H_3AsO_4 \rightarrow FeAsO_4.2H_2O + H_2O \quad (3.6)$$

$$_{=}FeOH° + AsO_4^{3-} + 3H^+ = FeH_2AsO_4 + H_2O \quad (3.7)$$

$$_{=}FeOH° + AsO_4^{3-} + 2H^+ \rightarrow {}_{=}FeHAsO_4^- + H_2O \quad (3.8)$$

For improved efficiency, oxidation of As into As(V) Immobilization of As by iron oxide (hydrous) as demonstrated in Equations 3.6 to 3.8, is required for As immobilization by iron oxide (hydrous). The As elimination from water is influenced by pH (Bissen and Frimmel, 2003; Saavedra et al., 2018). The pH range from 7.2 to 75 is most effective for the successful removal of As in the coagulation process with alum. Whereas, in the process of coagulation using iron salt the efficient As removal is accomplished between the pH

range of 6.0 to 8.5 (Sandoval et al., 2021). Fig. 3.3. shows different techniques for As treatment from water.

The main disadvantage of this process is the massive volume of secondary sludge generation. The resulting sludge is very difficult to manage, transport and disposed of properly and the accompanying of this technique adds downside. So, the development of new technology is necessary to overcome these concerns.

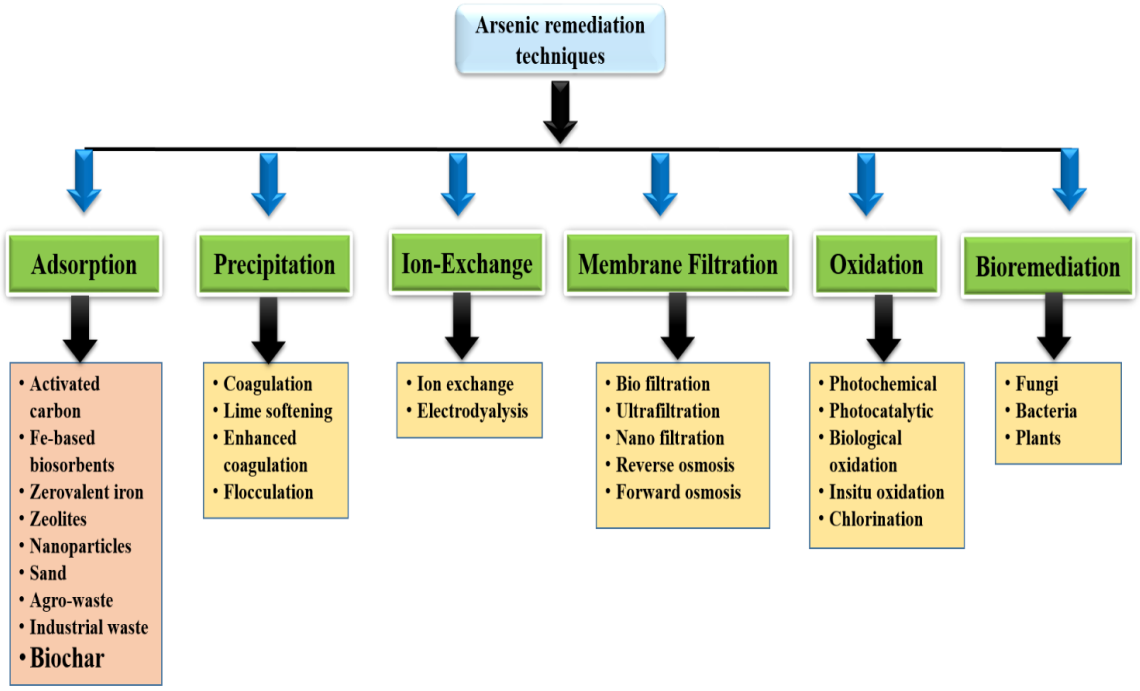


**Fig. 3.3. Common water treatment techniques related to removal of As.**

### 3.6.2. Ion-exchange

Ion exchange is a physicochemical process of water treatment that involves the removal of heavy metals including arsenic and other contaminants. The ions are electrostatically held on the solid phase surface and can be exchanged with ions of a similar charge from the solution (Alka et al., 2021). The solid is usually a synthetic resin (anion exchange) which is most commonly used to remove specific unwanted anions and cations

from water. Ion exchange is a reversible ion transfer method in which the solid's structure does not change permanently. To remove As, at the exchange sites an ion resin that is commonly loaded with ions of chloride, is placed in a container. Water containing As is then circulated through the vessel, where the As exchanges for chloride ions. The water leaving the vessel contains less As but more chloride ions than the water entering it through the inlet (Chen et al., 2020a; Dixit et al., 2021). When the resin gets exhausted, it must be regenerated meaning that almost all the exchange sites that were previously loaded with chloride ions are now occupied with As or the other ions (Holl, 2010). The chloride ions that were previously on the solid resin were replaced or exchanged for As and other anions present in the treated water. Equation 9 and 10 shows the As exchange and regeneration process, respectively, with a solution of common salt as a regeneration agent are given as follows:

$$2R - Cl + HAsO_4^{2-} = R_2HAsO_4 + 2Cl^- \quad (3.9)$$

$$R_2HAsO_4 + 2Na^+ + 2R - Cl + HAsO_4^{2-} + 2Na^+ \quad (3.10)$$

Here, R is the ion exchange resin.

It was reported that because nitrate and sulfate are exchanged earlier than As, the capacity of As removal is influenced or dependent on the raw water's nitrate and sulfate levels (Ahmed, 2001). The water pH has less impact on the process of ion exchange. Pre-oxidation of As(III) to As(V) improves the effectiveness of the process of ion exchange deeply, although excess oxidant must be eliminated before the ion exchange process to minimize the destruction of resins (Magana et al., 2021).

The use of the ion-exchange process is generally confined to small to medium scale due to its greater cost of treatment as compared to the available traditional and conventional methods of treatment (Chiban et al., 2012).

### 3.6.3. Oxidation

Although oxidation is not a process of removal itself, it may significantly improve the efficacy of different technologies used for As removal from water (Rashid et al., 2021). In groundwater As is present in varying amounts as As(III) and As(V). Most of the conventional treatment methods are very helpful in removing pentavalent form of As hence, As(III) needs to be pretreated with the oxidation process for conversion into As(V) (Raessler, 2018). Ozone, hypochlorite, hydrogen peroxide, oxygen, permanganate, etc. are the As(III) oxidizing agents (Nayak et al., 2019). Among these oxidizing agents hypochlorite, atmospheric oxygen, chlorine, chlorine dioxide, and potassium permanganate are generally used in developing countries for oxidation. The oxidation of As(III) to As(V) by hypochlorite, atmospheric oxygen, and potassium permanganate is given below:

$$H_3AsO_3 + HClO = HAsO_4^{2-} + Cl^- + 3H^+ \quad (3.11)$$

$$H_3AsO_3 + 1/2O_2 = H_2AsO_4^- + 2H^+ \quad (3.12)$$

$$3H_3AsO_3 + 2KMnO_4 = 3HAsO_4^{2-} + 2MnO^+ + 2K^+ + 4H^+ + H_2O \quad (3.13)$$

It takes a long time for the oxidation of arsenite to arsenate by atmospheric oxygen however the chemical oxidizing agents under various conditions rapidly oxidize As(III) into As(V). In a study conducted by Bissen and Frimmel, (2003) it was reported that only

55 % of total arsenite content in 5 days was oxidized by purging pure oxygen and air in groundwater.

### 3.6.4. Membrane Filtration

Membrane filtration is a technology for removing various toxins including As from water. Membrane technology is broadly recognized as an effective technology that can reduce about 96 % As contamination in groundwater. It stops bacteria from flowing across the membrane and prevents As accumulation by dissolving it from polluted water (Ungureanu et al., 2015). Membranes are often synthetic materials containing billions of holes that act as selective barriers and prevent some water constituents from passing through. As membranes are the selective barriers that separate dissolved components and suspended components to varying degrees, according to the size from tiny ions up to bigger molecules and large particles of approximately 100 µm. The pressure gradient between the two sides of the membrane results in the movement of molecules across the membrane because of this the membrane filtration is referred to as pressure-driven technology. Membrane filtration technology includes nanofiltration, microfiltration, reverse osmosis, and ultrafiltration that remove different types of particles dissolved in water including As (Gonzalez et al., 2019; Maitlo et al., 2019). Reverse osmosis and nanofiltration have been identified as the most encouraging technology for the removal of As from polluted water (Xu et al., 2013). With a pore size of about 0.1 microns, microfiltration may be used to eliminate the bacteria as well as the suspended particles. While ultrafiltration removes viruses, colloids and some proteins also have a pore size ranging from 0.0003 to 0.1 microns. Nanofiltration involves the physical elimination based on molecule size and

charge and the pore size varies from 0.001 to 0.003 microns. Reverse osmosis is used mainly for the desalination of water and has a pore size of 0.0005 microns. To pass water across the membrane from high concentration to low concentration high pressure is required. Typically selectivity increases with an increased driving force (Richards, 2012). Recently, Jadhav et al. (2018) investigated the removal of As using nanofiltration technology and found 97 % rejection of As. Mukhopadhyay et al. (2019) in their study used a nanocomposite membrane for the removal of As from an aqueous solution and observed that the rejection rate of As increased with an increased dose of nanocomposite with the highest rejection of 94% for 1 mg/L of initial As concentration.

This removal technology is more costly than other treatment processes and creates a huge amount of residual waste. Although reverse osmosis has been recognized as a successful technique to remove As, it requires high operating pressure and energy, raising the process's cost and lowering its efficiency.

### 3.6.5. Adsorption

The process of adsorption uses solids for removing pollutants from gaseous medium and liquid solutions. As (adsorbate) adsorption is defined as the adherence to the surface of the solid sorbent from a solution (Zakhar et al., 2018; Liu et al., 2020a). Thus, the effectiveness of adsorptive As removal is reliant on the affinity of adsorbent and adsorbate. Time of exposure, pH of the solution, presence of various chemical species, operating temperature, As initial concentration, and the dosage of adsorbent, all impact the efficacy of this method (Choong et al., 2007). In general, the removal of As by the process of adsorption is dependent on As speciation and pH of the solution, in a study it was observed that with lower pH (<7) exhibits higher removal of As(V) than that of As(III)

(Yang et al., 2017). Other ions present in water/solution such as silica, phosphate, calcium, and alkalinity compete for the active adsorption sites that affect the adsorption rate as well as the capacity of adsorbent to adsorb As. Adsorption of As also depends on various properties of the adsorbent like particle density, size of adsorbent, pore characteristics, zeta potential, surface functional groups, mineralogy, condition of activation, etc. (Sen and Pal, 2009; Zhu et al., 2013). Several conventional adsorbents that were successfully used for the remediation of As including clay minerals, commercially available activated carbon, iron-based adsorbents, zeolites, activated alumina, pristine biochar, engineered biochar, etc. and some other adsorbents like modified activated carbon, synthetic and natural oxides, sand, biomaterials, etc., that are reported as a potentially cost-effective adsorbent for removal of As (Gupta et al., 2012; Kumar et al., 2019; Mohan et al., 2019). Huang et al. (2020) reported 1.315 mmol/g and 1.325 mmol/g of adsorption capacity for the removal of As(III) and As(V), respectively, by using adsorbent ferrihydrite infused biochar via the process of adsorption. In another study, it was observed that the removal of As(V) by the process of adsorption 0.082 mg/g adsorption capacity was found, in which Zr-modified adsorbent has been applied for As(V) removal (Velazquez et al., 2019).

The method of adsorption compared to other methods discussed above is most often used in water treatment processes because it is simple in design, cost-effective, has regeneration capability, easy to operate and handling as well as the fact that it is sludge-free. The process of adsorption also attracted a lot of attention because of the following benefits: it generally does not require a big volume or any extra chemicals and it produces no toxic by-products. Several advantages and disadvantages of the removal techniques has been listed in Table 3.1.

**Table 3.1. Comparison of arsenic removal technologies**

| Treatment Method | Types | Mechanism | Advantages | Disadvantage | Reference |
|---|---|---|---|---|---|
| Chemical precipitation | Coagulation, Flocculation, Lime softening | Firstly forms a separable solid material and removes dissolved metals from the solution | Simple in operation and effective in removal; specific components removed; low cost | High processing cost; produces toxic sludge; in some cases, pre-oxidation is required; produces harmful by-products; removes As(V) effectively and medium removal of As(III) | Senn et al. (2018) |
| Ion exchange | Natural resins Synthetic resin | Solid-phase ions from polluted water were shared with an equal ion number | Limited production of sludge; to remove As specific resin is used | Regular rejuvenation is needed to ensure complete removal; high-tech operation is required; resins life; expensive | Laatikainen et al. (2016) |
| Membrane techniques | Nanofiltration, Reverse osmosis, | The membrane structure serves as a selective | High efficiency; high performance | Expensive and high rejection of water; pre-treatment is | Zakhar et al. (2018) |

| | | | | | |
|---|---|---|---|---|---|
| | Forward osmosis | barrier, allowing molecules to flow through with the assistance of a driving force, resulting in a high residual volume | for filtration; chemical-free | needed; high-tech operation and maintenance | |
| Electro-coagulation | Aluminium sulfate, Ferric chloride | Metallic cations are directly created by applying a current between iron electrodes to liquefy soluble anodes in the waste processed, as an alternative to chemical precipitation | Chemical-free; easy maintenance; simple operation; novel strategy for As removal | Commercially not available; not suitable for effective removal of As(III); high energy consumption; high affected by form of coagulant, solution pH and dose | Rosales et al. (2018) |
| Phyto-remediation | Phytoextraction Phyto-stabilization, Phytofiltration | Plants are used to combat soil, water pollution | Eco-friendly; chemical free; land restoration | Time-taking process; strong development is needed; | Karakurt, (2019) |

| | | | | | |
|---|---|---|---|---|---|
| | | | | commercially not available | |
| Adsorption | Activated carbon Sand, polymeric adsorbents, zeolites, nanoparticles, Biochar | Solids are used to remove chemicals from gaseous or liquid solutions | Safe operation handling; low cost; high removal efficiency; sludge free; no harmful by-products | Adsorption bed gets exhausted; not self-monitoring | Ghosal et al. (2018) |

### *3.6.5.1. Activated carbon*

Activated carbon materials are successful in the treatment of a wide range of pollutants in drinking water and wastewater (Yin et al., 2007; Power et al., 2018). Its strong affinity for pollutants is due to its huge hydrophobic surface. Despite the accessible availability, meeting the USPA, WHO permissible standard of 10 ppb for drinking water is challenging due to the poor or moderate adsorption capacities of unmodified activated carbon. As a result, activated carbon modification is gaining traction as a viable method for achieving remarkable affinities for a variety of targets (heavy metals ion). Restricted adsorption capacity has been observed for As adsorption via unmodified activated carbon. Several research has been reported on the use of microwaves for synthesizing activated carbon (Kosheleva et al., 2019; Gao et al., 2020). Several feedstocks have been utilized for the preparation of activated carbon such as coconut husk/shell, coal, crop residue, woods, etc. that further been applied for the treatment of wastewater (Gan, 2021; Elbehiry et al., 2021). Mostly, different sorts of acidic and basic chemicals like $H_2SO_4$, KOH, iron salts,

etc. are used to activate the carbon materials, therefore it is designated as activated carbon. Though many researchers have discussed the removal of As through activated carbon. Hao et al. (2018) conducted a study in which they utilized sugarcane bagasse to synthesize two types of activated carbon one was unmodified and another was modified with ferric chloride. The result indicates that the maximum removal (70 %) of As(III) was obtained by modified activated carbon and only 29 % removal was achieved by unmodified activated carbon. Activated carbon infused with Fe/Mg has a much greater adsorption capacity i.e., 19.35 mg/g for adsorption of pentavalent As, compared with other modified activated carbon or untreated activated carbon (Gallios et al., 2017). Various other studies also used activated carbon for the removal of As from water (Hashim et al., 2019; Joshi et al., 2019; Mani et al., 2021; Wang et al., 2020)

Globally, activated carbon has been extensively used as an adsorbent for the treatment of water, but its high cost of production and regeneration cost limits its usage on a broad scale for organic and inorganic contaminants removal.

#### *3.6.5.2. Fly ash*

Combustion of coal generates large quantities of residues and fly ash is one of them, whose disposal is a major problem these days. It is a complex compound including closely connected and finely distributed liquid, gaseous and solid components with a distinctive heterogeneous changeable composition. The mineral composition of these by-products (fly ashes) generally consists of a fluid (<0.5 %), organic (~1-9%), and inorganic (~90-99 %) components (Polowczyk et al., 2007). The fly ash mainly consists of alumina and silica particles and is a strong alkaline substance having a pH of 10-13, when mixed with water.

Therefore, by the process of electrostatic and precipitation adsorption, it can remove metal ions from an aqueous solution. Numerous researchers have used fly ash as an adsorbent to eliminate the pollutants from the environment. Removal of As(V) was observed highest at acidic pH (pH 4) rather than at neutral and alkaline pH via fly ash of coal power plant (Diamaddopoulos et al., 1993). The minerals in fly ash like Fe and Al are accountable for As captured from the water. It was reported that fly ash agglomerates were easy to be used because it is less dust and can be easily separated from the liquid solution and they also adsorb As at a high rate (Ultowska et al., 2014). It was also observed that components of fly ash might be dissolved at severe pH, thus interfering with As adsorption by increasing the concentration of total soluble As (Ochedi et al., 2020). In comparison to activated carbons, row fly ash possesses a low surface area that restricts it to adsorb more As ions (Zhang et al., 2016). Another drawback of fly ash is its comically inert surface structure that limits its use as an adsorbent for the removal of As. Thus various modifications have been employed to increase its efficiency to remove As by improving its pore structure and surface area.

#### *3.6.5.3. Zeolite*

Zeolites are crystalline in nature and aluminum, silicates are the main constituents that can be found in nature or can be manufactured on a massive scale in the industrial sector. Synthetic zeolites have greater benefits than naturally occurring zeolites, more functional zeolites should be designed and produced (Szerement et al., 2021). For the selective separation of cations from synthetically prepared solution, zeolites have been used because of their high adsorption and ion exchange capabilities. Zeolites have a variety of useful properties, including sieve, catalytic, and adsorbent, and were the 1$^{st}$ ion exchanger

to be utilized on a large scale to clean drinking water. Reversely, the zeolites gain and lose water as well as interchange component cations without undergoing structural changes. Over 30 different types of zeolites are naturally present, but just seven (analcime, phillipsite, erionite, chabazite, mordenite, ferrierite, and clinoptilolite) out of 30 natural zeolites are abundant to be used as an adsorbent (Kianfar and Mahler, 2020). The chemical properties of zeolite are further explored for its application in removing a variety of heavy metals present in the environment. Recently, the modification of natural zeolites with various metal salts (Fe, Zr, Al, FeZr, etc.) was applied for As removal (Xu et al., 2002; Velazquezpena-Pena et al., 2019). The zeolite modified with Zr and composite (FeZr) were found to have good efficiency in removing As(V) from an aqueous solution with 0.072 mg/g and 0.065 mg/g, respectively. Composite based on zeolite reduced graphene oxide has been used for the removal of As from water and the results revealed that the adsorption capacity of this adsorbent was 0.045 mg/g for As adsorption (Soni and Shukla, 2019). Several other studies have also been conducted to check the efficiency of zeolite for As removal from contaminated water (Yang et al., 2020; Ranjan et al., 2020; Pizarro et al., 2021; Abdellaoui et al., 2021).

#### *3.6.5.4. Nanomaterials*

Advancement in nanomaterial science has recently cleared the problem of the production of different nanomaterial for the treatment of water. Over the past few years, nanomaterials have been considered novel adsorbents for contaminants remediation because of their high surface area and high specificity (Ibrahim et al., 2021). These materials can be applied for the removal of heavy metals including As from an aqueous

solution. The most commonly used nanoparticles for As removal from contaminated water includes nano-composites, carbon nanotubes (CNT), and metal-based (Fe, Ti, etc.) nanoparticles. Although all of the nanomaterials mentioned have great removal powers, one of the most notable shortcomings is the non-selective elimination function (Alshehri et al., 2016).

Due to their distinctive chemical, physical and mechanical characteristics, nanomaterials especially carbon nanotubes and graphene are increasingly being used in a variety of fields, comprising heavy metal removal from contaminated water, and the size of nanomaterials is between 1 to 100 nm (Kumar et al., 2022). They have high resistance, thermal stability and electrical conductivity. Various nanomaterials were reported to remove As successfully from aqueous solution and groundwater contaminated with As. Among all these, metal oxides and zero-valent nanoparticles are stated as effective adsorbents for the removal of As (Tang et al., 2011; Mou et al., 2011; Manquian-Cerda et al, 2017). Luo et al. (2018) checked the ability of adsorption of nanofibers synthesized using $\alpha MnO_2$ (MO-2) to remove trivalent and pentavalent As. The highest capacity was 60.90 mg/g and 117.72 mg/g obtained for As(V) and As(III), correspondingly, through MO-2 (material synthesized in the study), which were much greater than the values informed for other $MnO_2$ infused nanofibers used in this study. Various other studies have also reported the removal of As using nanomaterials (Lal et al., 2020; Alidokht et al., 2021; Samuel et al., 2022).

As nanomaterials are adsorbents and possess several environmental problems, such as a sophisticated environment is needed for their fabrication and use of chemical reagents making them costly. Likewise, due to their tiny size, they can interact with living beings

and may get accumulated within the body or change metabolic processes, resulting in severe negative consequences.

#### *3.6.5.5. Biochar*

Biochar is the 'charred solid substance' produced during the process of thermochemical breakdown of organic biomass and is solid material resultant of biomass carbonization as described by International Biochar Initiative (IBI, http://www.biochar-international.org/biochar). A vast range of biochar was produced at varying degrees of carbonization, which was further utilized as an adsorbent or as a fuel (Mohan et al., 2014). To minimize the emission of greenhouse $CO_2$ from decomposing biomass, biochar can be used as a carbon sink. Biochar has been broadly employed in the removal of various organic and inorganic contaminants from the surroundings (air, water, and soil) (Oliveira et al., 2017). An economically efficient carbonaceous material, biochar is developing as a cost-effective alternative to activated carbon for treating large amounts of contaminants like antibiotics, volatile organic compounds, dyes, polychlorinated biphenyls, polycyclic aromatic carbon, agrochemicals, etc. and, some inorganic contaminants including heavy metals.

In addition to the remediation of pollutants, biochar has uses in a variety of fields including catalysis, sensing, energy and the development of products. Recently, biochar is used in supercapacitors and fuel cells (Gupta et al., 2015; Vivekanandhan, 2018; Andrade et al., 2020). The latest research on biochar has mostly focused on customizing the characteristics of biochar to enhance pollutants removal efficacy more effectively. Biochar is mainly the by-product of thermochemical conversion (gasification, pyrolysis, hydrothermal carbonization, etc.) of organic or carbonaceous biomass, such as agriculture

waste, forest residues, energy crops, aquatic weeds, digestate, manures, etc. at high temperatures (300-900 °C) under low oxygen condition (Kambo and Dutta, 2015). Due to the unique properties of biochar, including specific surface area, ion exchange capacity, higher adsorption capacity, and microporosity, it offers a broader range of environmental applications. The particular physicochemical features of biochar are very much related to the type and source of feedstock and pyrolytic conditions used during its manufacture, which determine the variability and predominance of a specific reaction. These parameters have a significant impact on the physical as well as chemical characteristics of biochar, including polarity, pH, atomic ratio, polarity, surface area and surface functional groups. These differences in properties of biochar have a big impact on its efficacy for the treatment of targeted pollutants (Sohi et al., 2010; Hassan et al., 2020). Several research has been done to find novel uses of waste biomass since biochar is ecofriendly, affordable and may be utilized for a range of purposes such as greenhouse reduction, waste management, water treatment, soil remediation, and energy production. While carbon is the most abundant element of biochar, it also constitutes oxygen, ash, hydrogen, sulfur and trace quantities of nitrogen (Saeed et al., 2019). The biochar's elemental composition varies depending on the raw material (biomass) used to prepare it and the process of carbonization. Fig**. 3.4.** showing different factors affecting adsorption process along with the physic-chemical properties of biochar.

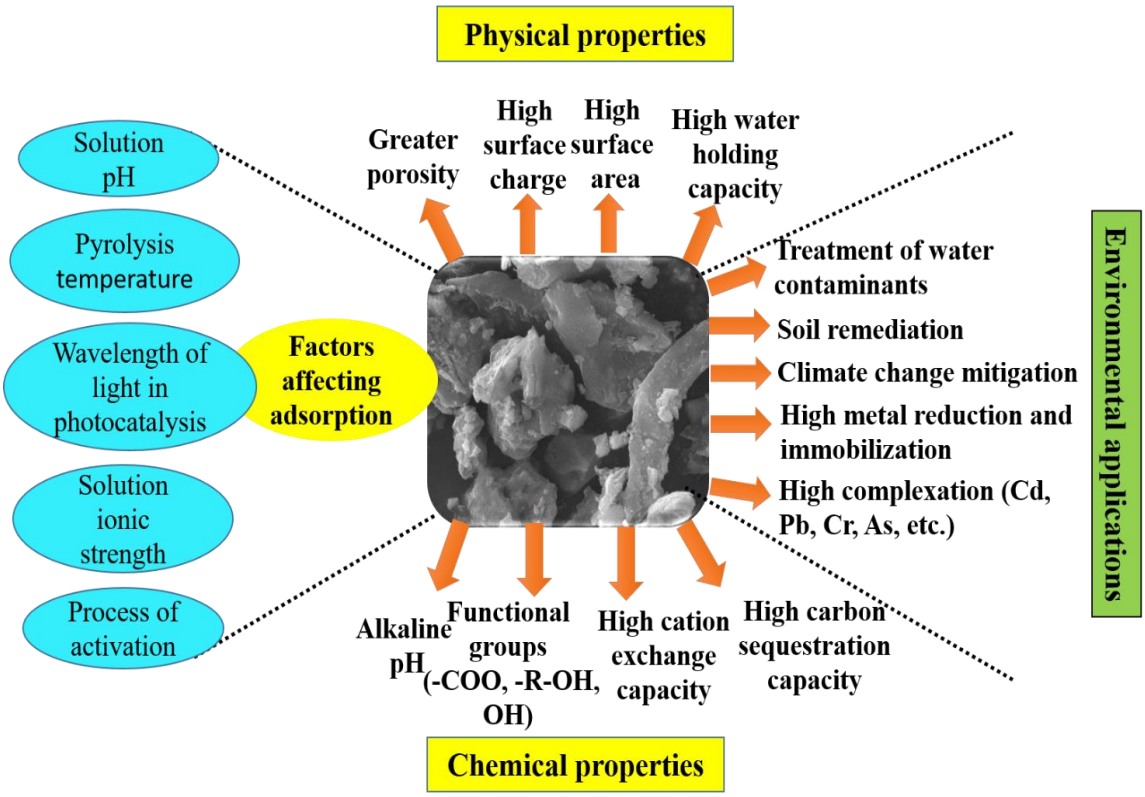


**Fig. 3.4. Factors affecting the process of adsorption and physical chemical properties of biochar along with its application for environmental remediation.**

### 3.7. Synthesis of biochar

#### 3.7.1. Gasification

Gasification is the process of thermochemical partial oxidation using gasification agents like air, oxygen, carbon dioxide, steam and a mixture of gases to transform the carbonaceous materials into gaseous products. Gaseous products (hydrogen, carbon monoxide, carbon dioxide, nitrogen), solid products (ash and char), and liquid products (oil and tar) are all created during the process of gasification (Cha et al., 2016; Arun et al., 2020). Residence time, gaseous composition, the particle size of biomass, temperature and the catalyst type all influence the products formed during the process of gasification (solid,

liquid, and gas). Among these factors, temperature is considered the most critical parameter that directly impacts the gasification process. As per the study conducted by Taba et al. (2012) it was found that raising the temperature increased the production of some of the gaseous products ($H_2$, carbon and CO) while lower the $CO_2$, hydrocarbons $CH_4$, and tar content. As gasification is intended to produce a gaseous product, biochar yield is about 5-10 % of the raw biomass, which is very less as compared to fast pyrolysis (~15-20 %). The amount of carbon converted, composition and heating value of resulting gaseous products, varying depending on the gasification agent utilized, as reported by Gomez-Barea et al. (2013). Azargohar et al. (2019) in their study reported that the production of biochar using gasification has a larger H/C atomic ratio, less developed aromatic structure, and relatively more content of ash. Slow pyrolysis produced more char aromaticity than the gasification process as revealed by Brewer et al. (2009) after characterizing the chars synthesized from rapid pyrolysis and gasification of biomass (corn stover and switchgrass).

### 3.7.2. Torrefaction

In the process of torrefaction, the biomass is pyrolyzed at a low heating rate in an inert environment with temperatures ranging between ~250 °C-350 °C and produces a dark brown or black color product having lower strength (Yang et al., 2021). The process of torrefaction involves the removal of carbon dioxide, oxygen and moisture present in biomass and depolymerization of long polysaccharide chains for the production of a solid component, which is hydrophobic in nature and has less O/C ratio (Mamvura and Danha, 2020). This process is also called mild pyrolysis because the process is operated at a low temperature with a low heating rate. Torrefaction is often done to enhance the

thermochemical characteristics of biomass that were further used for gasification, co-combustion, and combustion and the focus is on the generation of gas (Toro et al., 2021). Torrefaction raises the density of biomass, improves hydrophobicity, decreases weight, and makes it useful for energy generation by improving the viability of wood by lowering the cost of transportation. It does not often produce adsorbents or char since simply partial decomposition of biomass happens to avoid rot and induces loss of moisture (Chen et al., 2021a). The biochar in a study was produced by the process of torrefaction of food sludge for only 20 min at 150 °C and a high improvement in heating value as well as in carbon content was observed. Improved quality of biochar with higher fixed carbon content and reduced ash content was achieved after torrefaction performed on a blend of food sludge with a husk called macadamia at different ratios (Zheng et al., 2021). Recently, Pulka et al. (2019) reported that increasing torrefaction temperature reduces the higher heating value.

### 3.7.3. Hydrothermal carbonization

When the moisture content is low in biomass, the dry processes like gasification and pyrolysis can generate a high yield of products with minimal loss of energy. But most of the waste biomass contains lots of moisture in it, which necessitates a distinct drying step to attain a high yield of products and lower process energy (Mohan et al., 2014). The hydrothermal technique is anticipated as the best process that compensates for this flaw of the dry process, as it directly utilized the biomass for preparing char without its drying. Through the process of hydrothermal, the char produced is commonly referred to as hydrochar to differentiate it from the product produced using dry processes.

Hydropyroysis is a high-efficient method that occurs in a hydrogen-rich environment (Stummann et al., 2020). The poly-condensation and hydrogenation processes are made possible in the presence of a hydrogen medium. This process takes place at a high temperature and is characterized by a rapid reaction. In hydrothermal process, the feedstock is combined with water in a closed reactor and after a set amount of time, the temperature is raised for stabilization. The pressure is also increased in order to keep it liquid at a temperature exceeding 100 °C. On the basis of temperature at saturated pressure, biochar (250 °C), bio-oil (250-400 °C), and gaseous products (>400°C) are formed during the hydrothermal process (Chan et al., 2014). As a result, hydrothermal processes at different temperature ranges are referred to as hydrothermal carbonization, liquefaction and gasification. The production of biochar is reduced with decreased temperature and the overall ash concentration is determined by the type of feedstock used. To increase biochar yield in a short residence time and greater hydrogen pressure are desired (Chen et al., 2020b). Wiedner et al. (2013) reported that the hydrochars are less stable than that biochar because of their different chemical structures. Hydrochar consists of alkyl moieties and biochar is dominated by aromatic compounds.

### 3.7.4. Pyrolysis

It is a process of thermal degradation of biomass materials in an oxygen-deficient environment or when there is not much oxygen needed for full combustion. The process of pyrolysis can considerably affect the quality as well as the quantity of produced biochar. The technique of pyrolysis is commonly used to convert the biological or organic waste materials into fuel and biochar materials having large porosity and surface area (Tomczyk

et al., 2020). For the production of biochar, pyrolytic temperature plays a very significant role and is a major limiting factor in biochar production although the elemental composition and surface characteristics are very much dependent on the type of feedstock used. The pyrolysis process has been divided into two categories one is conventional or slow pyrolysis and another is fast pyrolysis based on residence time and temperature used (Akhil et al., 2021).

The process of slow pyrolysis has been used to produce charcoal for thousands of years. The process of slow pyrolysis takes place at 300 °C-600 °C temperature. Generally, the duration of air drying and temperature is determined by the feedstock used. In the absence of oxygen, the biomass is heat-treated slowly to around 500 °C and unlike the fast pyrolysis process, the vapors in slow pyrolysis do not escape quickly as the residence time of vapors varies from 5 min to 30 min (Bandara et al., 2017; Kim et al., 2020). In fast pyrolysis, dry biomass with less than 10 % moisture content, quick transfer of heat, rapid increase in temperature to 400-500 °C, and the vapor residence time of min 1 s to a maximum of 5 s, are required (Dai et al., 2017a; Yuan et al., 2020). Pyrolysis is one of the most used methods for biochar synthesis as it produces biochar with a 20-40 % yield along with a large specific surface area and due to this, it may be better for the removal of arsenic and many other contaminants from water.

### 3.8. Modification of biochar

As pristine biochar has a lower capacity for adsorption than activated or modified biochar. The adsorption behavior of biochar depends on various factors such as functional groups, porosity, cation exchange capacity, specific surface area, etc. Physical and

chemical approaches can be used to modify not only the surface area and functional groups of biochar, but also improves the structural properties and pore size distribution (Panwar et al., 2020; Li et al., 2021b). The type of activation process, temperature, activator, activation time, and soaking time (especially for chemical methods) are all factors that alter the properties of biochar. The physicochemical properties of biochar may be affected differently by a different method of modification. The mechanism and adsorption efficacy of biochar can be directly influenced by the method used for modification and the modifier utilized (An et al., 2018; Premarathana et al., 2019). As a result, it is critical to choose the right methods of biochar modification for the removal of environmental contaminants based on their physicochemical properties. Some of the recently used medication methods include metal oxide and acid-base modification.

### 3.8.1. Acid and alkali modification

Chemical activation of char is accomplished by using acids, such as sulphuric acid ($H_2SO_4$), phosphoric acid ($H_3PO_4$), hydrochloric acid (HCl), etc., and basic chemicals such as potassium hydroxide (KOH), ammonia ($NH_3$), sodium hydroxide (NaOH), zinc chloride ($ZnCl_2$), etc. (Shen et al., 2015; Bushra and Remya, 2020). The most frequent approach for changing the surface properties of biochar is to utilize alkali and acid based treatment of biomass, which involves the enhancement in pore structure and specific surface area of biochar that might affects the physical adsorption of contaminants. Furthermore, the functional groups C-OH and C-H produces by modification with acid and base that plays a very significant role in the process of chemical adsorption and ultimately change the biochar's adsorption capacity (Hu et al., 2018). It was reported that the activation efficiency

of the chemical modification method is higher than the physical activation process (Peter et al., 2021). It was reported that the surface area of biochar on treating with alkali and the acidic solution was amplified by 14 and 10 times, correspondingly (Wang et al., 2019b).

### 3.8.2. Metallic modification

Modification of biochar using metal salts and oxides of metal can increase the efficiency for adsorption and allow biochar to have variable adsorption capacity for various pollutants depending on their different characteristics. After being modified with metal salts and metal oxides, biochar possesses a good ability of electrostatic attraction, ion-exchange capacity and precipitation, consequently increasing its environmental contaminants adsorption capacity (Wu et al., 2019). Wan et al. (2020) in their study simultaneously removed three different heavy metals using magnetic biochar and the results show within 24 h, 20-30 % removal of As, Cd and lead was observed. Due to the modification with Fe, 65 % of the recovery rate of biochar was found. Other studies showed that adsorption of As(III) was successfully done after oxidizing it into As(V) and was successively adsorbed by biochar modified with $MnO_2$. Best results were obtained in neutral and acidic conditions than in alkaline conditions because of the mechanism of electrostatic repulsion (Cuong et al., 2021). Table 3.2 represents the adsorption capacities of different biochar materials.

**Table 3.2. Adsorption capacity of unmodified and modified biochar for As removal.**

| Adsorbent | As(III)/ As(V) | pH, contact time, agitation | Dose (g/L) | Initial concentration | Removal rate (%) | Adsorption Capacity (mg/g) | References |
|---|---|---|---|---|---|---|---|
| ***Unmodified biochar*** | | | | | | | |
| Chestnut shell biochar | As(V) | 7,24 h,- | 0.4 | 0.2-50 mg/L | - | 43.15 | Zhou et al. (2017) |
| Perilla leaf biochar | As(III) | 7, 2h,- | 1.0 | 0.05-7.0 mg/L | 63 | 4.71 | Niazi et al. (2018) |
| | As(V) | 7,2h,- | 1.0 | 0.04-7.0 mg/L | 37 | 3.85 | |
| Orange peel biochar | As | -,4h,- | - | 10-100 µg/L | 100 | - | Tabassum et al. (2019) |
| Pinewood biochar | As(V) | 4.1,40h, 40rpm | 2 | 0-400 mg/L | - | 124.5 | Wang et al. (2017) |
| Pinewood biochar | As(III) | - | 10 | 0.01-0.1 mg/L | - | 2.6 | Mohan and Pittman Jr. (2007) |

| | | | | | | | |
|---|---|---|---|---|---|---|---|
| Rice husk char | As(V) | -,16h, 30rpm | 2 | 0-200 mg/L | - | 0.35 | Norazlina et al. (2014) |
| Sewage sludge biochar | As(III) | - | 10 | 1 mg/L | - | 0.07 | Tavares et al. (2012) |
| Corn straw char | As(V) | 7, 48h, 180rpm | 5 | 0.25-100 mg/L | 3.80 | 6.80 | He et al. (2018) |
| ***Modified biochar*** | | | | | | | |
| Corn stem iron modified biochar | As(III) | 7, 800 min, 2000 rpm | 10 | 0.2-50 mg/L | - | 4.70 | Lin et al. (2019) |
| Cottonwood Magnetic biochar | As(V) | -,24h, 200 rpm | 2 | 5-200 mg/L | - | 3.14 | Zhang et al. (2013) |
| Bismuth infused wheat straw biochar | As(III) | 6.5-7,24h, 150rpm | 2 | 50 mg/L | | 0.182 | Zhu et al. (2016) |

| | | | | | | | |
|---|---|---|---|---|---|---|---|
| Corn straw iron incorporated biochar | As(V) | 7,48h, 180rpm | 5 | 0.25-100 mg/L | 85.98 | 0.017 | He et al. (2018) |
| Al modified rice straw biochar | As(V) | 5, 24h,- | 2 | 54-270 mg/L | - | 25.97 mM/kg | He et al. (2020b) |
| Coffee husk ZnO impregnated biochar | As(V) | -, 48h,- | 4 | 15-100 mg/L | - | 1.545 | Cruz et al. (2020) |
| Corn cob ZnO impregnated biochar | As(V) | | 4 | 15-100 mg/L | - | 25.9 | Cruz et al. (2020) |

### 3.9. Biochar application for As removal

Biochar is very effective in removing different kinds of organic and inorganic pollutants from the air, water, and soil. Inorganic metals like As is the most toxic contaminants, thus causing many negative impacts on human health and also affecting aquatic life. Biochar is a cost-effective and eco-friendly way to remove As from contaminated environments. Biochar synthesized using oak wood has shown 75-81 % removal of As(III) and ~84 % of As(V) at pH 3-7 and pH 6, respectively. Removal of both the As species was found to be decreased beyond and above this pH range (Niazi et al., 2018). Similar results were also achieved in another study in which pH-specific removal of both the As species was reported (Alam et al., 2018). Biochar was synthesized using Cu particles, rice husk, and iron and then applied for As(III) and As(V) adsorption and also investigated its effect on killing pathogenic microbes from an aqueous solution. As a result, it was concluded that modification of biochar matrix using any antimicrobial metals might give dual benefits, disinfection as well as metal adsorption (Priyadarshni et al., 2020). Asere et al. (2019) revealed that because of the negative charge surface, unmodified biochar has lower adsorption capacities for As(III) as well as for As(V). So, according to Amen et al. (2020) for the considerable adsorption of As from contaminated water surface modification of biochar was needed if possible using a cationic modifier. Agrafotiet et al. (2014b) reported that the electrostatic attraction mechanism is the most significant factor in the elimination of heavy metals especially As. Whereas, chemical reduction and oxidation in natural water, were the main mechanism involved in the removal of As ($AsO_3^{3-}$ and $AsO_4^{3-}$) (Dong et al., 2014). The legend exchange was identified as the main mechanism preferable involved in the removal of As ($AsO_3^{3-}$) using biochar modified with metal zinc oxide and biochar composites, in various studies (Xia et al., 2016). When silver

and iron infused biochar were used for the removal of As ($AsO_3^{3-}$) chemical reduction was observed to be the chief mechanism (Wang et al., 2017).

# Chapter-4
# Materials and Methods

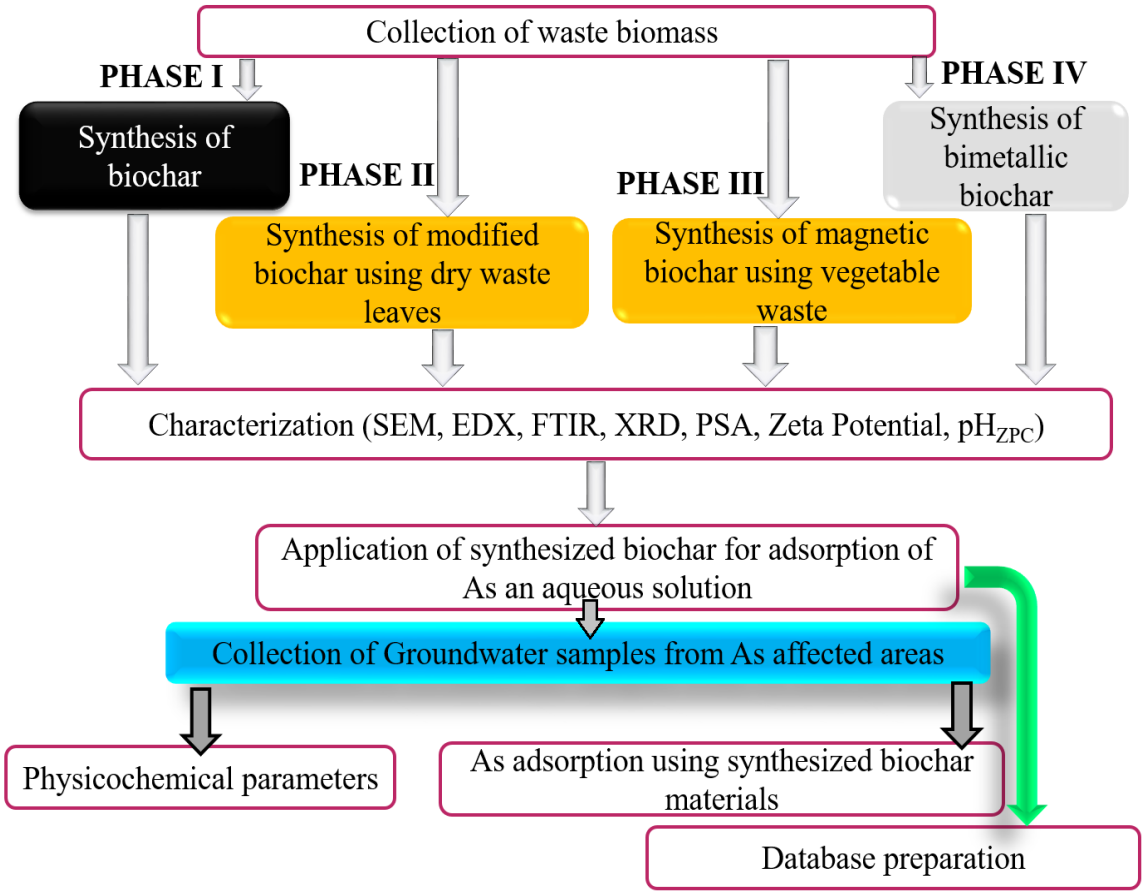


**Fig. 4.1. Flow diagram for experimental design.**

### 4.1. Collection of waste biomass

Waste dry leaves of different trees (*Lagerstroemia speciosa* and *Tectona species*) were collected from the campus of Babasaheb Bhimrao Ambedkar University Lucknow (26.7646º N, 80.9333º E), India. Waste vegetable biomass (*Raphanus sativa* (leaves) and *Artocarpus heterophyllus* (peel)) were collected from local market of Rajnikhand (26.4646° N, 805558° E) located near Babasaheb Bhimrao Ambedkar University, Lucknow, Uttar Pradesh, India (Fig. 4.2).


**Fig. 4.2. Different collected waste biomass.**

## 4.2. Chemicals required

Stock solutions for As(III) and As(V) were prepared by dissolving sodium arsenite ($NaAsO_2$) and sodium arsenate ($Na_2HAsO_4.7H_2O$) in distilled water and adjusted the pH 6.8–7, analytical grade chemicals were used without performing any further purification. Prepared stock solution of 1000 mg/L was further diluted to make working solutions to perform the experiment. Hydrochloric acid (HCl, > 36%), potassium phosphate ($KH_2PO_4$,

> 99.5%), potassium iodate ($KIO_3$, > 99.0%), L-ascorbic acid ($C_6H_8O_6$, > 99.7%), ammonium molybdate ($(NH_4)_6Mo_7O_{24}.4H_2O$, > 99.0%), antimony potassium tartrate ($C_4H_4O_6KSbO.1/2H_2O$, > 99.0%), sulphuric acid ($H_2SO_4$, > 95.0%), iron sulfate ($FeSO_4$), iron chloride ($FeCl_3$) and manganese dioxide ($MnO_2$) were procured from Fisher Scientific. Double distilled water was used for all the experiments.

### 4.3. Synthesis of Biochar

#### 4.3.1. Prestine biochar

Leaves of two different types of plants were used as feedstock materials: *Lagerstroemia speciosa* (an ornamental plant) and *Tectona species* (timber tree) to prepare pristine biochar. The feedstock materials were washed using deionized water and shade dried for 2–3 days. Dried samples were crushed and ground to convert into powdered form and sieved with 0.25 mm mesh. The powdered samples filled in the quartz crucible (upper diameter 60 mm, and capacity of 100 mL), this crucible was capped with a fitted lid. *Lagerstroemia speciosa* and *Tectona* biomass was subjected to heating in a muffle furnace for pyrolysis with heating rate of 10 °C $min^{-1}$ to achieve 800 °C temperature and kept constant for 60 min (Chen et al., 2018). The samples were allowed to cool till room temperature inside the muffle furnace. The obtained biochar was washed 3–4 times with deionized water to remove impurities like bio-oil and followed by drying in the oven for 12 h. The oven dried material was stored in the air tight container and used for the biochar characterization and other application (Fig. 4.3). The biochar was also prepared at 400 °C and 600 °C though, it was not suitable candidate for removal of As due to its leaching characteristics resulting color developed in the As solution and makes it slightly turbid. The reason behind the leaching is that some of the plant leaves contains high amount of

bio-oil and syngas and could not converted into carbon form completely. Therefore, biochar was prepared at 800 °C and found that leaching was not observed.

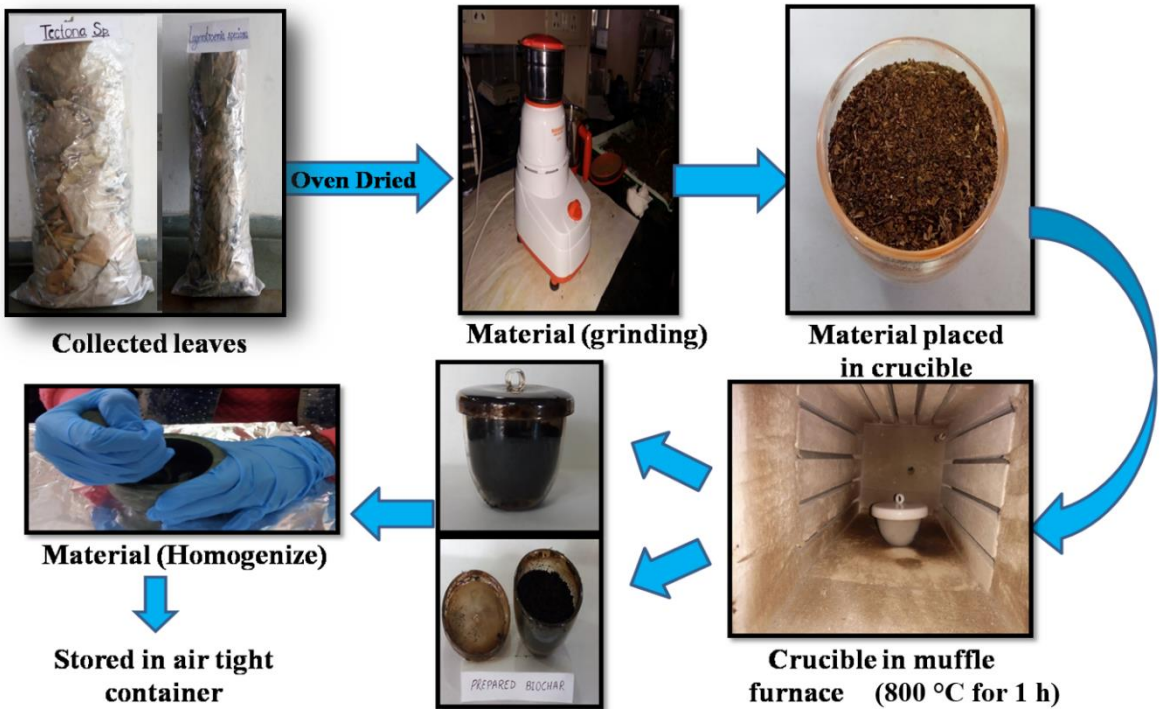


**Fig. 4.3. Synthesis of pristine biochar.**

### 4.3.2. Modified biochar

#### *4.3.2.1. Magnetic biochar*

Four different types of waste biomass i.e. Radish leaves (*Raphanus raphanistrum*) and Jackfruit peel (*Artocarpus heterrophyllus*), Banaba tree (*Lagerstroemia speciosa*) and Teak (*Tectona species*) were used for the synthesis of magnetic biochar materials. The waste biomasses were rinsed with normal tap water 2-3 times to remove the dust particles and other contaminants and finally washed with deionized (DI) water. After that, all waste biomasses were dried in an oven at 105 °C temperature. The dried waste biomass were

crushed and grounded with the help of a grinder and powdered material was obtained and used for the preparation of magnetic biochar. The synthesis of iron impregnated biochar was done by the following methodology described by Zhang et al. (2013) after some alteration. The solution of Ferric chloride was made by dissolving 40 g of $FeCl_3 6H_2O$ in 60 mL of double-distilled water and then 60 g of powdered feedstock was immersed in the $FeCl_3$ solution, the mixture was then pre-heated at 80 °C for 2 h. The material was then kept in a closed crucible and pyrolyzed at 800 °C for in a muffle furnace for 1 h. The obtained biochar was homogenized, washed, dried and kept in a sealed container (Fig. 4.4). The final obtained product was abbreviated as MRB-800 and MJB-800 for Magnetic Radish Biochar and Magnetic Jackfruit Biochar, respectively. However, MTB-800 and MLB-800 was abbreviated for Magnetic *Tectona* Biochar and Magnetic *Lagerstroemia* Biochar, correspondingly.

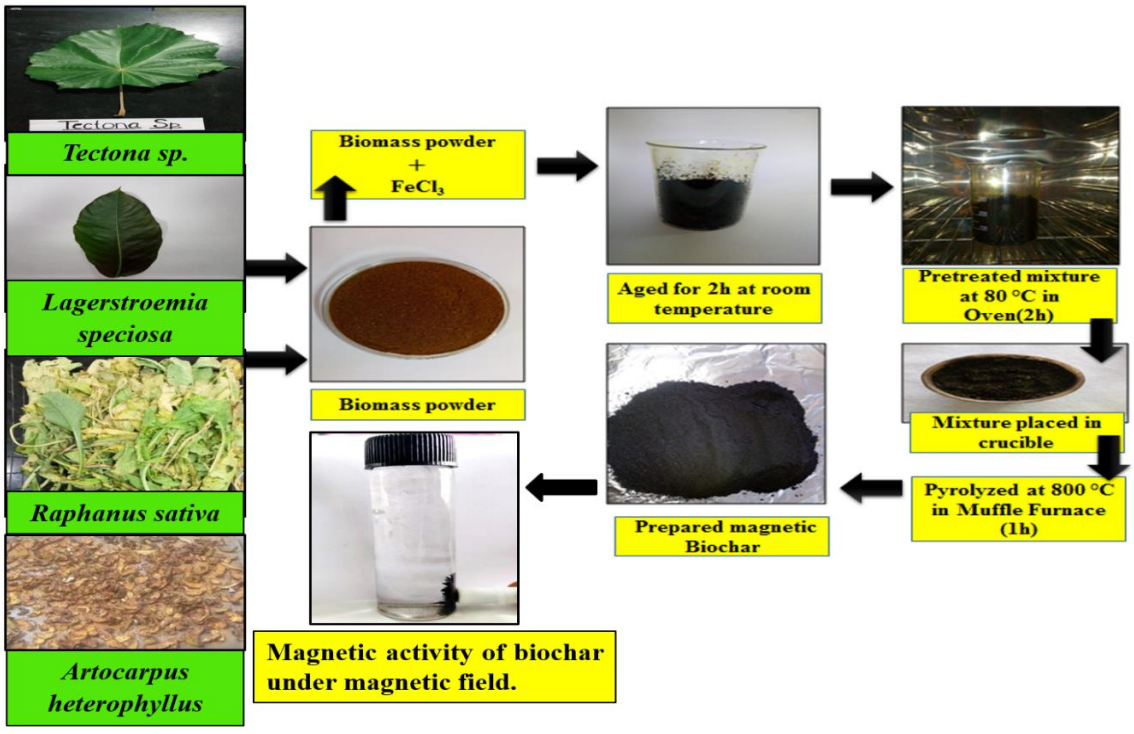


**Fig. 4.4. Magnetic biochar synthesis.**

#### *4.3.2.2. Monometallic and bimetallic biochar*

Waste biomass of *Tectona sp*. was utilized for synthesizing monometallic and bimetallic biochar. Collected waste was firstly washed with distilled water and oven dried at 105 °C temperature. The biochar was synthesized using method described by Lunge et al, (2014) after some modification. The dried biomass was grounded and sieved to obtain homogenized powder. A 30 g powdered biomass was added in the solution of $FeSO_4$ (10 g dissolved in 150 mL distilled water) separately to synthesize two different biochar. Fe/Mn biochar composite was synthesized by mixing 5 g $FeSO_4$ and 5 g $MnO_2$ salts dissolved together in 150 mL distilled water and 30 g of powdered biomass was added to it. The blend was then magnetically agitated for 4 h and filtered using vacuum filter to remove excess chemical. Filtered pretreated biomass was kept in oven at 80 °C overnight and then the material was pyrolyzed at 800 °C in muffle furnace for 1 h. The final biochar materials were homogenized, washed, dried and stored for further application (Fig. 4.5).

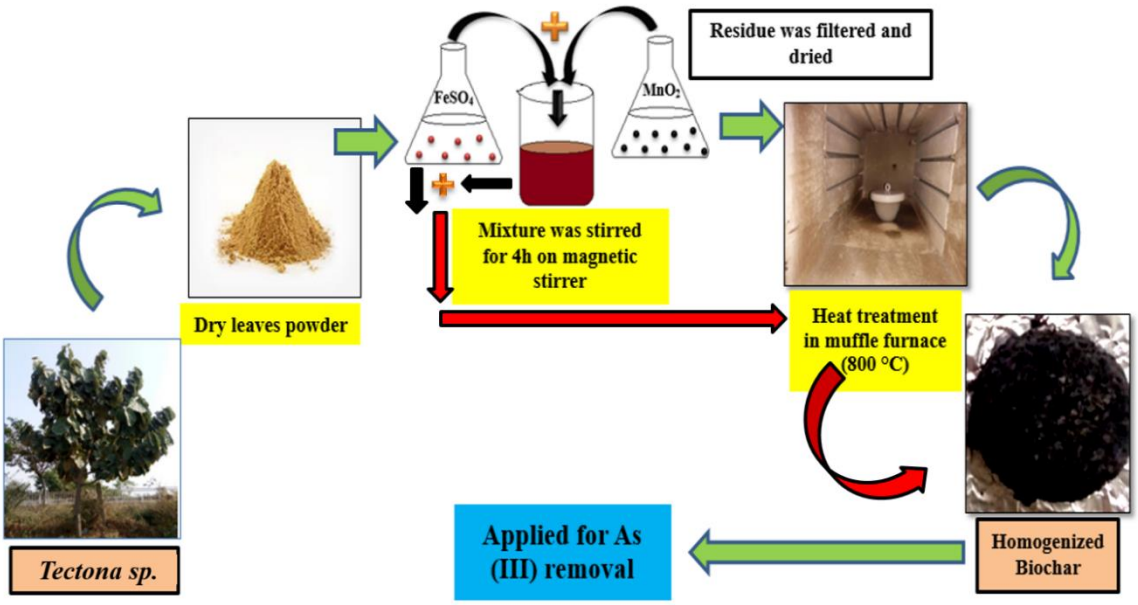


**Fig. 4.5. Preparation of monometallic and bimetallic biochar.**

### 4.4. Characterization techniques

#### 4.4.1. Proximate analysis

The collected raw waste biomass were considered for proximate analysis which include the determination of moisture content, ash content, volatile organic compounds (VOCs) and fixed carbon. The proximate analysis was performed using method described by Garcia et al. (2012). For the moisture content estimation the sample was kept in a hot air oven at 105 °C for 24 h and the percent moisture was assessed by calculating the difference in initial and final weight of the raw biomass. The dried waste biomass was then ignited at 550 °C in a muffle furnace for 3-4 h in a crucible not covered with the lid for ash content determination and in a closed crucible for estimation of volatile organic content. The ash content and VOC was calculated using equation (2) and (3), respectively. After muffle treatment, the weight loss represents the volatile compound and the remaining was ash content. Fixed carbon was identified by subtracting the sum of volatile and ash content from 100. All the values of parameters of proximate analysis were calculated by using following equations (Rawat et al., 2021):

$$Moisture\ content\ (MC)\% = \left(\frac{W_0 - W}{W_0}\right) \quad (4.1)$$

Where, $W_0$ signifies the weight of sample before oven treatment and $W$ represent the weight of sample after oven treatment.

$$Ash\ content\ (AC)\% = 100 - \left(\frac{W_0 - W}{W_{ds0}}\right) \quad (4.2)$$

Here, $W_0$ and W symbolizes the weight of the sample along with the crucible (without lid) before and after muffle treatment, correspondingly.

$$Volatile\ Matter\ (VM)\% = \left(\frac{W_0 - W}{W_{ds0}}\right) - Moisture(\%) \quad (4.3)$$

Where, $W_0$ and W represents the weight of sample along with crucible (closed with lid) before and after treating in muffle furnace, respectively.

$$Fixed\ Carbon\ (FX)\% = 100 - (AC + VM) \quad (4.4)$$

### 4.4.2. Biochar yield

The biochar yield was determined by using following equation (Shakya et al., 2019):

$$Biochar\ Yield\ (\%) = \left(\frac{mass\ of\ biochar(g)}{total\ mass\ of\ biomass(g)}\right) \times 100 \quad (4.5)$$

### 4.4.3. $pH_{ZPC}$

$pH_{ZPC}$ of the synthesized biochar materials were determined by adjusting the pH of 0.1 M NaCl solution in the range of 2.0-10.0 (with intervals of 2) by using 0.1 M HCl and 0.1 M NaOH. A 0.2 g of biochar was incorporated in 20 mL solution of 0.1 M NaCl. After 48 h final pH of the solution was measured using a multi parameter water analyzer (SYSTONIC 371, India) (Singh et al., 2016).

### 4.4.4. SEM and EDS

The surface morphology and structure of biochar was determined using scanning electron microscope (JSM 4490, JEOL Japan) endowed with energy dispersive spectroscopy that helps in the identification of elemental composition of the synthesized bioadsorbents.

### 4.4.5. FTIR

The dried biochar material was ground with potassium bromide (KBr) in a ratio of 1:100 (w/w). The pellet of this mixture was formed by hydraulic press of 130 lbs and the IR absorbance of the sample was read using a FTIR spectroscopy (Thermo-Scientific Nicole 6700, USA) in the ranges from 400-4000 $cm^{-1}$.

### 4.4.6. XRD

The crystalline and amorphous nature of synthesized biochar materials were analyzed using X-ray powder diffractometer (PW 3040/60, PaNanalytical Netherland) and the scanning of the material was done in the range of 10°-90° with the speed rate 2°/min.

### 4.4.7. PSA and Zeta Potential

Zeta potential is a technique used to examine the stability of synthesized biochar materials. To determine the size of the biochar particles, particle size analysis (PSA) was done. The analysis was carried out using a zeta nanosizer (Zeta Nano ZS90, Malvern Instruments, UK). A zeta nanosizer was used to determine the particle size distribution, which is based on light-scattering methodology and gives the average particle size from the Brownian motion of the particle.

### 4.4.8. BET

Surface area analyzer (BELSORP-max, JAPAN) is used for the identification of specific surface area, pore diameter and size of the biochar. A certain quantity of biochar was heated for 5-6 h under pretreatment at temperature of 120 °C in vacuum. Afterwards, the adsorption and desorption process of $N_2$ was also accomplished.

### 4.4.9. XPS

The XPS analysis was done to determine the elements comprises by the biochar surface, its composition and valance state of elements. This analysis was done by irradiating the x-rays on biosorbents surface. The pellets of the samples were formed and was dried for 6 h at 70 °C and subjected for XPS analysis using x-ray photoelectron spectroscopy (PHI 5000 Versa Probe II, FEI, Inc.).

### 4.4.10. VSM

The magnetization of biochar is measured by using vibrating sample magnetometer (VSM 8600 series, lakeshore cryotonics, USA). The magnetic constraints such as retentivity, coercivity and magnetization were measured through this technique of characterization.

### 4.4.11. Raman spectroscopy

The microstructure of a carbon material was evaluated using Raman spectroscopy (Invia Reflax Raman Microscope, Renishaw Metrological System, UK) equipped with 515/488 and 785 nm laser diode and the temperature range was from -160 °C to 300 °C.

## 4.5. Batch adsorption study

The batch adsorption experiments were performed for As (III) and As (V) separately in triplicate in 250 mL conical flask. A 50 mL of As(III and V) solution was taken along with the fixed dose of biochar and then shaken in water bath shaker (LI-WBIS-20, Labard Instruchem. Pvt. Ltd.) at 90 ± 2 rpm shaking speed at room temperature. After shaking for optimum time duration, samples were centrifuged and the supernatant was

analyzed for determining the remaining concentration of As by SPECTRO MOLYBDATE METHOD at 880 nm (Dhar et al., 2004) using UV–Visible spectrophotometer (117 Systronics, India). The batch adsorption studies of As(III) and As(V) were performed separately (mono metal adsorption) at 25 °C. Process optimization was studied by varying the dose (0.5–4 g/L), pH (3–10), temperature (25–55 °C), and initial arsenic concentration (0.5–2.5 mg/L). The pH of solution was maintained to 7 ± 0.5 during the adsorption experimental process, in each case by using the HCl or NaOH solution (0.1 N). For process parameter optimization, batch adsorption study was performed with different parameters manually without using any software. Each test was performed in duplicates in order to minimize the error and the average values were reported in the result. The removal percentage and adsorption capacity was calculated using the following equation (Shanmugarajah et al., 2019; Rawat and Singh. (2021):

$$\%\ \boldsymbol{Adsorption} = \frac{\boldsymbol{C_0 - C_t}}{\boldsymbol{C_0}} \times \mathbf{100} \tag{4.6}$$

$$\boldsymbol{q_t} = \frac{\boldsymbol{C_0 - C_t \times V}}{\boldsymbol{m}} \tag{4.7}$$

Here, $C_0$ and $C_t$ (mg $L^{-1}$) are the concentration of As(III) and As(V) at the initial and at time *t*, *V* is volume of liquid phase (L), and *m* (g) is the weight of the biochar.

### 4.6. Fixed Bed column study

The continuous study for adsorption of As(III) and As(V) was conducted in a glass column using magnetic biochar at ambient temperature with neutral pH. The glass vertical

column used in the study with length-38.3 cm and diameter-1.5 cm is shown in Fig. 4.6. Two different bed heights 3 cm and 6 cm with different amounts of biochar 2.7 g and 5.4 g, respectively, have been taken to examine the effect of bed height on Arsenic removal in the continuous study. Influence of flow rate on As adsorption was examined with two different flow rates (2.5 and 5 mL/min) and 1 mg/L initial concentration of adsorbate.

The biochar bed was packed in-between 1 cm glass wool layer and a sieve of 0.5 mm size to provide a consistent flow of adsorbate in the column. The material used in the column study has been divided into subsections using cotton fiber to reduce the compaction of biochar material inside the column and it also helps to maintain the flow rate of the adsorbate. Due to the lesser size of biochar, it gets compacted resulting water will not pass through it in a uniform manner. The influent with 1 mg/L initial concentration, flowed downwards and the treated solution was collected in sample tubes in a definite time interval.

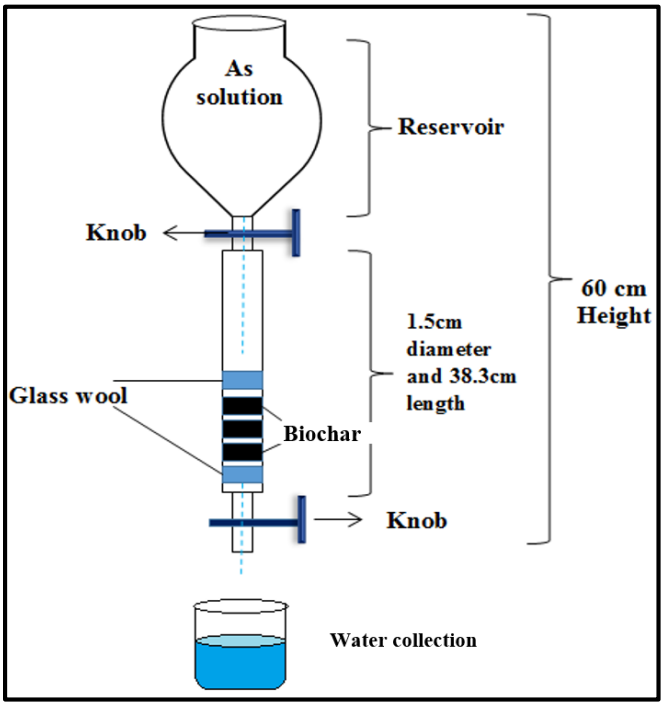


**Fig. 4.6. Pictorial presentation of column.**

### 4.6.1. Breakthrough curve

The adsorption functioning of a fixed column bed is demonstrated by the breakthrough curve. The time of breakthrough curve appearance and its shape are two very significant features for governing the operational and the active response of column adsorption. When the effluent As concentration reaches up to 95.5 % of the influent concentration of As, that point is taken as the breakthrough point (Chen et al., 2012). Adsorption behavior of As from an aqueous solution in a fixed bed column is manifested as a function of $C_t/C_0$ in terms of time and effluent volume at a particular bed height, forming a breakthrough curve. The total amount of As adsorbed in the fixed bed column i.e., $q_{total}$ can be estimated using the equation expressed below:

$$q_{total} = \frac{Q}{1000} \int_{t_0}^{t_{total}} C_{ad}\ dt \tag{4.8}$$

Where the flow rate is denoted by $Q$ (mL/min); total flow time is signified by $t_{total}$. $C_{ad}=C_{in}-C$ (mg/L), $C_{in}$ and $C$ is the influent and effluent concentration, respectively.

The adsorption capacity i.e., the quantity of adsorbate adsorbed per unit dry weight of biochar, can be evaluated by the equation bellowed:

$$q_e = \frac{q_{total}}{m} \tag{4.9}$$

Where $m$ is the total dry amount of biochar taken in a column.

The total treated volume of solution, $V_{eff}$ is calculated by the following equation:

$$V_{eff} = Q \times t_{total} \tag{4.10}$$

The total quantity of adsorbate passed through the fixed bed column, calculated by the equation bellowed:

$$m_{total} = \frac{C_{in} \times V_{eff}}{1000} \tag{4.11}$$

Total percent removal of As was calculated by the following expression:

$$Total\ removal\ percentage\ of\ As = \frac{m_{ad}}{m_{total}} \times 100 \quad (4.12)$$

Here, $m_{ad}$ is the dry amount of biochar.

### 4.6.2. Models for column study

#### *4.6.2.1.Thomas model*

The performance of the fixed-bed column for As removal was predicted by the Thomas model and it is the most commonly used model. The model follows Langmuir kinetics of the adsorption process and desorption process (Vilvanathan and Shanthakumar, 2017; Basu et al., 2019). The highest adsorption capacity of biosorbent in a fixed bed column is also evaluated by the Thomas model. The expression for Thomas model is given below:

$$\ln\left(\frac{C_0}{C_t} - 1\right) = \frac{k_{TH} q_e x}{Q} - k_{TH} C_0 t \quad (4.13)$$

Where, $k_{TH}$ is the Thomas rate constant and the flow rate of the solution is represented by $Q$ (mL/min). The adsorbents adsorption capacity is signified by $q_e$ (mg/g) and the mass of adsorbent is signified by $x$ (g).

#### *4.6.2.2. Yoon-Nelson Model*

The adsorption kinetics of the fixed-bed column has been specified by the Yoon-Nelson model. The model assumes that the rate of reduced probability of adsorbate molecule is proportionate to the rate of probability of adsorption of arsenic and the probability of its breakthrough on biosorbent. The linear equation for the Yoon-Nelson model is represented below:

$$ln\left(\frac{C_t}{C_0 - C_t}\right) = k_{YN}t - k_{YN}\tau \quad (4.14)$$

Here, the rate constant of Yoon-Nelson is signified by the $k_{YN}$ (1/min), and $\tau$ is acquired for 50% of the breakthrough.

#### *4.6.2.3. Adams-Bohort model*

The Adams-Bohart model has grounded on the supposition that the adsorption rate is relational to the biosorbents residual capacity and the adsorbing species concentration (Patel, 2019). The initial segment of the breakthrough curve is explained by the Adams-Bohart model and its equation is written as follow:

$$ln\left(\frac{C_t}{C_0}\right) = k_{AB}N_0\frac{z}{\mu_0} - k_{AB}C_0t \quad (4.15)$$

Where, $N_0$ and $k_{AB}$ are the highest adsorption capacity of biosorbent in a column per unit volume and rate constant for the Adams-Bohart model. The linear flow rate of the feeding solution is implied by $\mu_0$ (cm/min).

#### *4.6.2.4. Clark model*

This model for the column study was presented by Clark for the evaluation of mass transfer using the Freundlich constant *(n).* The model explained the new imitations of the breakthrough curve (Pantic et al., 2019). The equation of the Clark model is presented below:

$$\ln\left[\left(\frac{C_0}{C_t}\right)^{n-1} - 1\right] = \ln A - rt \quad (4.16)$$

Here, the Clark constant were *A* and *r* (1/h) and Freundlich rate constant is implied by *n*. to determine the values of these constants the linear plot was plotted between $ln[(C_0/C_t)^{n-1}-1]$ and *t* (min).

### 4.7. Arsenic determination remaining in the solution after adsorption

After filtration, samples were acidified immediately with 1% solution of HCl. A 5 mL of acidified sample was taken in a conical flask and mixed with 0.25 mL of 10 μM $KH_2PO_4$ solution after that the 0.5 mL of ~2 mmol $L^{-1}$ oxidizing agent ($KIO_3$) was also added to it. After 30 min, 0.5 mL of color reagent was added and the samples and then samples were analyzed with UV-vis spectrophotometer at the wavelength 880 nm (Spectro molybdate method) (Dhar et al., 2004). In case of As (V), oxidizing agent ($KIO_3$) was not added to the samples. Coloring reagent was prepared by adding 10.8% of ascorbic acid, 3% of ammonium molybdate, 0.56% antimony potassium tartrate and sulphuric acid in a ratio of 2:2:1:5, respectively. UV-vis spectrophotometer (Model no. 117, Systronics India Ltd.) was used for the analysis of residual concentration of arsenic at 880 nm.

#### 4.7.1. Reagents preparation

(1) 2 mmol $L^{-1}$ $KIO_3$ i.e., oxidizing agent was prepared by dissolving 0.085 g of potassium iodate salt in 200 mL of distilled water that contains 2% hydrochloric acid.

(2) 10 μM $KH_2PO_4$ i.e., the reducing agent was prepared by diluting the 1 M solution of $KH_2PO_4$ to 10 μM.

(3) Coloring reagent include the preparation of 10.8% solution of L-Ascorbic acid, ammonium molybdate (3% solution), 0.56 % solution of antimony potassium tartrate and $H_2SO_4$ (13.98 %). The reagents were prepared using standard methods (Johnson

and Pilson, 1972; Dhar et al., 2004). The ascorbic acid and ammonium molybdate solutions were firstly mixed together and sulphuric acid was mixed immediately after adding antimony potassium tartrate to circumvent the generation of turbidity in the prepared coloring reagent solution. All these reagents were mixed in the ratio of 2:2:1:5.

### 4.8. Adsorption isotherm

The isotherm models were used for the evaluation of experimental data obtained through batch adsorption study. Isotherm study defines the association between the adsorption capacity of the biochar and the initial adsorbate concentration (As(III) and As(V)).

#### 4.8.1. Langmuir isotherm model

Langmuir isotherm adsorption model implies homogeneous monolayer adsorption of adsorbate over the surface of biochar that comprises determinate identical sites with uniform adsorption activated energy (Ibrahim et al., 2019). Langmuir isotherm equation can be expressed as follows:

$$\frac{C_e}{q_e} = \frac{1}{Q_0 b} + \left(\frac{1}{Q_0}\right) C_e \qquad (4.17)$$

Where, $C_e$ and $q_e$ denote the concentration of As (III and V) (mg/L) and quantity of adsorbate adsorbed (mg/g) by biosorbent at the equilibrium state. . The Langmuir constants are $Q_0$ (mg/g) and $b$ (L/mg) that relate to the adsorption capacity of the biochar and binding energy, respectively. The values of both the Langmuir constants and $R^2$ were evaluated by

the values of slope and intercept obtained from the graph $C_e$ and $C_e/q_e$. The values of $R_L$ i.e., the dimensionless factor calculated by following equation:

$$R_L = \frac{1}{1 + bC_0} \tag{4.18}$$

Here, the Langmuir constant is denoted by $b$ (L/g) and $C_0$ represents initial adsorbate concentration (mg/L). The favorability of process of adsorption is designated by the value of $R_L$. When the values of $R_L$=0 and $R_L$=1 the process of adsorption is said to be irreversible and linear, respectively, and the value of $R_L$>1 and 0>$R_L$>1 indicates the process of adsorption is unfavourable and favourable, respectively (Shahnaz et al., 2021).

### 4.8.2. Freundlich isotherm model

Freundlich model of isotherm defines the multilayer adsorption process of adsorbate on biochar with the heterogeneous surfaces (Zhu et al., 2020). Freundlich isotherm equation is expressed as follows:

$$lnq_e = lnK_F + \left(\frac{1}{n}\right) lnC_e \tag{4.19}$$

Where, the $q_e$ (µg/g) relates the amount of adsorbate adsorbed onto the biochar at equilibrium, initial concentration was denoted by $C_0$ (mg/L). $K_F$ are relates to the maximum amount of biochar to adsorb the adsorbate ((mg/g)(L/mg)$^{1/n}$). $K_F$ (mg/g(L/mg)$^{1/n}$) and n are the constant of Freundlich. The values of both the constants were assessed by the slope and intercept values obtained after plotting the graph between $lnq_e$ and $lnC_e$. Adsorbent surface is said to be highly heterogeneous when the value of the slope is closer to zero.

### 4.8.3. Temkin isotherm model

The Temkin isotherm model distinctly explains the interaction among the adsorbate and synthesized biochar. The Temkin isotherm commences the heat of adsorption reduction of complete layer of molecule linearly with coverage and the adsorption process is exemplified by an equivalent dispersal of binding energies up to maximum specific binding (Abdel-Ghani et al., 2016; Kar and Equeenuddin. 2019). The equation for Temkin isotherm is equated as follows:

$$q_e = BlnK_T + BlnC_e \quad (4.20)$$

Where, the constant of the heat of adsorption is denoted by B (J/mol), Temkin equilibrium binding constant is signified by $K_T$. The adsorption capacity of biochar is implied by $q_e$ (mg/g) and $C_e$ represents the initial adsorbate concentration (mg/L) at the equilibrium point.

## 4.9. Adsorption kinetics

Adsorption kinetics includes the study of three kinetics model like pseudo-first-order, pseudo-second-order and intraparticle diffusion model. The kinetics study was performed to understand the characteristics of adsorption process.

### 4.9.1. Pseudo-first-order kinetics

The pseudo-first-order kinetics was used to determine the adsorption rate constant in the adsorption kinetics study (Gautam et al., 2018). The adsorption constants for As removal was identified by the pseudo-first-order kinetics. The equation for the pseudo-first-order kinetics is written as follows:

$$log q_e - q_t = log q_e - \left(\frac{k_1}{2.303}\right) t \quad (4.21)$$

Where, $q_e$ is the quantity of adsorbate adsorbed by the MTB-800 and MLB-800 at the equilibrium state and $q_t$ is the quantity of adsorbate adsorbed by both the biosorbents at a time (t). Pseudo-first-order kinetics constant is denoted by the $_{k1}$ and its value was calculated by the slope and intercept value obtained by the graph of log($q_e$-$q_t$) against *t*.

### 4.9.2. Pseudo-second-order kinetics

The obtained investigational data was also analyzed through pseudo-second-order kinetics. The second-order kinetics was given by Ho and Mckay (1998) and the equation is expressed as follows:

$$\frac{t}{q_t} = \frac{1}{k_2 q_e^2} + \left(\frac{1}{q_e}\right) t \quad (4.22)$$

Here, the adsorption capacity of MTB-800 and MLB-800 is signified by $q_e$ (mg/g) at equilibrium point and $k_2$ is the constant for pseudo-second-order kinetics. The $k_2$ value was evaluated by the linear graph of $t/q_t$ against *t*.

### 4.9.3. Intraparticle diffusion

The intraparticle diffusion model is the rate-limiting factor for most of the adsorption process and was described by Weber and Morris, (1963). If the biochar is porous, then the adsorption process is controlled either by pore diffusion (adsorbate mass transfer into biochar pores) or film diffusion (transfer of mass of As(III and V) from solution to the outer biochar surface) (Nikic et al., 2019). Thus, to recognize the process that is the rate-controlling step the experimental data was analyzed using an intraparticle diffusion model. The equation of adsorption diffusion model is equated bellow:

$$q_t = k_i t^{1/2} + C \quad (4.23)$$

Here, $k_i$ is the intraparticle diffusion model constant (mg/g $min^{1/2}$) and $C$ is the constant associated with the boundary layer of biochar. The values of both constants were determined by plotting $q_t$ vs $t^{1/2}$.

### 4.10. Thermodynamics

The influence of different temperatures (25, 35, 45 and 55 °C) for the adsorption of As(III and V) on the biochar surface were examined by thermodynamics parameters. All parameters of thermodynamic were calculated by using the following equations (Chen et al., 2021b):

$$\boldsymbol{K_c = \frac{q_e}{C_e}} \quad (4.24)$$

$$\boldsymbol{lnK_C = \frac{\Delta S}{R} - \frac{\Delta H}{RT}} \quad (4.25)$$

$$\boldsymbol{\Delta G = \Delta H - T\Delta S} \quad (4.26)$$

Where, the initial As concentration at equilibrium state is denoted by $C_e$ (mg/L) and the quantity of adsorbate adsorbed by biochar at equilibrium point is signified by $q_e$ (mg/g). ΔS° (kJ/mol K) is the change in entropy and ΔH (kJ/mol) is the change in enthalpy, correspondingly. ΔG° (kJ/mol) is the Gibbs free energy and the gas constant is $R$ (8.314 J/mol). The graph was plotted between the values of *lnKc* and *1/T* to evaluate the values of ΔS, ΔH and ΔG using *m* and *c* values of the linear plot**.**

### 4.11. Regeneration Study

Reusability of adsorbent is one of the most important parameter which can describe the materials stability in removing contaminants. Adsorption study was done to test the recyclability potential of the biosorbent. The whole study was carried out by using 0.1 M Sodium hydroxide as a desorbing solution to release the adsorbed As(III) and As (V) to solution. After that the material once used for adsorption was kept in contact with 50 mL of 0.1 M NaOH solution for 2 h and then washed with distilled water, until the solution pH become neutral. After that the desorbed biochar were again used for adsorption of arsenic (Padungthon et al., 2015).

### 4.12. Groundwater sample collection

The groundwater samples were collected from different villages of district Bahraich, U.P., India, it is situated near the border of Nepal (Fig. 4.7). These areas of Bahraich are highly affected by groundwater arsenic contamination. This city is situated near the bank of River Ghaghra, which is the largest tributary of the Ganga River. Four samples were collected from village Mahurikala (27.226373°N 81.575693°E), Hazipur (27.221905°N. 81.581032°E), Bariyagothi (27.2300°N. 81.5775°E), one sample (duplicate) from each village and two samples from Jhiliya (27.328412°N. 81.602911°E), named as MK, HP, BG J-I and J-II, respectively. Assessment of removal percentage of arsenic from the collected sample was done by evaluating the concentration of arsenic before and after adsorption. The process of adsorption was regulated with predetermined dose of biochar, 7 pH, and 25 °C temperature with 80 rpm shaking speed for 4 h.

**Fig. 4.7. Groundwater sample collection.**

### 4.12.1. Physicochemical parameters of collected ground water samples

The physicochemical parameters of collected groundwater; pH and Electrical Conductivity, Total dissolved solids (TDS) (water analyzer, 371, systronic, India), Fluoride (digital Ion-pH meter (EUTECH Handheld Meter Kit; Thermo Scientific) and As concentration was analyzed using standard spectromolybdate method (Dhar et al., 2004) at 880 nm absorbance UV–Visible spectrophotometer (117 Systronics, India). Total hardness was analyzed as per the standard protocol outlined in "Standard Methods for the Examination of Water and Wastewater" (APHA, 2005).

# Chapter-5
# Results and Discussion

### 5.1. Initial characterization of raw waste biomass

#### 5.1.1. Proximate analysis

The obtained result of proximate analysis has been given in Table 5.1. The maximum ash content and fixed carbon was found in *Tectona* leaves waste biomass and had lower moisture content whereas the lowest ash content and fixed carbon was preserved in waste biomass of *Raphanus sativa* and also it consists highest moisture content. The highest volatile solids percentage was observed in waste dry leaves of *Lagerstroemia speciosa* while lower most volatile solids was found in *Artocarpus heterophyllus.*

**Table 5.1. Proximate analysis of waste biomass.**

| Biomass | Ash (%) | Volatile solids (%) | Moisture content (%) | Fixed Carbon (%) |
|---|---|---|---|---|
| *Tectona* | 14.12 | 30.12 | 10.52 | 45.24 |
| *Lagerstroemia speciosa* | 11.11 | 31.33 | 15.52 | 42.04 |
| *Raphanus sativa* | 1.06 | 11.55 | 57.37 | 30.02 |
| *Artocarpus heterophyllus* | 4.6 | 9.4 | 49.4 | 33.6 |

#### 5.1.2. Biochar yield

The biochar yield was calculated and it was observed that the yield percent of biochar (LB 800 and TB 800 was 27.24 % and 20.23 %) was lowest than that of modified biochar. Amongst various modified biochars, the maximum yield was 48.32 % obtained for bimetallic biochar (Fe/Mn-TB) synthesized by waste biomass of *Tectona sp.,* while the

lower yield was 39.44 % acquired for magnetic biochar (MTB-800) synthesized using *Lagerstroemia speciosa* waste leaves biomass (Table 5.2.).

**Table 5.2. Yield of synthesized biochar materials.**

| **Pristine Biochar** | | **Yield (%)** |
|---|---|---|
| *Tectona* sp. | TB-800 | 20.23 |
| *Lagerstroemia speciosa* | LB-800 | 27.24 |
| **Modified biochar** | | |
| *Tectona* sp. | MTB-800 | 47 |
| *Lagerstroemia speciosa* | MLB-800 | 39.44 |
| *Raphanus sativa* | MRB-800 | 40.11 |
| *Artocarpus heterophyllus* | MJB-800 | 47.79 |
| *Tectona* sp. | Fe-TB | 40.21 |
| | Fe/Mn-TB | 48.32 |

### 5.1.3. Physico-chemical parameters of collected groundwater samples

Due to natural as well as anthropogenic sources groundwater has been contaminated with various organic and inorganic pollutants. Arsenic and fluoride are the main groundwater pollutant. It was observed that the pH, TDS, electrical conductivity and fluoride concentration in collected samples were found under permissible limits, whereas the Arsenic concentration in the groundwater samples were observed above its prescribed limits. Hardness of groundwater samples were also found above the permissible limits. Magnesium and calcium are the principle ions that causes the hardness of water and are also essential mineral elements of food. Consumption of hard water can cause several health effects to humans (Akram and Rehman, 2018). The detected concentration of As(III)

before adsorption was 0.088, 0.078, 0.101 and 0.092 mg/L, in Mahurikala, Hazipur, Bariyagothi and Jhiliya samples, respectively, that was above the prescribed limits. Various studies also reported Bahraich District of Uttar Pradesh poorly contaminated groundwater with Arsenic (Singh et al., 2022; Singh and Singh, 2020; Bindal et al., 2020). The obtained results were presented in Table 5.3.

**Table 5.3. Physicochemical parameters of collected groundwater.**

| Parameters | Permissible limit | Mahurikala (MK) | Hazipur (HP) | Bariyagothi (BG) | Jhiliya (J) |
|---|---|---|---|---|---|
| **pH** | **6.5-8.5** | 7.150±1.10 | 7.6±0.50 | 7.4±0.05 | 7.2±0.50 |
| **TDS (mg/L)** | **500** | 450.2±2.12 | 420.12±1.00 | 430.1±2.50 | 330.2±1.00 |
| **Electrical conductivity (µS/cm)** | **200-800** | 300.12±2.12 | 250.2±1.2 | 406±0.51 | 400.23±1.11 |
| **Hardness (mg/L)** | **200** | 240.21±0.25 | 220.11±0.50 | 205.13±0.33 | 225.11±2.22 |
| **Fluoride (mg/L)** | **1.5** | 0.00±0.00 | 0.00±0.00 | 0.00±0.00 | 0.00±0.00 |
| **Arsenic(III) (mg/L)** | **0.01** | 0.088±0.003 | 0.078±0.007 | 0.101±0.007 | 0.092±0.004 |
| **Arsenic(V) (mg/L)** | **0.01** | 0.082±0.010 | 0.054±0.043 | 0.097±0.035 | 0.112±0.025 |

## 5.2. PHASE I: Characterization and application of pristine biochar for the removal of As(III) and As(V) synthesized using waste dry leaves of *Tectona sp.* and *Lagerstroemia speciosa* from aqueous solution and groundwater

### 5.2.1. Characterization of TB 800 and LB 800

#### *5.2.1.1. SEM*

The SEM analysis was done for the determination of shape, size and surface morphological structure of both the biochar materials (TB 800 and LB 800). The Fig. 5.1a and c shows that both the biochar materials have irregular in shape with rough surface and consists of large surface area with high porosity. Fig. 5.1b and d describe the elemental composition of both the adsorbents which shows that the TB 800 has 62.55 % carbon by weight whereas LB 800 contains 57.98 % of carbon by weight.

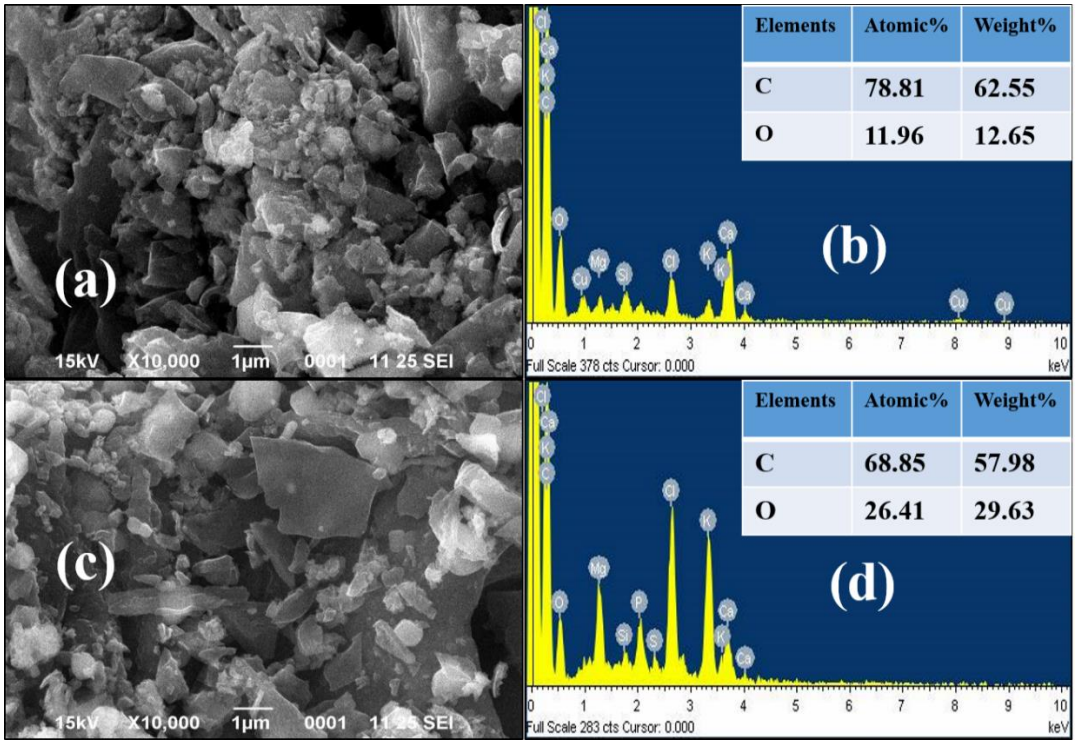


**Fig. 5.1. (a) and (c) SEM image of TB 800 and LB 800, (b) and (d) EDS graph of TB 800 and LB 800, respectively.**

### *5.2.1.2. FTIR analysis*

The FTIR spectrum is shown in Fig. 5.2a and b, represents the functional groups on both the biochar material freshly prepared and after the adsorption of both the arsenic species. FTIR spectra of both the biochar materials show the lesser number of peaks because of the high temperature at which the biochar was prepared. Under high temperature most of the functional groups from the lignocellulosic materials were lost due to high carbonization intensity (Li et al., 2017a). The peaks found in a spectrum of biochar materials before and after adsorption and show almost similar wavenumbers. The bands obtained around wavenumber 3435 $cm^{-1}$ and 3433 $cm^{-1}$ attribute hydroxyl group stretching and $–NH_2$ groups in aromatic amines, respectively, peak 1642 $cm^{-1}$ represents C=O stretching (Li et al., 2017b), C=C bonds of alkenes and $NH_2$ groups in primary amide. Benzene ring of aromatic compounds and $NO_2$ stretch vibration of aromatic nitro compound was represented by wavenumber 1548 $cm^{-1}$, this peak was only present in TB 800 before adsorption of arsenic species. Peak on 1414 $cm^{-1}$ attributes to OH group of carboxylic acid and aromatic C=C bond stretching that shows the OH bending, wavenumber 1048 $cm^{-1}$ attributes the C-O stretching bond and R-C-$H_2$-OH group of primary alcohol or –OH deformation vibration (Dai et al., 2017b) and 868 $cm^{-1}$ corresponds to –C-H aromatic out of plane stretch vibration (Lambert, 1987). Peak with wavenumber 1548 $cm^{-1}$ was present on TB 800 biochar surface but disappeared after adsorbing As(III) and As(V) that may be due to the adsorption of Arsenic species on the biochar surface and in case of LB 800 a new peak was appeared at wavenumber 1618 $cm^{-1}$ after adsorbing arsenic onto its surface that represents the $NH_3^-$ group of amino acid or $NH_3$ deformation.

After adsorption, the intensities of peaks (3435, 1642, 1414 and 868 $cm^{-1}$) slightly changes that might be responsible for the adsorption of Arsenic on the surface of both the biochar materials.

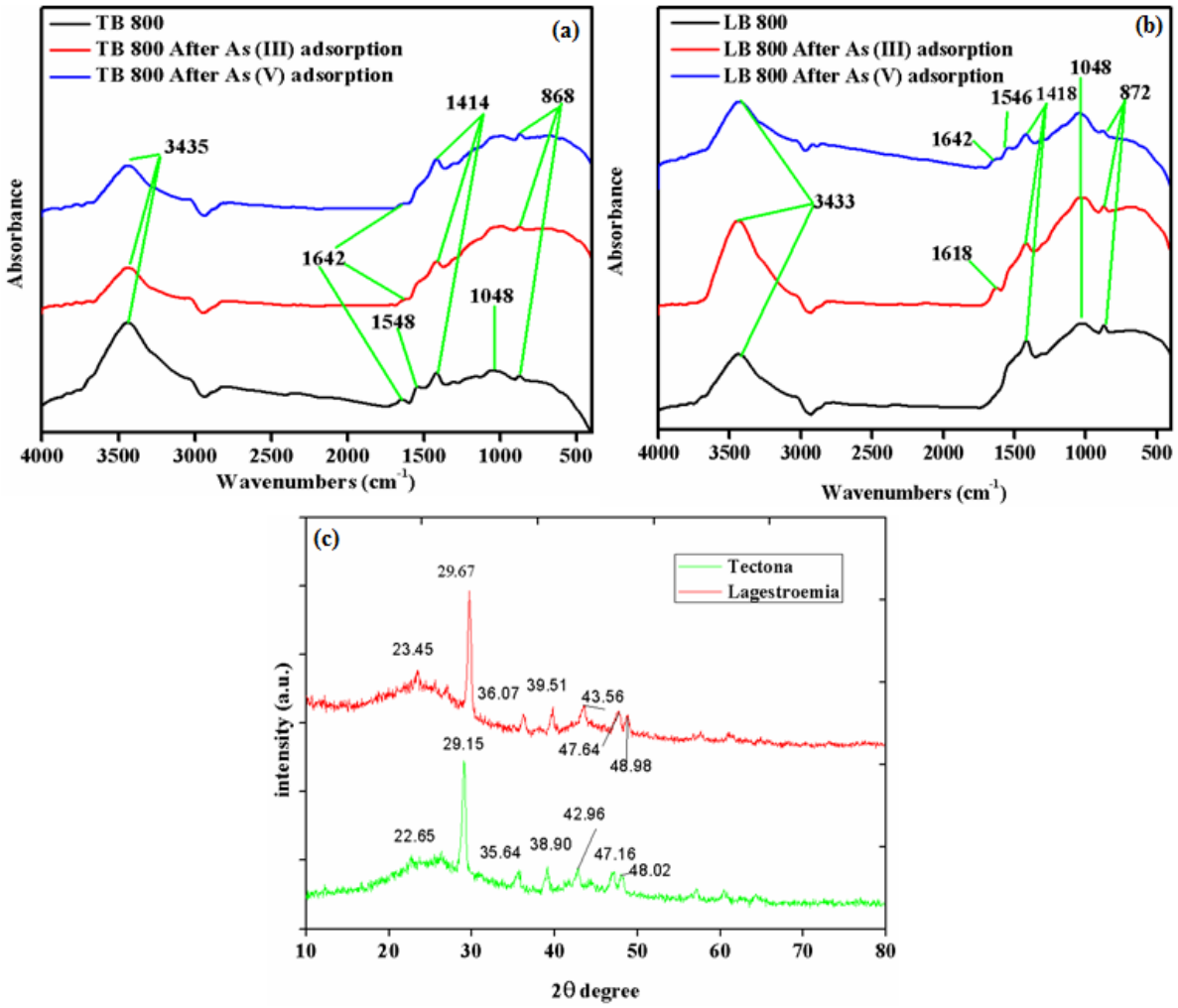


**Fig. 5.2. FTIR spectra of (a) TB 800 and (b) LB 800 before and after adsorption of As(III) and As(V) and (c) XRD analysis of TB 800 and LB 800.**

### *5.2.1.3. XRD*

XRD analysis was done for the determination of crystalline and amorphous structure of the prepared biochar materials. The XRD spectrums of both the adsorbents were seems to be almost similar showing the crystalline nature of the adsorbents (TB 800 and LB 800) (Fig. 5.2c) (Xu et al., 2014). The fine and sharper peaks were found at 2θ values of nearby 20-30$^{o}$. These peaks that were obtained for both the biochar materials indicated the development of carbonized material and also ensure the presence of graphene like structure in the prepared biochar materials (TB 800 and LB 800) (Zeng et al., 2018). These peaks designate the formation of aromatic carbon compounds in the biochar materials (Chutia et al., 2014). The peak found at 29.67° and 29.5° was assigned to $SiO_2$. The diffraction peaks present at 38.9°, 39.51°, 42.96° and 43.56° correspond to calcium silicate and diffraction peaks at 47.16°, 47.64°, 48.02° and 48.98° attributed to the presence of calcite (He et al., 2018). The XRD pattern was supported by the FTIR spectrum that shows the presence of aromatic carbon compounds in the biochar materials.

### *5.2.1.4. Zeta potential*

Zeta potential defines the stability of adsorbents at particular pH. If the value of zeta potential is more the 30 (negative or positive) the material is said to be stable. Zeta potential's magnitude describes the stability of adsorbent in a dispersed medium, which accomplishes electro-statistical repulsion between the adsorbent and dispersion medium (Sun et al., 2007). Fig. 5.3a shows that both the biochar (TB 800 and LB 800) were highly stable in alkaan line medium means at pH 10, the stability of both the adsorbents was negligible at lower pH.

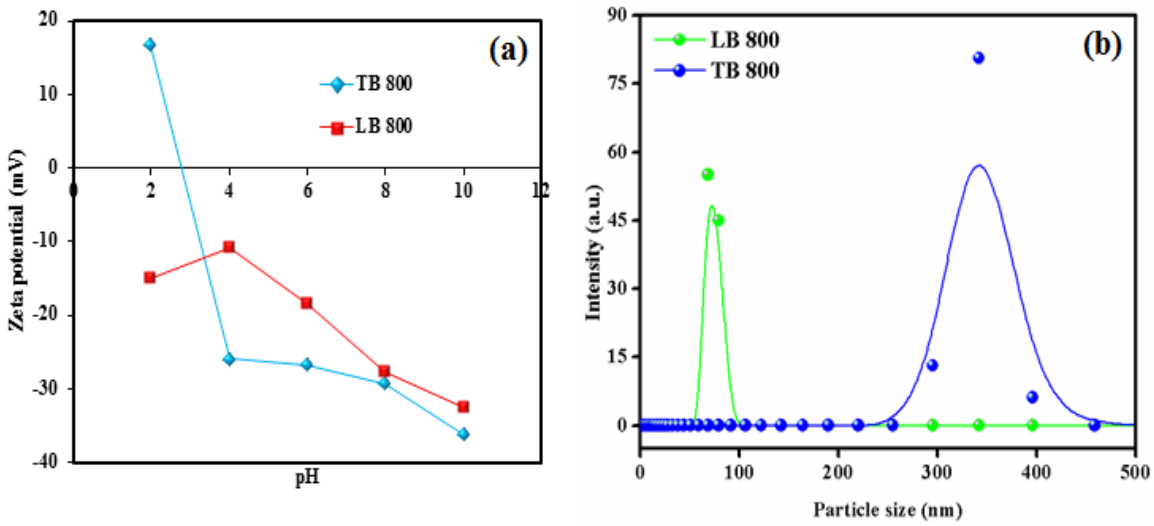


**Fig. 5.3. Plot of (a) Zeta potential and (b) PSA analysis for TB 800 and LB 800.**

### *5.2.1.5. PSA*

For the determination of particle size, the biochar materials were added to ethyl alcohol at room temperature after homogenizing them. The obtained result was plotted, as shown in Fig. 5.3b represents the broad peaks observed between 250-450 nm for TB 800 and 60-90 nm for LB 800. The obtained result revealed that the LB 800 particle size was very less means having larger surface area.

### *5.2.1.6. BET analysis*

The porosity and surface area of the synthesized biochar materials were determined by using Brunaur Emmitt Teller (BET) at 77 K. The results obtained through BET analysis shows the surface area of TB 800 and LB 800 are 34.55 $m^2g^{-1}$ and 6.18 $m^2g^{-1}$, respectively. It has been indicated in Fig. 5.4a that TB 800 possesses a microporous structure, which is confirmed by Fig. 5.4c, and the obtained results for LB 800 shown in Fig. 5.4a revealed that the LB 800 exhibits micro-mesoporous structure due to the weak interaction between

the adsorbed gas and the material, Fig. 5.4d confirmed the result. The mean pore diameter and total pore volume for TB 800 was 2.233 nm and 0.1929 $cm^3/g$ and for LB 800 were 39.310 nm and 0.0499 $cm^3/g$, respectively, (Fig. 5.4b). Similar BET analysis results were also observed in the study of Zhu et al. (2016); Zazycki et al. (2018), which also observed the microporous and micro-mesoporous structure of the biochar material.

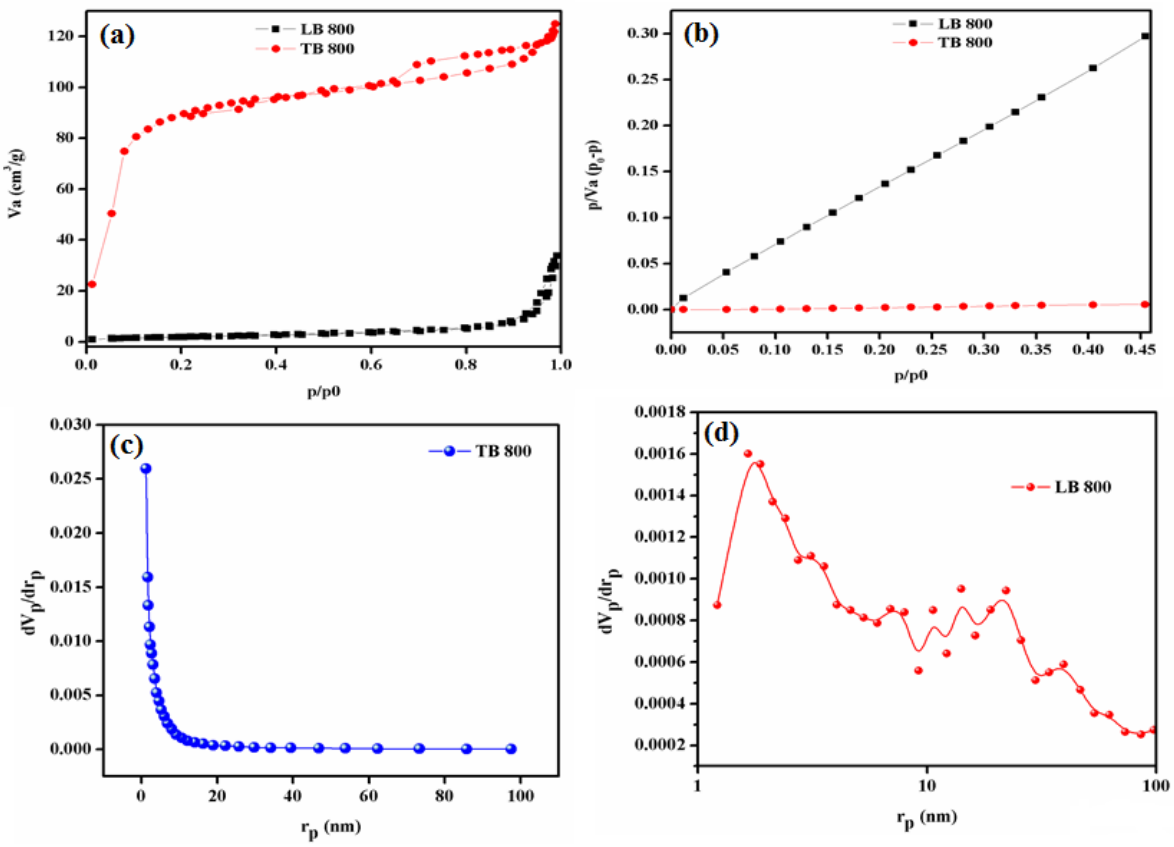


**Fig. 5.4. Curve (a) adsorption/ desorption of nitrogen with increase/decrease in pressure, (b) BET plot and (c) and (d) relationship between pore radius and change in pore volume with pore radius for TB 800 and LB 800, respectively.**

### *5.2.1.7. XPS*

Fig. 5.5 shows the XPS scan for TB 800 and LB 800. The obtained result of XPS shows the sharp peaks that indicate the presence of oxygen and carbon. The presence of higher amount of carbon and lesser amount of oxygen for TB 800 and LB 800 was also observed. In case of TB 800, the amount of oxygen was higher in comparison with LB 800; but, the carbon content was less than LB 800. The presence of carbon content was due to carbonization of material at high temperatures. The O 1s consisted one broad peak ~529 eV, which corresponds to oxygen carbonyl or quinone on the surface of both the biochar materials but the intensity of peaks were different (Fig. 5.5b). The spectrum of C 1s shows two distinct peaks: ~283 eV represents graphitic and aromatic carbon and ester and carboxylic groups at ~290 eV (Fig. 5.5c) (Dong et al., 2013).

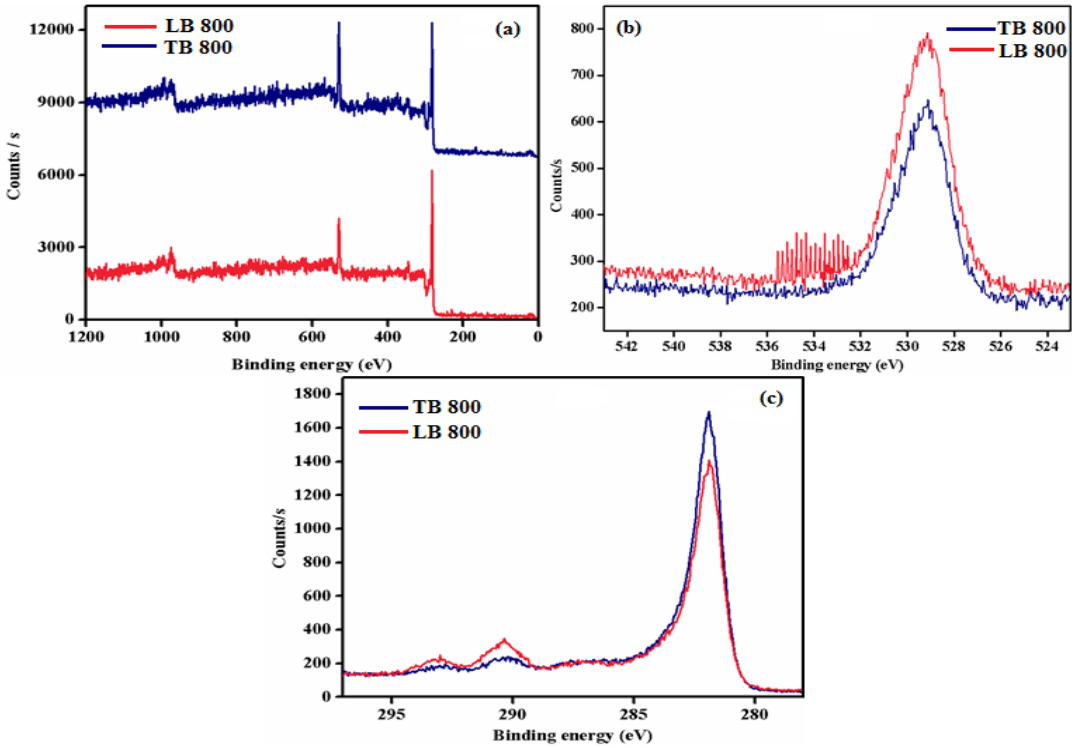


**Fig. 5.5. (a) XPS spectra of TB 800 and LB 800, (b) XPS spectra of O 1s and (c) XPS spectra of C 1s.**

#### *5.2.1.8. $pH_{ZPC}$*

It was observed that the $pH_{ZPC}$ of both the materials were basic in nature, having negative surface charge of adsorbent. A $pH_{ZPC}$ for TB 800 was ~8.2 and LB 800 ~8. Both biochar materials are basic in nature due to the emancipation of alkaline minerals (Ca and Mg) that occurs from thermal decomposition of waste biomass feedstock during the process of pyrolysis (Yoon et al., 2017).

### 5.2.2. Influence of operating parameters on Arsenic removal efficiency

#### *5.2.2.1. Effect of dose*

As shown in Fig. 5.6a, five different doses (1, 2, 3, 4 and 5 g/L) of TB 800 and LB 800 were taken for the dose study for As(III) and As(V) removal, the maximum removal percentage was obtained at 4 g/L but with TB 800 for As(V) removal, the maximum adsorption was obtained at 2 g/L of dose i.e., 95.6%. The study was operated under optimal conditions with contact time (360 min), at neutral pH, concentration (1 mg/L) and temperature 25 °C. Maximum adsorption capacities of As(III) were found as 0.625 mg/g and 0.504 mg/g for TB 800 and LB 800, respectively. Conversely, adsorption capacities of As(V) were achieved about 0.831 mg/g and 0.536 mg/g for TB 800 and LB 800, respectively (Fig. 5.7a). TB 800 shows high removal percentage in case of As(III) and As(V) in comparison with LB 800. Adsorption capacities of biochar materials decrease on increasing dose of adsorbent. It is due to the diminution of active functional sites present on surface of adsorbent and this reduction is because of increase in intermolecular attraction between adsorbent (Kazi et al., 2018).

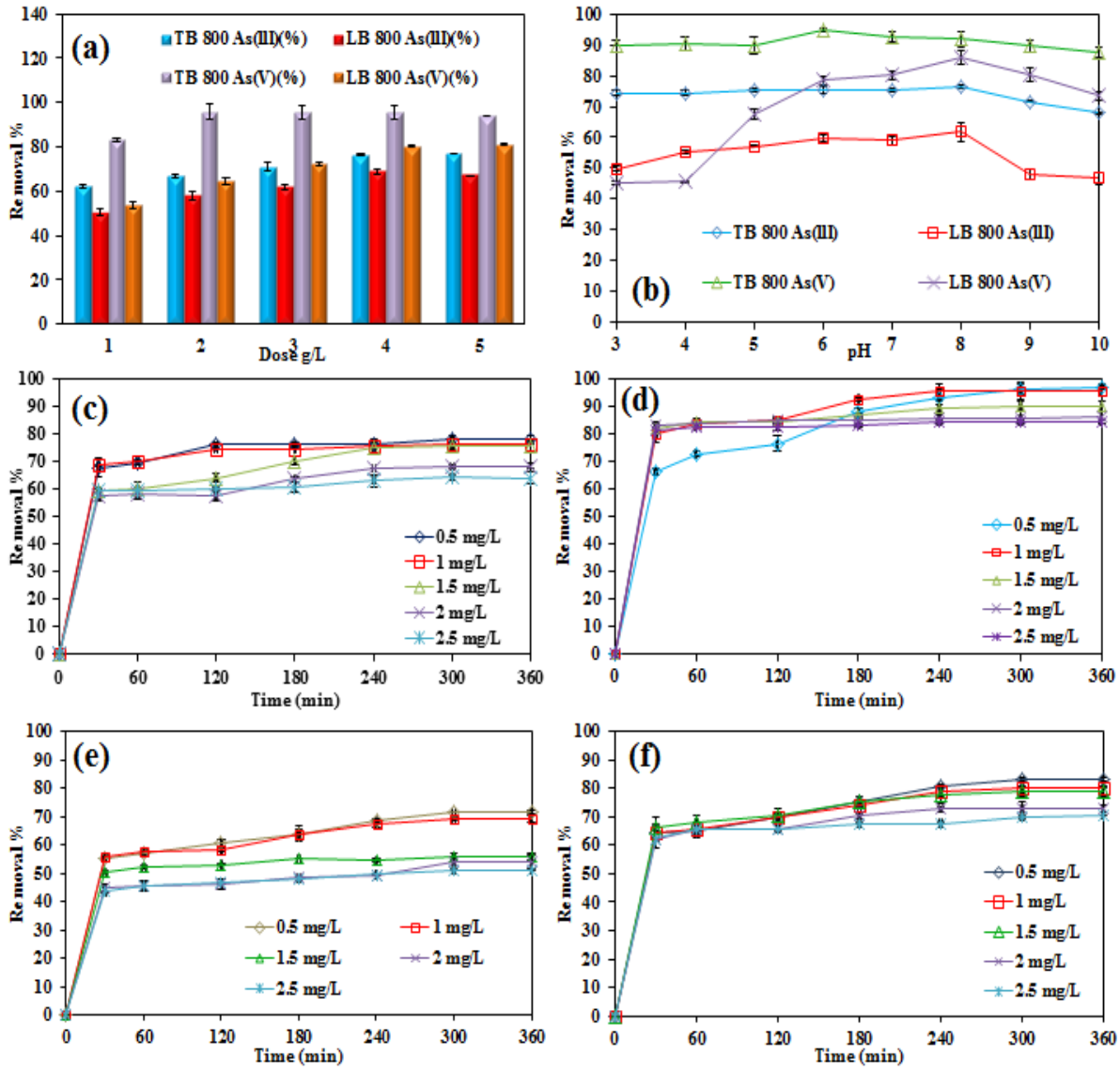


**Fig. 5.6. Effect of (a) adsorbent dose, (b) pH, (c) and (d) initial concentration on As(III) and As(V) adsorption by TB 800, (e) and (f) effect of initial concentration of As(III) and As(V) on adsorption by LB 800.**

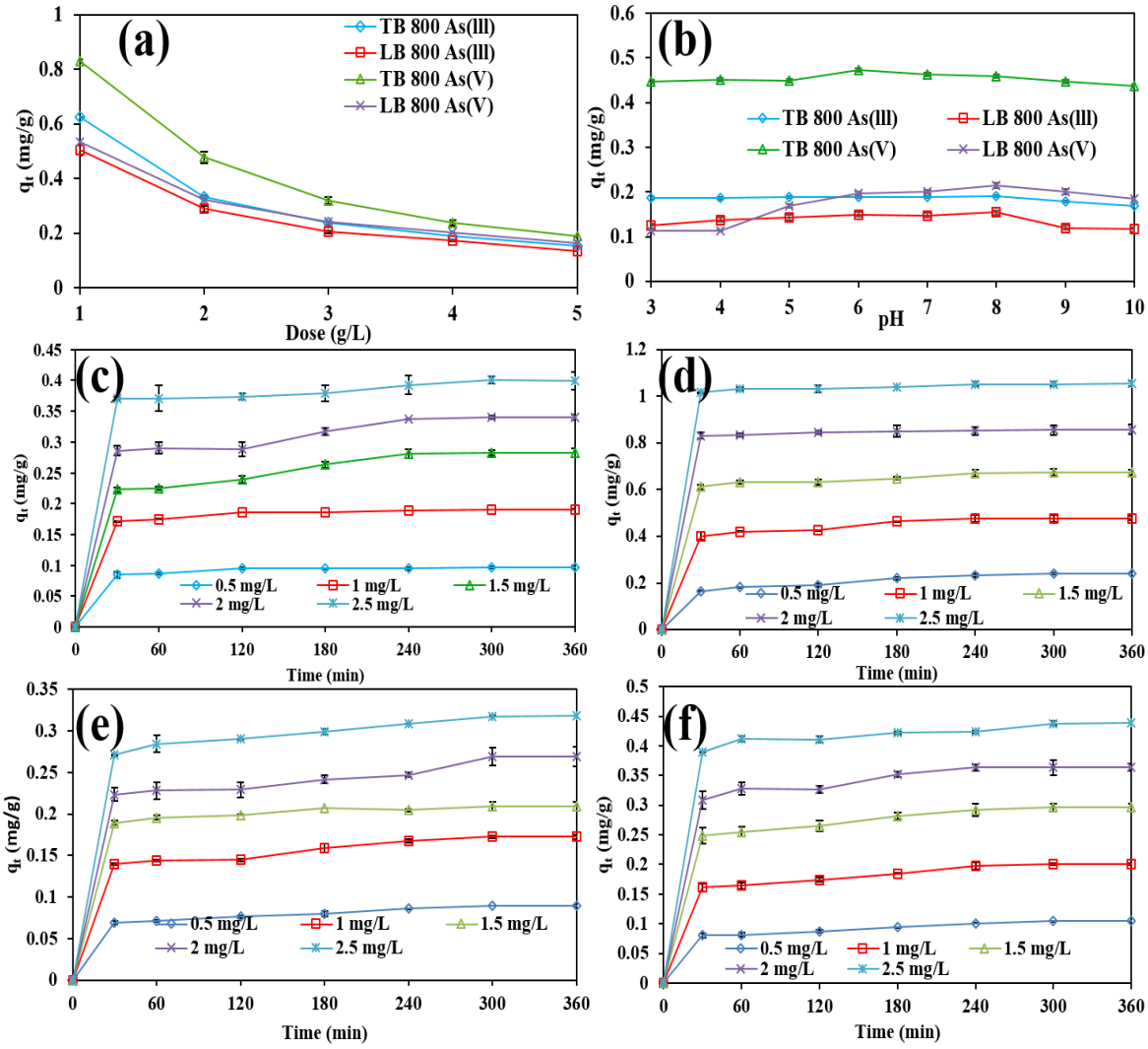


**Fig. 5.7. Effect of (a) adsorbent dose, (b) pH, (c) and (d) initial concentration of As(III) and As(V) on adsorption capacity by TB 800, (e) and (f) effect of initial concentration of As(III) and As(V) on adsorption capacity by LB 800.**

### *5.2.2.2. Effect of concentration*

The effect of concentration of adsorbate was studied by differing As(III) and As(V) initial concentration from 0.5-2.5 mg/L distinctly, with 4 g/L dose except TB 800 in case of As(V) (2 g/L) and at pH 7. The obtained results specifies that on increasing As(III) and As(V) initial concentration from 0.5-2.5 mg/g, $q_e$ value was also increased in the range of

0.097-0.400 mg/g and 0.089-0.317 mg/g for As(III) by applying TB 800 and LB 800, respectively (Fig. 5.7c and e). The $q_e$ values of As(V) were increased in the range of 0.241-1.054 mg/g and 0.104-0.439 mg/g by using TB 800 and LB 800, respectively (Fig. 5.7d and f). On further increasing the As(III) and (V) initial concentration, there was no effect observed on adsorption capacities of both adsorbents (TB 800 and LB 800) due to the saturation of active sites present on adsorbent surface (Saikia et al., 2017).

The adsorption percentage decreased with an increasing initial concentration of both the species of arsenic (As(III) and As(V)). The highest removal percentage of As(III) and As(V) were achieved 77.9 % and 96.5 %, respectively, by using TB 800 (Fig. 5.6c and d). Though, the highest removal about 82 % for As(V) and 72 % for As(III) was observed by using LB 800 at the lowest concentration i.e. 0.5 mg/L (Fig. 5.6e and f). The removal efficiency of TB 800 was better than that of LB 800, it shows good removal capacity for Arsenic (III and V) removal from an aqueous solution.

#### *5.2.2.3. Effect of pH*

The pH of the solution is one of the most important factors for the adsorption study because the pH of the solution stimulates the $H^+$ ions of functional groups present on biochar surface and also varies the form of As in an aqueous medium (Shakoor et al., 2016). So, the pH study was performed by varying pH in the range of pH 3-10, while keeping other experimental parameters constant (Temperature- 25°C, concentration- 1 mg/L and shaking speed-80 cycles/min). As shown in the Fig. 5.6b that the maximum removal percentage of As(III and V) was found at higher or basic pH with both the adsorbents (TB 800 and LB 800). TB 800 removed a maximum 76.42 % of As(III) at pH 8 with 0.191 mg/g adsorption capacity and the removal of As(III) decreased on further increasing pH of a

solution, removal of As(V) was lower at acidic pH but increased with an increasing in pH value and the highest removal was observed at 6 pH (94.6 %) and the slightly decreased on further increased in pH of solution. The highest removal percentage of As(III) (61.67 %) and As(V) (85.85 %) at 8 pH with adsorption capacities 0.154 and 0.214 mg/g, respectively, by using LB 800 (Fig. 5.7b).

The removal of As(III and V) with both the adsorbents (TB 800 and LB 800) were obtained within the pH range of 6-8, that is also the pH of natural groundwater. Hence, both the adsorbents could be used for the removal of both the arsenic species (As(III) and As(V)) from the natural groundwater. In the study of Niazi et al. (2018), the maximum removal of arsenic was observed at higher pH range from 7-9 pH on the perilla leaf biochar. Removal of As was totally dependent on species of arsenic and solution pH as described by Vithanage et al. (2017).

#### *5.2.2.4. Effect of temperature*

Temperature is a highly significant parameter that could have an exert influence on rate of reaction of adsorption process. All the reaction conditions, like removal capacity, pH, net concentration were somewhat correspond to the different temperatures. The temperature study was performed at various temperatures such as 25°C, 35°C, 45°C and 55°C, while retaining other constraints constant (dose-4g/L, initial concentration-1 mg/L and pH-7). It was found that the removal capacity was increased with an increasing temperature except in case of TB 800 As(V), in which the removal capacity decreased with an increase in temperature.

When TB 800 was used for the As(III) removal, the maximum adsorption was observed 94.17 % at 55 °C (Fig. 5.8a) and the highest removal of As(V) was found 95.6

% at 25 °C (Fig. 5.8b). A removal percentage was also obtained the highest 73.6 % for As(III) and 95.1% for As(V) by applying LB 800 at 55 °C (Fig. 5.8c and d).

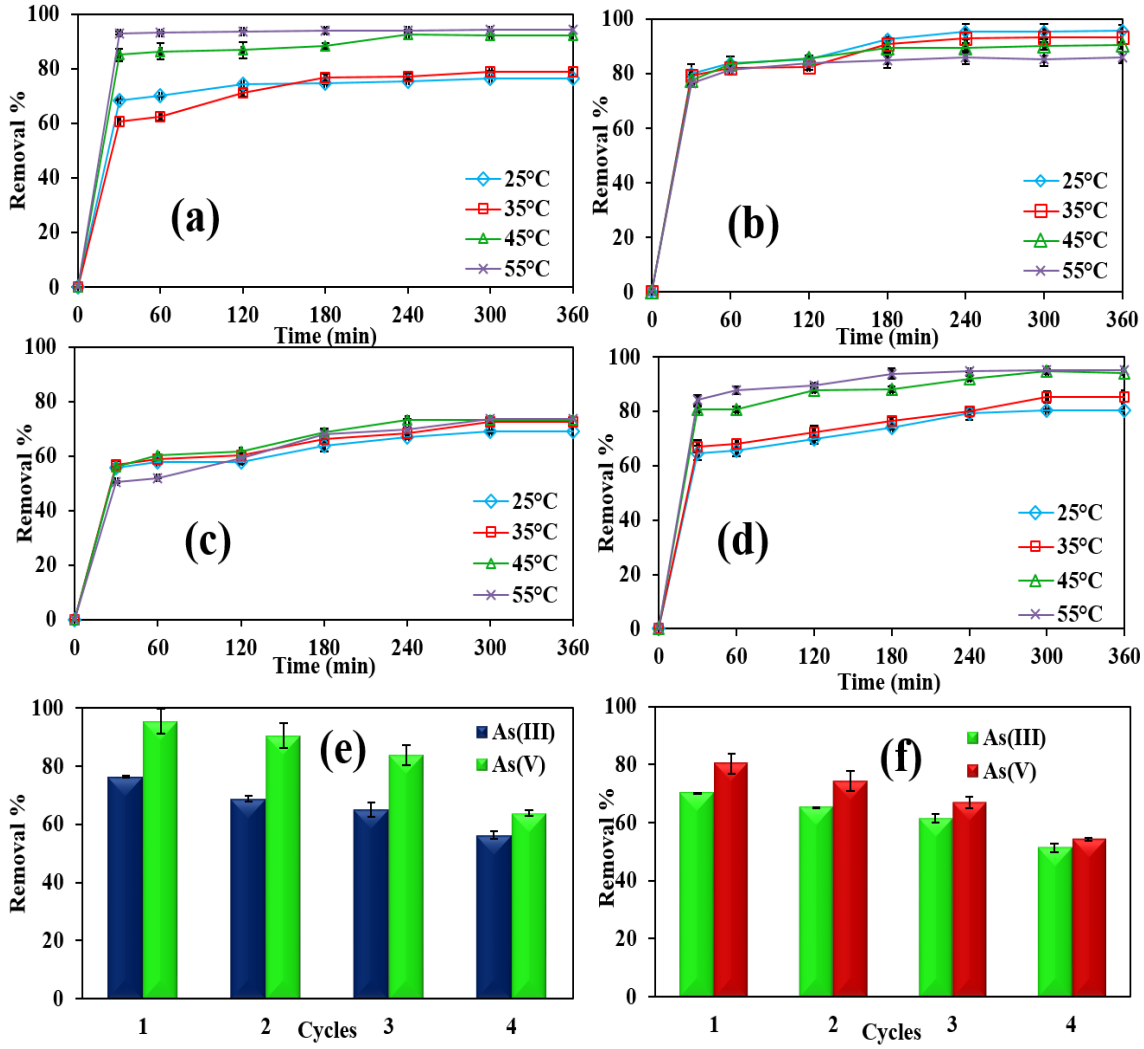


**Fig. 5.8. Effect of temperature on adsorption of (a) and (b) As(III) and As(V) by TB 800, (c) and (d) As(III) and As(V) by LB 800, respectively, and regeneration of (e) and (f) TB 800 and LB 800 for As(III) and As(V) adsorption, respectively.**

The reason behind the obtained highest adsorption at the highest temperature is that certain adsorptive sites are present on adsorbent's surface, which requires particular temperature

to become active, sometimes low or sometimes high temperature is required to activate the adsorption sites (Kazi et al., 2018).

### 5.2.3. Regeneration study

The regeneration study is very important constraint that reveals the stability of adsorbent and how many times it can be used for As species removal from an aqueous solution. The regeneration study was performed for TB 800 and LB 800 adsorbents and shows good results for both the species of arsenic i.e., As(III) and As(V) adsorption. A 0.1 M NaOH solution was used as a desorbing agent for As(III) and As(V). It was found that both the biochar materials were successfully used up to four regeneration cycles. The removal percentage in fourth cycle was greater than 50 %, by using TB 800 and LB 800. The removal percentage for As(III) through TB 800 were found to be 76.4 %, 68.8 %, 65.1 % and 56.3 % in first, second, third and fourth cycle, whereas, through TB 800, the As(V) removal percentage were achieved as 95.6 %, 90.6 %, 83.85 % and 63.85 %, respectively. In comparison with TB 800, the adsorption percentage of both Arsenic species was decreased. The As(III) adsorption shows 70.2 %, 65.2 %, 61.4 % and 51.4 %, whereas removal percentages of As(V) shows 80.4 %, 74.4 %, 66.9 % and 54.4 % in LB 800 in first, second, third and fourth regeneration cycle, respectively, (Fig. 5.8e and f).

### 5.2.4. Adsorption Isotherms

The isotherms were used to optimize the experimental conditions for the Arsenic species adsorption (Li et al., 2019). After studying adsorption isotherms it was found that the adsorption of As(III) by TB 800 followed Temkin isotherm with $R^2$ value 0.9924, while adsorption of As(V) by TB 800 experimental data best fitted to Langmuir isotherm

model with $R^2$ value of 0.9689. The experimental data of As(III) removal by LB 800 followed Frendliuch model of isotherm with $R^2$= 0.9651and the As(V) adsorption by LB 800 followed Langmuir model of isotherm (Fig. 5.9). All the values obtained through isotherms study are listed in Table 5.4.

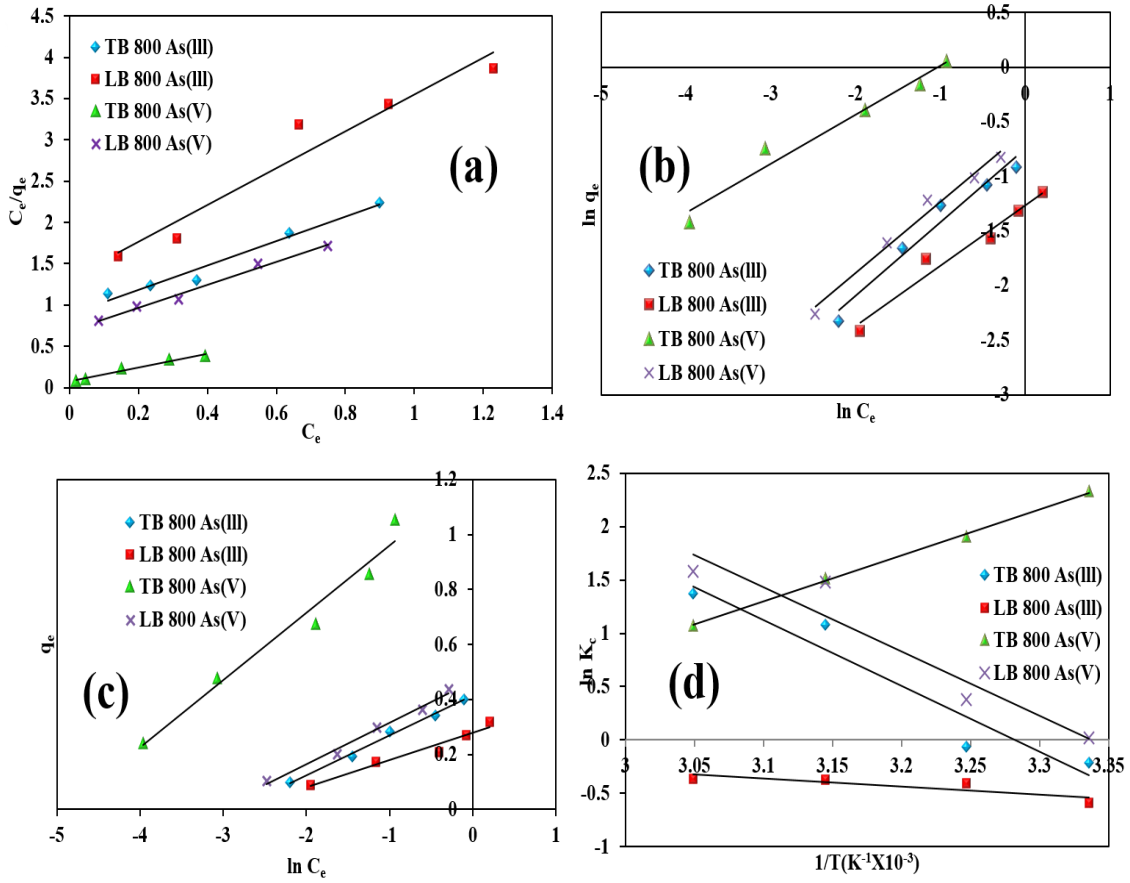


**Fig. 5.9. Plots of (a) Langmuir isotherm, (b) Freundlich isotherm, (c) Temkin isotherm for As(III) and As(V) adsorption by TB 800 and LB 800 and (d) Plot for thermodynamic.**

**Table 5.4. Isotherm parameters for removal of As(lll) and As(V) by synthesized TB 800 and LB 800.**

| | | TB 800 As(lll) | LB 800 As(lll) | TB 800 As(V) | LB 800 As(V) |
|---|---|---|---|---|---|
| | $q_{max}$ (mg/g) | 0.675±0.121 | 0.447±0.011 | 1.206±0.146 | 0.715±0.010 |
| **Langmuir isotherm** | **B (L/mg)** | 1.665±0.493 | 1.708±0.070 | 11.294±1.248 | 2.042±0.091 |
| | **RL** | 0.194±0.0431 | 0.181±0.006 | 0.034±0.025 | 0.164±0.006 |
| | $R^2$ | 0.9706 | 0.9447 | 0.9689 | 0.9875 |
| **Freundlich Isotherm** | $K_F$ $(mg/g(L/mg)^{1/n})$ | 4.594±1.4119 | 3.543±1.883 | 1.582±0.178 | 0.558±0.010 |
| | **N** | 1.491±0.1499 | 1.8155±0.025 | 2.237±0.857 | 1.532±0.009 |
| | $R^2$ | 0.9616 | 0.9651 | 0.9658 | 0.9821 |
| **Temkin isotherm** | **B** | 0.145±0.0165 | 0.0980.002 | 0.245±0.067 | 0.151±0.002 |
| | $K_T$ (L/g) | 17.262±2.8850 | 16.9960.393 | 13.599±5.064 | 21.88±0.249 |
| | $R^2$ | 0.9924 | 0.9578 | 0.9674 | 0.987 |

### 5.2.5. Thermodynamic study

The results obtained through thermodynamic study revealed that the adsorption of As(III) by TB 800 was increased with an increasing temperature, which means adsorption process was found to be endothermic and it was also recognized by the positive value of ΔS° (0.1685 kJ/mol K), ΔH° (0.513 kJ/mol) and with a negative value of ΔG° and the removal of As(V) through TB 800 was based on exothermic process of adsorption in which the removal percentage decreased on increasing temperature having positive value of ΔG°

and negative value of ΔS° (-0.101 kJ/mol K) and ΔH° (-0.036 kJ/mol). On the other hand, the adsorption of As(III) through LB 800 followed endothermic process with negative values of ΔG° and positive value of ΔH° (0.0061 kJ/mol) and ΔS° (0.0159 kJ/mol K). However, adsorption of As(V) by LB 800 also followed endothermic process (Fig. 5.9d). The values of the thermodynamics study parameters are listed in Table 5.5.

**Table 5.5. Thermodynamic parameters of As (III) and As(V) adsorption onto TB 800 and LB 800 adsorbent.**

| Parameters | Temperature (K) | TB 800 | | LB 800 | |
|---|---|---|---|---|---|
| | | As(lll) | As(V) | As(lll) | As(V) |
| ΔG° (kJ/mol) | 298 | -50.154±2.144 | 30.012±3.102 | -4.7377±0.362 | -49.7665±3.323 |
| | 308 | -51.839±2.216 | 31.020±3.206 | -4.8969±0.374 | -51.4381±3.434 |
| | 318 | -53.524±2.288 | 32.029±3.310 | -5.0561±0.386 | -53.1098±3.546 |
| | 328 | -55.208±2.360 | 33.037±3.415 | -5.2153±0.398 | -54.7815±3.657 |
| ΔH° (kJ/mol) | | 0.0513±0.002 | -0.036±0.003 | 0.0061±0.000 | 0.0501±0.004 |
| ΔS° (kJ/mol K) | | 0.1685±0.007 | -0.101±0.010 | 0.0159±0.001 | 0.1672±0.011 |

### 5.2.6. Adsorption kinetics

The adsorption experimental data was best described by the pseudo-second-order kinetics that was proved by the obtained values of correlation coefficient (Table 5.6). Pseudo-first-order kinetics was not fitted well to the experimental data (Fig. 5.10). The $R^2$ value for As(III) found greater than 0.999 and for As(V), this value was calculated greater than 0.995, when the adsorption was performed by TB 800.

Whereas, the value of $R^2$ was >0.996 for As(III) and As(V) removal by the LB 800 as shown in the Fig. 5.11. The obtained values of kinetics study has been listed in Table 5.6.

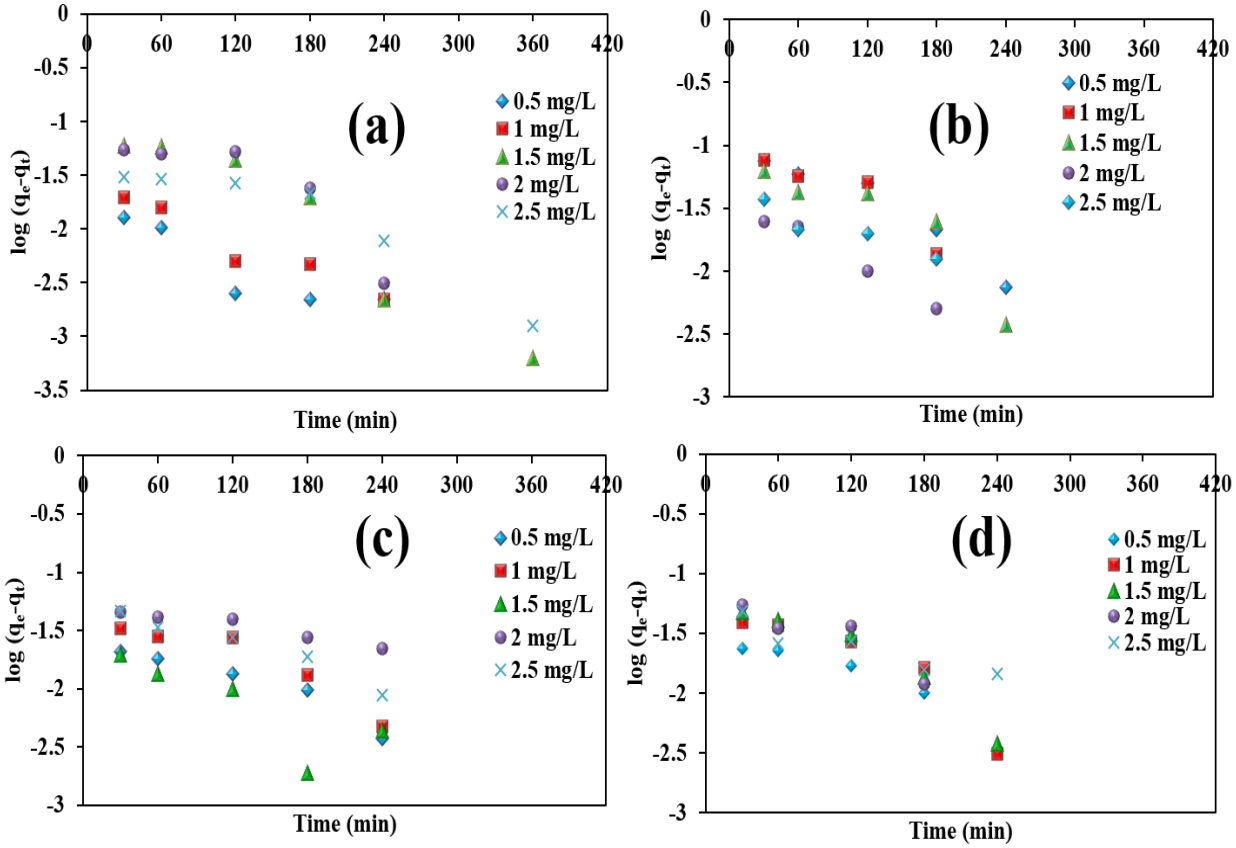


**Fig. 5.10. Plots for pseudo-first-order kinetics, (a) and (b) of As(III) and As(V) adsorption by the application of TB 800 and (c) and (d) of As(III) and As(V) adsorption by the application of LB 800.**

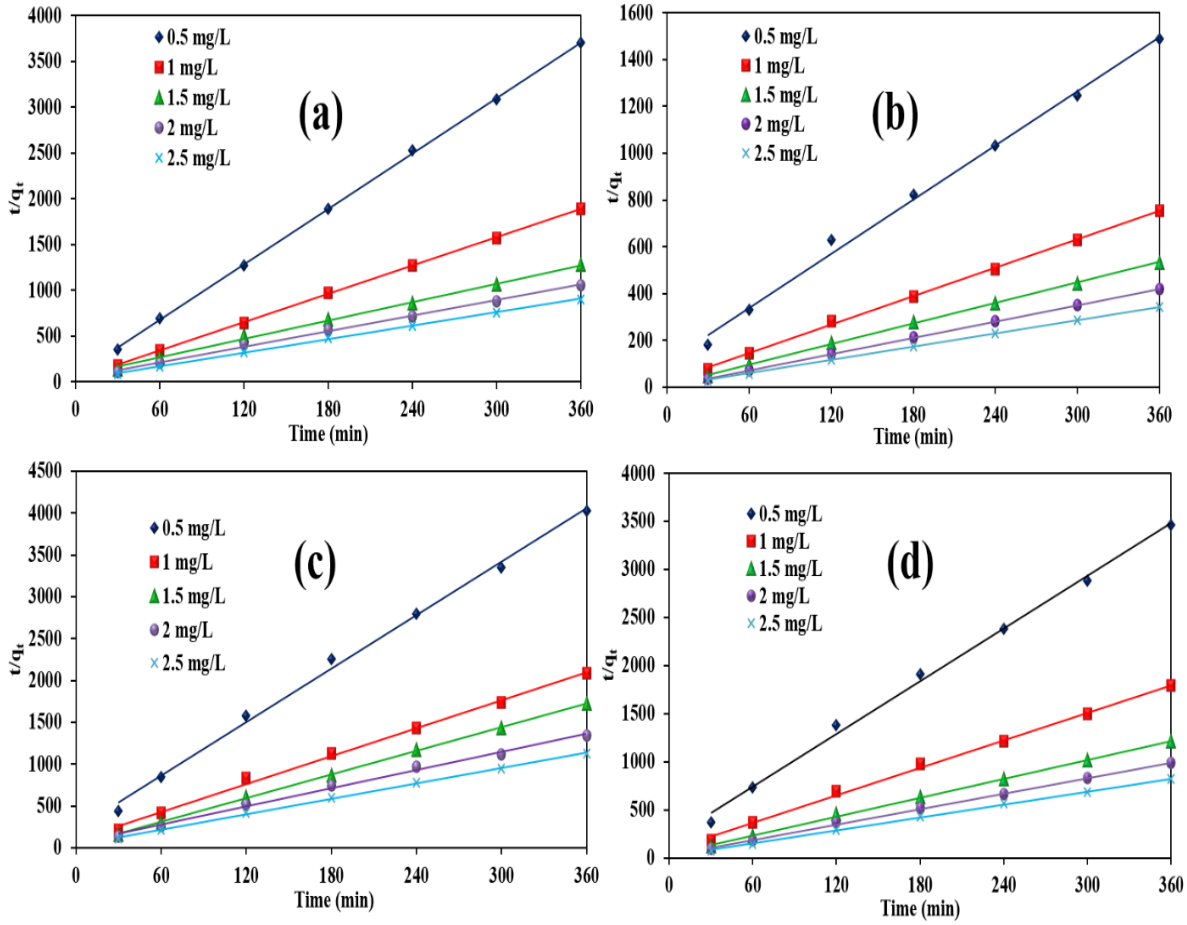


**Fig. 5.11. Plots for pseudo-second-order kinetics, (a) and (b) of As(III) and As(V) adsorption by the application of TB 800 and (c) and (d) of As(III) and As(V) adsorption by the application of LB 800.**

**Table 5.6. Values of kinetic parameters pseudo first order and second order.**

| Kinetics | Pseudo first order kinetics | | | | Pseudo second order | | |
|---|---|---|---|---|---|---|---|
| | $C_0$ (mg/L) | $q_e$ (mg/g) | $k_1$ ($min^{-1}$) | $R^2$ | $q_e$ (mg/g) | $k_2$ (g/mg min)) | $R^2$ |
| TB 800 As(lll) | 0.5 | 0.0140±0.001 | 0.0017±0.009 | 0.797 | 0.0990±0.003 | 1.5193±0.952 | 0.9998 |
| | 1 | 0.0256±0.001 | 0.0020±0.001 | 0.9393 | 0.1938±0.001 | 0.9455±0.062 | 0.9999 |
| | 1.5 | 0.1538±0.001 | 0.0029±0.041 | 0.9253 | 0.2973±0.004 | 0.1804±0.041 | 0.9974 |
| | 2 | 0.1211±0.000 | 0.0023±0.028 | 0.7584 | 0.3544±0.001 | 0.1837±0.034 | 0.997 |
| | 2.5 | 0.0634±0.007 | 0.0018±0.039 | 0.8725 | 0.4053±0.003 | 0.3594±0.024 | 0.9992 |
| LB 800 As(lll) | 0.5 | 0.0293±0.013 | 0.0014±0.002 | 0.9163 | 0.0938±0.061 | 0.5208±0.028 | 0.9964 |
| | 1 | 0.0529±0.033 | 0.0017±0.000 | 0.8693 | 0.1797±0.124 | 0.3224±0.050 | 0.997 |
| | 1.5 | 0.0232±0.056 | 0.0017±0.001 | 0.6885 | 0.2117±0.183 | 0.8934±0.296 | 0.9997 |
| | 2 | 0.0524±0.043 | 0.0007±0.001 | 0.9357 | 0.2765±0.225 | 0.2137±0.016 | 0.9944 |
| | 2.5 | 0.0585±0.031 | 0.0014±0.000 | 0.9499 | 0.3253±0.246 | 0.2932±0.076 | 0.999 |
| TB 800 As(V) | 0.5 | 0.1223±0.015 | 0.0020±0.000 | 0.925 | 0.2591±0.005 | 0.1392±0.012 | 0.9955 |
| | 1 | 1.0000±0.522 | 0.0020±0.000 | 0.8442 | 0.4932±0.022 | 0.1812±0.084 | 0.999 |
| | 1.5 | 0.1088±0.047 | 0.0022±0.001 | 0.7984 | 0.6854±0.016 | 0.2307±0.227 | 0.9996 |
| | 2 | 0.0388±0.042 | 0.0021±0.001 | 0.9837 | 0.8608±0.032 | 0.6219±1.339 | 1 |
| | 2.5 | 0.0390±0.010 | 0.0012±0.001 | 0.8638 | 1.0595±0.015 | 0.4580±1.566 | 1 |
| LB 800 As(V) | 0.5 | 0.004±0.003 | 1.4053±0.789 | 0.8914 | 0.1095±0.001 | 0.4318±0.108 | 0.9967 |
| | 1 | 0.0049±0.004 | 1.1289±0.686 | 0.8455 | 0.2098±0.001 | 0.2809±0.058 | 0.9978 |
| | 1.5 | 0.0051±0.004 | 1.0646±0.644 | 0.9104 | 0.3055±0.001 | 0.2714±0.134 | 0.9991 |
| | 2 | 0.0039±0.003 | 1.1449±0.697 | 0.8263 | 0.3741±0.013 | 0.2698±0.096 | 0.9991 |
| | 2.5 | 0.0023±0.002 | 1.3362±0.805 | 0.8553 | 0.4446±0.003 | 0.3196±0.066 | 0.9993 |

### 5.2.7. Intraparticle diffusion model of kinetics

In this study, the linear regression drawn on the graph does not passed through the origin of the plot and resulted that As(III) and As(V) adsorption by TB 800 and LB 800, the intraparticle diffusion model was not only the rate controlling factor (Fig. 5.12).

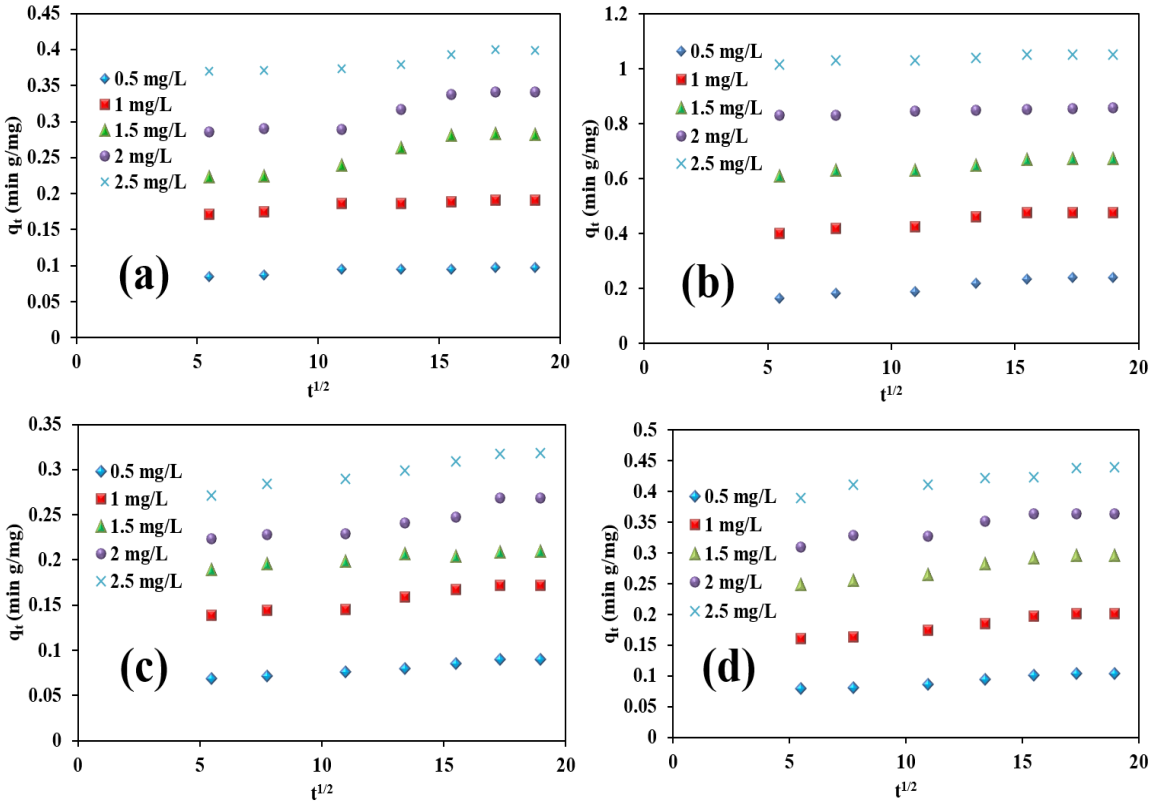


**Fig. 5.12. Intraparticle diffusion model for (a) and (b) As(III) and As(V) adsorption by the application of TB 800 and (c) and (d) As(III) and As(V) adsorption by LB 800.**

### 5.2.8. Arsenic removal from groundwater samples

In this study the maximum adsorption capacity for As adsorption was achieved by TB 800. So, TB 800 was used to treat the groundwater contaminated with As. The adsorption of As(III) was ~71.17, ~79.79, ~78.38, ~81.00 and 82.25 %, and respectively

for MK, HP, BG, J-I and J-II. However, for the sample MK, HP, BG, J-I and J-II the removal percentage of As(V) was ~89.72, ~87.98, ~90.67, ~87.36 and ~93.96 %, respectively.

### 5.2.9. Mechanism involve in adsorption of arsenic

The Fig. 5.13, shows the adsorption mechanism of As on biochar. The As(III) and As(V) adsorption was might be due to the electrostatic interaction, complexation of surface (Niazi et al., 2018; Zhang et al., 2013). As it was observed that the many of oxygenated functional groups were present on the biochar surface like hydroxyl and carboxyl group that play a vital role in sorption mechanism of As on biochar (Zhang et al., 2015).

Electrostatic interaction mainly depends on the surface charge of biochar and the charge on the adsorbent. TB 800 and LB 800 contains negative charge on it means $OH^-$ ions ($pH_{ZPC}$ ~8 and pH~9) and the Arsenic species exhibits positive charge. Hence, the arsenic with positive charges was attracted towards the biochar with negative surface charge. A pH of solution and surface charge on adsorbent play a vital role in adsorption of Arsenic species on the biochar surface. The pH study revealed that the maximum removal of arsenic was obtained in basic medium except As(V) removal by TB 800 (6 pH), Samsuri et al. (2013) also reported similar results, in which the maximum adsorption of arsenic was observed at alkaline pH around 6-9.

Complexation of arsenic with the functional groups present on biochar regulates As adsorption through biochar. Change in the pH of the solution also changes the complexation behavior of the functional group like carbonyl, hydroxyl and amino and increased pH results deprotonation of carbonyl group that effectively complex with the

metal with positive charge (Pulido-Novicio et al., 2001; Zhang et al., 2013; Yuan et al., 2011). The adsorption of As on biochar is based on the chemisorption and physisorption mechanism. When the biochar interacts with the As solution then due to the presence of $OH^-$ and $COO^-$ ions the As gets attracted towards the biochar. After the first level of chemisorption the biochar makes a complex structure with the As molecule.

FTIR spectra shows the shift and decreased intensities of hydroxyl (3435 $cm^{-1}$), C=C bond of alkenes (1548 $cm^{-1}$) and carboxylic acid group (1414 $cm^{-1}$) after arsenic loading on biochar. It was observed that a peak with wavenumber 1548 $cm^{-1}$ present on the TB 800 that was further disappeared after the process of adsorption that may be due to the adsorption of As species on that active site of adsorbent. The appearance of a new peak with wavenumber 1618 $cm^{-1}$ in the FTIR spectrum of LB 800 after the adsorption of As onto its surface, which were indicative to the As adsorption (Wang et al., 2015).

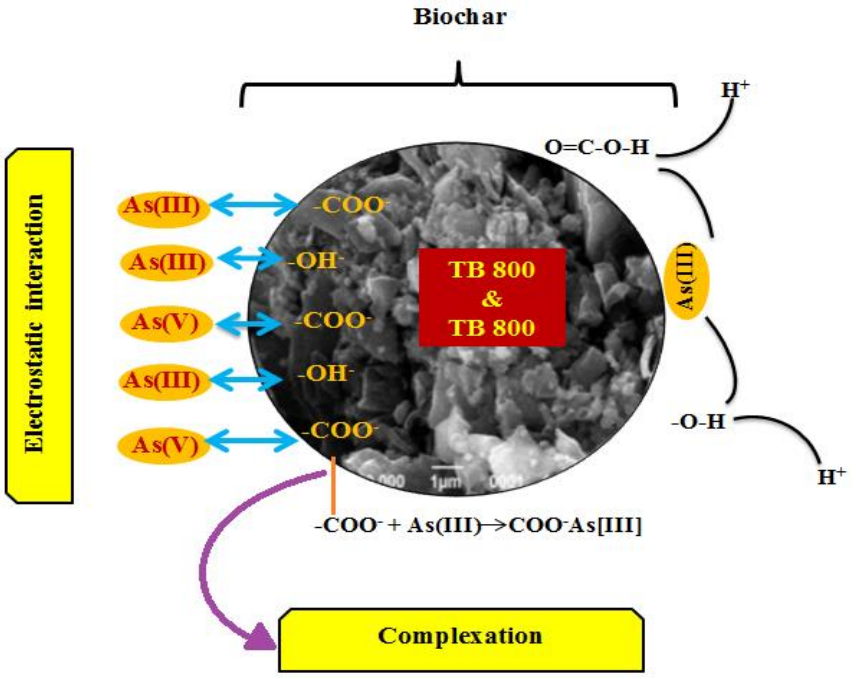


**Fig. 5.13. Proposed mechanism of As(III and V) adsorption onto the surface of TB 800 and LB 800.**

## 5.3. Phase II: Characterization of magnetic biochar synthesized using waste dry leaves and their application for the removal of As(III) and As(V) from aqueous solution and groundwater

### 5.3.1. Characterization of biochar

#### *5.3.1.1. SEM and EDX*

SEM analysis was conducted to evaluate the surface morphological structure of the biosorbents. Obtained results revealed that the MTB-800 (Fig. 5.14a) has a rough surface and is irregular in shape and MLB-800 (Fig. 5.14c) entails a smooth surface with an irregular structure. EDX analysis illustrated the elemental composition of both the biosorbents (Fig. 5.14b and d).

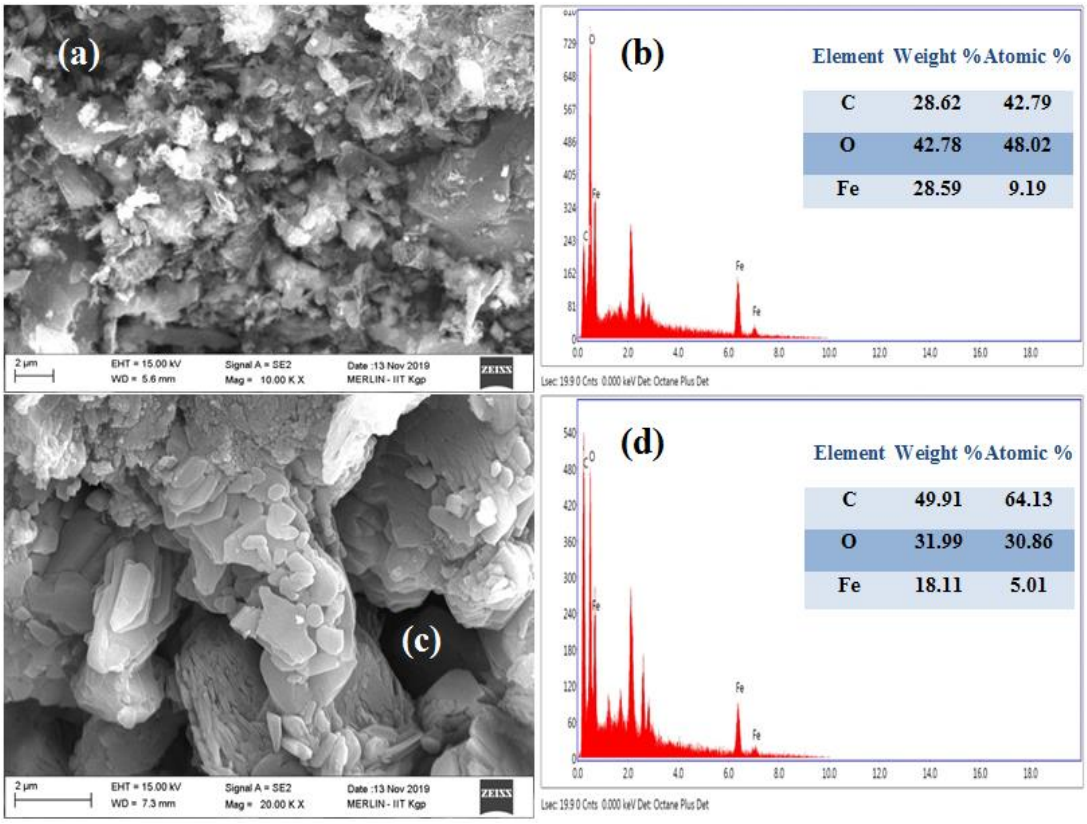


**Fig. 5.14. SEM images of the (a) and (c) MTB-800 and MLB-800, respectively, (b) and (d) EDX images of MTB-800 and MLB-800, respectively.**

The results portrayed that the MTB-800 contains 42.79 % carbon by an atomic percentage which is less than the carbon content of MLB-800 i.e., 64.13 %. MTB-800 (9.19 %) consist higher amount of iron than the MLB-800 (5.01%).

#### *5.3.1.2. FTIR*

FTIR was performed for surface functional groups determination present on MTB-800 and MLB-800 before and after As(III) and As(V) adsorption (Fig. 5.15). Before loading of As (III) and As(V), numbers of peaks were found at wavenumber ranges from 3408 $cm^{-1}$ -3827.87 $cm^{-1}$ (MTB-800) and 3338.44 $cm^{-1}$ -3911.35 $cm^{-1}$ (MLB-800) were assigned for the presence of hydroxyl group (-OH) (Ali et al., 2020). Peaks at wavenumber 2340.35 $cm^{-1}$ and 2374.82 $cm^{-1}$ correspond to $CH_2$ stretching, respectively for MTB-800 and MLB-800. The peaks at 1522.84 $cm^{-1}$ (MTB-800) and 1530.23 $cm^{-1}$ (MLB-800) wavenumber corresponds to the carboxyl group (-COOH). Whereas, the peaks near wavenumber 1138.71 $cm^{-1}$, 1132.14 $cm^{-1}$ are assigned to O=C-O or C-O stretching. Peaks appear at wavenumber 977.83 (MLB-800) and 880.16 (MTB-800 and MLB-800) representing aromatic hydrogen group (C-H) (He et al., 2018). The functional group band of C-C=O of a carboxylic acid group or Fe-O exists at peaks with wavenumber 573.18 $cm^{-1}$and 566.62 $cm^{-1}$ (Ajmal et al., 2020). The existence of functional group C-N-C was found at 482.07 $cm^{-1}$ and 447.60 $cm^{-1}$ wavenumbers.

After As(III) and As(V) adsorption, it was examined that some of the corresponding FTIR peaks were shifted at 3855.54, 3799.72, 3666.75 $cm^{-1}$ for OH, 2382.21, 2277.15 $cm^{-1}$ for $CH_2$ group, and 1565.70, 1375.92 $cm^{-1}$ for COOH in case of As(III) adsorption by MTB-800 (Fig. 5.15a). However, after adsorption of As(V) by MTB-800 peaks were shifted for some of the functional groups like $CH_2$ and COOH at 2291.10 $cm^{-1}$ and 1565.70

$cm^{-1}$, correspondingly. The intensities of peaks near wavenumber 3408-3827.87 $cm^{-1}$and 1138.71-482.07 $cm^{-1}$ were found to be changed after the adsorption of both As species.

After loading of As(III) and As(V) onto MLB-800, spectral peaks were shifted at 3757.86, 1508.89, 1369.35 $cm^{-1}$ for OH, $CH_2$, and COOH functional groups, respectively, for adsorption of As(III) and As(V) the peaks were shifted for hydroxyl and $CH_2$ at 3925.30 or 3422.16 $cm^{-1}$ and 1564.70 $cm^{-1}$, correspondingly (Fig. 5.15b). Intensities of some of the peaks also observed that confirmed the involvement of surface functional groups in the adsorption process of Arsenic.

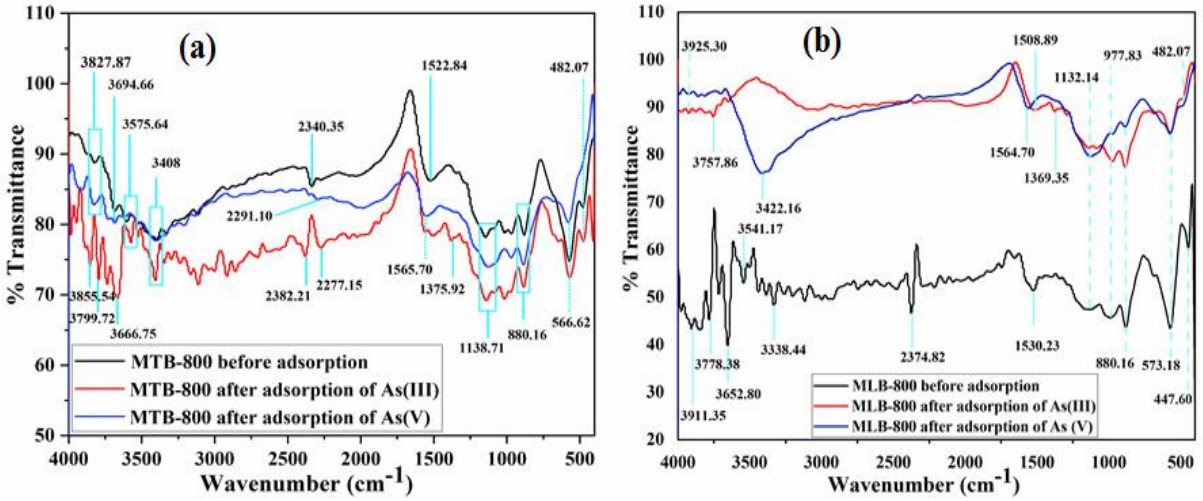


**Fig. 5.15. FTIR spectrum a) MTB-800 and b) MLB-800, before and after As adsorption.**

### *5.3.1.3. XRD Analysis*

The XRD was performed to identify the amorphous and crystalline nature of synthesized biosorbents. A similar XRD spectrum was exhibited by both biosorbents (MTB-800 and MLB-800) as shown in Fig. 5.16a. Both the biosorbents were demonstrated with narrower and distinct peaks that represent the crystalline nature of MTB-800 and

MLB-800. The sharp peaks were obtained at 2θ= 29.9, 34.12, 35.11, 36.29, 41.32, 50.55 and 57.25 that attributes to the occurrence of $Fe_3O_4$ (Ibrahim et al., 2019; Nath et al., 2019).

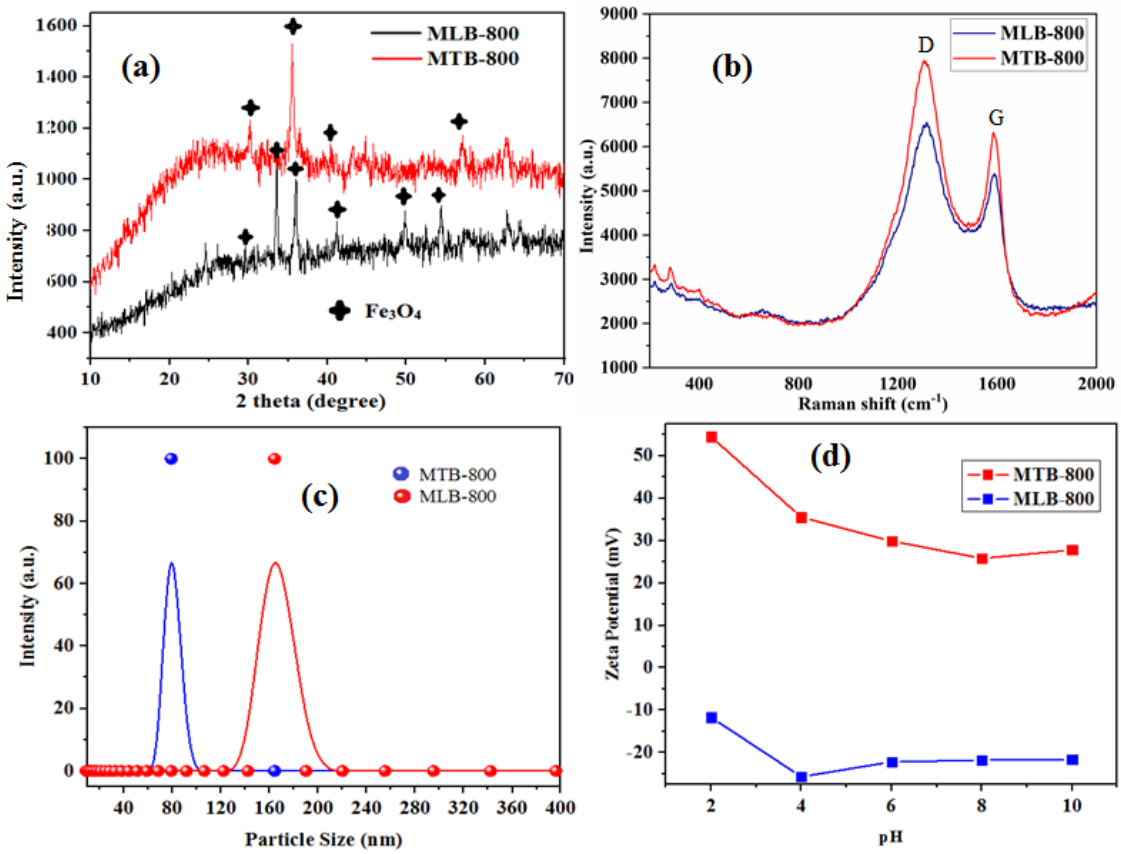


**Fig. 5.16. (a) XRD spectrum, (b) Raman spectroscopy, (c) Particle Size analysis and (d) Zeta potential of MTB-800 and MLB-800.**

### *5.3.1.4. Raman spectroscopy*

Raman spectroscopy is used to evaluate the microstructure of carbon materials. Fig. 5.16b, shows the spectra of biochar materials at 800°C, and range of spectra was 100 to 2000 $cm^{-1}$. Most of the biomass-derived carbon materials are illustrated two distinct peaks which are D-peak and G-peak. In-plane vibration of $sp^2$-bonded crystallite carbon creates G-band at ~1580 $cm^{-1}$, while D-band at ~1350$cm^{-1}$ is attributed to defected structure in the

carbonaceous biochar which comes from in-plane vibration of $sp^2$-bonded carbon. Usually, the D and G bands intensity ratio was used for the determination of crystallization of carbonaceous materials. The ID/IG ratio for MTB-800 and MLB-800 was 1.26 and 1.22, respectively. The high value of ID/IG elucidates that during the process of carbonization structural disorders increased due to the development of pores (Tam et al., 2020). $I_D/I_G$ ratio at 800 °C was found 2.65 in a study performed by Eshun et al, (2019). They were also suggested that the temperature elevation is also increased the $I_D/I_G$. However, the addition of minerals decreases the $I_D/I_G$ ratio of biochar (Chia et al., 2012). Biomass materials have various sate of a combination of chemical structures such as aromatic rings, alkanes, arene which vary in various sources of biomass such as husk, straw and wood (Xu et al., 2020; Mohanty et al., 2013).

#### *5.3.1.5. Particle Size Analysis*

Particle size analysis of MTB-800 and MLB-800 was done by dispersing the MTB-800 and MLB-800 particles in dispersal medium (alcohol) at room temperature and neutral pH. The results of particle size analysis were shown in Fig. 5.16c and reveal that the particle size of the biosorbents was in the nanometer and micrometer range. The size of MTB-800 was found in the range of 60-100 nm whereas; the size of MLB-800 was in the range of 125-220 nm. The intensity of smaller particles of MTB-800 was high as compared to MLB-800, this is might be due to the difference in biomasses used for biosorbents synthesis.

#### *5.3.1.6. Zeta Potential*

The stability of bioadsorbent was examined by the zeta potential at a particular pH. The magnitude of zeta potential designates the bioadsorbents stability in a dispersal

medium that undertakes electrostatic repulsion between the dispersal medium and the bioadsorbent (Verma et al., 2019). The material is said to be stable if the zeta potential value is more than ±30. As presented in Fig. 5.16d the values of zeta potential for MLB-800 were less than ±30 at all the pH hence, the bioadsorbents were unstable. Whereas, the value of zeta potential for MTB-800 at pH 2 was 54.5 mV and at pH 4 was 35.5 mV these values were higher than the zeta potential of MLB-800 (at ±30) at the same pH values.

#### *5.3.1.7. $pH_{ZPC}$*

The net surface charge of synthesized biosorbents was described by $pH_{ZPC}$. It was found that the $pH_{ZPC}$ for MTB-800 was 2.3 and 6.5 for MLB-800. The $pH_{ZPC}$ is the solution at which the biosorbent surface charge is neutral and it plays a very efficient role in the adsorption mechanism of the adsorbate.

### 5.3.2. Adsorption experiment

#### *5.3.2.1. Effect of dose*

The As (III and V) adsorption was conducted at neutral pH, 1 mg/L initial concentration at 25 °C and varying dosages of biochar (MTB-800 and MLB-800) i.e., in the range of 0.5 to 3 g/L (with the interval of 0.5). Fig. 5.17a shows that the removal of As(III) was maximum of 79.4 % at 1.5 g/L doses and 85 % at dose 2.5 g/L on the application of MTB-800 and MLB-800, respectively. On increasing the dose further, there was a slight or no increase in the removal of As occurred. The highest adsorption capacity was attained 1.381 mg/g and 1.501 mg/g for As(III) using MTB-800 and MLB-800, respectively at the lowest dose (0.5 g/L). On increasing the dose of the biosorbent the

adsorption capacity was decreased up to 0.529 mg/g (1.5 g/L dose of MTB-800) and 0.340 mg/g at dose 2.5 g/L of MLB-800.

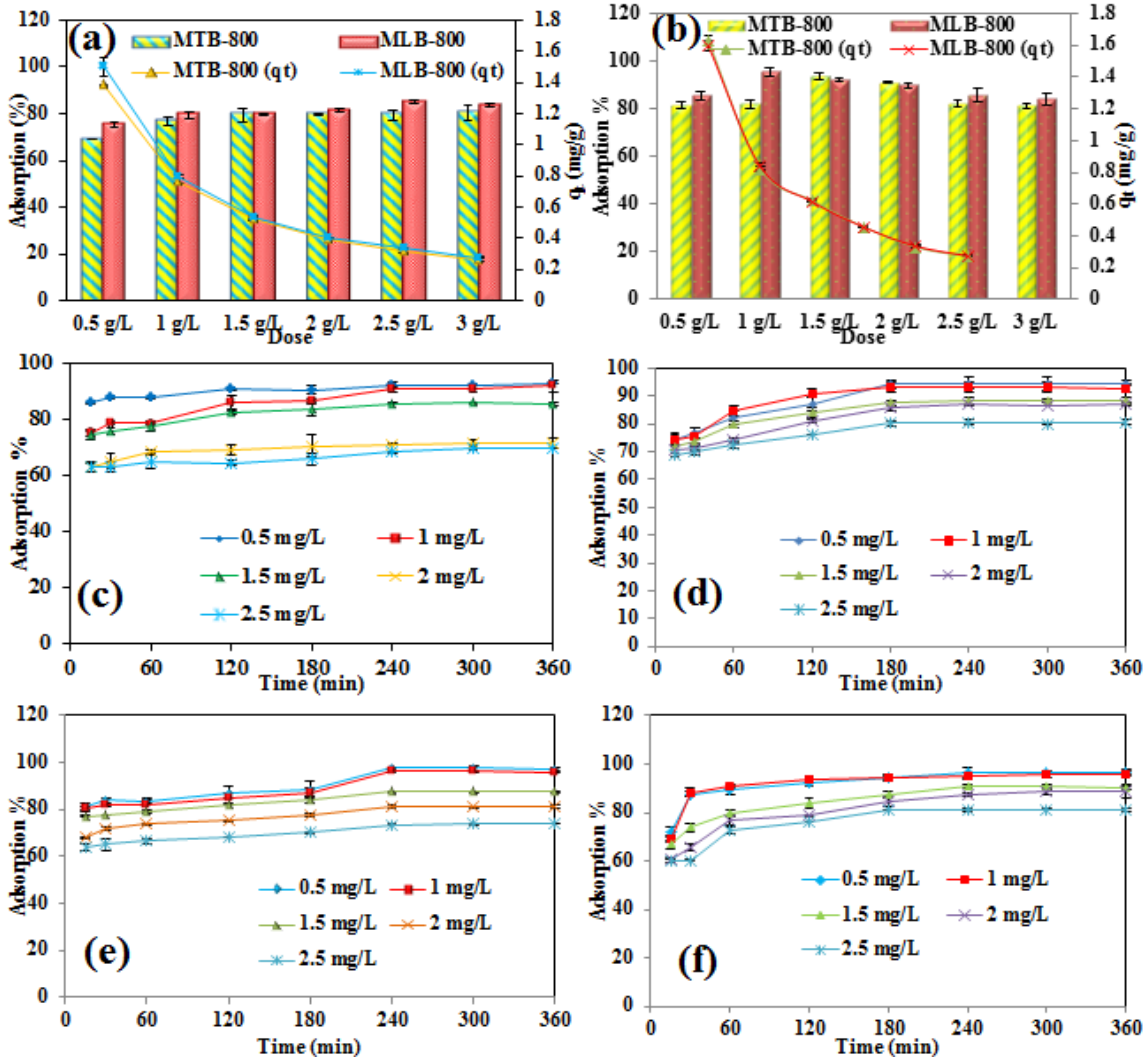


**Fig. 5.17. Effect of adsorbent dose on adsorption of (a) As(III), (b) As(V) by MTB-800 and MLB-800, (c) and (d) Effect of initial concentration on adsorption of As(III) and As(V), respectively, by MTB-800, (e) and (f) Effect of initial concentration on adsorption of As(III) and As(V), respectively, by MLB-800.**

However, the highest removal of As(V) was observed at 1.5 g/L (93.6 %) by MTB-800 and at dose 1 g/L (95.6 %) using MLB-800. As indicated in Fig. 5.17b that the

maximum adsorption capacity was found at the lowest dose i.e., 1.627 mg/g and 0.597 mg/g for As(V) using MTB-800 and MLB-800, separately, on further increasing dose the adsorption capacity of both the biochar materials were decreased. It was obtained that the with increasing dose of biochar, removal percentage of adsorbate also increased but after certain limits, an increasing the amount of biochar removal of As was not increased due to the agglomeration of the biosorbent particles that forms a cluster which ultimately decreases the available active sites and surface area (Siddiqui et al., 2019).

#### *5.3.2.2. Effect of initial concentration of arsenic and contact time*

Varying initial As concentration from 0.5 mg/L to 2.5 mg/L were used for the study of the influence of As concentration on its adsorption with a fixed amount of dose, neutral pH and 25 °C temperature. The results demonstrated that the removal of As was decreased with an increasing initial concentration. The maximum removal of As(III) was found to be 92.1 % and 97.8 % by MTB-800 (Fig. 5.17c) and MLB-800 (Fig. 5.17e), correspondingly. However, the highest adsorption of As(V) was 94.7 % and 96.7 % on applying MTB-800 (Fig. 5.17d) and MLB-800 (Fig. 5.17f) biosorbents, respectively, at lower As initial concentration i.e., 0.5 mg/g.

The adsorption capacity of both the biosorbents (MTB-800 and MLB-800) was increased with increasing the initial concentration of As. The maximum adsorption capacity for As(III) was 1.157 mg/g and 0.739 mg/g for MTB-800 and MLB-800, respectively (Fig. 5.18a and c), whereas the highest capacity for As(V) adsorption was obtained 1.345 mg/g using MTB-800 and 1.354 mg/g for MLB-800 at 2.5 mg/L initial As concentration (Fig. 5.18b and d).

The whole study was conducted for a total of 6 h, on using MTB-800 and MLB-800 both the As species show a similar pattern of adsorption i.e., with an increasing time the As(III) and As(V) adsorption was also increased and the equilibrium was achieved within 4 h after that no significant increase in As (III and V) adsorption was noticed. The obtained result was explained as, initially, there were many available vacant active sites on biosorbent surface hence, more As molecules get adsorbed by the biochar materials readily at a fast rate but after saturation of the active sites, no adsorption was possible further because of unavailability of vacant active sites for As adsorption (Kim et al., 2019).

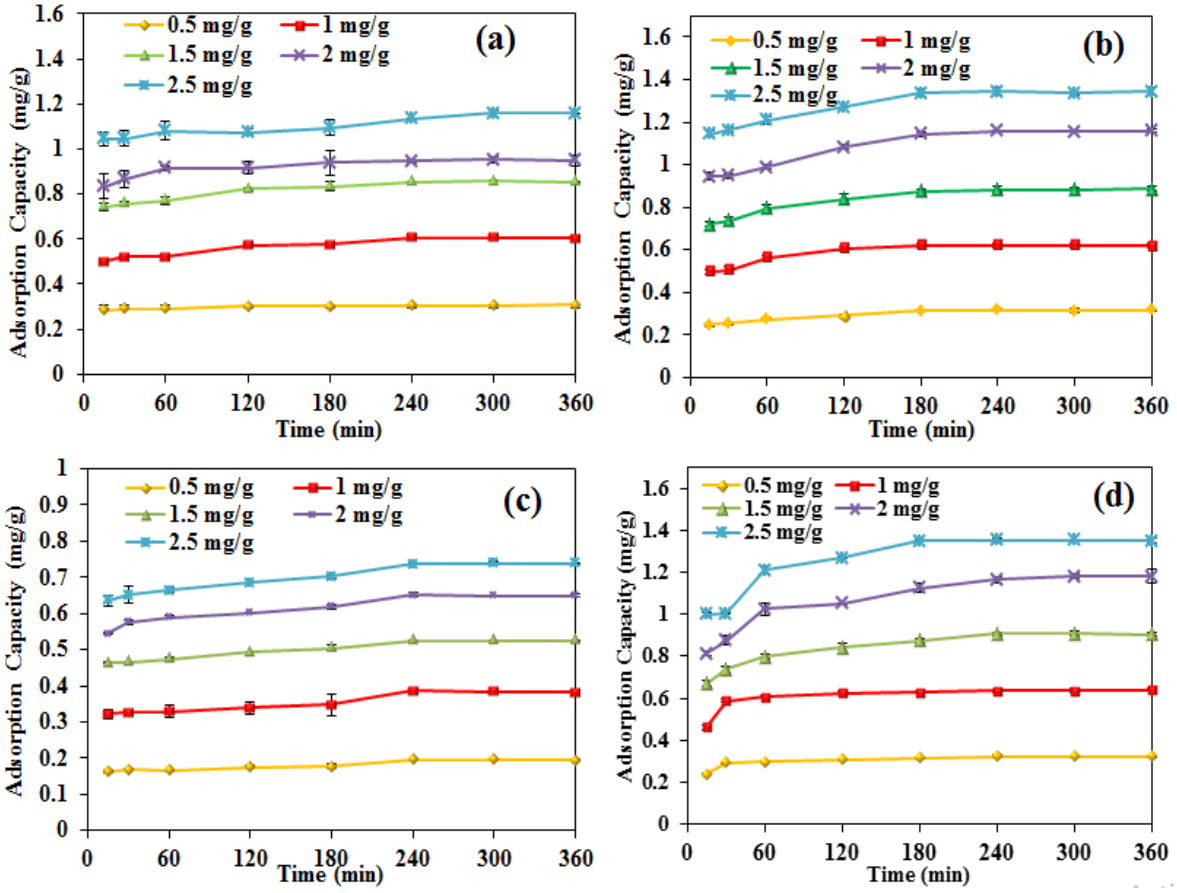


**Fig. 5.18. Adsorption capacity of (a) and (b) As(III) and As(V) adsorption, respectively, by MTB-800, (c) and (d) As(III) and As(V) adsorption, respectively, by MLB-800.**

### *5.3.2.3. Effect of pH on Arsenic adsorption*

The solution pH is one of the truly significant aspects in the process of adsorption. The pH of the solution affects the adsorption process by changing the biosorbents surface charge, stimulating the functional groups of biochar, and altering the As form in an aqueous solution (Shakoor et al., 2016).

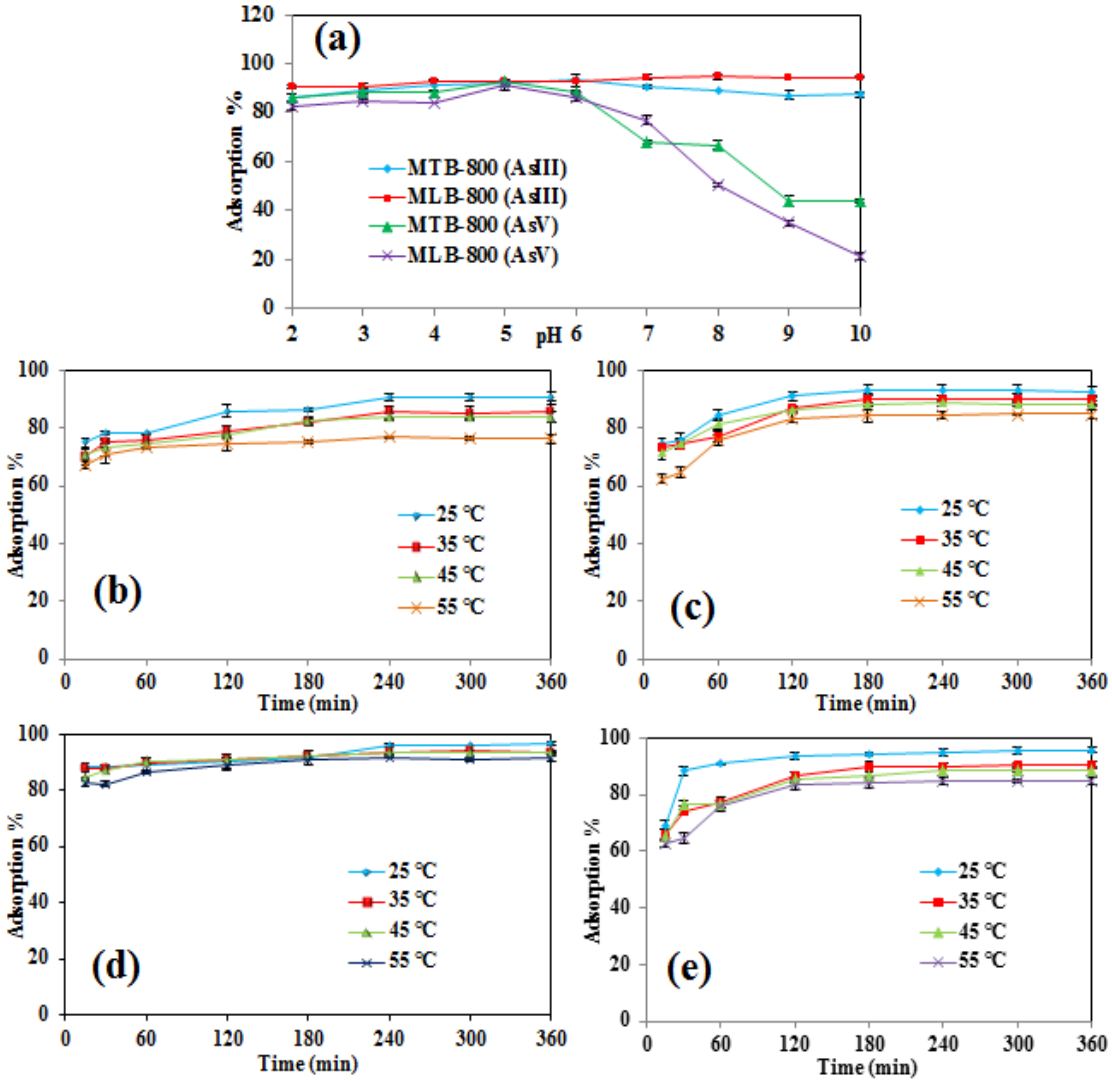


**Fig. 5.19. (a) Effect of pH on As(III) and As(V) adsorption by MTB-800 and MLB-800, Effect of temperature on adsorption of (b) and (c) As(III) and As(V) by MTB-800, respectively, (d) and (e) As(III) and As(V) by MLB-800, respectively.**

The Fig. 5.19a represents the obtained result of the pH study that reveals that the highest As(III) adsorption was 93.6 % found at pH 6 by applying MTB-800, however, at pH 8 removal was found to be 94.6 % by applying MLB-800. Although, the highest adsorption of As(V) was 92.85 % and 91.1 % obtained at pH 5 by using MTB-800 and MLB-800, respectively. The removal of As(V) was highly decreased in an alkaline medium. The adsorption of both the As species by applying MTB-800 and MLB-800 was found in between the pH range of 5-8. As acquires a positive charge and the $pH_{ZPC}$ of MTB-800 was 2.3 beyond this pH the biosorbent consists negative charge on it and attracts positive charge on As species while, the $pH_{ZPC}$ value of MLB-800 was 6.5 that means at this pH biosorbent entails zero charge or neutral charge thus, attracts both negatively and positively charged adsorbate. As removal is greatly dependent on the pH of the solution and species of As to be adsorbed (Vithanage et al., 2017).

#### *5.3.2.4. Influence of temperature on Arsenic removal*

The study of temperature effect on the process of adsorption of both the species of As is one of the most significant parameters that help to stimulate the rate of reaction. The obtained results describe that on increasing temperature from 25°C to 55°C the adsorption percentage was decreased for adsorption of As(III) and As(V) on the application of both the biosorbents (MTB-800 and MLB-800) (Fig. 5.19b-e).

Fig. 5.19b and d shows that the maximum adsorption of As(III) was 90.9 % ($q_e$=0.606 mg/g) and 96.8 % ($q_e$=0.387 mg/g) obtained at lowest temperature by applying MTB-800 and MLB-800, correspondingly. A similar removal pattern was also obtained for the removal of As(V) and the highest adsorption percentage was found at 25°C temperature by both the prepared biosorbents MTB-800 (90.35% ) with $q_e$ value 0.602 mg/g and MLB-

800 (95.6 % and $q_e$=0.634 mg/g) (Fig. 5.19c and e). As (III and V) removal decreased on increasing temperature the process of adsorption was exothermic. Almost similar outcomes were also reported by Shakoor et al. (2018). The removal of As(III and V) was increased with an increasing temperature because the activation of the active sites on biosorbents surface was maximum at low temperature that facilitates the As removal at the minimal temperature (Kazi et al, 2018; Verma et al., 2019).

### 5.3.3. Regeneration study

Regeneration study is a most essential factor that assistances to check the biosorbents stability to adsorb the adsorbate i.e., (As(III and V) from an aqueous solution. For the desorption of As from the used biochar (MTB-800 and MLB-800) NaOH solution (0.1 M) was used.

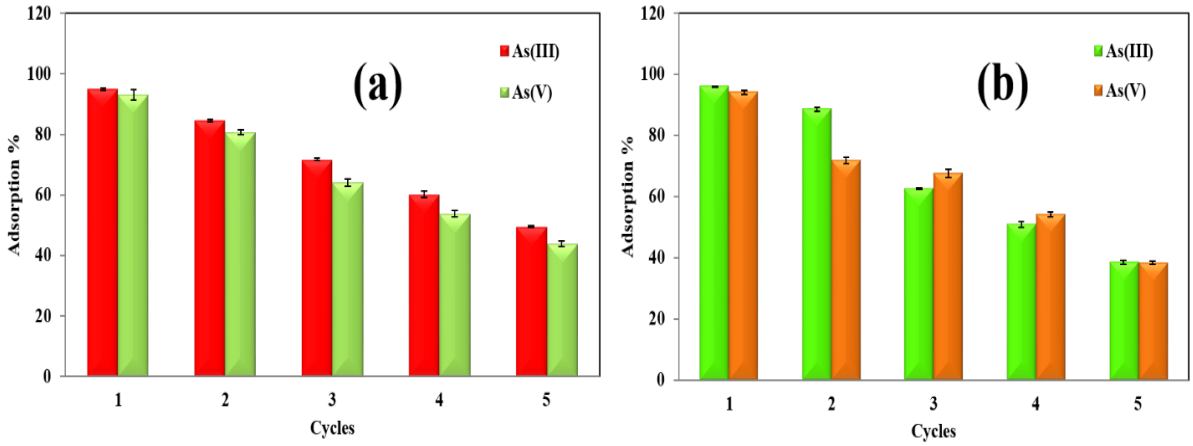


**Fig. 5.20. Regeneration study (a) MTB 800 and (b) MLB 800 for adsorption of As(III) and As(V).**

The regeneration study was conducted for both the biochar materials and the obtained results revealed that both the biosorbents were successfully recycled up to five cycles.

The adsorption of As(III) by MTB-800 was 94.92 % in the first cycle, 84.55% in the second cycle, 71.67% in the third cycle and decreased in the fourth (60.17%) and fifth cycle (49.55%), whereas, the adsorption of As(V) was 93.1 % in an initial cycle and was 43.85% in the fifth cycle by MTB-800 (Fig. 5.20a). Fig. 5.20b shows that the removal of As(III) was 95.9 % and it was decreased to 38.55 % in the fifth cycle by MLB-800. The removal of As(V) was decreased from 94.1 % to 38.35% (first to the fifth cycle) using MLB-800. The efficiency of the biosorbents was analyzed through the number of cycles and the removal percentage of the adsorbate. An almost similar desorption pattern was obtained for the As removal by both the biochar materials (MTB-800 and MLB-800).

### 5.3.4. Adsorption isotherms

Isotherm study revealed that the Langmuir model of isotherm was best fitted to the As(III) adsorption process as well as As(V) by both the synthesized biosorbents (MTB-800 and MLB-800) with $R^2$ values close to 1. The values of $R^2$ were 0.9793 and 0.9913 for As(III) adsorption by MTB-800 and MLB-800, respectively. Whereas, for As(V) adsorption, the $R^2$ value was 0.9913 and 0.9944 by using MTB-800 and ML5B-800, respectively (Fig. 5.21a-c). The values of the isotherm study was given in Table 5.7.

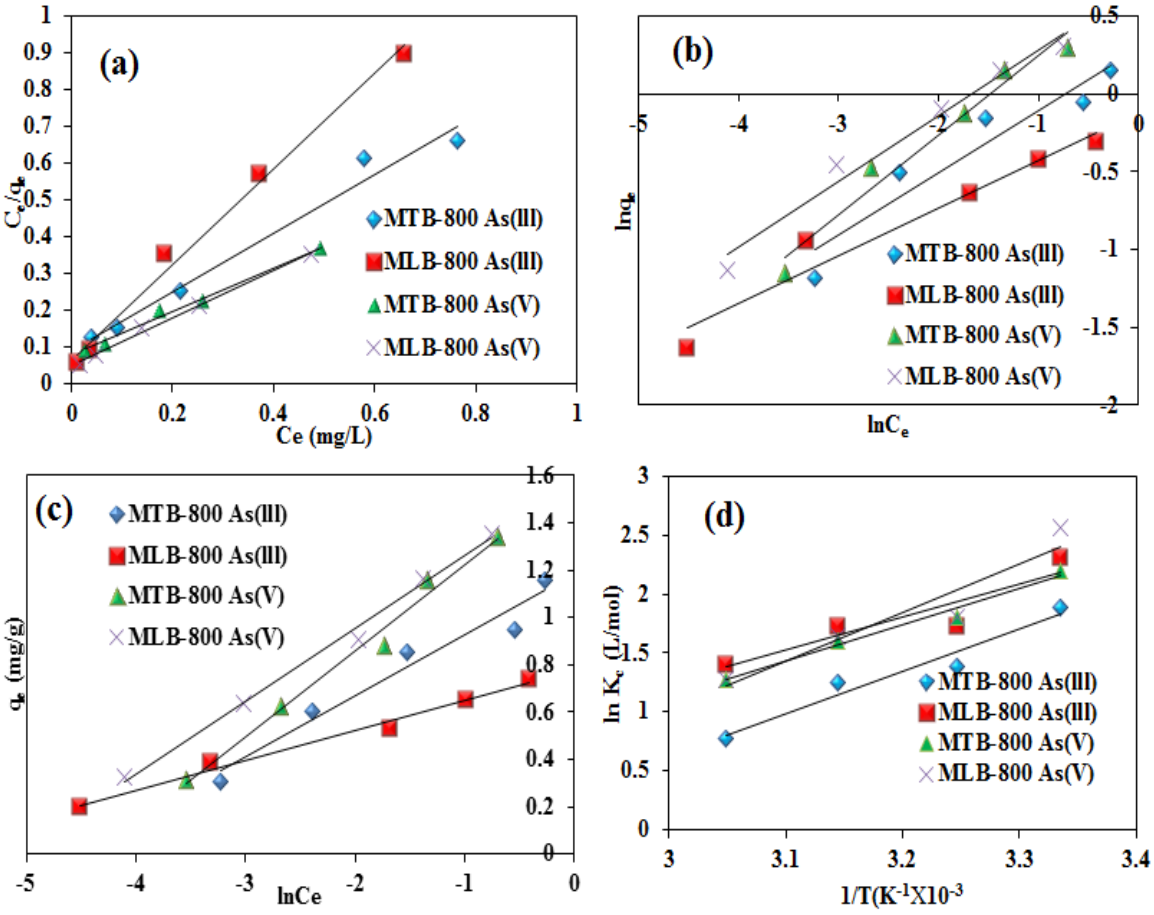


**Fig. 5.21. Plot of (a) Langmuir isotherm (b) Freundlich isotherm (c) Temkin isotherm for As(III) and As(V) adsorption by MTB-800 and MLB-800 and (d) Plot of thermodynamics for As(III) and As(V) adsorption by MTB-800 and MLB-800.**

**Table 5.7. Isotherm parameters for removal of As(lll) and As(V) by synthesized MTB-800 and MLB-800.**

| Isotherms | | As(lll) | | As(V) | |
|---|---|---|---|---|---|
| | | MTB-800 | MLB-800 | MTB-800 | MLB-800 |
| Langmuir isotherm | $Q_e$ (mg/g) | 1.256±0.002 | 0.773±0.006 | 1.682±0.034 | 1.543±0.048 |
| | b (L/mg) | 8.672±0.121 | 19.399±1.727 | 7.690±0.524 | 13.198±2.693 |
| | RL | 0.044±0.001 | 0.020±0.002 | 0.049± 0.003 | 0.029±0.006 |

| | | | | | |
|---|---|---|---|---|---|
| | $R^2$ | 0.9793 | 0.9913 | 0.9913 | 0.9944 |
| **Freundlich Isotherm** | $K_F$ $(mg/g(L/mg)^{1/n})$ | 1.331±0.007 | 0.881±0.009 | 2.122±0.060 | 2.022±0.132 |
| | **n** | 2.505±0.037 | 3.284±0.151 | 1.966±0.059 | 2.362±0.345 |
| | $R^2$ | 0.9055 | 0.9512 | 0.9659 | 0.9745 |
| **Temkin isotherm** | **B** | 0.258±0.002 | 0.126±0.005 | 0.364±0.015 | 0.307±0.044 |
| | $K_T$ **(L/g)** | 98.396±3.703 | 466.47±8.303 | 78.909±8.450 | 163.48±6.231 |
| | $R^2$ | 0.9566 | 0.9862 | 0.9862 | 0.9943 |

### 5.3.5. Thermodynamics

The thermodynamics study revealed that the As(III) and As(V) adsorption by MTB-800 and MLB-800 was exothermic which means the adsorption was reduced on rising temperature. The positive ΔG value supports the obtained result (Fig. 5.21d). All the values of thermodynamics constraints are given in Table 5.8. The value of ΔH for As(III) removal was -0.0299 kJ/mol and -0.0231 kJ/mol, when the adsorption process was performed using MTB-800 and MLB-800, respectively. Whereas, the value of ΔH was found to be -0.0254 kJ/mol and -0.0342 kJ/mol through MTB-800 and MLB-800, separately. The negative value of enthalpy of adsorption (ΔH) assessed that the process of adsorption is exothermic, validating the diminution in the adsorption capacity at equilibrium state with an increasing temperature. The value of ΔH indicates that the process of adsorption was dominated by physisorption than the process of chemisorption (Ma et al., 2018). The ΔS value for As(III) adsorption was -0.0846 kJ/mol and -0.0592 kJ/mol via MTB-800 and MLB-800, individually. The value of ΔS for As(V) adsorption was -0.0254 kJ/mol (MTB-800) and -0.0943 kJ/mol (MLB-800).

**Table 5.8. Thermodynamic parameters of As (III) and As(V) adsorption onto MTB-800 and MLB-800 biosorbents.**

| Parameters | Temperature (K) | As(lll) | | As(V) | |
|---|---|---|---|---|---|
| | | MTB-800 | MLB-800 | MTB-800 | MLB-800 |
| ΔG° (KJ/mol) | 298 | 25.247±5.752 | 17.633±2.121 | 19.976±3.237 | 28.096±6.634 |
| | 308 | 26.093±5.945 | 18.224±2.192 | 20.647±3.345 | 29.040±6.863 |
| | 318 | 26.939±6.138 | 18.817±2.263 | 21.318±3.454 | 29.984±7.086 |
| | 328 | 27.785±6.331 | 19.410±2.335 | 21.988±3.563 | 30.927±7.309 |
| ΔH° (KJ/mol) | | -0.030±0.01 | -0.023±0.002 | -0.026±0.004 | -0.0343±0.007 |
| ΔS° (KJ/mol K) | | -0.085±0.02 | -0.059±0.007 | -0.067±0.011 | -0.094±0.022 |

### 5.3.6. Adsorption kinetics

After studying pseudo-first-order kinetics (Fig. 5.22a-d) and pseudo-second-order kinetics the kinetics model it was revealed that the As(III) and As(V) adsorption by MTB-800 and MLB-800 was best fitted to the pseudo-second-order kinetics. The $R^2$ value for As(III) adsorption was greater than 0.9991 and 0.9995 for As(V) by MTB-800 (Fig.5.23a-d). However, for adsorption of As(III) and As(V) the $R^2$ value was more than 0.9968 and 0.9992, correspondingly on the application of MLB-800 (Table 5.9).

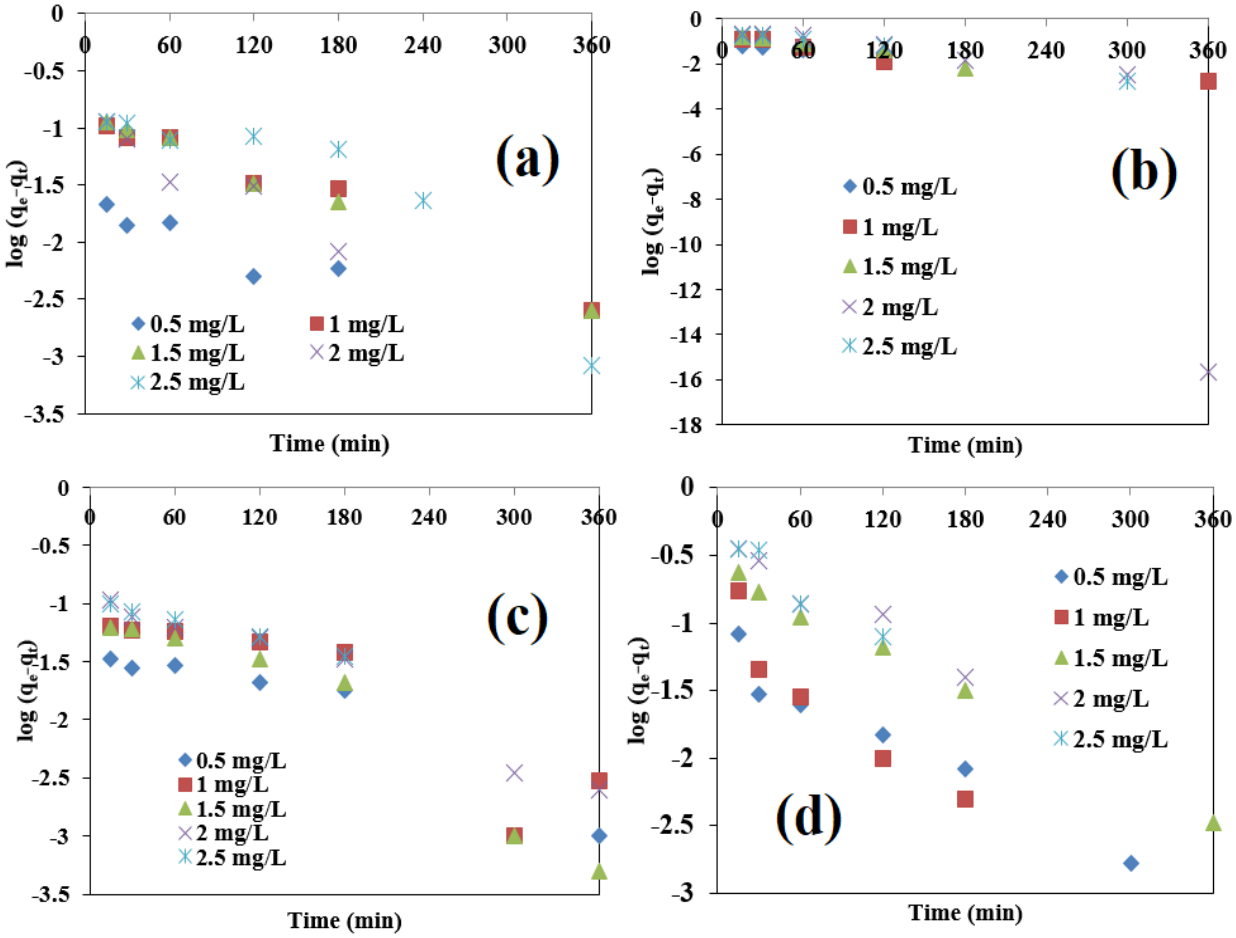


**Fig. 5.22. Graphs of pseudo first order kinetics for adsorption of (a) and (b) As(III) and As(V) by MTB-800, respectively, (c) and (d) As(III) and As(V) adsorption by MLB-800, respectively.**

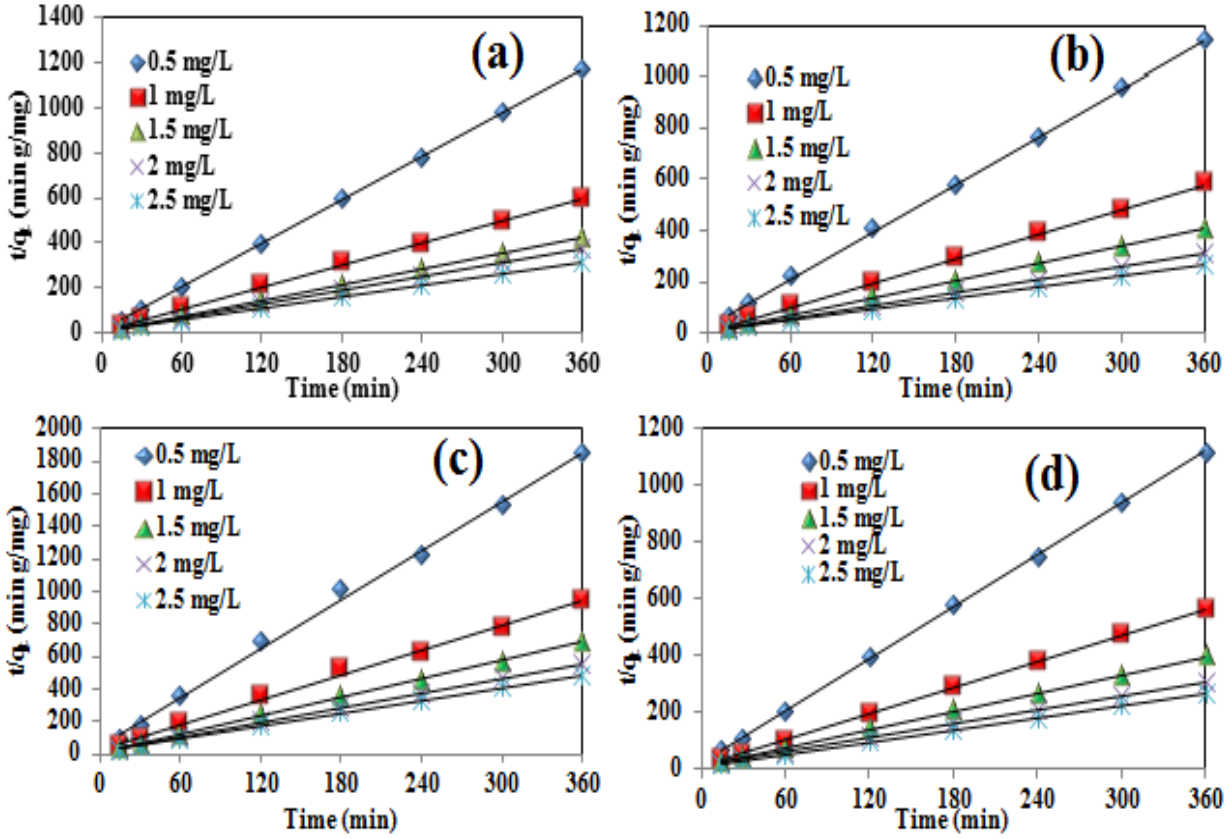


**Fig. 5.23. Plots for pseudo second order kinetics for adsorption of (a) and (b) As(III) and As(V) by MTB-800, respectively, (c) and (d) As(III) and As(V) by MLB-800, respectively.**

**Table 5.9. Values of kinetic parameters pseudo first order and second order.**

| Kinetics | | Pseudo-first-order kinetics | | | Pseudo-second-order | | |
|---|---|---|---|---|---|---|---|
| | $C_0$ (mg/L) | $q_e$ (mg/g) | $k_1$ ($min^{-1}$) | $R^2$ | $q_e$ (mg/g) | $k_2$ (g/mg min)) | $R^2$ |
| MTB-800 As(lll) | 0.5 | 0.02099±0.0021 | 0.0016±0.0002 | 0.8115 | 0.3094±0.0007 | 1.2643±0.2363 | 0.9999 |
| | 1 | 0.13406±0.0179 | 0.0011±0.0003 | 0.9736 | 0.6159±0.0126 | 0.2246±0.0344 | 0.9993 |
| | 1.5 | 0.1414±0.0065 | 0.0020±0.0005 | 0.9932 | 0.8663±0.3210 | 0.2304±0.7633 | 0.9998 |
| | 2 | 0.1196±0.0344 | 0.0027±0.0013 | 0.9177 | 0.9590±0.0100 | 0.3117±1.2939 | 0.9999 |
| | 2.5 | 0.2299±0.0537 | 0.0024±0.0007 | 0.8129 | 1.1670±0.0021 | 0.1526±0.0271 | 0.9991 |
| MTB-800 As(V) | 0.5 | 0.0770±0.0018 | 0.0019±0.0002 | 0.9948 | 0.3232±0.0038 | 0.3799±0.0038 | 0.9995 |
| | 1 | 0.1221±0.0218 | 0.0023±0.0008 | 0.9471 | 0.6323±0.0058 | 0.2856±0.0058 | 0.9998 |
| | 1.5 | 0.2543±0.0637 | 0.0035±0.0010 | 0.9567 | 0.9020±0.0035 | 0.1754±0.0035 | 0.9999 |
| | 2 | 25.972±14.8171 | 0.0135±0.0063 | 0.5838 | 1.1864±0.0043 | 0.1061±0.0043 | 0.9995 |
| | 2.5 | 0.3211±0.0564 | 0.0032±0.0007 | 0.979 | 1.3656±0.0193 | 0.1331±0.0193 | 0.9997 |
| MLB-800 As(III) | 0.5 | 0.0511±0.0082 | 0.0018±0.0003 | 0.8941 | 0.1993±0.0012 | 0.5104±0.0488 | 0.9973 |
| | 1 | 0.1103±0.0231 | 0.0021±0.0005 | 0.8066 | 0.3922±0.0008 | 0.2480±0.0589 | 0.9968 |
| | 1.5 | 0.1229±0.0274 | 0.0028±0.0009 | 0.9412 | 0.5329±0.0000 | 0.3184±0.0239 | 0.9995 |
| | 2 | 0.1372±0.0066 | 0.0021±0.0002 | 0.9538 | 0.6596±0.0021 | 0.2325±0.0103 | 0.9993 |
| | 2.5 | 0.10571±0.0455 | 0.0012±0.0007 | 0.9951 | 0.7505±0.0021 | 0.1962±0.0201 | 0.9992 |
| MLB-800 As(V) | 0.5 | 0.0627±0.0108 | 0.0023±0.0005 | 0.9527 | 0.3270±0.0024 | 0.5445±0.0594 | 0.9999 |
| | 1 | 0.1187±0.0917 | 0.0036±0.0036 | 0.8967 | 0.6465±0.0007 | 0.3471±0.0099 | 1 |
| | 1.5 | 0.2597±0.0603 | 0.0023±0.0006 | 0.9964 | 0.9289±0.0085 | 0.1246±0.0233 | 0.9996 |
| | 2 | 0.3935±0.0635 | 0.0023±0.0004 | 0.9456 | 1.2183±0.0223 | 0.0682±0.0159 | 0.9992 |
| | 2.5 | 0.4486±0.0614 | 0.0028±0.0002 | 0.9286 | 1.3902±0.0127 | 0.0843±0.0079 | 0.9996 |

### 5.3.7. Intraparticle diffusion model

As presented in Fig. 5.24a-d, which the linear line of the plot was not passing the origin that means the intraparticle diffusion was not the only rate-limiting factor that affects the rate of reaction.

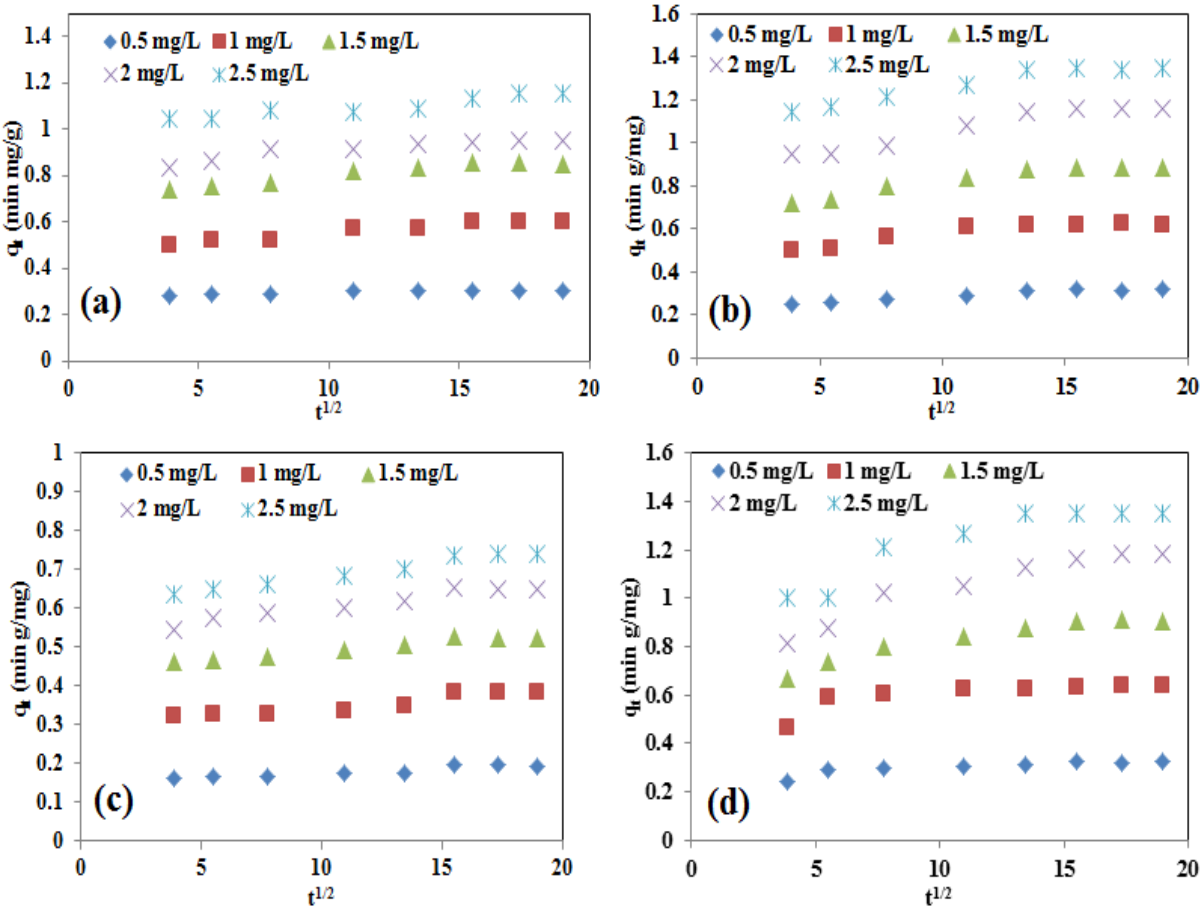


**Fig. 5.24. Graphs of intraparticle diffusion model for adsorption of (a) and (b) As(III) and As(V) by MTB-800, respectively, (c) and (d) As(III) and As(V) adsorption by MLB-800, respectively.**

### 5.3.8. Column adsorption study

#### *5.3.8.1. Effect of influent flow rate*

The breakthrough curve for removal of As(III and V) was obtained at two different influent flow rates (2.5 and 5 mL/min) with a constant 6 cm bed depth and initial

concentration of As 1 mg/L. the obtained breakthrough curve has been shown in Fig. 5.25a and the values of other constraints were epitomized in Table 5.10.

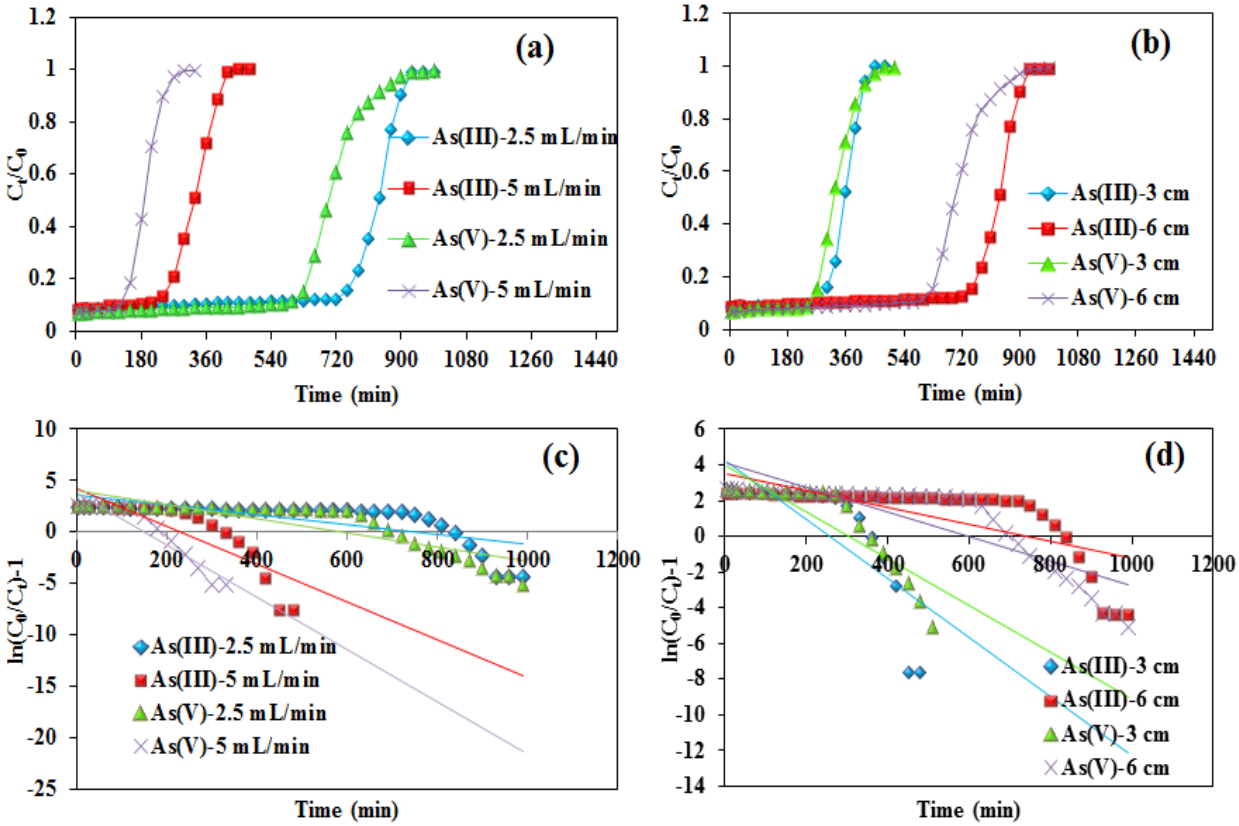


**Fig. 5.25. Breakthrough curve (a) effect of flow rate (b) effect of bed height; plots for Thomas model, (c) effect of flow rate and (d) effect of bed height.**

The experimental data revealed that with increasing flow rate the exhaustion time and breakthrough time have been decreased because at a higher influent flow rate the contact time of adsorbate with the adsorbent bed in the column also decreased. While at a lower As feed flow rate the time of exhaustion and the breakthrough time increases due to more residence time of Arsenic in the column.

**Table 5.10. Parameters of fixed bed column study (breakthrough curve) and Thomas model**

| | Column parameters | | | | | | | | Thomas model parameters | | |
|---|---|---|---|---|---|---|---|---|---|---|---|
| | $C_0$ (mg/L) | Z (cm) | Q (mL/min) | $t_{total}$ (min) | $m_{total}$ | $q_{total}$ (mg) | $q_{eq}$ (mg/g) | $V_{eff}$ (mL) | $K_{TH}$ m($min^{-1}$ $mg^{-1}$) | $Q_0$ (mg/g) | $R^2$ |
| As(III) | 1 | 3 | 2.5 | 480 | 1.2 | 0.8144 | 0.3017 | 1200 | 0.0166±0.0008 | 238.7439±8.0954 | 0.6147 |
| | 1 | 3 | 5 | 240 | 1.2 | 0.655 | 0.2426 | 1200 | 0.0316±0.0028 | 206.9567±5.1870 | 0.8722 |
| | 1 | 6 | 2.5 | 990 | 2.475 | 1.8688 | 0.3461 | 2475 | 0.0048±0.0002 | 342.0043±7.4577 | 0.5188 |
| | 1 | 6 | 5 | 480 | 2.4 | 1.475 | 0.2732 | 2400 | 0.0183±0.0008 | 215.5283±4.8339 | 0.7191 |
| As(V) | 1 | 3 | 2.5 | 510 | 1.275 | 0.7642 | 0.2831 | 1275 | 0.0131±0.0014 | 283.0224±19.429 | 0.7639 |
| | 1 | 3 | 5 | 270 | 1.35 | 0.7281 | 0.2697 | 1350 | 0.0294±0.0007 | 239.8967±1.9447 | 0.8933 |
| | 1 | 6 | 2.5 | 990 | 2.475 | 1.6344 | 0.3027 | 2475 | 0.0069±0.0003 | 275.383±4.8713 | 0.7411 |
| | 1 | 6 | 5 | 330 | 1.65 | 0.8710 | 0.1613 | 1650 | 0.0255±0.0010 | 141.8011±2.0040 | 0.8938 |

### *5.3.8.2. Effect of bed height*

In a fixed-bed column study the influence of bed height was evaluated at two different bed depths (3 cm and 6 cm) and the initial As concentration was 1 mg/L. The breakthrough curve was epitomized in Fig. 5.25b and the interpreted values are given in Table 5.10. It was noted that the breakthrough time was increased from 300 min to 750 min with an increasing bed depth from 3 cm to 6 cm, respectively, for As(III) adsorption at 2.5 mL/min. The breakthrough time for As(V) adsorption was 270 min and 630 min at 3 cm to 6 cm, correspondingly. The adsorbent in lower bed depth gets exhausted quickly because of the less amount of biosorbent, however at 6 cm bed depth more active sites were available for adsorbate adsorption and enhanced removal of As was observed.

### *5.3.8.3. Models for column study*

To evaluate the experimental data obtained from the column study four different models have been studied i.e., Thomas, Yoon-Nelson, Clark and Adams-Bohort models. The linear plot of $ln(C_0/C_t\text{-}1)$ vs $t$ is shown in Fig. 5.25c and d for Thomas model and the values evaluated from the Thomas model are given in Table 5.10. The value of $K_{TH}$ increased and $q_0$ value decreased on increasing flow rate from 2.5 to 5 mL/min at 6 cm bed height. The reason behind the obtained result was the driving force amongst biosorbents and adsorbate. Similar results were also reported by Nguyen et al. (2019), where the $K_{TH}$ value increased and $q_0$ value declined with an increasing flow rate. The results revealed that the maximum As adsorption was obtained at a lower flow rate and 6 cm bed height.

The adsorption kinetics of the fixed-bed column has been quantified by using Yoon-Nelson model (Fig. 5.26a and b). It was observed that the value of $k_{YN}$ (rate constant of Yoon-Nelson) increased on increasing bed depth from 3 to 6 cm for the removal of both

the species of As (Table 5.11). The value of the Adams-Bohart rate constant increased on increasing bed height as well as flow rate (Fig. 5.26c and d). Though, the $N_0$ value was decreased on increasing bed depth of biosorbent in a column (Table 5.11). The obtained values of Clark model were given in Table 5.11, which revealed that the Clark model constant increased on the increasing flow rate (2.5-5 mL/min) and bed depth (3-6 cm) (Fig. 5.26e and f).

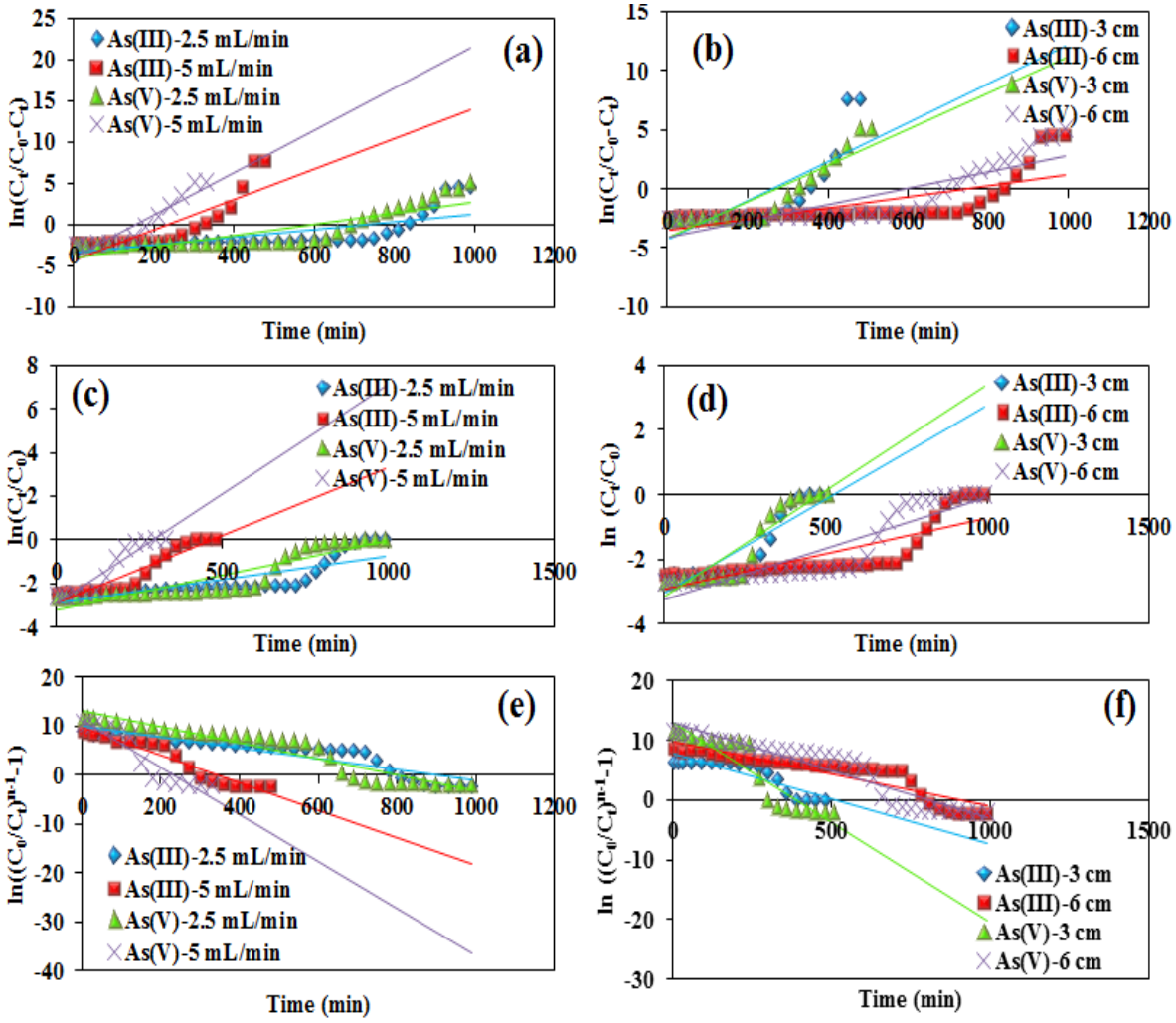


**Fig. 5.26. Plots for Yoon-Nelson model (a) effect of flow rate and (b) effect of bed depth; Adams-Bohart model c) effect of flow rate and (d) effect of bed depth; Clark model (e) effect of flow rate and (f) effect of bed depth.**

**Table 5.11. Parameters of Yoon-Nelson Model, Clark Model and Adams-Bohart Model.**

| | | | | Yoon-Nelson Model | | | Adams-Bohart Model | | | Clark Model | | |
|---|---|---|---|---|---|---|---|---|---|---|---|---|
| | $C_0$ (mg/L) | Q (mL/ min) | L (cm) | $K_{YN}$ (1/min) | τ (min) | $R^2$ | $K_{AB}$ (mg/min. mg) | N0 (mg/L) | $R^2$ | r (1/h) | A | $R^2$ |
| As (III) | 1 | 2.5 | 3 | 0.0166±0.001 | 257.84±7.579 | 0.647 | 0.0058±0.00 | 437.23±0.941 | 0.7941 | 0.0093±0.003 | 1080.74 | 0.5641 |
| | 1 | 5 | 3 | 0.0316±0.003 | 113.38±4.662 | 0.8722 | 0.0126±0.00 | 368.48±0.410 | 0.9029 | 0.0542±0.013 | 6172.75 | 0.9098 |
| | 1 | 2.5 | 6 | 0.0048±0.000 | 746.40±18.04 | 0.5188 | 0.0022±0.00 | 553.77±1.894 | 0.6667 | 0.0109±0.003 | 17210.93 | 0.8313 |
| | 1 | 5 | 6 | 0.0183±0.001 | 232.77±4.696 | 0.7191 | 0.0062±0.00 | 392.66±0.995 | 0.8901 | 0.0281±0.007 | 13301.07 | 0.9263 |
| As (V) | 1 | 2.5 | 3 | 0.0153±0.001 | 270.42±3.106 | 0.8214 | 0.0066±0.00 | 401.58±1.970 | 0.8631 | 0.0337±0.009 | 509915.34 | 0.8706 |
| | 1 | 5 | 3 | 0.0294±0.001 | 129.54±1.051 | 0.8933 | 0.0122±0.00 | 406.53±0.941 | 0.9197 | 0.0598±0.016 | 107366.13 | 0.9093 |
| | 1 | 2.5 | 6 | 0.0069±0.000 | 594.83±10.52 | 0.7411 | 0.0032±0.00 | 420.34±2.214 | 0.815 | 0.0162±0.005 | 429338.1 | 0.9064 |
| | 1 | 5 | 6 | 0.0255±0.001 | 153.15±2.164 | 0.8938 | 0.0101±0.00 | 243.64±0.849 | 0.9084 | 0.0483±0.013 | 79459.29 | 0.89 |

### 5.3.9. Removal of As from groundwater

The MTB-800 was applied for the removal of As from groundwater samples because the $q_{max}$ value obtained in the batch adsorption study was higher than the MLB-800 and shows better adsorption of As. Removal of As(III) was 84.94, 82.85, 85.13, 84.10, 86.63 % and As(V) was 90.80, 94.44, 90.16, 89.69, 97.76 % for collected samples MK, HP, BG J-I and J-II, correspondingly.

### 5.3.10. The proposed mechanism for As adsorption on MTB-800 and MLB-800

The adsorption mechanism of As on magnetic biochar includes four possible mechanisms, electrostatic attraction, surface complexation, hydrogen bonding and π-π interaction the adsorption is also greatly influenced by the pore structure, chemical bonds and surface functional groups on biosorbents. The occurrence of various oxygenated functional groups on magnetic biochar such as -OH and provides potential sites for As adsorption.

In the electrostatic attraction mechanism, the adsorption depends on the As speciation and surface functional groups. The interaction between negatively charged As anions and positively charged surface functional groups on magnetic biochar. The highest As(III) adsorption by MTB-800 was observed at pH 6 and 7 pH by MLB-800 whereas, the highest adsorption of As(V) was found on pH 7 by both MTB-800 and MLB-800. The As(III) exists in the neutral form at pH range 6-9 and As(V) was present in its anionic form at pH>3 (Samadzadeh and Khodadadi, 2010) hence, get attracted towards iron present on the surface of both the biosorbents through electrostatic attraction. A study performed for As adsorption from an aqueous solution through magnetic grass biochar showed the main mechanism for As adsorption was the electrostatic attraction (Baig et al., 2014). The

magnetic biochar contains more oxygenated groups than of unmodified biochar. The surface functional groups of MTB-800 and MLB-800 can facilitate the hydrogen bond formation with the molecules of arsenate and arsenite, consequently helping in improved adsorption capacity of biochar materials (Jing et al., 2014). The magnetic biochar also contains an aromatic compound on its surface, the adsorption of As(III and V) can be dominated by π-π interaction among the aromatic ring of biosorbent and molecules of As (Tan et al., 2020a; Li et al., 2020b). The probable mechanism of Arsenic adsorption based on the above-discussed point is presented in Fig. 5.27.

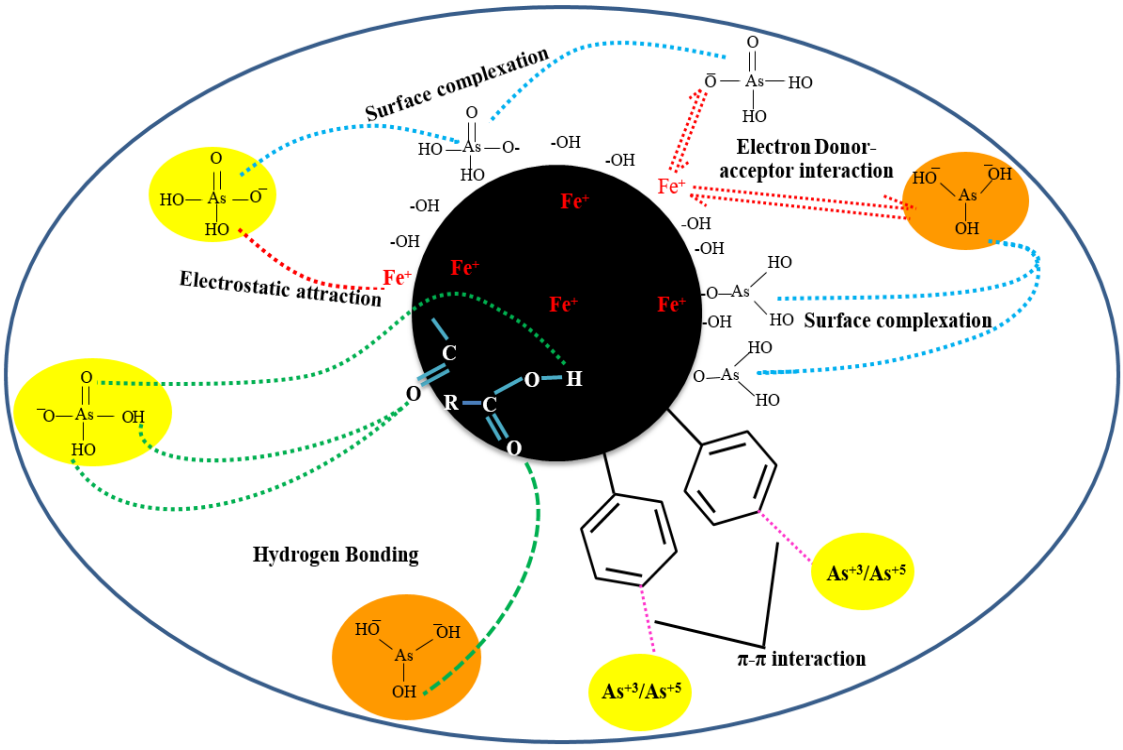


**Fig. 5.27. Proposed mechanism of As(III) and As(V) adsorption by MTB-800 and MLB-800.**

The adsorbate and biosorbent interaction might lead to the development of new complexes with hydroxyl groups. It was found that on both the magnetic biochar hydroxyl group is the major functional group. FTIR spectrum after As adsorption shows significant

changes in the peak of hydroxyl functional groups. Change in the peak intensity and peak shift was observed after loading of As(III) and As(V) on MTB-800 and MLB-800 as discussed in the FTIR result. This showed that the Arsenic ions might coordinate with the surface functional groups (-OH) of MTB-800 and MLB-800.

## 5.4. Phase III: Characterization and application of magnetic biochar synthesized using vegetable waste for As(III) and As(V) removal from an aqueous solution and groundwater.

### 5.4.1. Characterizations

#### *5.4.1.1. SEM and EDS*

The Fig. 5.28a and c, shows that MRB-800 and MJB-800 having irregular morphology with a somewhat rough surface. EDS analysis of both biadsorbents shows MRB-800 consists of higher iron content by weight percentage i.e., 3.08 % than MJB-800 (6.58 %), which means the Radish and Jackfruit waste biomasses were successfully impregnated with iron, which imparted magnetic properties to both the bioadsorbents (Fig. 5.28b and d).

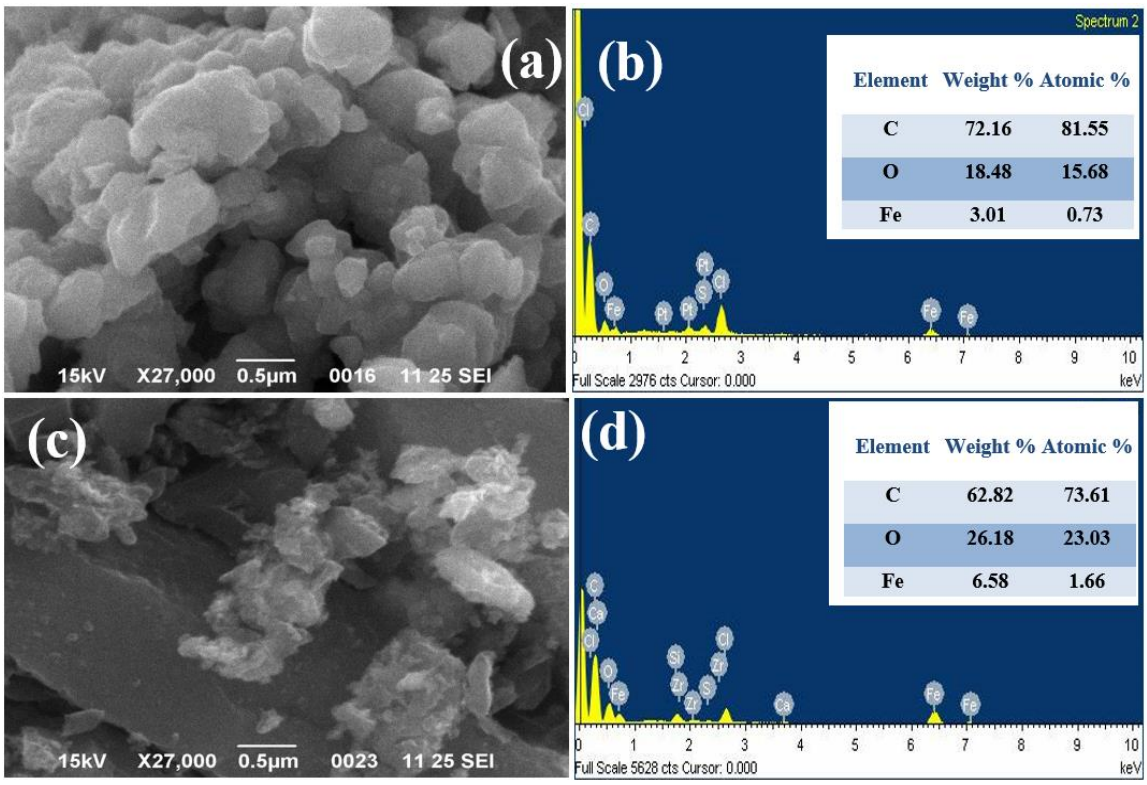


**Fig. 5.28. SEM images of the a) and c) MTB-800 and MLB-800, respectively, b) and d) EDX images of MRB-800 and MJB-800, respectively.**

### *5.4.1.2. FTIR analysis*

For the determination of surface functional groups of MRB-800 and MJB-800, before and after As(III and V) adsorption FTIR analysis was performed. Fig. 5.29a and b, represent FTIR spectra of both bioadsorbents before and after As adsorption. Nearly similar peaks were found for both bioadsorbents before and after adsorption of As. The peaks appear at wavenumber 3454.99 $cm^{-1}$ and 3467.38 $cm^{-1}$ corresponds to the hydroxyl group (-OH) (Liu et al., 2019b), peaks at wavenumber 2937.07 $cm^{-1}$ and 2923.11 $cm^{-1}$ represents $CH_2$ or bonds of C-H (Wang et al., 2018). The peaks were found at wavenumber 1614.70 $cm^{-1}$, 1633. 65 $cm^{-1}$ and 1421.06 $cm^{-1}$ attributed to the presence of C=C, COOH (carboxyl group) and C-O or COO- of carboxyl group vibration, respectively, (Ali et al., 2020). Peaks at 1033.30 $cm^{-1}$ and 1022.16 $cm^{-1}$ wavenumbers were allocated for stretching of the C-O group of an alcoholic compound. Aromatic hydrogen group (C-H) was ascribed by the presence of a peak at 965.82 $cm^{-1}$ and 968.10 $cm^{-1}$ wavenumbers. The peaks at 569, 546.21 and 532.3 $cm^{-1}$ show the occurrence of C-C=O bonds of a carboxylic acid group (Verma et al., 2019) or Fe-O stretching of iron (Sarswat and Mohan, 2016) that confirms the impregnation of Iron on to the surface of biochar materials.

FTIR result revealed that the functional groups of bioadsorbents play a significant role in adsorption of As (III and V). The intensity of peaks varies after As (III and V) adsorption and shifting of peaks shows the involvement of some functional group in the process of As adsorption.

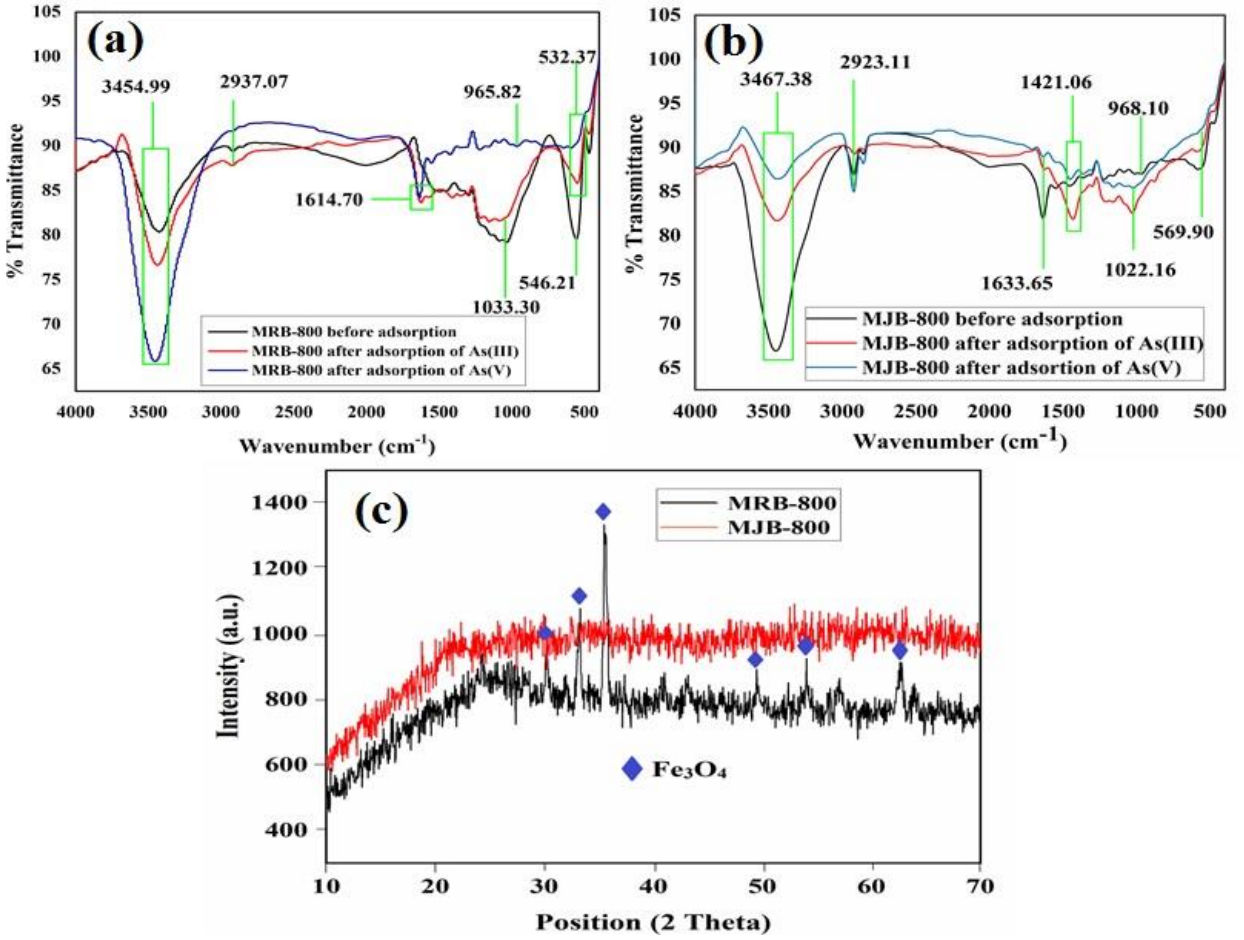


**Fig. 5.29. (a) and (b) FTIR spectra of MRB-800 and MJB-800, respectively, and (c) XRD analysis of MRB-800 and MJB-800.**

### *5.4.1.3. XRD*

The crystalline and amorphous nature of bioadsorbents was determined through XRD analysis. Fig. 5.29c shows that no distinct peaks were obtained for iron-modified MJB-800 bioadsorbent hence; MJB-800 was amorphous. That is might be due to the incorporation of iron (hydr) oxide into the bioadsorbent was amorphous (Kim et al., 2019). The study done by Yin et al. (2017), it was also found that the iron oxide inclusion into pyrolyzed granulated attapulgite (GAP) was amorphous. The graph of MRB-800 shows some distinct peaks with 2θ= 29.97°, 33.28°, 35.53°, 49.29°, 54.03° and 62.60° that

corresponds to the occurrence of $Fe_3O_4$ (Nath et al., 2019). The nature of MRB-800 was crystalline.

### *5.4.1.4. Particle Size Analysis*

PSA is one of the most significant characteristics of any bioadsorbent. The small size of particles having more surface area that is available for adsorption of As. It was found that for MRB 800 the broad two peaks were found between the two different ranges one was at 80 – 270 nm and the other shown the broad peak at 270- 1300 nm (Fig. 5.30a) and the broad peak found at 400-1000 nm represent the particle size of MJB-800, that illustrate the size of the material.

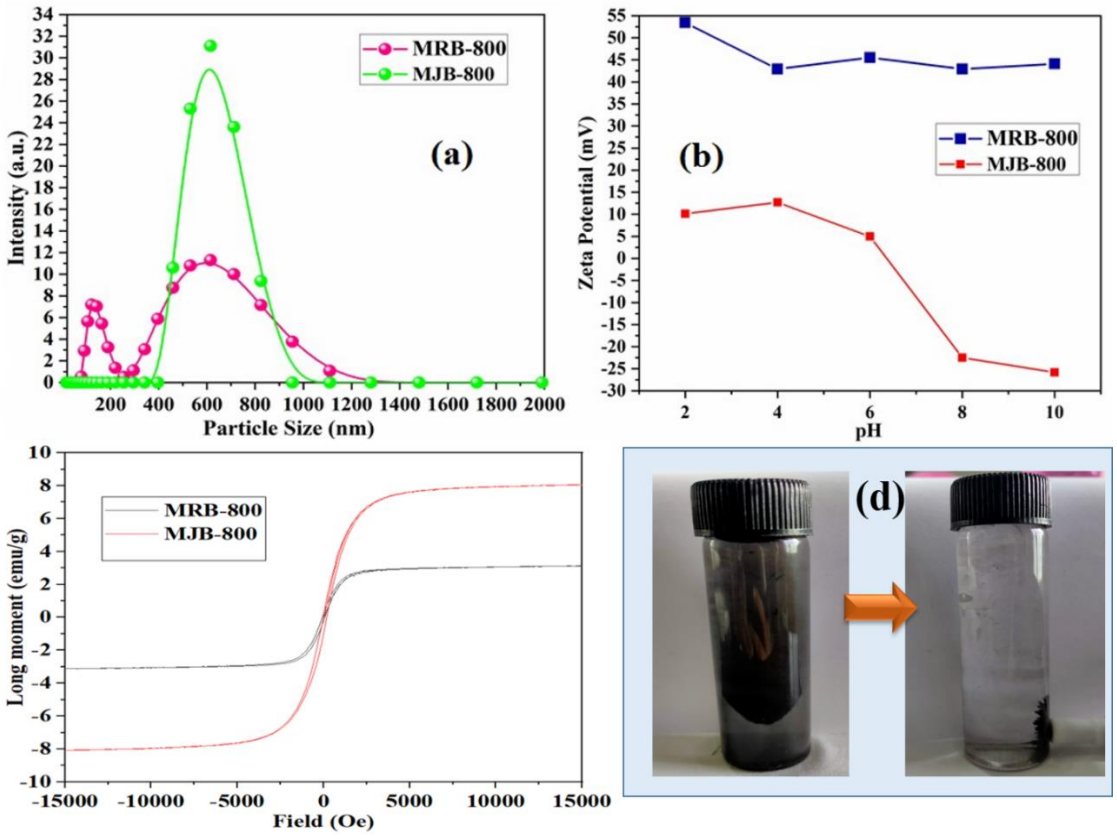


**Fig. 5.30. (a) Particle Size Analysis (b) zeta potential of MRB-800 (c) Magnetization curve of MRB-800 and MJB-800 and (d) Magnetic activity of biochar under magnetic field.**

#### *5.4.1.5. Zeta potential*

The stability of bioadsorbents was checked by zeta potential at a definite pH in a dispersion medium. The zeta potential of bioadsorbents was measured at five diverse pH values (2, 4, 6, 8 and 10). The results show that MRB-800 was very stable at the alkaline as well as acidic pH range because the zeta potential value was higher than ±30 mV (Fig. 5.30b). Whereas the value of zeta potential for MJB-800 was quite less, this indicates that MJB-800 was unstable.

#### *5.4.1.6. VSM*

The magnetic parameters like retentivity, magnetization and coercivity were determined by vibrating sample magnetometer (VSM). The magnetic hysteresis curve of MRB-800 and MJB-800 was measured at -15kOe to +15kOe range of magnetic field at room temperature (Fig. 5.30c). The rise in magnetization with rising magnetic field and saturates at 3.13 emu/g (MRB-800) and 8.08 emu/g (MJB-800), signifying significant quantity of ferric compound were effectively infused to surface of bioadsorbent (Liu et al., 2020b). The high magnetization values demonstrated superparamagnetic properties of both the bioadsorbents (Priyan et al., 2021). Whereas, excellent magnetic properties of bioadsorbents was confirmed by the Fig. 5.30d and this also illustrate the solid-liquid method of separation so that the biosorbents after adsorption can be recycled effectively.

#### *5.4.1.7. $pH_{ZPC}$*

The $pH_{ZPC}$ is known for the identification of net surface charge of synthesized bioadsorbent and at this pH the bioadsorbent contains net neutral surface charge. The $pH_{ZPC}$ of MRB-800 and MJB-800 was found to be 2 beyond this pH the bioadsorbent surface

charge was negative. The $pH_{ZPC}$ helps in characterizing the type of surface of both the biochar materials. It also stipulates that the surface of the MRB-800 and MJB-800 has zero electrical charge density (Vinayagam et al., 2020).

### 5.4.2. Batch adsorption study

#### *5.4.2.1. Effect of dose*

Effect of biosorbent dose was studied using a different dose and it was observed that removal efficiencies of both As (III) and As (V) were increased with an increasing dose from 0.5 g/L -1.5 g/L, but it decreased on further increasing dose up to 3 g/L. Fig. 5.31a shows that the adsorption percentage obtained for As (III) was ~79.3 % and ~82.9 % by MRB-800 and MJB-800, respectively. Whereas, maximum adsorption of As (V) was ~60.85 % and ~89.1 % obtained at dose 1.5 g/L for MRB-800 and MJB-800, correspondingly. The highest As (III) and As (V) adsorption was observed at 1.5 g/L doses of MRB-800 and MJB-800. The adsorption capacities of both bioadsorbents were decreased with an increasing doses after 1.5 g/L. For As(III) removal, the adsorption capacities of MRB-800 and MJB-800 were decreased from 1.493 mg/g to 0.240 mg/g and 1.223 mg/g to 0.270 mg/g, respectively, with an increasing dose from 0.5 g/L to 3 g/L. Whereas, adsorption capacities of MRB-800 and MJB-800 for As(V) removal were decreased from 0.962 mg/g to 0.184 mg/g and 1.452 mg/g to 0.290 mg/g, correspondingly.

The adsorption of adsorbate by the adsorbent generally depends on the accessibility of active sites and surface area thus, on increasing the bioadsorbent dose after certain limits it gets agglomerated and forms small clumps that may reduce the surface area and ultimately reduce the surface active sites resulting in a lower adsorption of adsorbate (Zeng et al., 2018).

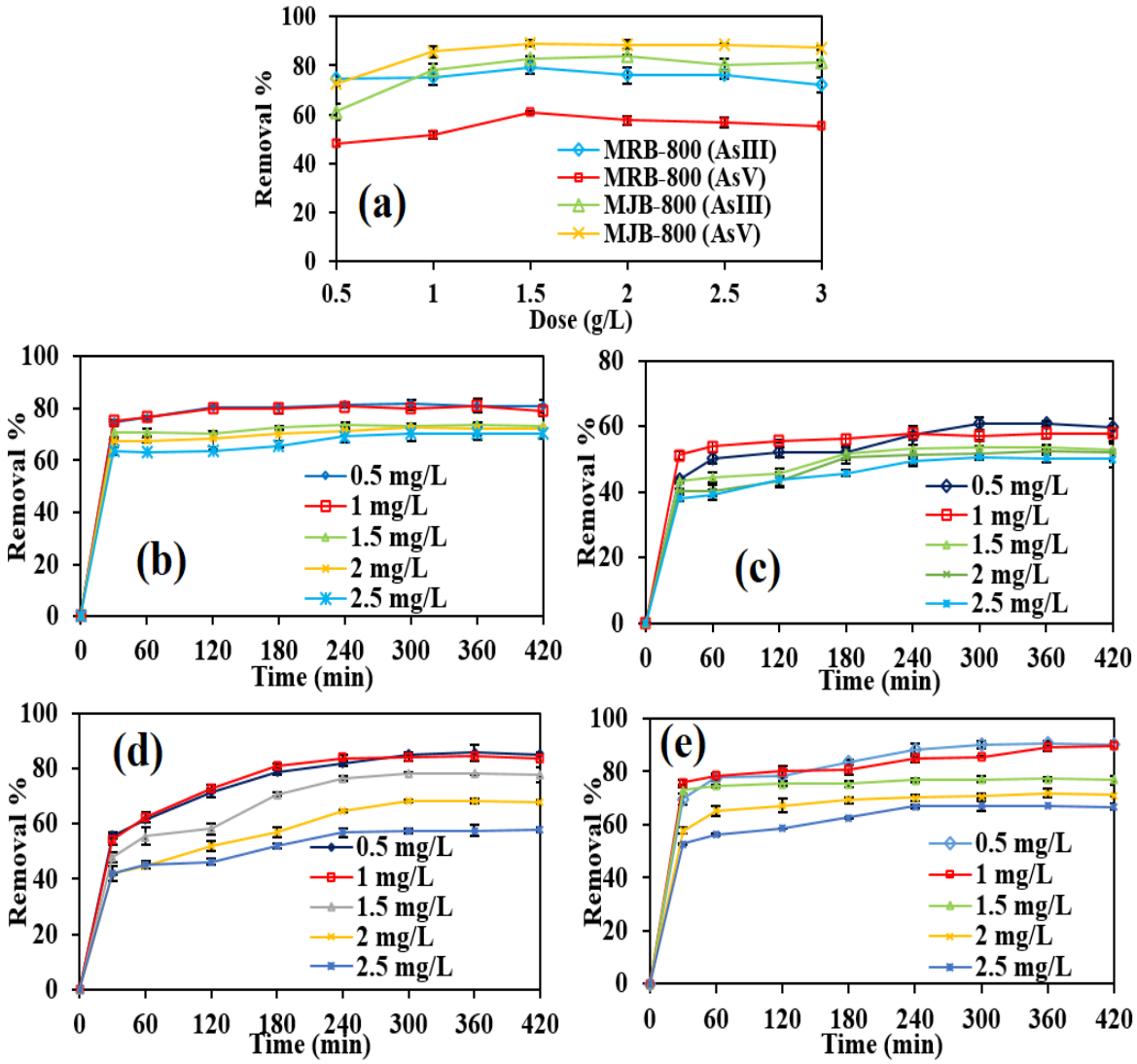


**Fig. 5.31. Influence of (a) dose of biadsorbent, (b) and (c) Effect of initial As(III) and As(V) concentration of by MRB-800, respectively, (d) and (e) Effect of initial concentration of As(III) and As(V) by MJB-800, respectively, on process of adsorption.**

### *5.4.2.2. Effect of concentration and contact time*

The influence of initial adsorbate concentration was examined at varying As concentrations (0.5 mg/L to 2.5 mg/L). At lowest initial concentration (0.5mg/L), the

highest As (III) removal was ~81.85 % and ~85.80 % for MRB-800 and MJB-800, respectively (Fig. 5.31b and d), whereas the highest removal of As (V) was ~60.7 % and ~90.7 % for MRB-800 and MJB-800, correspondingly (Fig. 5.31c and e). Fig. 5.32 shows that the adsorption capacities of both the bioadsorbents i.e., MRB-800 and MJB-800 were increased with an increasing initial concentration of As (III) and As (V). The highest adsorption capacity of MRB-800 for As (III) adsorption was 1.17 mg/g, and it was found to be 0.84 mg/g for As (V) adsorption (Fig. 5.32a and b). The maximum capacity of MJB-800 for adsorption of As (III) was 0.95 mg/g and for adsorption of As (V) was 1.11 mg/g (Fig. 5.32c and d). A necessary dynamic potency for immobilizing mass transfer resistance force between the solid phase and liquid phase is delivered by the initial concentration of adsorbate (Prabhakar and Samaddar, 2020).

The effect of contact time was evaluated by differing shaking time from 5 min to 420 min with the initial As concentration (1 mg/L) and 1.5 g/L bioadsorbent dose. The obtained results indicated that adsorption of As was increased with an increasing contact time up to 240 min then on further increasing the contact time there was no substantial amount of As adsorption observed (Fig. 5.31b-e). The equilibrium for As adsorption by MRB-800 and MJB-800 was achieved at 240 min. Initially, the active binding sites were vacant but with an increasing time these available binding sites were inhabited by the As ions and decreased the number of vacant active sites available for As adsorption hence, adsorption was decreased after a certain period (Alam et al., 2018). At lower initial concentration, As adsorption was higher and at higher initial concentration adsorption of As was decreased. The lower removal ability of both the biochar materials with an increasing concentration was due to the occurrence of less number of MRB-800 and MJB-800 than As molecules, which inclines the removal efficiency (Priyan et al., 2021).

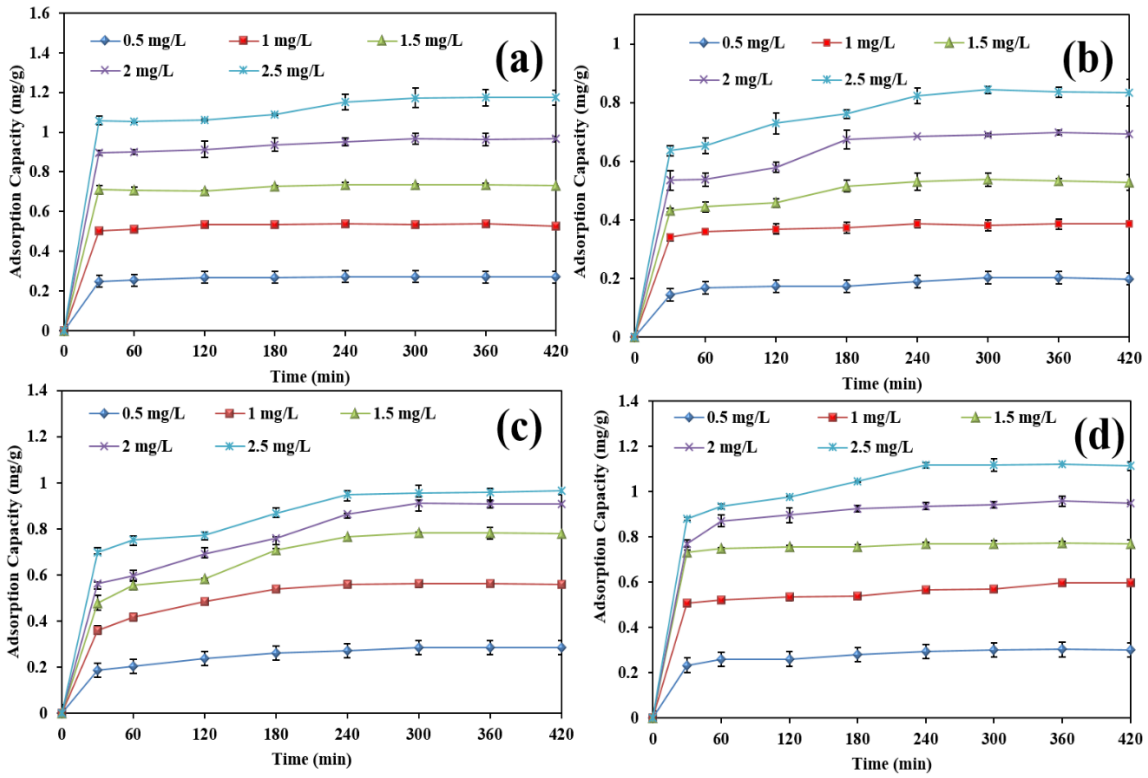


**Fig. 5.32. Adsorption capacity for removal of (a) As(III) and (b) As(V) by MRB-800, correspondingly and (c) As(III) and (d) As(V) by MJB-800, respectively.**

### *5.4.2.3. Influence of pH on As adsorption*

The pH of the working solution is another main constraint and had a significant effect on the adsorption process. The study was performed by changing the pH of the solution from 2-10 and kept other constraints constant. The removal of As (III) was ~72.67 % and ~88.4 % found maximum at 5 pH and 6 pH by MRB-800 and MJB-800, respectively; however, the maximum adsorption of As (V) was ~72.35 % by MRB-800 and ~92.65 % by MJB-800. The highest adsorption capacity of MRB-800 and MJB-800 for As (III) adsorption was 0.484 mg/g (pH 5) and 0.589 mg/g (pH 6), respectively. While the highest

adsorption capacity of MRB-800 and MJB-800 was discovered to be 0.482 mg/g (pH 5) and 0.617 mg/g (pH 6) for adsorption of As (V), correspondingly.

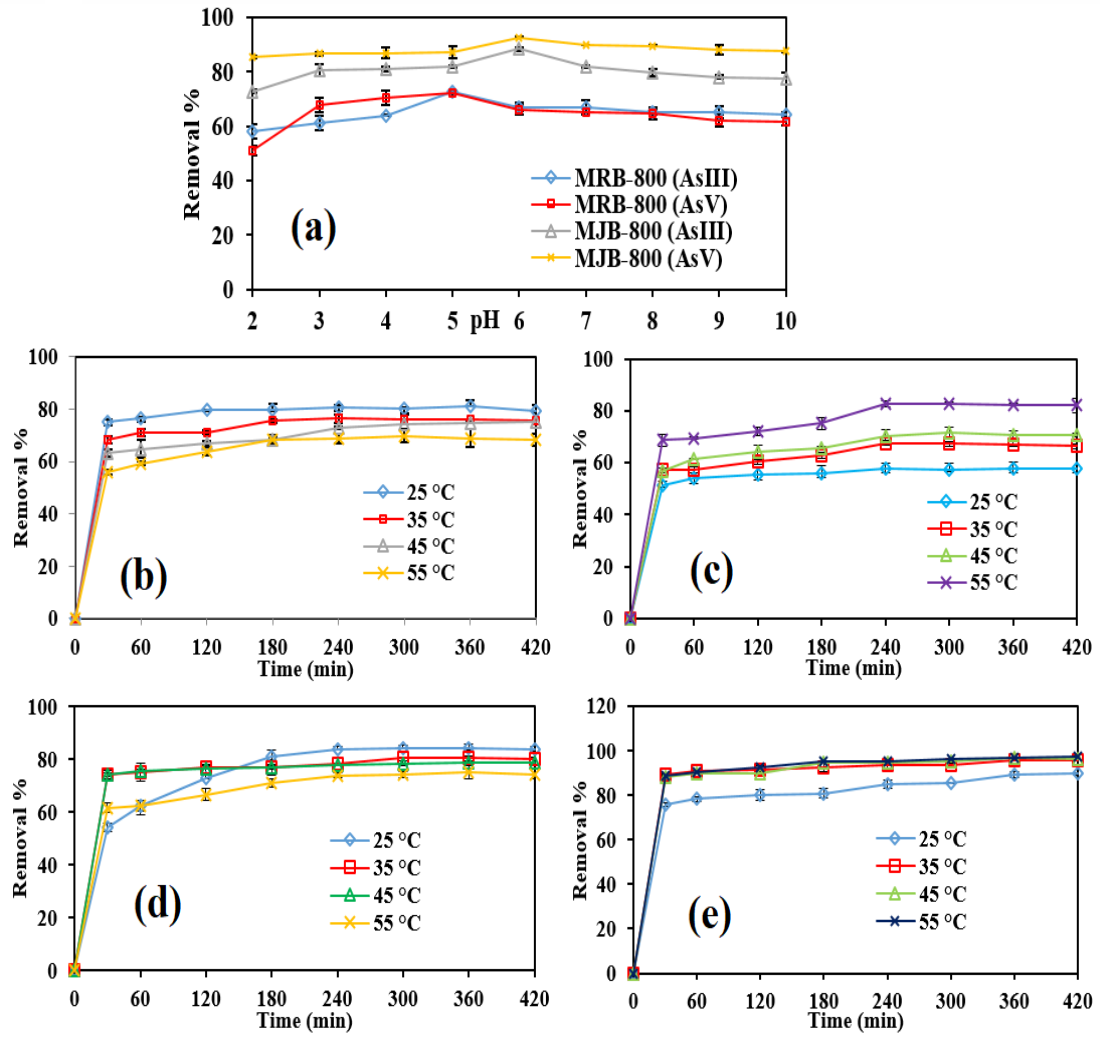


**Fig. 5.33. Effect of (a) pH, (b) and (c) Effect of Temperature on adsorption of As(III) and As(V) by MRB-800, respectively, (d) and (e) Effect of Temperature on adsorption of As(III) and As(V) by MJB-800, respectively.**

The adsorption efficiencies of both As species were lower at a high alkaline medium. Fig. 5.33a directs that adsorption of both the As species were found maximum at slightly acidic pH. Under high alkaline conditions, there were more $OH^-$ ions that compete with the As

anions for active sites of bioadsorbent, giving rise to the blockage of As adsorption onto the surface of both the iron impregnated biochar (MRB-800 and MJB-800). This is due to the As (III) found mainly in form of $H_2AsO_3^-$ (anionic) at a pH range of 2-8, although, As (V) appears especially in the form of $H_3AsO_4^-$ at a pH range of 2-6 (Gubler and ThomasArrigo, 2021). Thus on increasing the protons concentration in an aqueous solution increased As (III and V) adsorption under slightly acidic conditions (Nguyen et al., 2019).

#### *5.4.2.4. Temperature effect on adsorption of As (III) and As (V)*

Fig. 5.33b and d revealed that the removal of As (III) was decreased from ~80.92 % to ~68.3 % by MRB-800 and ~84.4% to ~74.9 % by MJB-800 with an increasing temperature. Hence, the process of adsorption was exothermic because the removal was decreased on increasing temperature. With increasing temperature, the adsorption capacities of MRB-800 and MJB-800 for As (III) removal were decreased from 0.538 mg/g to 0.464 mg/g and 0.562 mg/g to 0.499 mg/g, respectively. Though, the removal of As (V) through both bioadsorbents was endothermic. The adsorption of As (V) was maximum at 55 °C i.e., ~82.1 % by MRB-800 and ~97.35 % by MJB-800 (Fig. 5.33c and e). The adsorption capacities of MRB-800 and MJB-800 for As (V) removal were enhanced from 0.385 mg/g to 0.549 mg/g and 0.597 mg/g to 0.649 mg/g with an increasing temperature from 25 °C to 55°C. The obtained result was due to several binding active sites present on the surface of modified biochar requires more temperature for the activation so that the As ions get adsorbed on these active sites. In some cases, adsorbent needs a lesser temperature for activation of active binding sites that enhances the As removal at a lower temperature (Verma and Singh, 2019; Kazi et al., 2018).

### 5.4.3. Regeneration study

The result of regeneration study revealed that both the magnetic biochar materials were recycled up to four cycles (Fig. 5.34a and b). For removal of As(III) using MRB-800 and MJB-800 it was observed that 80.93 % and 86.05 % adsorption in first cycle and was reduced to 53.8 % and 50.93 %, respectively. Whereas, for As(V) the adsorption was found to be 57.1 % and 89.35 % in first cycle which was then reduce up to 30.6 % and 46.35 %, respectively, using MRB-800 and MJB-800.

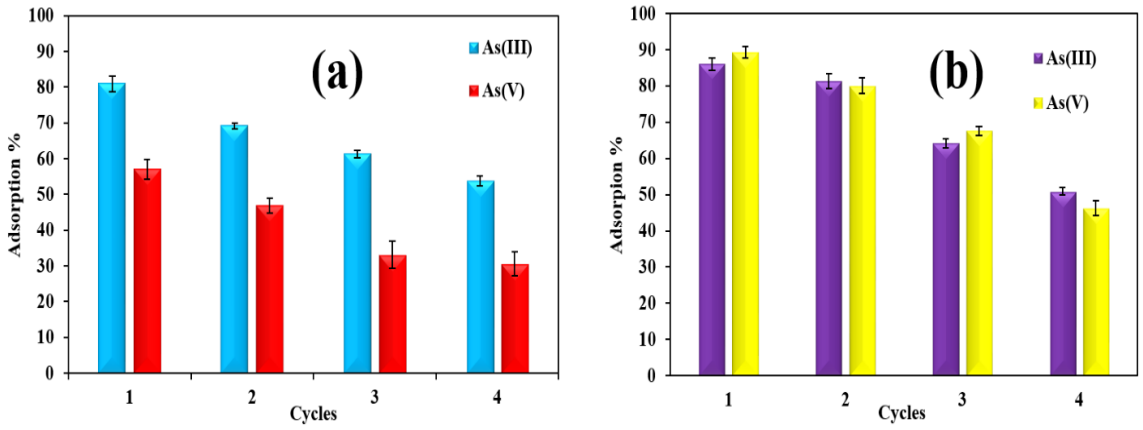


**Fig. 5.34. Regeneration for As(III) and As(V) adsorption (a) by MRB-800 and (b) by MJB-800.**

### 5.4.4. Adsorption isotherms

For the optimization of operating conditions to remove As (III) and (V) three different adsorption isotherms were used. The obtained result disclosed that the As (III) removal by MRB-800 fitted well to the Temkin isotherm model with a value of $R^2$ =0.9924 though, the adsorption of As (V) by MRB-800 best followed to the Freundlich isotherm with 0.9975 $R^2$ value. The adsorption process of As (III and V) by MJB-800 was best followed to the Langmuir model of isotherm with correlation coefficient values 0.9939 and

0.9753, correspondingly (Fig. 5.35a-c). The value of $q_0$ i.e., the Langmuir constant was 2.08 mg/g and 1.13 mg/g for As (III) adsorption by MRB-800 and MJB-800, respectively. The $q_0$ value for As (V) was 2.03 mg/g and 1.26 mg/g, respectively, for MRB-800 and MJB-800. The values of the Langmuir isotherm are given in Table 5.12.

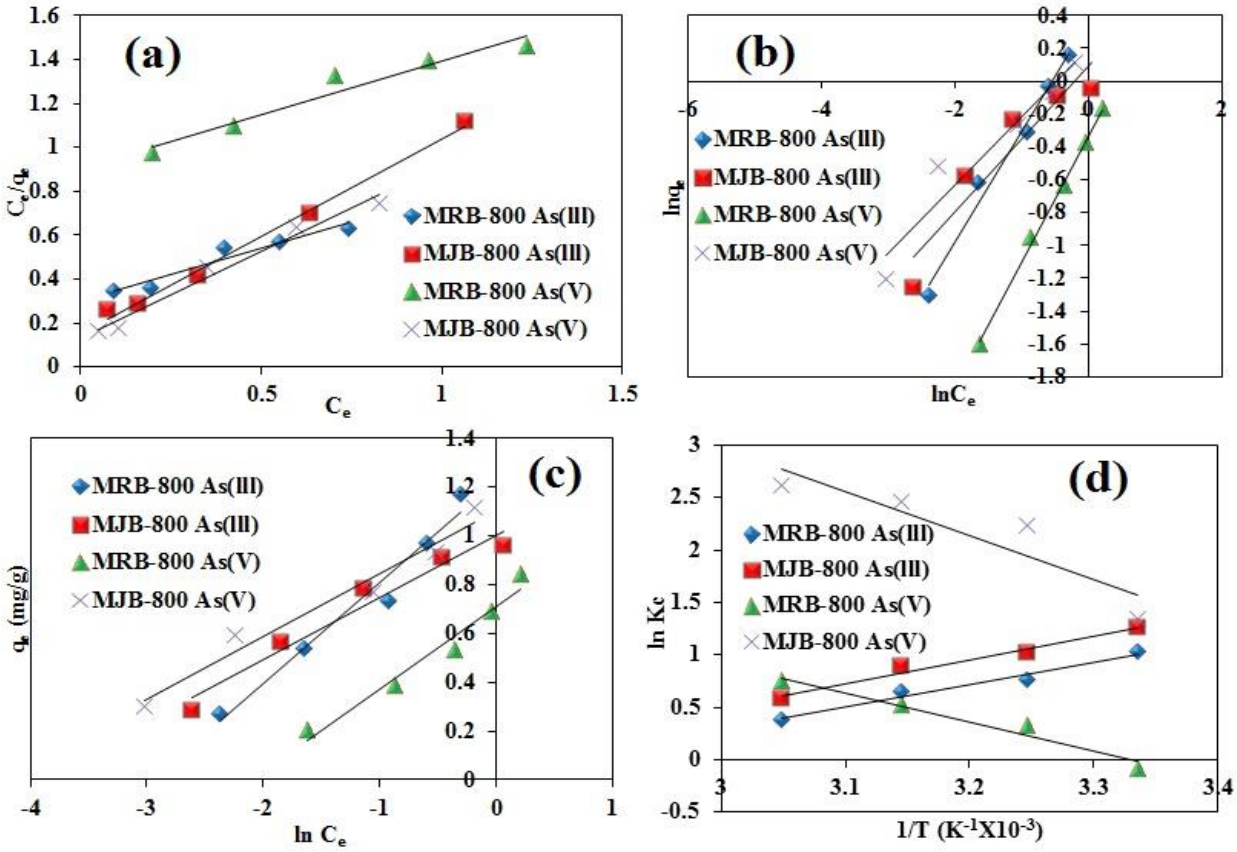


**Fig. 5.35. Plots of (a) Langmuir isotherm, (b) Freundlich isotherm, (c) Temkin isotherm for MRB-800 and MJB-800 and (d) Plot for thermodynamic.**

**Table 5.12. Isotherm parameters for removal of As (lll) and As (V) by synthesized MRB 800 and MJB 800.**

| Isotherms | | MRB 800 As(lll) | MJB 800 As(lll) | MRB 800 As(V) | MJB 800 As(V) |
|---|---|---|---|---|---|
| Langmuir isotherm | $Q_e$ (mg/g) | 2.083±0.120 | 1.131±0.031 | 2.031±0.022 | 1.269±0.013 |
| | b (L/mg) | 1.608±0.122 | 5.741±0.506 | 0.542±0.014 | 6.001±0.938 |
| | $R_L$ | 0.199±0.011 | 0.065±0.005 | 0.425±0.006 | 0.062±0.009 |
| | $R^2$ | 0.9367 | 0.9939 | 0.9442 | 0.9753 |
| Freundlich Isotherm | $K_F$ (mg/g(L/mg)$^{1/n}$) | 1.450±0.025 | 1.088±0.060 | 0.714±0.038 | 1.213±0.136 |
| | N | 1.475±0.047 | 2.263±0.011 | 1.307±0.017 | 2.414±0.018 |
| | $R^2$ | 0.9818 | 0.887 | 0.9975 | 0.9324 |
| Temkin isotherm | B | 0.413±0.010 | 0.255±0.007 | 0.337±0.008 | 0.337±0.047 |
| | $K_T$ (L/g) | 19.146±0.305 | 51.278±4.300 | 8.253±0.179 | 72.142±17.887 |
| | $R^2$ | 0.9924 | 0.9581 | 0.9584 | 0.9629 |

### 5.4.5. Thermodynamics

For adsorption of As (III), the value of ΔH° was calculated to be negative -0.01762 kJ/mol for MRB-800 and -0.01906 kJ/mol for MJB-800, which shows the exothermic process. The value of ΔG° was positive which designated that As (III) adsorption by MRB-800 and MJB-800 was non-spontaneous. The negative value of ΔS° (-0.05039 kJ/mol for MRB-800 and -0.05311 kJ/mol for MJB-800) specifies that on the increasing temperature the randomness between the interface of adsorbate and the bioadsorbent was declined (Imran et al., 2021).

The obtained results show that for adsorption of As (V) value of ΔH° was positive viz., 0.023112 kJ/mol and 0.03468 kJ/mol by MRB-800 and MJB-800, respectively, which

represents that adsorption of As (V) was endothermic process. The positive value of ΔS° (0.076949 kJ/mol for MRB-800 and 0.12875 kJ/mol for MJB-800) implied increased randomness between the As (V) and both these (Fig. 5.35d). The value of ΔG° was negative for As (V) adsorption that indicates the adsorption process was spontaneous. The negative value of ΔG° was increased with temperature increase shows that adsorption process was thermodynamically favorable (Massoudinejad et al., 2020) (Table 5.13).

**Table 5.13. Thermodynamic parameters of As (III) and As(V) adsorption onto MRB 800 and MJB 800 adsorbent.**

| Parameters | Temperature (K) | MRB 800 | | MJB 800 | |
|---|---|---|---|---|---|
| | | As(lll) | As(V) | As(lll) | As(V) |
| ΔG° (kJ/mol) | 298 | 14.999±0.458 | -22.9078±7.130 | 15.8089±3.721 | -38.3355±8.008 |
| | 308 | 15.503±0.473 | -23.6773±7.369 | 16.3400±3.846 | -39.6231±8.277 |
| | 318 | 16.007±0.488 | -24.4468±7.609 | 16.8712±3.971 | -40.9107±8.546 |
| | 328 | 16.510±0.504 | -25.2163±7.848 | 17.4023±4.096 | -42.1982±8.815 |
| ΔH° (kJ/mol) | | -0.018±0.000 | 0.02311±0.007 | -0.0191±0.019 | 0.03468±0.009 |
| ΔS° (kJ/mol K) | | -0.050±0.002 | 0.07694±0.024 | -0.0531±0.053 | 0.12875±0.027 |

### 5.4.6. Adsorption Kinetics

Obtained experimental data were analyzed by pseudo-first-order and pseudo-second-order kinetics to define the adsorption rate constant (Gautam et al., 2018). The pseudo-first-order kinetics was not followed by the experimental data of As adsorption (Fig. 5.36).

The obtained value of correlation coefficient indicates that As (III and V) adsorption experimental data was best followed to pseudo-second-order kinetics (Fig. 5.37). The values of $R^2$ were close to 1 and are well presented in Table 5.14.

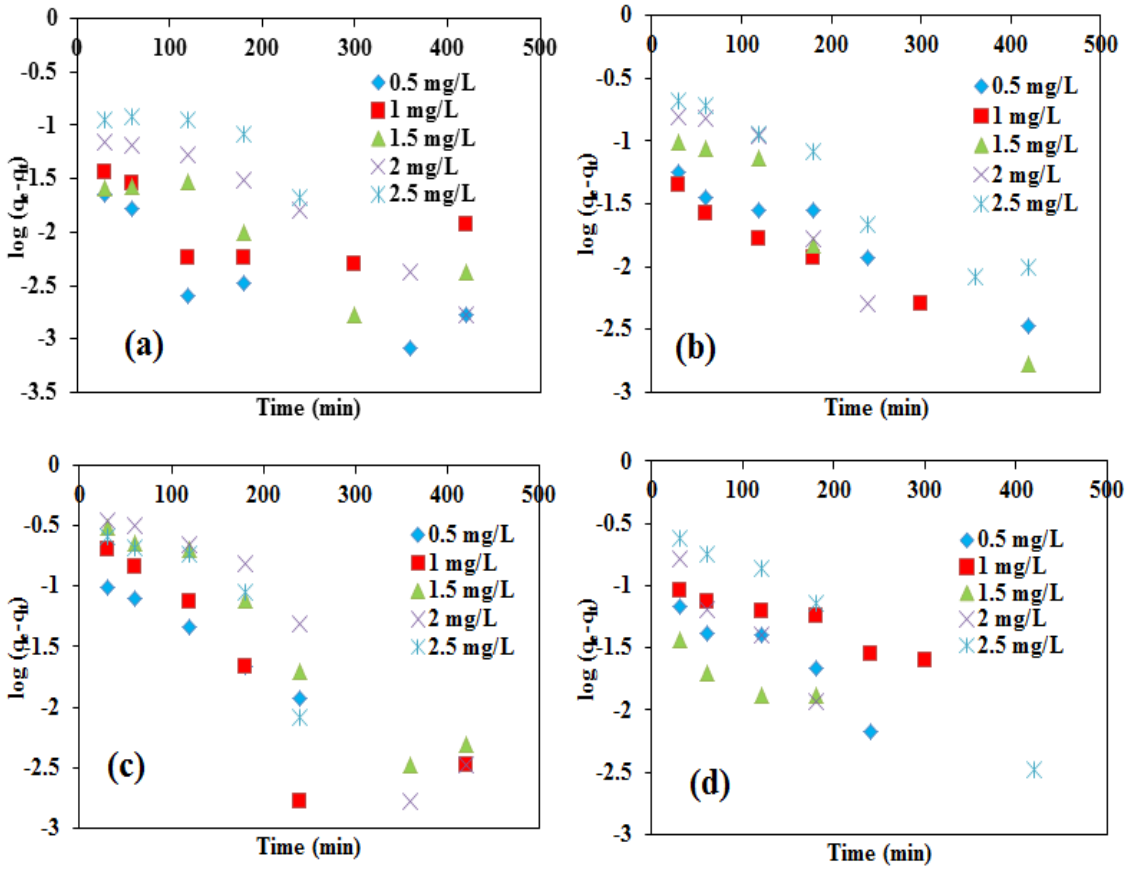


**Fig. 5.36. Graphs for pseudo First order kinetics, (a) and (b) of As(III) and As(V) adsorption by using MRB-800 and (c) and (d) of As(III) and As(V) adsorption by using of MJB-800.**

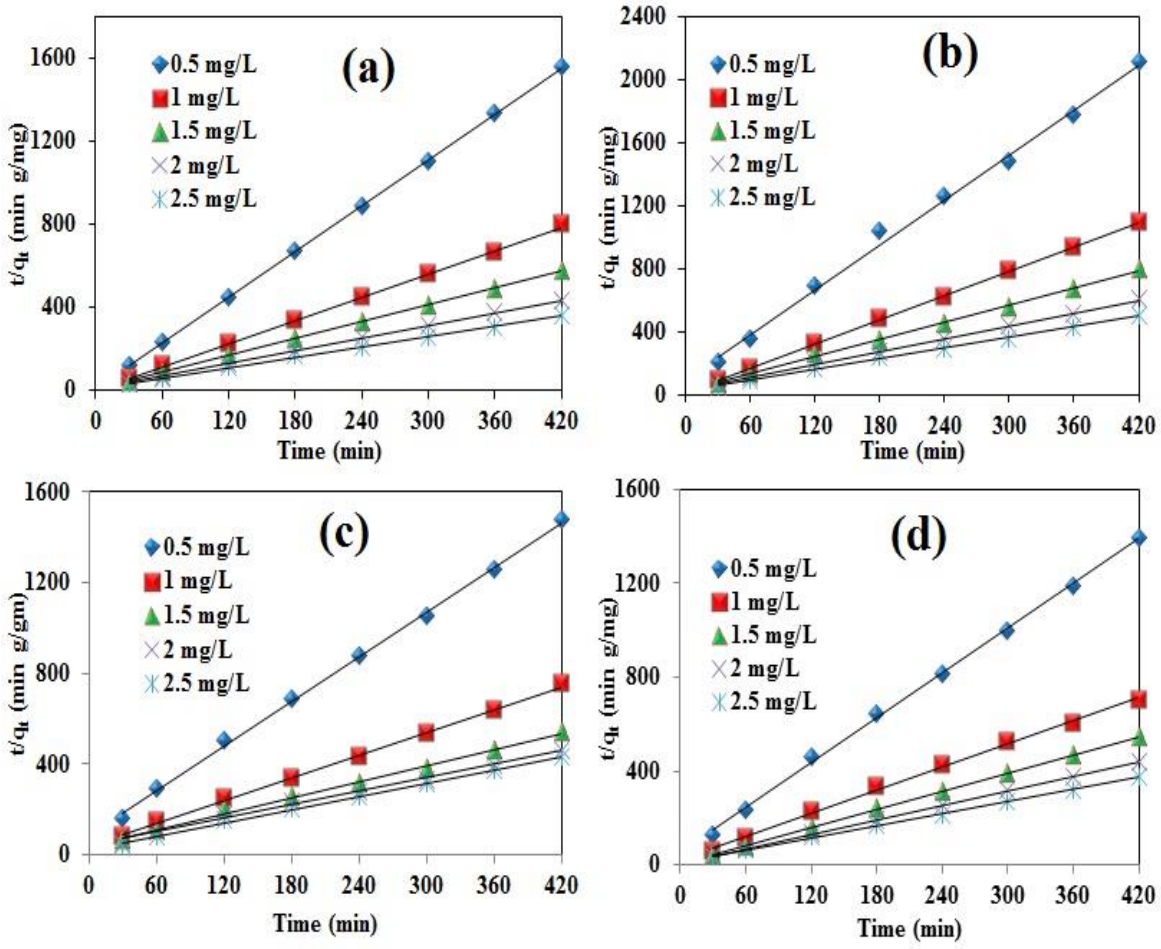


**Fig. 5.37. Graphs for pseudo second order kinetics, (a) and (b) of As(III) and As(V) adsorption by using MRB-800 and (c) and (d) of As(III) and As(V) adsorption by using of MJB-800.**

**Table 5.14. Values of kinetic parameters pseudo first order and second order.**

| Kinetics | Pseudo first order kinetics | | | | Pseudo second order | | |
|---|---|---|---|---|---|---|---|
| | $C_0$ (mg/L) | $q_e$ (mg/g) | $k_1$ ($min^{-1}$) | $R^2$ | $q_e$ (mg/g) | $k_2$ (g/µg min)) | $R^2$ |
| MRB 800 As(lll) | **0.5** | 0.0156±0.007 | 0.0013±0.001 | 0.7304 | 0.2726±0.001 | 1.3904±0.394 | 0.9999 |
| | **1** | 0.0197±0.007 | 0.0006±0.001 | 0.2686 | 0.5349±0.016 | 1.7915±1.360 | 0.9996 |
| | **1.5** | 0.0367±0.011 | 0.0013±0.001 | 0.7183 | 0.7386±0.000 | 0.5092±0.020 | 0.9999 |
| | **2** | 0.1335±0.053 | 0.0018±0.001 | 0.9676 | 0.9773±0.022 | 0.1838±0.480 | 0.9998 |
| | **2.5** | 0.1911±0.153 | 0.0014±0.000 | 0.7063 | 1.2019±0.053 | 0.0802±0.044 | 0.9989 |
| MJB 800 As(lll) | **0.5** | 0.1451±0.019 | 0.0020±0.000 | 0.9934 | 0.3046±0.005 | 0.1228±0.016 | 0.9988 |
| | **1** | 0.2123±0.051 | 0.0023±0.002 | 0.7491 | 0.5946±0.010 | 0.0784±0.010 | 0.9989 |
| | **1.5** | 0.5390±0.099 | 0.0023±0.001 | 0.9455 | 0.8511±0.013 | 0.0347±0.001 | 0.9949 |
| | **2** | 0.9202±0.395 | 0.0027±0.001 | 0.9062 | 0.9993±0.014 | 0.0250±0.002 | 0.9936 |
| | **2.5** | 0.5922±0.149 | 0.0027±0.001 | 0.791 | 1.0213±0.031 | 0.0405±0.007 | 0.9968 |
| MRB 800 As(V) | **0.5** | 0.0672±0.019 | 0.0013±0.001 | 0.9569 | 0.2100±0.004 | 0.2341±0.057 | 0.9962 |
| | **1** | 0.0472±0.014 | 0.0014±0.001 | 0.9772 | 0.3906±0.008 | 0.4481±0.028 | 0.9998 |
| | **1.5** | 0.1630±0.076 | 0.0021±0.001 | 0.9613 | 0.5521±0.021 | 0.1330±0.054 | 0.9984 |
| | **2** | 0.4101±0.162 | 0.0033±0.002 | 0.9087 | 0.7284±0.003 | 0.0748±0.001 | 0.9998 |
| | **2.5** | 0.3028±0.028 | 0.0017±0.000 | 0.9445 | 0.8769±0.207 | 0.0605±0.044 | 0.9989 |
| MJB 800 As(V) | **0.5** | 0.0963±0.011 | 0.0019±0.000 | 0.8977 | 0.3129±0.003 | 0.2027±0.025 | 0.9988 |
| | **1** | 0.1060±0.061 | 0.0009±0.000 | 0.9316 | 0.6088±0.007 | 0.1197±0.021 | 0.9979 |
| | **1.5** | 0.0351±0.008 | 0.0012±0.001 | 0.7657 | 0.7755±0.012 | 0.4657±0.294 | 0.9999 |
| | **2** | 0.2303±0.060 | 0.2769±0.015 | 0.9586 | 0.9708±0.016 | 0.1237±0.049 | 0.9999 |
| | **2.5** | 0.4079±0.064 | 0.0021±0.000 | 0.9819 | 1.1589±0.020 | 0.0591±0.011 | 0.9988 |

### 5.4.7. Intraparticle diffusion model

As shown in Fig. 5.38, the linear regression does not cross the origin; representing that the intraparticle diffusion mechanism is not the only rate-controlling step for the As (III) and As (V) adsorption by both MRB-800 and MJB-800.

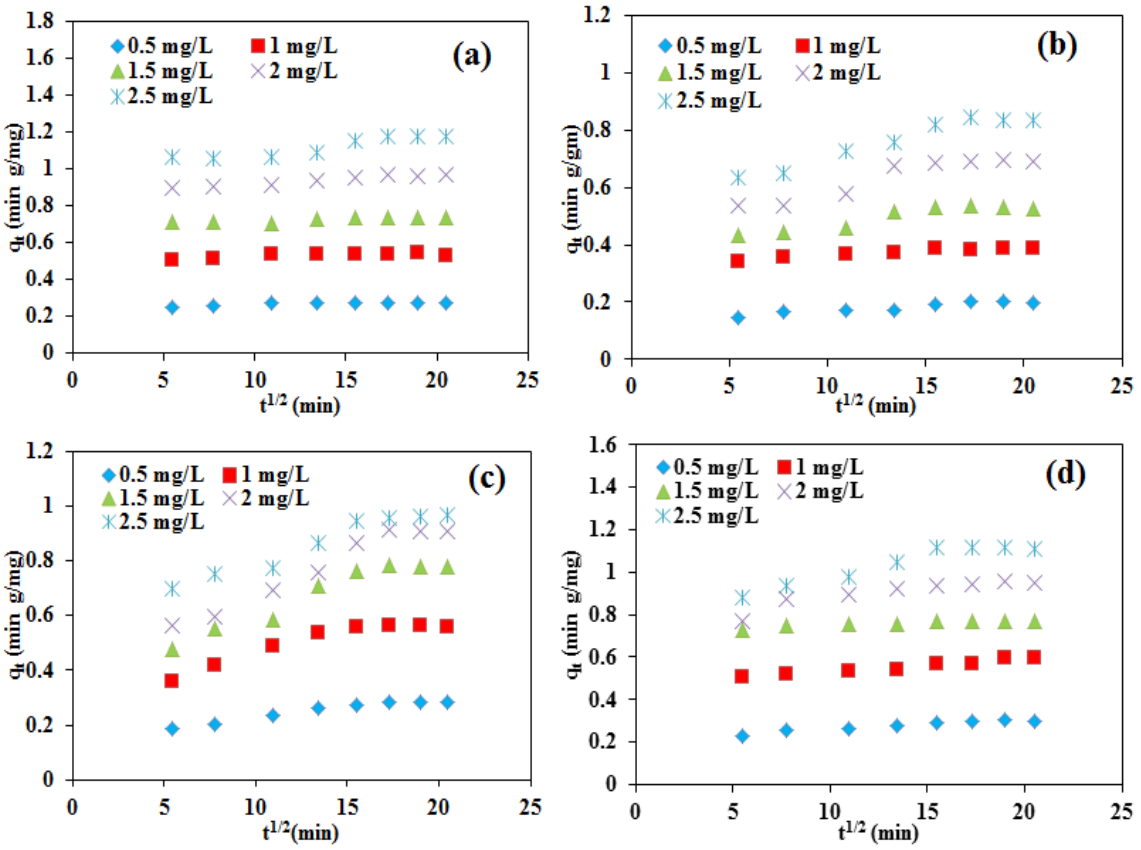


**Fig. 5.38. Graphs for intraparticle diffusion model, (a) and (b) for adsorption of As(III) and As(V) by using MRB-800 and (c) and (d) for adsorption of As(III) and As(V) by using of MJB-800.**

### 5.4.8. As removal from collected ground water samples

The MRB-800 shows good removal percentage than MJB-800. Thus, MRB-800 was further used for groundwater treatment contaminated with As. The removal of As(III)

was ~92.71, ~94.44, ~88.16, ~92.69 and ~96.76 % while the adsorption of As(V) was ~81.17, ~81.71, ~88.38, ~81.00 and ~92.25 %, respectively, for MK, HP, BG, J-I and J-II.

### 5.4.9. Mechanism involved in Arsenic adsorption

Fig. 5.39 illustrated the adsorption mechanism of As on both iron-modified bioadsorbents MRB-800 and MJB-800. Surface complexation and electrostatic attraction were the two most dominant mechanisms involved in the As(III and V) adsorption and were better understood by functional groups as well as by elemental composition of MRB-800 and MJB-800.

In electrostatic attraction, the adsorption mechanism generally depends on the adsorbate speciation and the bioadsorbents surface charge. MRB-800 and MJB-800 consist of more $H^+$ ions because of the acidic ($FeCl_3$) treatment of raw biomass. The negatively charged As oxyanions were attracted towards the positively charged bioadsorbents surface via electrostatic attraction (Lin et al., 2019; Ali et al., 2020).

It was observed that the adsorption of both As species was maximum at slightly acidic conditions by both MRB-800 and MJB-800 that was might be because of the complexation between the As ions and the hydroxyl group present on both the bioadsorbents surface. The complexation of hydroxyl and carboxylic acid groups on the surface of MRB-800 and MJB-800 forms more stable new complexes of As (Liu et al., 2019b).

As per the obtained results of FTIR, it was observed that iron modified magnetic biochar composites contain hydroxyl group or oxygenated functional groups on its surface. Oxidative modification of biochar introduces various oxygen comprising surface functional groups (-OH, -COOH, etc.) to the biochar (Wang et al., 2019c). After As loading

on MRB-800 and MJB-800 intensities of the peak at 3454.99 $cm^{-1}$ and 3467.38 $cm^{-1}$ that represents –OH group has been changed. In case of MRB-800 intensity of peaks after As adsorption was increased while a decrease in the peak intensity for MJB-800 was observed. The result designates that As ions might coordinate with the hydroxyl group present on the magnetic biochar surface. Two new peaks 1614.70 $cm^{-1}$ and 1022.16 $cm^{-1}$ were also appeared after As (III and V) adsorption by MRB-800 and MJB-800, respectively, that might be due to As adsorption by both bioadsorbents.

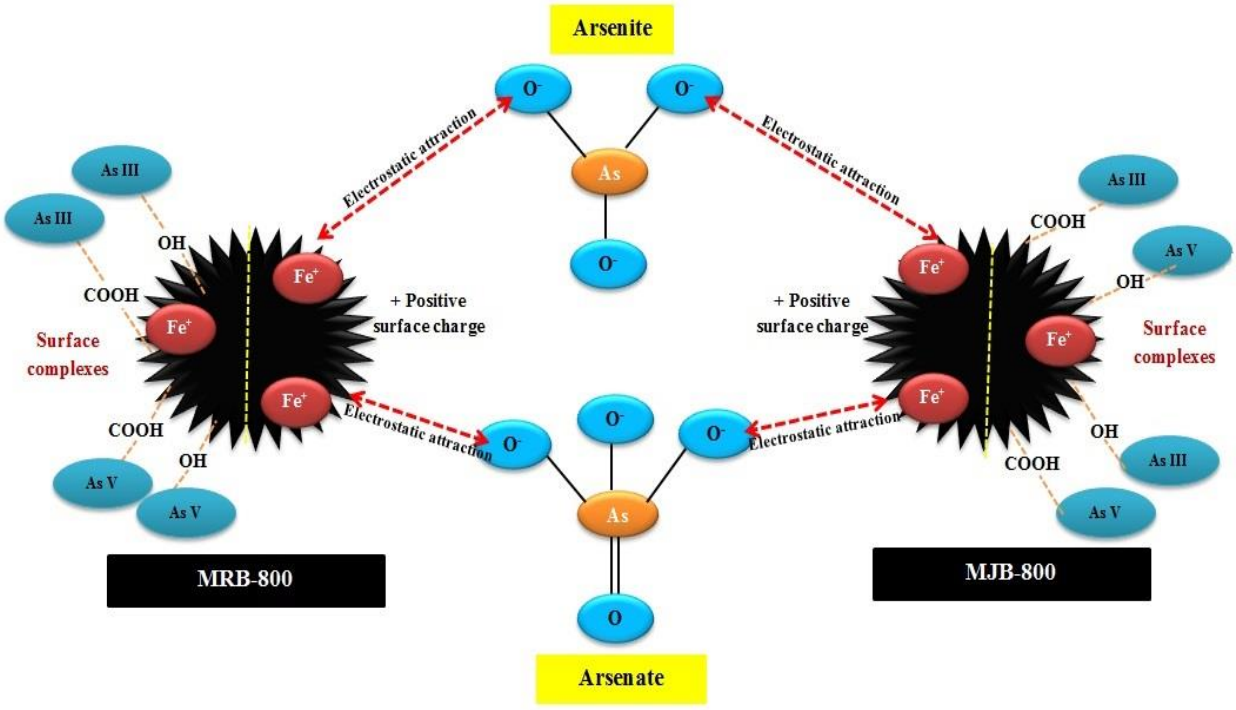


**Fig. 5.39. Proposed mechanism of As removal using MRB-800 and MJB.**

## 5.5. Phase IV: Characterization and application of monometallic and bimetallic biochar prepared using *Tectona* dry waste leaves for the removal of As(III) from aqueous solution and groundwater.

### 5.5.4. Characterization

#### *5.5.4.1. SEM and EDS*

Fig. 5.40a and c presented the SEM and EDS images of Fe-TB and Fe/Mn-TB before As(III) adsorption. The scanning electron micrographs indicated that both the biochar materials were irregular in shape with rough surface.

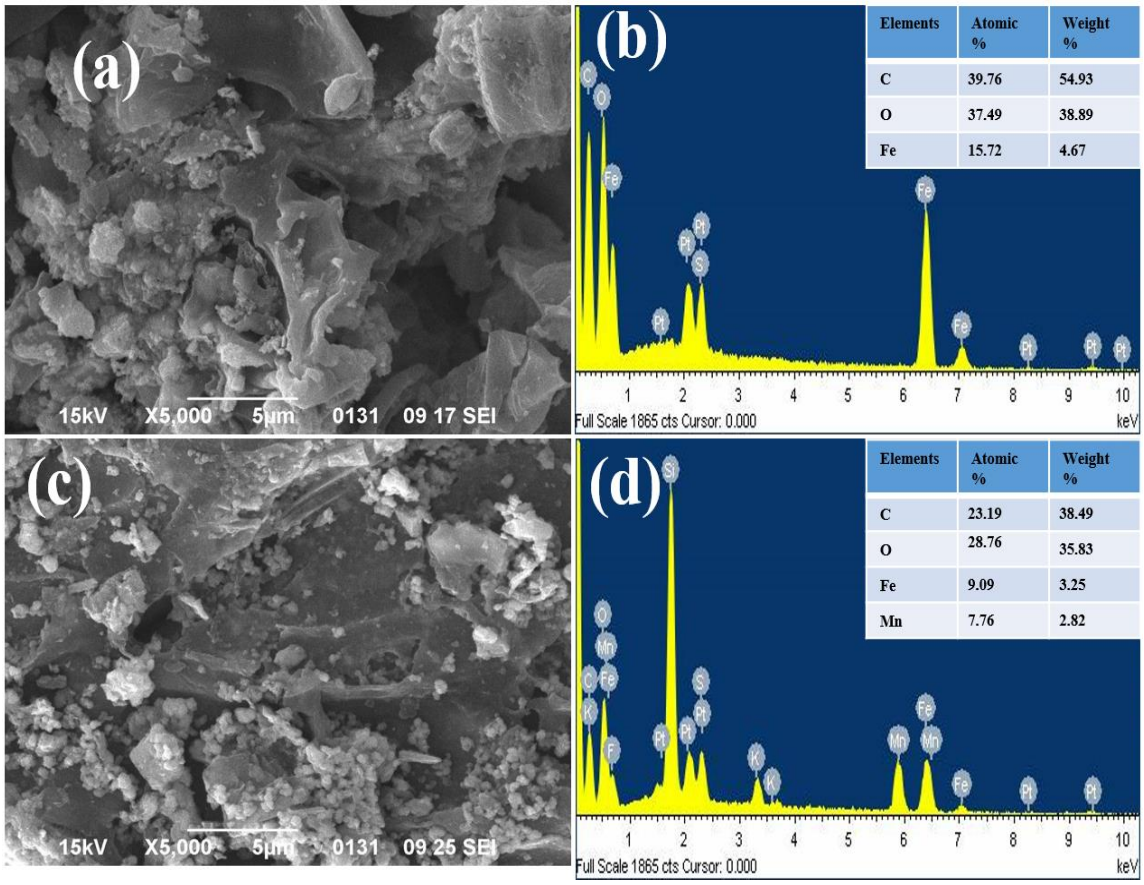


**Fig. 5.40. SEM images of the (a) and (c) Fe-TB and Fe/Mn-TB, respectively, (b) and (d) EDX images of Fe-TB and Fe/Mn-TB, respectively.**

Fig. 5.40b and d, represents the elemental composition of both biosorbent which reveals that the Fe-TB has 39.76 % and Fe/Mn-TB has 23.19 % of carbon by weight %. The presence of Fe and Mn shows the successful infusion of these elements to the waste biomass.

### *5.5.4.2. FTIR*

The surface functional group of Fe-TB and Fe/Mn-TB before and after loading of As(III) was analyzed using FTIR and the spectrum was shown in Fig. 5.41a and b. The FTIR spectra of Fe-TB and Fe/Mn-TB shows distinct number of peaks and also the variations in peaks before and after As(III) adsorption. In the spectra of FTIR, the peaks found between wavenumber 3855.54-3002.73 $cm^{-1}$ attributes the presence of stretching of –OH (hydroxyl) group. The peaks appeared between 2889.46 and 2332.14 $cm^{-1}$ corresponds to $CH_2$ or C-H bond. The peaks at 1730.50 or 1799.45 $cm^{-1}$ corresponds to –CO and C=C bond vibration whereas, the peaks with 1528.59, 1518.74 $cm^{-1}$ wavenumber ascribes to the presence of carboxyl group (-COOH) (Ali et al., 2020). The peaks at wavenumbers 1435.02, 1430.09, 1311.90, 1287.27$cm^{-1}$ attributed to the stretching of C=O vibration, bending vibration of C-H in the plane. The peaks at 1139.53, 1080.43, 1016.41 and 1075.51 $cm^{-1}$ shows the asymmetric stretching of O-H vibration and C-O groups of alcoholic compounds. Few aromatic hydrogen groups were also found in the spectrum that was designated by the 872.77 $cm^{-1}$ peak. The peaks found near 690.56 -552.66 $cm^{-1}$ indicated the occurrence of Fe-O iron stretching (Verma et al., 2021). Some small peaks were appeared near wavenumber 739.80 and 483.72 correspond to the Mn-O stretching (Xiong et al., 2017).

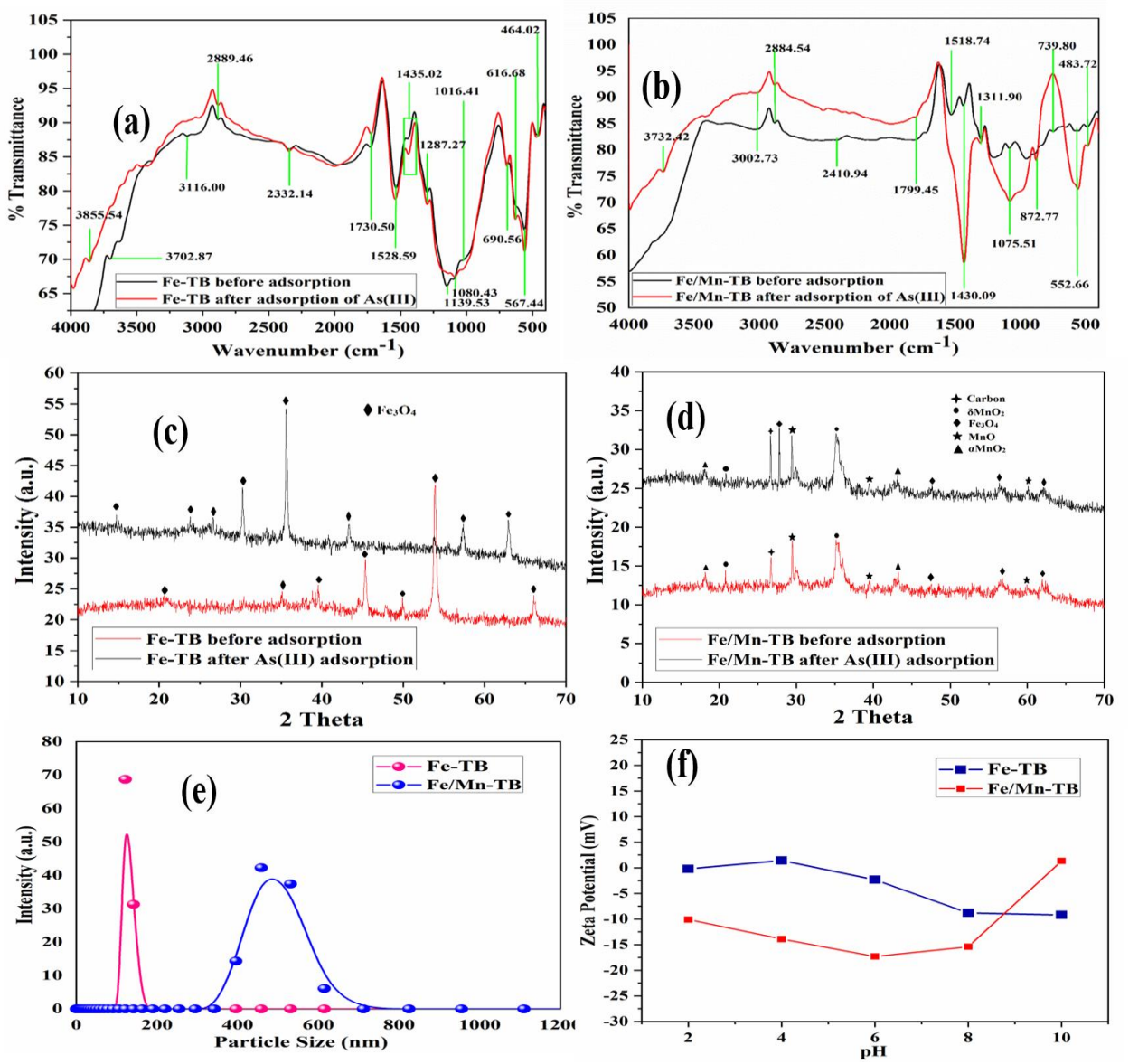


**Fig. 5.41. (a) and (b) FTIR analysis of Fe-TB and Fe/Mn-TB, respectively, (c) and (d) XRD analysis of Fe-TB and Fe/Mn-TB, respectively, (e) PSA analysis and (f) Zeta potential of Fe-TB and Fe/Mn-TB.**

Almost similar pattern of spectrum was found for Fe-TB before and after As(III) removal but the change in the peaks intensity was might be due to the adsorption of As on

to the biosorbent surface. In case of Fe/Mn-TB FTIR spectra before and after adsorption, the peak 739.80 $cm^{-1}$ disappeared, and the peak 1430.09 $cm^{-1}$ intensity was increased. Shift in peaks and change in peaks intensities might be due to the adsorption of As and this could be described by the some of the adsorbate and adsorbents (functional groups) interaction.

### *5.5.4.3. XRD*

The crystallographic and amorphous properties of biosorbents were evaluated through X-ray diffraction analysis. Fe-TB and Fe/Mn-TB, both the biochar materials were examined for determination of their crystalline and amorphous nature before and after adsorption of As(III). Fig. 5.41c shows sharp and narrower peaks at 2θ= ~14°, ~20°, ~35°, ~45°, ~50°, ~57°, ~62° and ~66° for Fe-TB indicates that Fe-TB consists single Fe compound in the $Fe_3O_4$ crystal structure. This validates the formation of biochar having magnetic properties. After adsorption process, certain peaks shows lower intensities at 2θ= ~43° and ~53°, it was also monitored that some new peaks were appeared at 2θ= ~26, ~30 and 53°. Higher intensity of peak at 2θ= ~35° was observed. As per the results obtained by Rahman et al. (2020) these peaks represent the ferric arsenate compound (Darezereshki et al., 2018).

The XRD pattern for FeMn-TB before and after As(III) adsorption were shown in Fig. 5.41d. The diffraction peaks of Fe/Mn-TB corresponds to the $Fe_3O_4$ (2θ= ~47°, ~56° and ~62°), δ$MnO_2$ (2θ= ~20° and ~35°), α$MnO_2$ (2θ= ~18°, and ~42°), MnO (2θ= ~29°, ~39° and ~60°) and few peaks of carbon as shown in the Fig. 2d. The change in the pattern and intensities of diffraction peaks was might be due to some interaction taking place between the adsorbate and biosorbents surface. Similar diffraction peaks were also reported in the study conducted by Tan et al. (2020b).

#### *5.5.4.4. Particle Size Analysis*

Particle size analysis of Fe-TB and Fe/Mn-TB was performed to examine the size of the biosorbent. For particle size analysis the biochar was initially homogenized and ultra-sonicated after being added in ethyl alcohol solution (dispersal medium). As presented in Fig. 5.41e, the average size of Fe-TB was in the range of 100-200 nm whereas, the average particle size of Fe/Mn-TB composite was found in the range of 350-750 nm.

#### *5.5.4.5. Zeta potential*

The stability of biochar material at a specific pH was analyzed by zeta potential. Any biosorbent is said to be stable when the zeta potential value is more than ±30. The magnitude of zeta potential illustrate the degree of stability of biosorbent in dispersion media, which undertake the electrostatic repulsion amongst dispersed medium and biosorbent. Fig. 5.41f shows that the zeta potential value was <±30, hence both the materials were not highly stable. The zeta potential value for Fe-TB was found in range of -0.209 mV-1.43 mV and -17.3 mV-1.36 mV. So, both these materials shows incipient stability.

#### *5.5.4.6. $pH_{ZPC}$*

The point of zero charge is one of the very essential parameter of biosorbent to be determined. The point of zero charge describing the pH dependent net surface charge on biosorbent is zero. The $pH_{ZPC}$ of both the biosorbent was determined after its synthesis and the values of point of zero charge for Fe-TB was 2.9 and 8.2 for Fe/Mn-TB.

### 5.5.2. Adsorption experiment

#### *5.5.2.1. Effect of biochar dosage on As(III) adsorption*

The biochar concentration in As(III) solution is one of the most essential factor in adsorption process. The process of adsorption is highly influenced by the increasing or decreasing the amount of biochar concentration in aqueous solution of As(III).

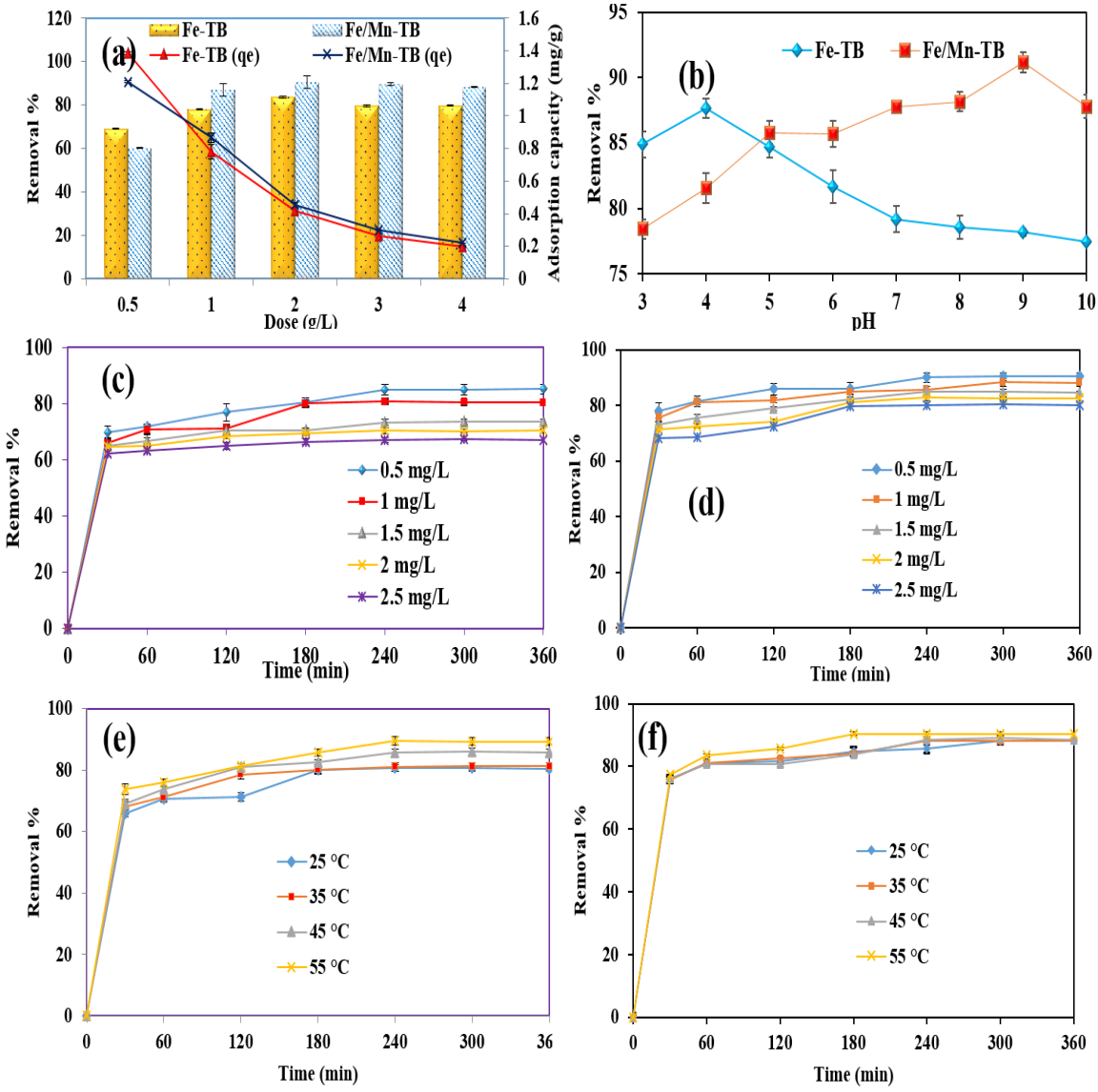


**Fig. 5.42. Effect of (a) Dose, (b) pH, (c) and (d) Initial concentration of As(III) on adsorption by Fe-TB and Fe/Mn-TB, respectively, (e) and (f) Effect of operating temperature on As(III) adsorption by Fe-TB and Fe/Mn-TB, respectively.**

The influence of biochar (Fe-TB and Fe/Mn-TB) dosage on As(III) adsorption was assessed by varying biochar quantity in the range of 0.5 g/L-4 g/L. Fig. 5.42a represents the outcomes of dose study and it was found that the adsorption of As(III) was maximum with 2 g/L (~83.8 %) and 2 g/L (~90 %) using Mn-TB, Fe-TB and Fe/Mn-TB, respectively. Further, on increasing the biosorbent dose, the adsorption efficiency was decreased. On increasing the biochar concentration, overlapping of active sites might occurs due to the aggregation or clump formation (Verma and Singh, 2019), resulting in decreased adsorption of As(III) increasing dosage of Fe-TB and Fe/Mn-TB.

#### *5.5.2.2. Effect of pH*

The solution pH is one of the very vital parameter defining surface charge, speciation of adsorbate, and degree of ionization etc. The pH effect on As(III) adsorption was examined by varying pH of the solution in the range of 3-10. The Fig. 5.42b presented the obtained results that illustrate that the maximum adsorption of As(III) by Fe-TB was ~87.68 % at 4 pH and the slightly decreased with increment in pH of solution. Whereas, the highest adsorption of As(III) was ~91.18 % achieved at 9 pH by using Fe/Mn-TB. Below pH 9.2 As(III) is present as $H_3AsO_3$ in an aqueous medium and beyond pH 9.3 this neutral form of As dissociated into negatively charged arsenite ions ($H_3AsO_3^-$). As the $pH_{ZPC}$ of Fe-TB and Fe/Mn-TB was 2.9 and 8.2, respectively, below this pH value both these materials were positively charged and above this pH the biosorbent surface have net negative charge (Cuong et al., 2021) and the neutral charged As ($H_3AsO_3$) species was adsorbed onto negatively charged biosorbent surface and effective adsorption was found at pH 4 and 9. The removal of As(III) was not much affected by the pH of the solution, only slight reduction in adsorption was observed with varying solution pH.

### *5.5.2.3. Effect of initial As concentration and contact time*

The impact of initial adsorbate concentration on adsorption process was illustrated in Fig. 5.42c and d. The experimental results shows that adsorption of As(III) by both biosorbents decreased with increasing concentration from 0.5 mg/L to 2.5 mg/L. The maximum adsorption was ~84.85 % by Fe-TB and ~90.35 % by Fe/Mn-TB, obtained at 0.5 mg/L initial concentration. Gradual decrease in adsorption of As(III) on an raise in initial concentration was because of the saturation of biosorbent surface that limits the active adsorption sites. Fig. described that the adsorption capacities of biosorbent increased with an increase in As(III) initial concentration. The maximum axdsorption capacity for As(III) removal by Fe-TB was 0.831 mg/g and 1.002 mg/g by Fe/Mn-TB at 2.5 mg/L initial adsorbate concentration (Fig 5.43a and b).

At initial point of adsorption experiment, the process of As(III) removal was less and increased as the contact time was increased and the time of equilibrium was attained in 240 min for both the biosorbents but there was no significant increase in As(III) adsorption was observed on further increasing contact time. Primarily, the number of vacant binding active sites were available abundantly but after a certain time period these vacant sites were occupied by the As ions and decrease in available active binding sites resulting in decreased As adsorption (Priyan et al., 2021; Ayub et al., 2020).

### *5.5.2.4. Effect of temperature*

The impact of temperature on adsorption of adsorbate i.e., was studied using different temperature (25 °C to 55 °C). The obtained experimental results are shown in Fig. 5.42e and f and the results shows that with increasing operating temperature from 25 °C to 55 °C, adsorption of As(III) was also increased. The maximum adsorption of As was found

to be ~89.42 % and ~90.42 % at 55 °C using Fe-TB and Fe/Mn-TB, correspondingly. The adsorption of As(III) via Fe-TB and Fe/Mn-TB was found to be endothermic. The adsorption capacity was also increased with an increase in temperature (Fig. 5.43c and d).

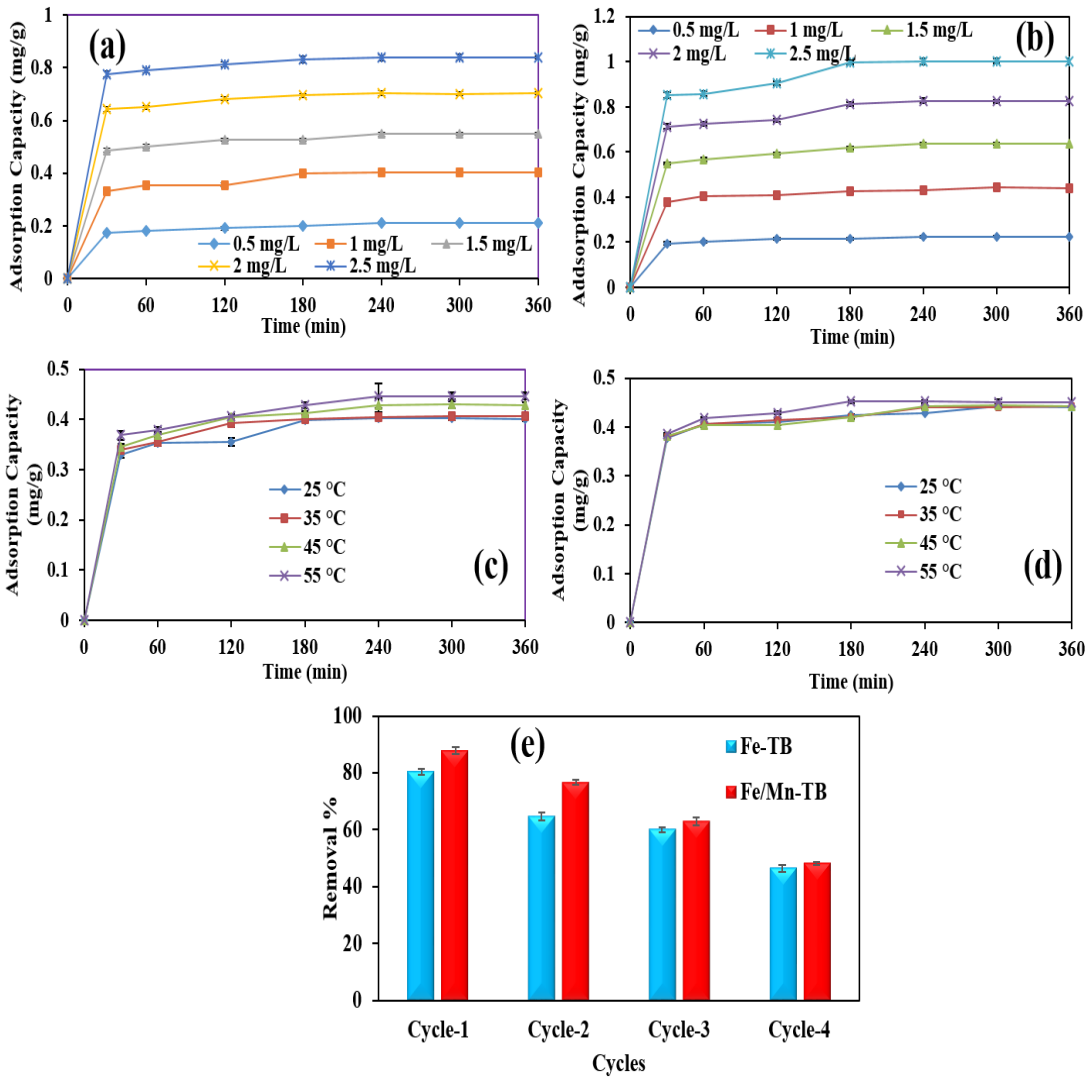


**Fig. 5.43. Effect of (a) and (b) Initial concentration of As(III) on adsorption capacity of Fe-TB and Fe/Mn-TB, respectively, (c) and (d) Operating temperature on adsorption capacity of Fe-TB and Fe/Mn-TB, respectively, and (e) Regeneration of Fe-TB and Fe/Mn-TB.**

Increased in removal percentage with temperature elevation was might be due to the high temperature help to incapacitate the high activation barrier, resulting in an increase in adsorption. As reported by Kazi et al. (2018) sometimes biosorbents need high temperature or sometimes needs low temperature for the activation of surface active binding sites.

### 5.5.3. Regeneration study

Regeneration of spent or used biochar is a very essential step and a very significant characteristics of any biosorbents. For recycling of Fe-TB and Fe/Mn-TB, the used biochar was separated out physically from As(III) solution after adsorption using magnet then kept into desorbing solution (0.1 M NaOH) for 24 h and then washed with deionized water until its pH reaches to neutral. The biochar materials were then dried and used for next adsorption cycle. The results shows that the removal percentage was decreased with number of cycles. The pattern of decreased adsorption percentage per cycle for both the biosorbent was alsmost similar. The Fig. 5.43e presented that the adsorption of As(III) was drops from ~80.3 % to ~46.4 % for Fe-TB and ~87.8 % to ~48.8 % from initial first to forth regeneration cycle.

### 5.5.4. Isotherm study

The experimental design of adsorption process was described by using the adsorption isotherms. The obtained results revealed that the adsorption of As(III) on Fe-TB ($R^2$=0.9926) and Fe/Mn-TB ($R^2$=0.9959) shows more conformity with Freundlich isotherm model with greater value of $R^2$ than that of Temkin and Langmuir isotherm (Fig. 5.44 a-c). The compliance of adsorption process with Freundlich model of isotherm explained the physiosorption and multilayer sorption mechanism (Araujo et al., 2018). The

process of As(III) adsorption is said to be favorable physical process when the value of Freundlich constant (1/n) is less than 1 and close to 0 (Verma et al., 2021). All the values were given in Table 5.15.

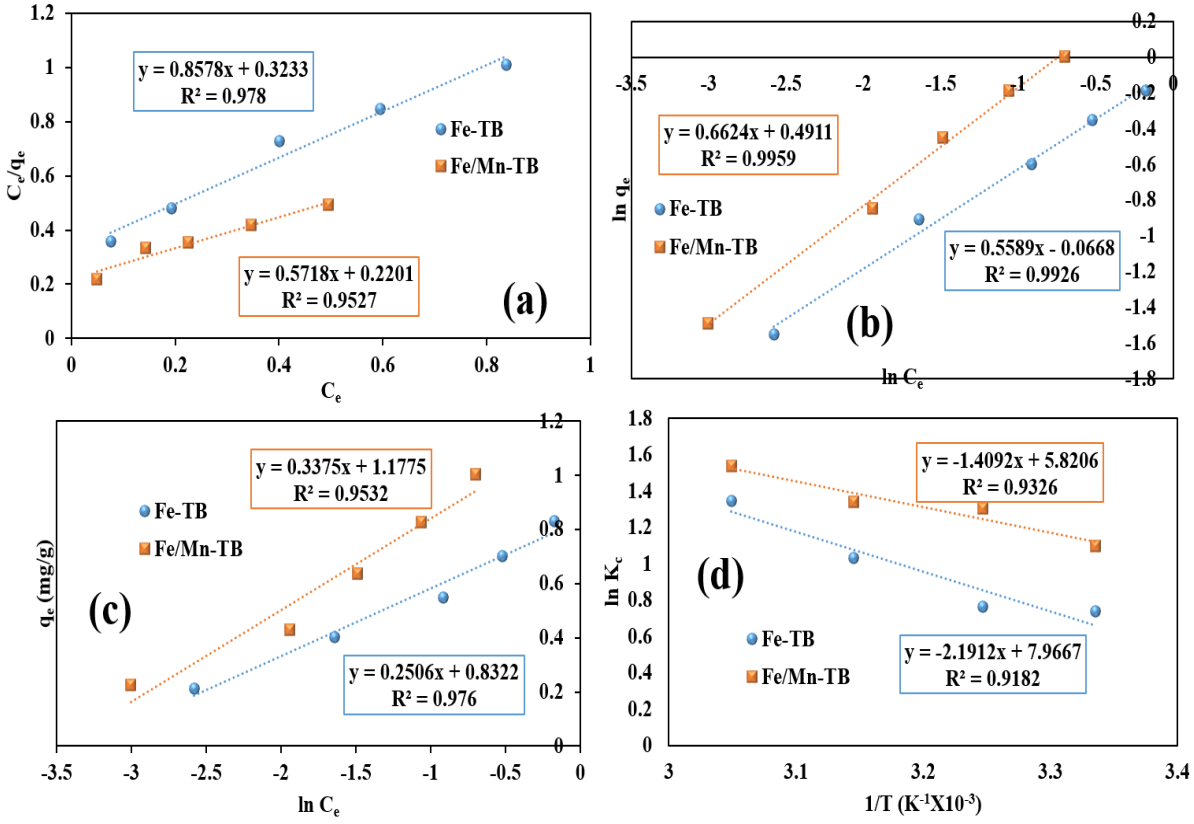


**Fig. 5.44. Plot for (a) Langmuir isotherm, (b) Freundlich isotherm, (c) Temkin isotherm and (d) Thermodynamics study for Fe-TB and Fe/Mn-TB.**

**Table 5.15. Isotherm parameters for As(III) adsorption using Fe-TB and Fe/Mn-TB.**

| Isotherm model | Parameters | Values | |
|---|---|---|---|
| | | Fe-TB | Fe/Mn-TB |
| Langmuir isotherm | *Q0 (mg/g)* | 1.1658±0.1700 | 1.7489±0.1317 |
| | *b (L/mg)* | 2.6533±0.7412 | 2.598±0.6015 |

| | | | |
|---|---|---|---|
| | $R_L$ | 0.1310±0.0256 | 0.1334±0.0262 |
| | $R^2$ | 0.978 | 0.9527 |
| **Freundlich isotherm** | $K_F$ $(mg/g(L/mg)^{1/n})$ | 0.9354±0.0174 | 1.6341±0.0046 |
| | $N$ | 1.7892±0.1004 | 1.5097±0.0941 |
| | $R^2$ | 0.9926 | 0.9959 |
| **Temkin isotherm** | $B$ | 0.251±0.0142 | 0.3375±0.017 |
| | $K_T$ (L/g) | 27.683±4.2733 | 32.7495±6.855 |
| | $R^2$ | 0.976 | 0.9532 |

### 5.5.5. Thermodynamics

The results of thermodynamic study revealed that the values of entropy and enthalpy was found to be positive. The adsorption of As(III) by both the synthesized biosorbents i.e., Fe-TB and Fe/Mn-TB was endothermic, the adsorption was increases as the operating temperature was raised from 25 °C to 55 °C (Fig. 5.44 d). The results were verified by the negative value of $\Delta G°$ for As(III) adsorption by Fe-TB and Fe/Mn-TB. The value of ΔS was 0.0662 kJ/mol for Fe-TB and 0.0484 kJ/mol for Fe/Mn-TB, respectively. Whereas, the value of $\Delta H°$ was 0.0182 kJ/mol and 0.0117 for As(III) adsorption using Fe-TB and Fe/Mn-TB, correspondingly. The process of adsorption is spontaneous and feasible represented by negative $\Delta G°$ values i.e., found in range of -19.720 to -21.707 kJ/mol and -14.409 to -15.861 kJ/mol using Fe-TB and Fe/Mn-TB, respectively, as biosorbent for As(III) removal (Table 5.16). The positive $\Delta S°$ values designates increases randomness between interface of solid biosorbent surface and liquid adsorbate whereas, the positive value of $\Delta H°$ represents the endothermic process of adsorption (Imran et al., 2021; Massoudinejad et al., 2020).

**Table 5.16. Thermodynamics parameters for As(III) adsorption by using Fe-TB and Fe/Mn-TB.**

| Parameters | Temperature (K) | Fe-TB | Fe/Mn-TB |
|---|---|---|---|
| **ΔG° (KJ/mol)** | 298 | -19.720±5.933 | -14.409±2.641 |
| | 308 | -20.382±6.132 | -14.893±2.730 |
| | 318 | -21.045±6.331 | -15.377±2.818 |
| | 328 | -21.707±6.531 | -15.861±2.907 |
| **ΔS° (KJ/mol)** | | 0.0662±0.006 | 0.0484±0.009 |
| **ΔH° (KJ/mol K)** | | 0.0182±0.020 | 0.0117±0.003 |

### 5.5.6. Kinetics study

The kinetic study was performed with different initial As(III) concentrations and contact time. Based on obtained results it was illustrated that the experimental data shows better compliance with the Pseudo-second order kinetics than pseudo-first order kinetics. The results shows the instant enhancement in uptake of As(III) with increasing contact time and obeyed slow adsorption rate to attain the equilibrium. Moreover, about 80 % of As was adsorbed through Fe/Mn-TB within 1 h, while ~70 % of As was adsorbed after 1-2 h using Fe-TB and did not show any rapid change. This was happened might be due to the elaboration of adequate Arsenic binding sites on the Fe/Mn-TB surface. The data was fitted well to the pseudo-second order kinetics with linear regression coefficient ($R^2$) with above than 0.9986 (Fig. 5.45c and d) (Table 5.17). The plots for pseudo-first order kinetics were presented in Fig. 5.45a and b.

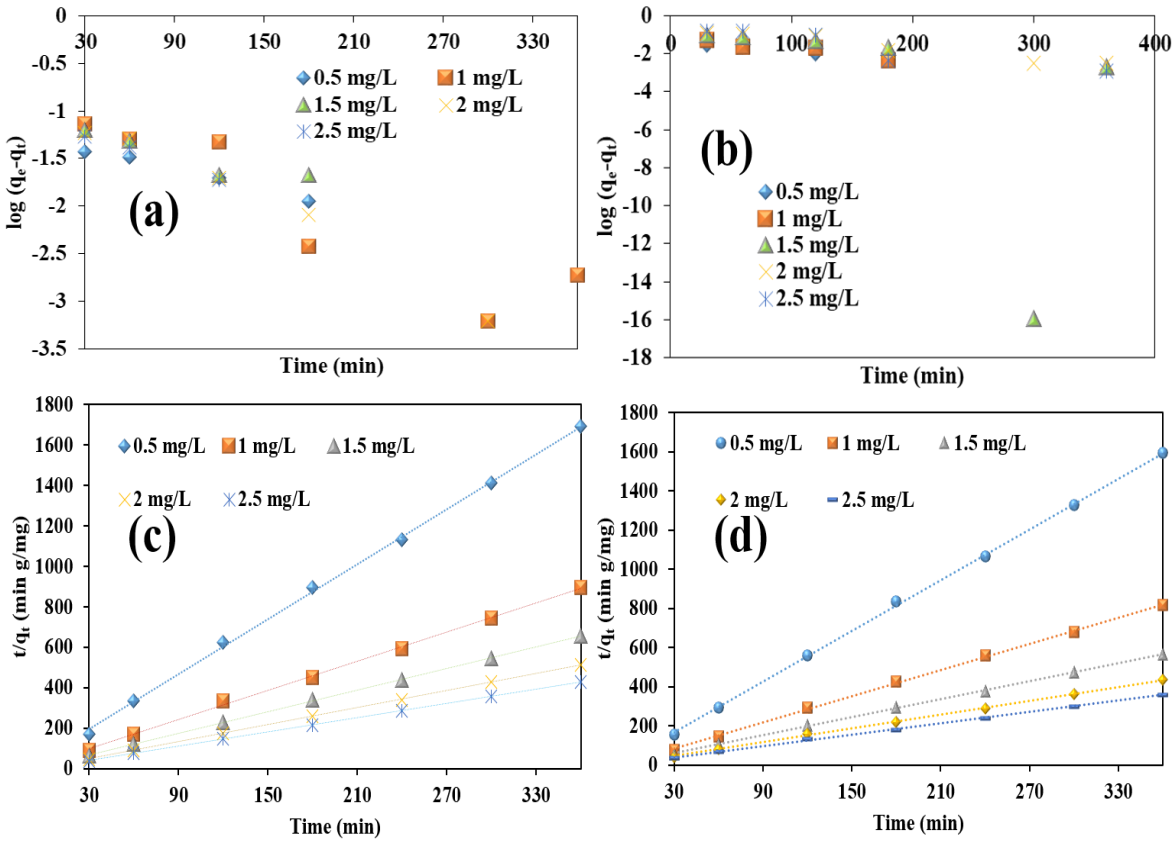


**Fig. 5.45. Plots of pseudo-first-order kinetics (a) Fe-TB and (b) Fe/Mn-TB and pseudo-second-order kinetics (c) Fe-TB and (d) Fe/Mn-TB for As(III) adsorption.**

**Table 5.17. Parameters of pseudo-first order and pseudo-second order kinetics.**

| Kinetics | | Pseudo-first order | | | Pseudo-second order | | |
|---|---|---|---|---|---|---|---|
| | $C_0$ (mg/L) | $q_e$ (mg/g) | $k_1$ ($min^{-1}$) | $R^2$ | $q_e$ (mg/g) | $k_2$ (g/mg min) | $R^2$ |
| Fe-TB | **0.5** | 0.0506±0.010 | 0.0015±0.000 | 0.9899 | 0.2203±0.003 | 0.3525±0.013 | 0.9991 |
| | **1** | 0.1113±0.022 | 0.0026±0.001 | 0.8374 | 0.4161±0.001 | 0.4921±0.158 | 0.9986 |
| | **1.5** | 0.0740±0.010 | 0.0015±0.001 | 0.8643 | 0.5343±0.017 | 0.6058±0.202 | 0.9997 |
| | **2** | 0.1328±0.039 | 0.0032±0.002 | 0.9808 | 0.7132±0.005 | 0.3060±0.042 | 0.9999 |
| | **2.5** | 0.0797±0.012 | 0.0023±0.001 | 0.992 | 0.8497±0.001 | 0.2927±0.083 | 0.9999 |
| Fe/Mn-TB | **0.5** | 0.0344±0.025 | 0.0014±0.003 | 0.8926 | 0.2309±0.001 | 0.5396±0.001 | 0.9996 |
| | **1** | 0.0722±0.005 | 0.0027±0.000 | 0.9000 | 0.4493±0.000 | 0.2665±0.001 | 0.9994 |
| | **1.5** | 2.1237±1.142 | 0.0107±0.005 | 0.305 | 0.6523±0.000 | 0.1793±0.000 | 0.9997 |
| | **2** | 0.2072±0.006 | 0.0024±0.000 | 0.9411 | 0.8488±0.001 | 0.1220±0.000 | 0.999 |
| | **2.5** | 0.2869±0.041 | 0.0030±0.001 | 0.8702 | 1.0350±0.001 | 0.0932±0.001 | 0.999 |

### 5.5.7. Intraparticle diffusion model

The intraparticle diffusion model was also examined to assess the rate controlling step and uptake mechanism for As(III) adsorption by synthesized Fe-TB and Fe/Mn-TB. The Fig. 5.46a and b, shows that the regression of intraparticle diffusion was not a straight line and does not pass through origin that might be due to the varying contact time and distinctive mass transfer rate. Thus, intraparticle diffusion was not the only rate limiting factor involved in As(III) adsorption process.

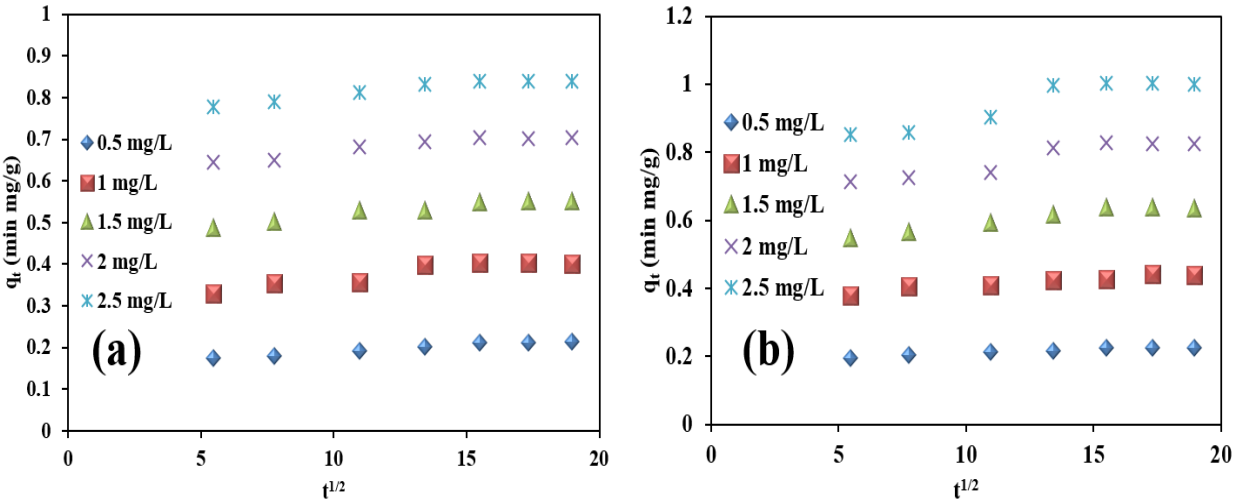


**Fig. 5.46. Plots of intraparticle diffusion model (a) Fe-TB and (b) Fe/Mn-TB.**

### 5.5.8. As removal from groundwater

The detected concentration in collected groundwater samples were higher than the permissible limits set by WHO. Then the samples were treated using 2.5 g/L dose of Fe/Mn-TB as the adsorption capacity of Fe/Mn-TB was better than that of Fe-TB. Adsorption of As(III) was 79.73, 84.32, 82.20, 83.80 and 80.05 %, correspondingly for MK, HP, BG, J-I and J-II.

### 5.5.9. Proposed mechanism of As adsorption on to Fe-TB and Fe/Mn-TB

Fig. 5.47 shows the proposed mechanism of As adsorption onto the synthesized monometallic and bimetallic biochar. Monometallic and bimetallic biochar comprises abundant in functional groups, that can provides enough adsorptive interaction sites on the biosorbent surface for the As adsorption (Zhong et al., 2019; Verma and Singh, 2019). For example, FTIR spectra of Fe-TB and FeMn-TB contains various oxygenated surface functional groups because of the oxidative modification or oxidative treatment of biomass. The oxidative modification was substantiates the presence of oxygen containing functional groups on biosorbents surface like; -OH, COOH etc. A minor alteration of spectral pattern was observed after As loading to Fe-TB. A peak near wavenumber 3116.00 $cm^{-1}$ was disappeared and the peak found at 1139.58 $cm^{-1}$ was shifted to 1080.43 $cm^{-1}$ which were allocated to –OH and C-O band stretching (Cuong et al., 2021). An increase in the 567.44 $cm^{-1}$ peaks intensity was also observed which was assigned to the Fe-O group and that show the involvement of iron in the adsorption of As in case of Fe-TB. Whereas, in case of Fe/Mn-TB, the peak at wavenumber 3732.42 $cm^{-1}$ was appeared and the intensity of peaks at 1430.09, 1475.15 and 552.66 and 483.72 $cm^{-1}$ was increased, which corresponds to C=O, C-H, Fe-O and Mn-O stretching, respectively, after loading of As on to the biosorbent. The change in the peaks intensities was might be due to the involvement of these functional groups in the As adsorption (Xiong et al., 2017) or these change was might be due to the formation of new complexes due to the interaction of biosorbent with the As and was supported by the complexation mechanism (Benis et al., 2020).

The electrostatic attraction was also a possible mechanism that favors the adsorption of As onto the biosorbent surface. As(III) was adsorbed by the Fe-TB and

Fe/Mn-TB at pH 4 and pH 9, correspondingly, as the $pH_{ZPC}$ of Fe-TB was 2.3 and Fe/Mn-TB was 8.2, that means the biosorbent contains more $OH^-$ ions above this pH and below this pH these biosorbents consists $H^+$ or positive surface charge. Below pH 9.2 As(III) is present in its neutral form i.e., $H_3AsO_3$ and was get adsorbed by the negatively charged biosorbents through electrostatic attraction (Baig et al., 2014; Tan et al., 2020b). Removal of As can also be accelerated by the formation of H-bonds between the aromatic groups present on biochar surface and molecules of arsenite. Similar adsorption mechanism was also reported by Jing et al. (2014).

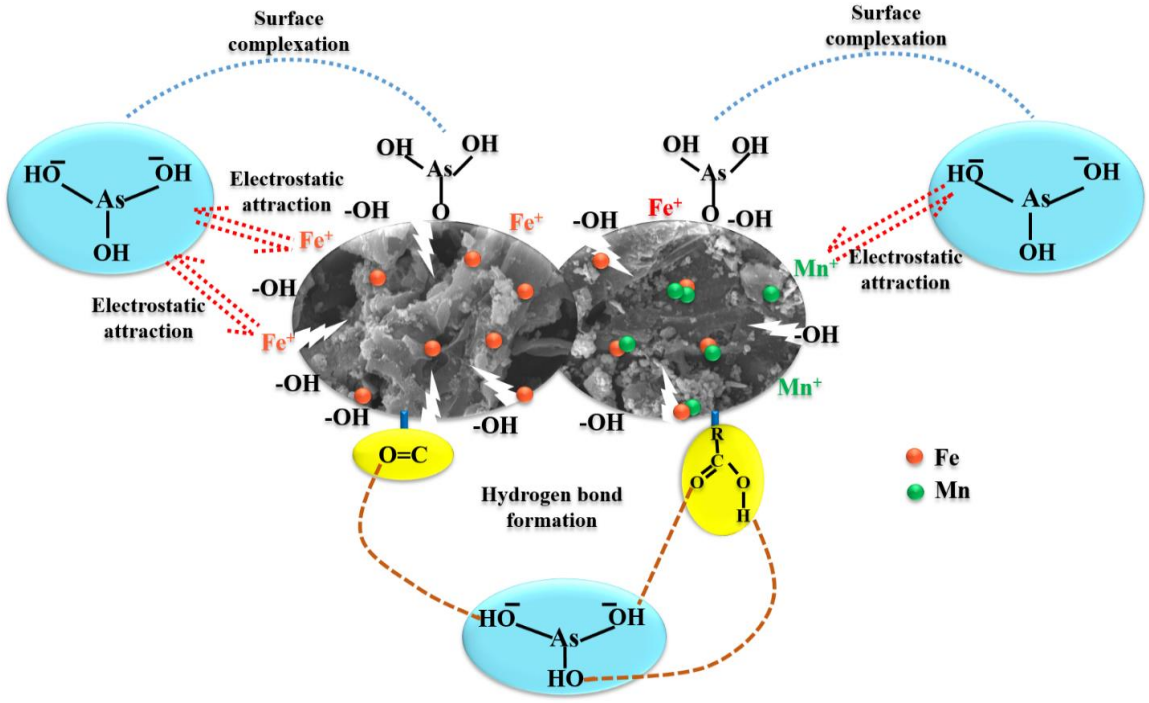


**Fig. 5.47. Proposed mechanism of As(III) adsorption on Fe-TB and Fe/Mn-TB.**

# *Chapter-6*
# *Summary*

# Chapter-6 Summary

Water is the most necessary and basic requirement for the survival of all life forms, on the planet earth. Noticeably only 1 % of total water resources is usable and in that 1 % groundwater contributes about 96%. Over the last several decades, As contaminated groundwater posing several health-related issues. As poisoning can cause skin diseases, obstructive lung illness, arsenicosis, black foot disease, etc., and also lead to cancer in numerous body organs. The geogenic origin is the primary cause of arsenic pollution in groundwater. Several anthropogenic activities, such as mining, geothermal discharge, agricultural activities, feed additives, medicine etc. also pollute groundwater. As enters the human body primarily through the consumption of As contaminated drinking water.

Several physicochemical techniques have already been used for the treatment of As contaminated water. However, the high cost, sludge generation, less efficacy in removing pollutants, high energy cost, and specialized manpower requirement necessitate the development of a new and advanced treatment system for remediation of As from contaminated water. Besides these conventional techniques of As removal, adsorption has evolved as a simple, eco-friendly, cost-effective, time-saving and sustainable approach for water treatment including As removal without generating harmful secondary toxic by-products. Many studies have been conducted in this area and different types of adsorbents were investigated for their efficacy towards As removal. Biochar is found to be the most effective adsorbent and an emerging technique for the cost-efficient and sustainable removal of pollutants from contaminated water. The feedstock for biochar synthesis is available in bulk and synthesizing biochar from these waste biomasses not only helps to

solve the problem of waste disposal but also encourages the production of multifunctional adsorbents for the removal of As from contaminated water. According to the available literature, significant work has been done on the adsorption of As using biochar. However, the feedstock is still not been used for the development of biochar and has not been explored for their removal efficiency, mechanism and other multiple aspects. This is a major gap to be addressed in order to improve the applicability of biochar in the adsorption process. Based on these assumptions, this work has been performed in four different phases and key findings of the entire study are as follows:

**Phase I: Characterization and application of pristine biochar for the removal of As(III) and As(V) synthesized using waste dry leaves of T*ectona sp.* and *Lagerstroemia speciosa* from an aqueous solution and groundwater.**

- Firstly, four different biochar were synthesized without any modification using waste biomass of plant leave litter (*Tectona sp.* and *Lagerstroemia speciosa*) and vegetable waste (*Raphanus staivus* and *Artocarpus heterophyllus*).
- Only two biochar materials synthesized using dry leaves of *Tectona sp.* (TB 800) and *Lagerstroemia speciosa* (LB 800) showed high removal percentage of both the As species (As(III) and As(V)). Whereas, less than 10 % adsorption of both species of As was observed via biochar materials synthesized using vegetable waste. So, for further study TB 800 and LB 800 was used and in Phase III of the study, vegetable waste was modified and applied for As removal.

- The biochar was pyrolyzed at 800 °C and was characterized using different instrumental techniques such as SEM, EDX, BET, FTIR, XRD, zeta potential, $pH_{ZPC}$, PSA and XPS.
- The SEM and EDX results showed irregular and rough morphological surfaces and the elemental composition of both the adsorbents revealed that the TB 800 and LB 800 have 57.38 % and 55.51 % carbon by weight, respectively.
- About 94.6 % and 85.85 % of As(V) were adsorbed at pH 6 and pH 8 via TB 800 and LB 800, respectively. However, the highest (76.42 %) removal of As(III) was observed at pH 8 through TB 800 but in the case of LB 800, the removal of As(V) was found to be 61.67 %.
- Adsorption of As(III) and As(V) was probably due to electrostatic interaction and surface complexation mechanism. The presence of several oxygenated functional groups on the biochar surface, such as hydroxyl and carboxyl groups that play a very important role in the adsorption mechanism of As on biochar. The results were confirmed by the FTIR analysis of adsorbent before and after adsorption.
- Using TB 800, the maximum removal percentage of As(III) and As(V) was attained, with 77.9 % and 96.5 %, respectively. Noticeably, the highest removal of about 82% for As(V) and 72% for As(III) was observed by using LB 800 at the lowest initial concentration i.e. 0.5 mg/L.
- Findings of the batch adsorption investigation revealed that both the biochar materials were extremely effective in removing As(III) and As(V) from an aqueous solution as well as from groundwater, due to effective adsorption of As species from the solution. Both these materials can be successfully recycled up to four cycles.

- For the elimination of As(III), the adsorption capacity of TB 800 and LB 800 was 0.66 mg/g and 0.45 mg/g, respectively, while for As(V) the adsorption capacities of TB 800 and LB 800 were 1.25 mg/g and 0.71 mg/g, respectively.
- Experimental data followed the Langmuir model for As(V) removal using TB 800 and LB 800, Freundlich model for As(III) removal by LB 800 and Temkin model for As(III) removal by TB 800. Pseudo-second-order kinetics was observed and best fitted with the obtained As(III) and (V) removal data. Thermodynamic study revealed that the process of adsorption was endothermic for the removal of As(III) and exothermic for the adsorption of As(V) using TB 800 and LB 800
- In the next phase of the study, *Tectona sp.* and *Lagerstroemia speciosa* biomass were modified with the $FeCl_3$ to improve the adsorption capacity of biochar material and to minimize the dose requirement for As removal.

**Phase II: Characterization of magnetic biochar synthesized using waste dry leaves and their application for the removal of As(III) and As(V) from an aqueous solution and groundwater.**

- Waste dry leaves of *Tectona sp*. (MTB-800) and *Lagerstroemia speciosa* (MLB-800) were used to develop magnetic biochar materials. The ability of these synthesized biochars to adsorb As(III) and As(V) from an aqueous solution and groundwater was investigated.
- Both biochar materials were characterized by using SEM, EDX, FTIR, Raman spectroscopy, $pH_{ZPC}$, XRD, PSA and zeta potential.

- The SEM results elucidated that MTB-800 has an irregular shape and rough surface while MLB-800 has a smooth surface with an irregular shape. The results of EDX analysis showed that MTB-800 and MLB-800 have 42.79 % and 64.13 % carbon content, respectively. The presence of Fe in the EDX results indicates that the iron was successfully bound to the biomass materials. MTB-800 and MLB-800 consists 9.19 % and 5.01 % iron content, respectively, by weight percentage.
- Both the Fe-infused biochar were found to be effective in removing As(III) and As(V) from an aqueous solution and groundwater samples. MTB-800 and MLB-800 had a maximum As(III) adsorption of 92.1 % and 97.8 %, respectively. MTB-800 and MLB-800 on the other hand obtained the highest As(V) adsorption rate of 94.7 % and 96.7 %, respectively, at 0.5 mg/L As concentration.
- Results of the pH study reveal that the maximum 93.6 % adsorption of As(III) was achieved at pH 6 by MTB-800; while using MLB-800 the maximum adsorption was found to be 94.6 % at pH 8. However, adsorption of As(V) was found to be 92.85 % and 91.1 % at pH 5 by using MTB-800 and MLB-800, respectively.
- Adsorption capacity for the removal of As(III) was observed as 1.25 mg/g and 1.68 mg/g with MTB-800 and MLB-800, respectively. Whereas, the adsorption capacity of MTB-800 and MLB-800 was found to be 0.77 mg/g and 1.54 mg/g, respectively.
- Reusability test of the biochar revealed that it can be successfully reprocessed up to five cycles. Different models were explored to evaluate the breakthrough curve obtained in the column study.
- The adsorption process was well-fitted to the Langmuir model of isotherm and pseudo-second-order kinetic. The thermodynamics study revealed that the As(III) and As(V)

adsorption by MTB-800 and MLB-800 was exothermic which means the adsorption was reduced with increase in temperature.

- Batch and column studies showed that the dry leaves biomass can be successfully converted into biochar with magnetic properties and can be a good adsorbent for As(III) and As(V) removal. Both these biochar were able to adsorb significant levels of As from aqueous solution as well as from groundwater.

**Phase III: Characterization and application of magnetic biochar synthesized using vegetable waste for As(III) and As(V) removal from an aqueous solution and groundwater.**

- In this phase, fabrication of magnetic biochar was done by pyrolysis of waste leaves of *Raphanus sativus* (MRB) and *Artocarpus heterophyllus* (MJB) peel pretreated with $FeCl_3$ and was subsequently examined for As(III and V) adsorption from an aqueous solution.
- The characterization techniques such as SEM, EDX, FTIR, PSA, zeta potential, $pH_{ZPC}$, and VSM were used for biochar characterization.
- MRB-800 and MJB-exhibited irregular structure and rough surface. MRB-800 had high iron content by weight 44.40 % than MJB-800 (6.58 %), indicating that the *Raphanus sativus* and *Artocarpus heterophyllus* waste biomasses were successfully impregnated with iron, imparting magnetic properties to both adsorbents, as per the results obtained by EDX analysis.

- The highest As(III) adsorption was 81.85 % and 85.80 % for MRB-800 and MJB-800, respectively, whereas the highest As(V) removal was 60.7 % and 90.7 % for MRB-800 and MJB-800, respectively, at 0.5 mg/L initial As concentration.
- The highest removal of As(III) was 72.67 % and 88.4 % by MRB-800 and MJB-800, respectively, at pH 5 and 6. Whereas, the maximum adsorption of As(V) was found to be 72.35 % by MRB-800 and 92.65 % by MJB-800.
- MRB-800 showed greater efficiency towards the removal of both As species with $q_{max}$ value 2.08 mg/g for As(III) and 2.03 mg/g for As(V). Whereas, the $q_{max}$ value was 1.13 mg/g for As (III) and 1.26 mg/g for As (V) adsorption using MJB-800.
- Both adsorbents are stable, have lower particle size and are more efficient in removing both As species because they have more oxygen-containing surface functional groups. Two main important processes involved in As (III and V) adsorption were surface complexation and electrostatic attraction, which were better demonstrated by functional groups as well as the elemental composition of MRB-800 and MJB-800.
- Temkin and Freundlich isotherm was best fitted to the adsorption of As(III) and As(V) by MRB-800. Langmuir isotherm was best followed by the adsorption of As (III and V) by MJB-800. Pseudo-second-order kinetics was well simulated by the experimental data of As adsorption using both the adsorbents. Thermodynamic study showed that As (III) removal was exothermic while the As (V) adsorption was endothermic for MRB-800 and MJB-800, respectively.

**Phase IV: Characterization and application of monometallic and bimetallic biochar prepared using *Tectona* dry waste leaves for the removal of As(III) from an aqueous solution and groundwater.**

- In this study, the plant waste biomass was utilized for the synthesis of monometallic and bimetallic biochar. The biomass waste was pretreated with $FeSO_4$ for the synthesis of monometallic biochar whereas, it was pretreated with $FeSO_4$ and $MnO_2$ for synthesizing bimetallic biochar. These biochar materials were applied for As(III) removal from an aqueous solution as well as from groundwater samples.
- Fe-TB and Fe/Mn-TB both were characterized by using different analytical techniques such as SEM, EDX, FTIR, XRD, PSA, zeta potential and $pH_{ZPC}$
- The results of EDX showed the presence of Fe content in monometallic while Fe and Mn content in bimetallic biochar. Results of FTIR spectroscopy also confirm the impregnation of these metal salts with the plant biomass material.
- Enhanced removal of As(III) was observed with Fe/Mn-TB biochar which was greater than Fe-TB. The maximum adsorption was achieved about 90 % with Fe/Mn-TB, though ~84.85 % As was adsorbed using Fe-TB when the initial As concentration was 0.5 mg/L.
- The maximum adsorption of As(III) by Fe-TB was ~87.68 % at 4 pH. Whereas, the highest adsorption of As(III) was ~91.18 % achieved at 9 pH using Fe/Mn-TB.
- Adsorption capacity was 1.16 mg/g and 1.75 mg/g for As(III) removal using Fe-TB and Fe/Mn-TB, respectively, further the Fe-TB and Fe/Mn-TB were successfully recycled up to four cycles with optimum removal.

- The As adsorption was also assessed by kinetic study and the adsorption process has good compliance with pseudo-second-order kinetics. The As adsorption was followed freundlich isotherm model.
- The adsorption of As(III) by both the synthesized biosorbents i.e., Fe-TB and Fe/Mn-TB was endothermic, the adsorption was increased as the operating temperature was raised from 25 °C to 55 °C.
- Fe-TB and Fe/Mn-TB were also applied for the removal of As from groundwater. The removal of Arsenic by these biosorbents were controlled by different mechanisms like; electrostatic attraction, surface complexation and h-bond formation. Various functional groups were present on the biosorbents surface and hence many reactive surface binding sites were available on the biosorbent surface for the removal of As.

# *Chapter-7*
# *Conclusion*

# Chapter-7 Conclusion

In the present study, a total of four waste biomasses namely *Tectona sp., Lagerstroemia speciosa, Raphanus sativus,* and *Artocarpus heterophyllus* were utilized for synthesizing biochar materials for removal of As from water. It was found that out of four only two biochar materials synthesized from dry leaves of *Tectona sp.* and *Lagerstroemia speciosa* were able to remove the As(III) and As(V) from aqueous solution as well as from groundwater whereas, *Raphanus sativus* and *Artocarpus heterophyllus* biochar have shown insignificant efficiency. At higher concentrations of As(III) and As(V) the adsorption efficiency of these biochars was very low and a large amount of biochar was required for the As removal. To overcome the inefficacy of synthesized biochar, these biochar were modified by the application of $FeCl_3$ and subsequently applied for As removal from water. It was found that application of $FeCl_3$ has raised the As removal efficiency of these biochar materials. Further, modification with $FeCl_3$ imparts magnetic properties to the biochar that enable separation of biochar after adsorption by applying an external magnetic field. The biomass of *Tectona sp.* was further modified to synthesize the monometallic (with $FeSO_4$) and bimetallic ($FeSO_4/MnO_2$) biochar. Results revealed that the As(III) removal efficiency of bimetallic was higher as compared to monometallic biochar. The present study is a small initiative for the effective management of locally available waste with its application to address the issue of As in aquatic environment. Present findings confirm that the magnetic biochar has great potential to remove As from aqueous solution and can be used at large-scale for the removal of arsenic from drinking contaminated groundwater.

To the best of our knowledge, the studied biomass were utilized first time for the removal of As from the contaminated water. The prime mechanism involved for the removal of As was found to be the adsorption with the help of surface complexation and electrostatic attraction. These biomass are potential candidates for the treatment of As contaminated water in a cost-effective and eco-friendly way. Results of this study were obtained through the experiments carried out under controlled conditions; however they may vary in ambient environment probably due to interference of co-existing chemical sp. and environmental variables. Thus, before large-scale application experiments should be performed to optimize the process with the help of present findings such as adsorbent dose, initial As concentration, contact time, pH of the solution, operating temperature and method of biochar synthesis.

# *References*

# References

Abdel-Ghani, N. T., Rawash, E. S. A., & El-Chaghaby, G. A. (2016). Equilibrium and kinetic study for the adsorption of p-nitrophenol from wastewater using olive cake based activated carbon. *Global Journal of Environmental Science and Management*, *2*(1), 11-18.

Abdellaoui, Y., El Ibrahimi, B., Abou Oualid, H., Kassab, Z., Quintal-Franco, C., Giácoman-Vallejos, G., & Gamero-Melo, P. (2021). Iron-zirconium microwave-assisted modification of small-pore zeolite W and its alginate composites for enhanced aqueous removal of As (V) ions: Experimental and theoretical studies. *Chemical Engineering Journal*, *421*, 129909.

Abdul, K. S. M., Jayasinghe, S. S., Chandana, E. P., Jayasumana, C., & De Silva, P. M. C. (2015). Arsenic and human health effects: A review. *Environmental Toxicology and Pharmacology*, *40*(3), 828-846.

Aghdam, M. M., Crowley, Q., Rocha, C., Dentoni, V., DaPelo, S., Long, S., & Savatier, M. (2021). A study of natural radioactivity levels and radon/thoron release potential of bedrock and soil in Southeastern Ireland. *International Journal of Environmental Research and Public Health*, *18*(5), 2709.

Agrafioti, E., Kalderis, D., & Diamadopoulos, E. (2014a). Ca and Fe modified biochars as adsorbents of arsenic and chromium in aqueous solutions. *Journal of environmental management*, *146*, 444-450.

Agrafioti, E., Kalderis, D., & Diamadopoulos, E. (2014b). Arsenic and chromium removal from water using biochars derived from rice husk, organic solid wastes and sewage sludge. *Journal of Environmental Management*, *133*, 309-314.

Ahangarpour, A., Zeidooni, L., Samimi, A., Alboghobeish, S., Khorsandi, L. S., & Moradi, M. (2018). Chronic exposure to arsenic and high fat diet additively induced cardiotoxicity in male mice. *Research in Pharmaceutical Sciences*, *13*(1), 47.

Ahmad, S. A., Khan, M. H., & Haque, M. (2018). Arsenic contamination in groundwater in Bangladesh: implications and challenges for healthcare policy. *Risk Management and Healthcare Policy*, *11*, 251.

Ahmed, M. F. (2001, May). An overview of arsenic removal technologies in Bangladesh and India. In *Proceedings of BUET-UNU international workshop on technologies for arsenic removal from drinking water, Dhaka* (pp. 5-7).

Ajmal, Z., Muhmood, A., Dong, R., & Wu, S. (2020). Probing the efficiency of magnetically modified biomass-derived biochar for effective phosphate removal. *Journal of Environmental Management*, *253*, 109730.

Akhil, D., Lakshmi, D., Kartik, A., Vo, D. V. N., Arun, J., & Gopinath, K. P. (2021). Production, characterization, activation and environmental applications of engineered biochar: a review. *Environmental Chemistry Letters*, *19*(3), 2261-2297.

Akram, S., & Rehman, F. (2018). Hardness in drinking-water, its sources, its effects on humans and its household treatment. *J Chem Appl*, *4*(1), 1-4.

Alam, M., Shaikh, W. A., Bhattacharya, T., Chakraborty, S., Show, B., & Saha, I. (2018). Adsorption of As (III) and As (V) from aqueous solution by modified Cassia fistula (golden shower) biochar. *Applied Water Science*, *8*(7), 1-14.

Alchouron, J., Navarathna, C., Chludil, H. D., Dewage, N. B., Perez, F., Pittman Jr, C. U., Vega, A. S., & Mlsna, T. E. (2020). Assessing South American Guadua chacoensis

bamboo biochar and Fe3O4 nanoparticle dispersed analogues for aqueous arsenic (V) remediation. *Science of The Total Environment*, *706*, 135943.

Ali, S., Rizwan, M., Shakoor, M. B., Jilani, A., & Anjum, R. (2020). High sorption efficiency for As (III) and As (V) from aqueous solutions using novel almond shell biochar. *Chemosphere*, *243*, 125330.

Ali, W., Rasool, A., Junaid, M., & Zhang, H. (2019). A comprehensive review on current status, mechanism, and possible sources of arsenic contamination in groundwater: a global perspective with a prominence of Pakistan scenario. *Environmental geochemistry and health*, *41*(2), 737-760.

Alidokht, L., Anastopoulos, I., Ntarlagiannis, D., Soupios, P., Tawabini, B., Kalderis, D., & Khataee, A. (2021). Recent advances in the application of nanomaterials for the remediation of arsenic-contaminated water and soil. *Journal of Environmental Chemical Engineering*, *9*(4), 105533.

Alka, S., Shahir, S., Ibrahim, N., Ndejiko, M. J., Vo, D. V. N., & Abd Manan, F. (2021). Arsenic removal technologies and future trends: a mini review. *Journal of Cleaner Production*, *278*, 123805.

Alshehri, R., Ilyas, A. M., Hasan, A., Arnaout, A., Ahmed, F., & Memic, A. (2016). Carbon nanotubes in biomedical applications: factors, mechanisms, and remedies of toxicity: miniperspective. *Journal of Medicinal Chemistry*, *59*(18), 8149-8167.

Ambaye, T. G., Vaccari, M., van Hullebusch, E. D., Amrane, A., & Rtimi, S. (2021). Mechanisms and adsorption capacities of biochar for the removal of organic and inorganic pollutants from industrial wastewater. *International Journal of Environmental Science and Technology*, *18*(10), 3273-3294.

Amen, R., Bashir, H., Bibi, I., Shaheen, S. M., Niazi, N. K., Shahid, M., Hussain, M. M., Antoniadis, V., Shakoor, M. B., Al-Solaimani, G., Wang, H., Bundschuh & Rinklebe, J. (2020). A critical review on arsenic removal from water using biochar-based sorbents: the significance of modification and redox reactions. *Chemical Engineering Journal*, *396*, 125195.

An, Q., Li, X. Q., Nan, H. Y., Yu, Y., & Jiang, J. N. (2018). The potential adsorption mechanism of the biochars with different modification processes to Cr (VI). *Environmental Science and Pollution Research*, *25*(31), 31346-31357.

Andrade, T. S., Vakros, J., Mantzavinos, D., & Lianos, P. (2020). Biochar obtained by carbonization of spent coffee grounds and its application in the construction of an energy storage device. *Chemical Engineering Journal Advances*, *4*, 100061.

APHA. (2005). Standard methods for the examination of water and wastewater. Washington DC: American Public Health Association.

Araújo, C. S., Almeida, I. L., Rezende, H. C., Marcionilio, S. M., Léon, J. J., & de Matos, T. N. (2018). Elucidation of mechanism involved in adsorption of Pb (II) onto lobeira fruit (Solanum lycocarpum) using Langmuir, Freundlich and Temkin isotherms. *Microchemical Journal*, *137*, 348-354.

Argos, M., Ahsan, H., & Graziano, J. H. (2012). Arsenic and human health: epidemiologic progress and public health implications. *Reviews on Environmental Health*, *27*(4), 191–195.

Argos, M., Kalra, T., Rathouz, P. J., Chen, Y., Pierce, B., Parvez, F., Islam, T., Ahmed, A., Rakibuz-Zaman, M., Hasan, R., Sarwar, G., Slavkovich, V., van Geen, A., Graziano, J., & Ahsan, H. (2010). Arsenic exposure from drinking water, and all-

cause and chronic-disease mortalities in Bangladesh (HEALS): a prospective cohort study. *The Lancet*, *376*(9737), 252-258.

Arun, J., Gopinath, K. P., Vo, D. V. N., SundarRajan, P., & Swathi, M. (2020). Co-hydrothermal gasification of Scenedesmus sp. with sewage sludge for bio-hydrogen production using novel solid catalyst derived from carbon-zinc battery waste. *Bioresource Technology Reports*, *11*, 100459.

Asere, T. G., Stevens, C. V., & Du Laing, G. (2019). Use of (modified) natural adsorbents for arsenic remediation: a review. *Science of the total environment*, *676*, 706-720.

Ayub, A., Raza, Z. A., Majeed, M. I., Tariq, M. R., & Irfan, A. (2020). Development of sustainable magnetic chitosan biosorbent beads for kinetic remediation of arsenic contaminated water. *International Journal of Biological Macromolecules*, *163*, 603-617.

Azargohar, R., Nanda, S., Dalai, A. K., & Kozinski, J. A. (2019). Physico-chemistry of biochars produced through steam gasification and hydro-thermal gasification of canola hull and canola meal pellets. *Biomass and Bioenergy*, *120*, 458-470.

Azimi, A., Azari, A., Rezakazemi, M., & Ansarpour, M. (2017). Removal of heavy metals from industrial wastewaters: a review. *ChemBioEng Reviews*, *4*(1), 37-59.

Baig, S. A., Sheng, T., Hu, Y., Xu, J., & Xu, X. (2015). Arsenic removal from natural water using low cost granulated adsorbents: a review. *CLEAN–Soil, Air, Water*, *43*(1), 13-26.

Baig, S. A., Zhu, J., Muhammad, N., Sheng, T., & Xu, X. (2014). Effect of synthesis methods on magnetic Kans grass biochar for enhanced As (III, V) adsorption from aqueous solutions. *Biomass and bioenergy*, *71*, 299-310.

Bakshi, S., Banik, C., Rathke, S. J., & Laird, D. A. (2018). Arsenic sorption on zero-valent iron-biochar complexes. *Water research, 137*, 153-163.

Bandara, T., Herath, I., Kumarathilaka, P., Hseu, Z. Y., Ok, Y. S., & Vithanage, M. (2017). Efficacy of woody biomass and biochar for alleviating heavy metal bioavailability in serpentine soil. *Environmental geochemistry and health*, *39*(2), 391-401.

Basu, A., Saha, D., Saha, R., Ghosh, T., & Saha, B. (2014). A review on sources, toxicity and remediation technologies for removing arsenic from drinking water. *Research on Chemical Intermediates*, *40*(2), 447-485.

Basu, M., Guha, A. K., & Ray, L. (2019). Adsorption of lead on lentil husk in fixed bed column bioreactor. *Bioresource Technology, 283,* 86-95.

Benis, K. Z., Shakouri, M., McPhedran, K., & Soltan, J. (2020). Enhanced arsenate removal by Fe-impregnated canola straw: assessment of XANES solid-phase speciation, impacts of solution properties, sorption mechanisms, and evolutionary polynomial regression (EPR) models. *Environmental Science and Pollution Research,* 1-18

Bhattacharya, A., Sarani, C., Kumar Roy, A., Karthik, D., Singh, A., Kumari, S., & Kumar Mishra, A. (2019). An analysis of arsenic contamination in the groundwater of India, Bangladesh and Nepal with a special focus on the stabilisation of arsenic-laden sludge from arsenic filters. *Electronic Journal of Geotechnical Engineering*, *24*(1), 1-34.

Bhattacharya, P., Welch, A. H., Stollenwerk, K. G., McLaughlin, M. J., Bundschuh, J., & Panaullah, G. (2007). Arsenic in the environment: biology and chemistry. *Science of the Total environment, 379,* 2-3.

Bindal, S., Kumar, A., Mallick, J., Shashtri, S., Kumar, P., & Singh, C. K. (2020). Geochemical, topographical, and meteorological controls on groundwater arsenic contamination in Sharda River Basin of Uttar Pradesh, India. *Journal of Climate Change*, *6*(2), 71-87.

Bissen, M., & Frimmel, F. H. (2003). Arsenic—a review. Part II: oxidation of arsenic and its removal in water treatment. *Acta hydrochimica et hydrobiologica*, *31*(2), 97-107.

Bozack, A. K., Saxena, R., & Gamble, M. V. (2018). Nutritional influences on one-carbon metabolism: effects on arsenic methylation and toxicity. *Annual review of nutrition*, *38*, 401-429.

Brewer, C. E., Schmidt-Rohr, K., Satrio, J. A., & Brown, R. C. (2009). Characterization of biochar from fast pyrolysis and gasification systems. *Environmental Progress & Sustainable Energy: An Official Publication of the American Institute of Chemical Engineers*, *28*(3), 386-396.

Bushra, B., & Remya, N. (2020). Biochar from pyrolysis of rice husk biomass—characteristics, modification and environmental application. *Biomass Conversion and Biorefinery*, 1-12.

Cai, L. M., Wang, Q. S., Luo, J., Chen, L. G., Zhu, R. L., Wang, S., & Tang, C. H. (2019). Heavy metal contamination and health risk assessment for children near a large Cu-smelter in central China. *Science of the Total Environment*, *650*, 725-733.

Carter, D. E., Aposhian, H. V., & Gandolfi, A. J. (2003). The metabolism of inorganic arsenic oxides, gallium arsenide, and arsine: a toxicochemical review. *Toxicology and Applied Pharmacology*, *193*(3), 309-334.

Cha, J. S., Park, S. H., Jung, S. C., Ryu, C., Jeon, J. K., Shin, M. C., & Park, Y. K. (2016). Production and utilization of biochar: A review. *Journal of Industrial and Engineering Chemistry*, *40*, 1-15.

Chakraborti, D., Singh, S. K., Rahman, M. M., Dutta, R. N., Mukherjee, S. C., Pati, S., & Kar, P. B. (2018). Groundwater arsenic contamination in the Ganga River Basin: a future health danger. *International Journal of Environmental Research and Public Health*, *15*(2), 180.

Chakraborty, M., Mukherjee, A., & Ahmed, K. M. (2015). A review of groundwater arsenic in the Bengal Basin, Bangladesh and India: from source to sink. *Current Pollution Reports*, *1*(4), 220-247.

Chan, Y. H., Yusup, S., Quitain, A. T., Uemura, Y., & Sasaki, M. (2014). Bio-oil production from oil palm biomass via subcritical and supercritical hydrothermal liquefaction. *The Journal of Supercritical Fluids*, *95*, 407-412.

Chatterjee, D., Adak, S., Banerjee, N., Bhattacharjee, P., Bandyopadhyay, A. K., & Giri, A. K. (2018). Evaluatıon of health effects, genetıc damage and telomere length ın children exposed to arsenic in West Bengal, İndia. *Mutation Research/Genetic Toxicology and Environmental Mutagenesis*, *836*, 82-88.

Chen, Y., & Karagas, M. R. (2013). Arsenic and cardiovascular disease: new evidence from the United States. *Annals of internal medicine*, *159*(10), 713-714.

Chen, A. S., Wang, L., Sorg, T. J., & Lytle, D. A. (2020a). Removing arsenic and co-occurring contaminants from drinking water by full-scale ion exchange and point-of-use/point-of-entry reverse osmosis systems. *Water Research*, *172*, 115455.

Chen, W., Lu, J., Zhang, C., Xie, Y., Wang, Y., Wang, J., & Zhang, R. (2020b). Aromatic hydrocarbons production and synergistic effect of plastics and biomass via one-pot catalytic co-hydropyrolysis on HZSM-5. *Journal of Analytical and Applied Pyrolysis*, *147*, 104800.

Chen, L., Song, D., Zhang, W., Zhang, C., & Zhang, L. (2019). The dynamic changes of arsenic bioaccumulation and antioxidant responses in the marine medaka Oryzias melastigma during chronic exposure. *Aquatic Toxicology*, *212*, 110-119.

Chen, S., Yue, Q., Gao, B., Li, Q., Xu, X., & Fu, K. (2012). Adsorption of hexavalent chromium from aqueous solution by modified corn stalk: a fixed-bed column study. *Bioresource technology*, *113*, 114-120.

Chen, T., Da, T., & Ma, Y. (2021b). Reasonable calculation of the thermodynamic parameters from adsorption equilibrium constant. *Journal of Molecular Liquids*, *322*, 114980.

Chen, W. H., Lin, B. J., Lin, Y. Y., Chu, Y. S., Ubando, A. T., Show, P. L., Ong, H. C., Chang, J. S., Ho, S. H., Culaba, A.B., Petrissans, A., & Pétrissans, M. (2021a). Progress in biomass torrefaction: Principles, applications and challenges. *Progress in Energy and Combustion Science*, *82*, 100887.

Chen, Y., Wang, B., Xin, J., Sun, P., & Wu, D. (2018). Adsorption behavior and mechanism of Cr (VI) by modified biochar derived from Enteromorpha prolifera. *Ecotoxicology and environmental safety*, *164*, 440-447.

Chia, C. H., Gong, B., Joseph, S. D., Marjo, C. E., Munroe, P., & Rich, A. M. (2012). Imaging of mineral-enriched biochar by FTIR, Raman and SEM–EDX. *Vibrational Spectroscopy 62*, 248-257.

Chiavola, A., D'Amato, E., Sirini, P., Caretti, C., & Gori, R. (2019). Arsenic removal from a highly contaminated groundwater by a combined coagulation-filtration-adsorption process. *Water, Air, & Soil Pollution*, *230*(4), 1-12.

Chiban, M., Zerbet, M., Carja, G., & Sinan, F. (2012). Application of low-cost adsorbents for arsenic removal: A review. *Journal of Environmental Chemistry and Ecotoxicology*, *4*(5), 91-102.

Chikkanna, A., Mehan, L., Sarath, P. K., & Ghosh, D. (2019). Arsenic exposures, poisoning, and threat to human health: arsenic affecting human health. In *Environmental Exposures and Human Health Challenges* (pp. 86-105). IGI Global.

Choong, T. S., Chuah, T. G., Robiah, Y., Koay, F. G., & Azni, I. (2007). Arsenic toxicity, health hazards and removal techniques from water: an overview. *Desalination*, *217*(1-3), 139-166.

Chutia, R. S., Kataki, R., & Bhaskar, T. (2014). Characterization of liquid and solid product from pyrolysis of Pongamia glabra deoiled cake. *Bioresource technology*, *165*, 336-342.

Cruz, G. J., Mondal, D., Rimaycuna, J., Soukup, K., Gómez, M. M., Solis, J. L., & Lang, J. (2020). Agrowaste derived biochars impregnated with ZnO for removal of arsenic and lead in water. *Journal of Environmental Chemical Engineering*, *8*(3), 103800.

Cuong, D. V., Wu, P. C., Chen, L. I., & Hou, C. H. (2021). Active MnO2/biochar composite for efficient As (III) removal: Insight into the mechanisms of redox transformation and adsorption. *Water Research*, *188*, 116495.

Dai, L., Fan, L., Liu, Y., Ruan, R., Wang, Y., Zhou, Y., Zhao, Y., & Yu, Z. (2017a). Production of bio-oil and biochar from soapstock via microwave-assisted co-catalytic fast pyrolysis. *Bioresource technology*, *225*, 1-8.

Dai, L., Tan, F., Li, H., Zhu, N., He, M., Zhu, Q., Hu, G., Wang, L., & Zhao, J. (2017b). Calcium-rich biochar from the pyrolysis of crab shell for phosphorus removal. *Journal of environmental management*, *198*, 70-74.

Darezereshki, E., khodadadi Darban, A., Abdollahy, M., & Jamshidi-Zanjani, A. (2018). Influence of heavy metals on the adsorption of arsenate by magnetite nanoparticles: Kinetics and thermodynamic. *Environmental Nanotechnology, Monitoring & Management*, *10*, 51-62.

Dhar, R. K., Zheng, Y., Rubenstone, J., & Van Geen, A. (2004). A rapid colorimetric method for measuring arsenic concentrations in groundwater. *Analytica Chimica Acta*, *526*(2), 203-209.

Dhillon, A. K. (2020). Arsenic contamination of India's groundwater: a review and critical analysis. *Arsenic Water Resources Contamination*, 177-205.

Diamadopoulos, E., Ioannidis, S., & Sakellaropoulos, G. P. (1993). As (V) removal from aqueous solutions by fly ash. *Water Research*, *27*(12), 1773-1777.

Dixit, F., Dutta, R., Barbeau, B., Berube, P., & Mohseni, M. (2021). PFAS removal by ion exchange resins: A review. *Chemosphere*, *272*, 129777.

Dong, X., Ma, L. Q., Gress, J., Harris, W., & Li, Y. (2014). Enhanced Cr (VI) reduction and As (III) oxidation in ice phase: important role of dissolved organic matter from biochar. *Journal of hazardous materials*, *267*, 62-70.

Dong, X., Ma, L. Q., Zhu, Y., Li, Y., & Gu, B. (2013). Mechanistic investigation of mercury sorption by Brazilian pepper biochars of different pyrolytic temperatures based on X-ray photoelectron spectroscopy and flow calorimetry. *Environmental Science & Technology*, *47*(21), 12156-12164.

Duttagupta, S., Bhanja, S. N., Dutta, A., Sarkar, S., Chakraborty, M., Ghosh, A., Mondal, D., & Mukherjee, A. (2021). Impact of Covid-19 lockdown on availability of drinking water in the arsenic-affected Ganges River Basin. *International Journal of Environmental Research and Public Health*, *18*(6), 2832.

Elbehiry, F., Alshaal, T., Elhawat, N., & Elbasiouny, H. (2021). Environmental-Friendly and Cost-Effective Agricultural Wastes for Heavy Metals and Toxicants Removal from Wastewater.

Engwa, G. A., Ferdinand, P. U., Nwalo, F. N., & Unachukwu, M. N. (2019). Mechanism and health effects of heavy metal toxicity in humans. *Poisoning in the Modern World-new Tricks for an old dog*, *10*.

Eshun, J., Wang, L., Ansah, E., Shahbazi, A., Schimmel, K., Kabadi, V., & Aravamudhan, S. (2019). Characterization of the physicochemical and structural evolution of biomass particles during combined pyrolysis and CO2 gasification. *Journal of the Energy Institute*, *92*(1), 82-93.

Faust, J. C., Tessin, A., Fisher, B. J., Zindorf, M., Papadaki, S., Hendry, K. R., Doyle, K. A., & März, C. (2021). Millennial scale persistence of organic carbon bound to iron in Arctic marine sediments. *Nature Communications*, *12*(1), 1-9.

Ferasat, Z., Panahi, R., & Mokhtarani, B. (2020). Natural polymer matrix as safe flocculant to remove turbidity from kaolin suspension: Performance and governing mechanism. *Journal of Environmental Management*, *255*, 109939.

Gallios, G. P., Tolkou, A. K., Katsoyiannis, I. A., Stefusova, K., Vaclavikova, M., & Deliyanni, E. A. (2017). Adsorption of arsenate by nano scaled activated carbon modified by iron and manganese oxides. *Sustainability*, *9*(10), 1684.

Gan, Y. X. (2021). Activated Carbon from Biomass Sustainable Sources. *C*, *7*(2), 39.

Gao, Y., Yue, Q., Gao, B., & Li, A. (2020). Insight into activated carbon from different kinds of chemical activating agents: A review. *Science of the Total Environment*, *746*, 141094.

García, R., Pizarro, C., Lavín, A. G., & Bueno, J. L. (2012). Characterization of Spanish biomass wastes for energy use. *Bioresource technology*, *103*(1), 249-258.

Garelick, H., Jones, H., Dybowska, A., & Valsami-Jones, E. (2009). Arsenic pollution sources. *Reviews of Environmental Contamination Volume 197*, 17-60.

Gautam, A., Rawat, S., Verma, L., Singh, J., Sikarwar, S., Yadav, B. C., & Kalamdhad, A. S. (2018). Green synthesis of iron nanoparticle from extract of waste tea: An application for phenol red removal from aqueous solution. *Environmental Nanotechnology, Monitoring & Management*, *10*, 377-387.

Ghosal, P. S., Kattil, K. V., Yadav, M. K., & Gupta, A. K. (2018). Adsorptive removal of arsenic by novel iron/olivine composite: insights into preparation and adsorption process by response surface methodology and artificial neural network. *Journal of Environmental Management*, *209*, 176-187.

Ghosh, A., Awal, M. A., Majumder, S., Sikder, M. H., & Rao, D. R. (2012). Arsenic residues in broiler meat and excreta at arsenic prone areas of Bangladesh. *Bangladesh Journal of Pharmacology*, *7*(3), 178-185.

Giuliani, A., Zuccarini, M., Cichelli, A., Khan, H., & Reale, M. (2020). Critical review on the presence of phthalates in food and evidence of their biological impact. *International Journal of Environmental Research and Public Health*, *17*(16), 5655.

Gómez-Barea, A., Ollero, P., & Leckner, B. (2013). Optimization of char and tar conversion in fluidized bed biomass gasifiers. *Fuel*, *103*, 42-52.

Gong, G., Basom, J., Mattevada, S., & Onger, F. (2015). Association of hypothyroidism with low-level arsenic exposure in rural West Texas. *Environmental research*, *138*, 154-160.

Gonzalez, B., Heijman, S. G. J., Rietveld, L. C., & van Halem, D. (2019). Arsenic removal from geothermal influenced groundwater with low pressure NF pilot plant for drinking water production in Nicaraguan rural communities. *Science of the Total Environment*, *667*, 297-305.

Gribble, M. O., Howard, B. V., Umans, J. G., Shara, N. M., Francesconi, K. A., Goessler, W., Crainiceanu, C. M., Silbergeld, E. K., Guallar, E., & Navas-Acien, A. (2012). Arsenic exposure, diabetes prevalence, and diabetes control in the Strong Heart Study. *American Journal of Epidemiology*, *176*(10), 865-874.

Gubler, R., & ThomasArrigo, L. K. (2021). Ferrous iron enhances arsenic sorption and oxidation by non-stoichiometric magnetite and maghemite. *Journal of Hazardous Materials*, *402*, 123425.

Guo, J., Yan, C., Luo, Z., Fang, H., Hu, S., & Cao, Y. (2019). Synthesis of a novel ternary HA/Fe-Mn oxides-loaded biochar composite and its application in cadmium (II) and arsenic (V) adsorption. *Journal of Environmental Sciences*, *85*, 168-176.

Gupta, A., Yunus, M., & Sankararamakrishnan, N. (2012). Zerovalent iron encapsulated chitosan nanospheres–A novel adsorbent for the removal of total inorganic Arsenic from aqueous systems. *Chemosphere*, *86*(2), 150-155.

Gupta, R. K., Dubey, M., Kharel, P., Gu, Z., & Fan, Q. H. (2015). Biochar activated by oxygen plasma for supercapacitors. *Journal of Power Sources*, *274*, 1300-1305.

Hao, L., Liu, M., Wang, N., & Li, G. (2018). A critical review on arsenic removal from water using iron-based adsorbents. *RSC Advances*, *8*(69), 39545-39560.

Hare, V., Chowdhary, P., Kumar, B., Sharma, D. C., & Baghel, V. S. (2019). Arsenic toxicity and its remediation strategies for fighting the environmental threat. In *Emerging and Eco-friendly Approaches for Waste Management* (pp. 143-170). Springer, Singapore.

Hashim, M. A., Kundu, A., Mukherjee, S., Ng, Y. S., Mukhopadhyay, S., Redzwan, G., & Gupta, B. S. (2019). Arsenic removal by adsorption on activated carbon in a rotating packed bed. *Journal of Water Process Engineering*, *30*, 100591.

Hassan, M., Liu, Y., Naidu, R., Parikh, S. J., Du, J., Qi, F., & Willett, I. R. (2020). Influences of feedstock sources and pyrolysis temperature on the properties of biochar and functionality as adsorbents: A meta-analysis. *Science of The Total Environment*, *744*, 140714.

He, R., Peng, Z., Lyu, H., Huang, H., Nan, Q., & Tang, J. (2018). Synthesis and characterization of an iron-impregnated biochar for aqueous arsenic removal. *Science of the Total Environment*, *612*, 1177-1186.

He, X., Jiang, J., Hong, Z., Pan, X., Dong, Y., & Xu, R. (2020b). Effect of aluminum modification of rice straw–based biochar on arsenate adsorption. *Journal of Soils and Sediments*, *20*(8), 3073-3082.

He, X., Li, P., Ji, Y., Wang, Y., Su, Z., & Elumalai, V. (2020a). Groundwater arsenic and fluoride and associated arsenicosis and fluorosis in China: occurrence, distribution and management. *Exposure and Health*, *12*(3), 355-368.

Ho, Y. S., & McKay, G. (1998). Kinetic models for the sorption of dye from aqueous solution by wood. *Process Safety and Environmental Protection*, *76*(2), 183-191.

Höll, W. H. (2010). Mechanisms of arsenic removal from water. *Environmental Geochemistry and Health*, *32*(4), 287-290.

Hong, J., Liu, L., Luo, Y., Tan, W., Qiu, G., & Liu, F. (2018). Photochemical oxidation and dissolution of arsenopyrite in acidic solutions. *Geochimica et Cosmochimica Acta*, *239*, 173-185.

Hong, N., Cheng, Q., Goonetilleke, A., Bandala, E. R., & Liu, A. (2020). Assessing the effect of surface hydrophobicity/hydrophilicity on pollutant leaching potential of biochar in water treatment. *Journal of Industrial and Engineering Chemistry*, *89*, 222-232.

Hsu, L. I., Chen, G. S., Lee, C. H., Yang, T. Y., Chen, Y. H., Wang, Y. H., Hsueh, Y.M., Chiou, H. Y., Wu, M. M., & Chen, C. J. (2013). Use of arsenic-induced

palmoplantar hyperkeratosis and skin cancers to predict risk of subsequent internal malignancy. *American Journal of Epidemiology*, *177*(3), 202-212.

Hu, X., Xue, Y., Long, L., & Zhang, K. (2018). Characteristics and batch experiments of acid-and alkali-modified corncob biomass for nitrate removal from aqueous solution. *Environmental Science and Pollution Research*, *25*(20), 19932-19940.

Hu, Y., Zhang, W., Cheng, H., & Tao, S. (2017). Public health risk of arsenic species in chicken tissues from live poultry markets of Guangdong province, China. *Environmental Science & Technology*, *51*(6), 3508-3517.

Huang, Y., Gao, M., Deng, Y., Khan, Z. H., Liu, X., Song, Z., & Qiu, W. (2020). Efficient oxidation and adsorption of As (III) and As (V) in water using a Fenton-like reagent,(ferrihydrite)-loaded biochar. *Science of the Total Environment*, *715*, 136957.

Ibrahim, A. O., Adegoke, K. A., Adegoke, R. O., AbdulWahab, Y. A., Oyelami, V. B., & Adesina, M. O. (2021). Adsorptive removal of different pollutants using metal-organic framework adsorbents. *Journal of Molecular Liquids*, *333*, 115593.

Ibrahim, M., Siddique, A., Verma, L., Singh, J., & Koduru, J. R. (2019a). Adsorptive removal of fluoride from aqueous solution by biogenic iron permeated activated carbon derived from sweet lime waste. *Acta Chimica Slovenica*, *66*(1), 123-136.

Ibrahim, M., Siddique, A., Verma, L., Singh, J., & Koduru, J. R. (2019b). Adsorptive removal of fluoride from aqueous solution by biogenic iron permeated activated carbon derived from sweet lime waste. *Acta Chimica Slovenica*, *66*(1), 123-136.

Imran, M., Iqbal, M. M., Iqbal, J., Shah, N. S., Khan, Z. U. H., Murtaza, B., Amjad, M., Ali, S., & Rizwan, M. (2021). Synthesis, characterization and application of novel

MnO and CuO impregnated biochar composites to sequester arsenic (As) from water: modeling, thermodynamics and reusability. *Journal of Hazardous Materials*, *401*, 123338.

Iob, E., & Steptoe, A. (2019). Cardiovascular disease and hair cortisol: a novel biomarker of chronic stress. *Current cardiology reports*, *21*(10), 1-11.

Jadhav, S. V., Häyrynen, P., Marathe, K. V., Rathod, V. K., Keiski, R. L., & Yadav, G. D. (2018). Experimental and modeling assessment of sulfate and arsenic removal from mining wastewater by nanofiltration. *International Journal of Chemical Reactor Engineering*, *16*(1).

Jiao, G. J., Ma, J., Li, Y., Jin, D., Ali, Z., Zhou, J., & Sun, R. (2021). Recent advances and challenges on removal and recycling of phosphate from wastewater using biomass-derived adsorbents. *Chemosphere*, *278*, 130377.

Jing, X. R., Wang, Y. Y., Liu, W. J., Wang, Y. K., & Jiang, H. (2014). Enhanced adsorption performance of tetracycline in aqueous solutions by methanol-modified biochar. *Chemical Engineering Journal*, *248*, 168-174.

Johnson, D. L., & Pilson, M. E. (1972). Spectrophotometric determination of arsenite, arsenate, and phosphate in natural waters. *Analytica Chimica Acta*, *58*(2), 289-299.

Jomova, K., Jenisova, Z., Feszterova, M., Baros, S., Liska, J., Hudecova, D., Rhodes, C. J., & Valko, M. (2011). Arsenic: toxicity, oxidative stress and human disease. *Journal of Applied Toxicology*, *31*(2), 95-107.

Joshi, S., Sharma, M., Kumari, A., Shrestha, S., & Shrestha, B. (2019). Arsenic removal from water by adsorption onto iron oxide/nano-porous carbon magnetic composite. *Applied Sciences*, *9*(18), 3732.

Jovanovic, B., Eiermann, N., Talwar, D., Boulougouri, M., Dick, T. P., & Stoecklin, G. (2021). Thioredoxin 1 is required for stress granule assembly upon arsenite-induced oxidative stress. *Food and Chemical Toxicology*, *156*, 112508.

Kambo, H. S., & Dutta, A. (2015). A comparative review of biochar and hydrochar in terms of production, physico-chemical properties and applications. *Renewable and Sustainable Energy Reviews*, *45*, 359-378.

Kanwar, V. S., Sharma, A., Srivastav, A. L., & Rani, L. (2020). Phytoremediation of toxic metals present in soil and water environment: a critical review. *Environmental Science and Pollution Research*, *27*(36), 44835-44860.

Kar, S., & Equeenuddin, S. (2019). Adsorption of hexavalent chromium using natural goethite: isotherm, thermodynamic and kinetic study. *Journal of the geological society of India*, *93*(3), 285-292.

Karakurt, S. (2019). Removal of carcinogenic arsenic from drinking water by the application of ion exchange resins. *Oncogen Journal*, *2*(1), 5.

Kazi, T. G., Brahman, K. D., Baig, J. A., & Afridi, H. I. (2018). A new efficient indigenous material for simultaneous removal of fluoride and inorganic arsenic species from groundwater. *Journal of hazardous materials*, *357*, 159-167.

Kianfar, E., & Mahler, A. (2020). Zeolites: properties, applications, modification and selectivity. *Zeolites: advances in research and applications*, *1*.

Kibenge, F. S., & Strange, R. J. (2021). Introduction to the anatomy and physiology of the major aquatic animal species in aquaculture. In *Aquaculture Pharmacology* (pp. 1-111). Academic Press.

Kim, J. Y., Oh, S., & Park, Y. K. (2020). Overview of biochar production from preservative-treated wood with detailed analysis of biochar characteristics, heavy metals behaviors, and their ecotoxicity. *Journal of hazardous materials*, *384*, 121356.

Kim, J., Song, J., Lee, S. M., & Jung, J. (2019). Application of iron-modified biochar for arsenite removal and toxicity reduction. *Journal of Industrial and Engineering Chemistry*, *80*, 17-22.

Kim, K. W., Chanpiwat, P., Hanh, H. T., Phan, K., & Sthiannopkao, S. (2011). Arsenic geochemistry of groundwater in Southeast Asia. *Frontiers of medicine*, *5*(4), 420-433.

Kosheleva, R. I., Mitropoulos, A. C., & Kyzas, G. Z. (2019). Synthesis of activated carbon from food waste. *Environmental Chemistry Letters*, *17*(1), 429-438.

Kumar, A., Ali, M., Kumar, R., Kumar, M., Sagar, P., Pandey, R. K., Akhouri, V., Kumar, V., Anand, G., Niraj, P. K., Rani, R., Kumar, S., Kumar, D., Bishwapriya, A., & Ghosh, A. K. (2021). Arsenic exposure in Indo Gangetic plains of Bihar causing increased cancer risk. *Scientific Reports*, *11*(1), 1-16.

Kumar, R., Patel, M., Singh, P., Bundschuh, J., Pittman Jr, C. U., Trakal, L., & Mohan, D. (2019). Emerging technologies for arsenic removal from drinking water in rural and peri-urban areas: Methods, experience from, and options for Latin America. *Science of the Total Environment*, *694*, 133427.

Kumar, V., Dwivedi, S. K., & Oh, S. (2022). A critical review on lead removal from industrial wastewater: Recent advances and future outlook. *Journal of Water Process Engineering*, *45*, 102518.

Laatikainen, M., Sillanpää, M., & Sainio, T. (2016). Comparison of ion exchange process configurations for arsenic removal from natural waters. *Desalination and Water Treatment*, *57*(29), 13770-13781.

Lal, S., Singhal, A., & Kumari, P. (2020). Exploring carbonaceous nanomaterials for arsenic and chromium removal from wastewater. *Journal of water process engineering*, *36*, 101276.

Lambert, J. B., Shurvell, H. F., Lightner, D. A., & Cooks, R. G. (1987). *Introduction to organic spectroscopy*. Macmillan Publishing Company.

Li, H., Dong, X., da Silva, E. B., de Oliveira, L. M., Chen, Y., & Ma, L. Q. (2017a). Mechanisms of metal sorption by biochars: biochar characteristics and modifications. *Chemosphere*, *178*, 466-478.

Li, M. F., Liu, Y. G., Zeng, G. M., Liu, S. B., Hu, X. J., Shu, D., Jiang, L.H., Tan, X.F., Cai, X.X., & Yan, Z. L. (2017b). Tetracycline absorbed onto nitrilotriacetic acid-functionalized magnetic graphene oxide: Influencing factors and uptake mechanism. *Journal of Colloid and Interface Science*, *485*, 269-279.

Li, M. F., Liu, Y. G., Zeng, G. M., Liu, N., & Liu, S. B. (2019). Graphene and graphene-based nanocomposites used for antibiotics removal in water treatment: a review. *Chemosphere*, *226*, 360-380.

Li, P., Karunanidhi, D., Subramani, T., & Srinivasamoorthy, K. (2021a). Sources and consequences of groundwater contamination. *Archives of Environmental Contamination and Toxicology*, *80*(1), 1-10.

Li, Y., Yu, H., Liu, L., & Yu, H. (2021b). Application of co-pyrolysis biochar for the adsorption and immobilization of heavy metals in contaminated environmental substrates. *Journal of Hazardous Materials*, *420*, 126655.

Li, X., Liu, H., Meng, W., Liu, N., & Wu, P. (2022). Accumulation and source apportionment of heavy metal (loid)s in agricultural soils based on GIS, SOM and PMF: A case study in superposition areas of geochemical anomalies and zinc smelting, Southwest China. *Process Safety and Environmental Protection*, *159*, 964-977.

Li, X., Wang, C., Zhang, J., Liu, J., Liu, B., & Chen, G. (2020a). Preparation and application of magnetic biochar in water treatment: A critical review. *Science of the Total Environment*, *711*, 134847.

Li, Z., Sun, Y., Yang, Y., Han, Y., Wang, T., Chen, J., & Tsang, D. C. (2020b). Biochar-supported nanoscale zero-valent iron as an efficient catalyst for organic degradation in groundwater. *Journal of Hazardous Materials*, *383*, 121240.

Lin, L., Song, Z., Khan, Z. H., Liu, X., & Qiu, W. (2019). Enhanced As (III) removal from aqueous solution by Fe-Mn-La-impregnated biochar composites. *Science of the Total Environment*, *686*, 1185-1193.

Lipshultz, S. E., Law, Y. M., Asante-Korang, A., Austin, E. D., Dipchand, A. I., Everitt, M. D., Hsu, D. T., Lin, K. Y., Price, J. F., Wilkinson, J. D., Colan, S. D., & American Heart Association Council on Cardiovascular Disease in the Young; Council on Clinical Cardiology; and Council on Genomic and Precision Medicine. (2019). Cardiomyopathy in children: classification and diagnosis: a scientific statement from the American Heart Association. *Circulation*, *140*(1), 9-68.

Litter, M. I., Morgada, M. E., & Bundschuh, J. (2010). Possible treatments for arsenic removal in Latin American waters for human consumption. *Environmental Pollution*, *158*(5), 1105-1118.

Liu, B., Kim, K. H., Kumar, V., & Kim, S. (2020a). A review of functional sorbents for adsorptive removal of arsenic ions in aqueous systems. *Journal of hazardous materials*, *388*, 121815.

Liu, N., Liu, Y., Tan, X., Li, M., Liu, S., Hu, X., Zhang, P., Dai, M., Xu, W., & Wen, J. (2020b). Synthesis a graphene-like magnetic biochar by potassium ferrate for 17β-estradiol removal: effects of Al2O3 nanoparticles and microplastics. *Science of the Total Environment*, *715*, 136723.

Liu, S. J., Liu, Y. G., Tan, X. F., Liu, S. B., Li, M. F., Liu, N., Yin, Z. H., Tian, S. R., & Zhou, Y. H. (2019a). Facile synthesis of MnOx-loaded biochar for the removal of doxycycline hydrochloride: effects of ambient conditions and co-existing heavy metals. *Journal of Chemical Technology & Biotechnology*, *94*(7), 2187-2197.

Liu, X., Gao, M., Qiu, W., Khan, Z. H., Liu, N., Lin, L., & Song, Z. (2019b). Fe–Mn–Ce oxide-modified biochar composites as efficient adsorbents for removing As (III) from water: adsorption performance and mechanisms. *Environmental Science and Pollution Research*, *26*(17), 17373-17382.

Lunge, S., Singh, S., & Sinha, A. (2014). Magnetic iron oxide (Fe3O4) nanoparticles from tea waste for arsenic removal. *Journal of Magnetism and Magnetic Materials*, *356*, 21-31.

Luo, J., Meng, X., Crittenden, J., Qu, J., Hu, C., Liu, H., & Peng, P. (2018). Arsenic adsorption on α-MnO2 nano fibers and the significance of (1 0 0) facet as compared with (1 1 0). *Chemical Engineering Journal, 331*, 492-500.

Ma, J., Li, T., Liu, Y., Cai, T., Wei, Y., Dong, W., & Chen, H. (2019). Rice husk derived double network hydrogel as efficient adsorbent for Pb (II), Cu (II) and Cd (II) removal in individual and multicomponent systems. *Bioresource Technology, 290,* 121793.

MacDonald, A. M., Bonsor, H. C., Ahmed, K. M., Burgess, W. G., Basharat, M., Calow, R. C., Dixit, A., Foster, S. S. D., Gopal, K., Lapworth, D. J., & Yadav, S. K. (2016). Groundwater quality and depletion in the Indo-Gangetic Basin mapped from in situ observations. *Nature Geoscience, 9*(10), 762-766.

Madhav, S., Ahamad, A., Singh, A. K., Kushawaha, J., Chauhan, J. S., Sharma, S., & Singh, P. (2020). Water pollutants: sources and impact on the environment and human health. In Sensors in Water Pollutants Monitoring: Role of Material (pp. 43-62). Springer, Singapore.

Magaña, N. M., González, E. A., Ix, M. L., Díaz, C. S., & Gómez, R. (2021). Improved photocatalytic oxidation of arsenic (III) with WO3/TiO2 nanomaterials synthesized by the sol-gel method. *Journal of Environmental Management, 282,* 111602.

Maitlo, H. A., Kim, J. H., Kim, K. H., Park, J. Y., & Khan, A. (2019). Metal-air fuel cell electrocoagulation techniques for the treatment of arsenic in water. *Journal of Cleaner Production, 207,* 67-84.

Maliva, R. G. (2020). Anthropogenic Aquifer Recharge and Water Quality. In *Anthropogenic Aquifer Recharge* (pp. 133-164). Springer, Cham.

Mamvura, T. A., & Danha, G. (2020). Biomass torrefaction as an emerging technology to aid in energy production. *Heliyon*, *6*(3), 03531.

Mani, P., Kim, Y., Lakhera, S. K., Neppolian, B., & Choi, H. (2021). Complete arsenite removal from groundwater by UV activated potassium persulfate and iron oxide impregnated granular activated carbon. *Chemosphere*, *277*, 130225.

Manquián-Cerda, K., Cruces, E., Rubio, M. A., Reyes, C., & Arancibia-Miranda, N. (2017). Preparation of nanoscale iron (oxide, oxyhydroxides and zero-valent) particles derived from blueberries: reactivity, characterization and removal mechanism of arsenate. *Ecotoxicology and Environmental safety*, *145*, 69-77.

Massoudinejad, M., Mohammadi, A., Sadeghi, S., Ghaderpoori, M., Sahebi, S., & Alinejad, A. (2020). Arsenic adsorption over dodecahedra ZIF-8 from solution aqueous: modelling, isotherms, kinetics and thermodynamics. *International Journal of Environmental Analytical Chemistry*, *102*(4), 855-871.

Matta, G., & Gjyli, L. (2016). Mercury, lead and arsenic: impact on environment and human health. *J Chem Pharm Sci*, *9*(2), 718-725.

Mazhar, S. H., Li, X., Rashid, A., Su, J., Xu, J., Brejnrod, A. D., Su, J. Q., Zhu, Y. G., Zhou, S. G., Feng, R., & Rensing, C. (2021). Co-selection of antibiotic resistance genes, and mobile genetic elements in the presence of heavy metals in poultry farm environments. *Science of The Total Environment*, *755*, 142702.

Mazumder, D. N. G., Ghosh, A., Majumdar, K. K., Ghosh, N., Saha, C., & Mazumder, R. N. G. (2010). Arsenic contamination of ground water and its health impact on population of district of Nadia, West Bengal, India. *Indian Journal of Community*

*Medicine: Official Publication of Indian Association of Preventive & Social Medicine*, *35*(2), 331.

Medunić, G., Fiket, Ž., & Ivanić, M. (2020). Arsenic contamination status in Europe, Australia, and other parts of the world. In *Arsenic in Drinking Water and Food* (pp. 183-233). Springer, Singapore.

Megharaj, M., Ramakrishnan, B., Venkateswarlu, K., Sethunathan, N., & Naidu, R. (2011). Bioremediation approaches for organic pollutants: a critical perspective. *Environment International*, *37*(8), 1362-1375.

Mershiba, S. D., Dassprakash, M. V., & Saraswathy, S. D. (2013). Protective effect of naringenin on hepatic and renal dysfunction and oxidative stress in arsenic intoxicated rats. *Molecular Biology Reports*, *40*(5), 3681-3691.

Moeck, C., Grech-Cumbo, N., Podgorski, J., Bretzler, A., Gurdak, J. J., Berg, M., & Schirmer, M. (2020). A global-scale dataset of direct natural groundwater recharge rates: A review of variables, processes and relationships. *Science of the Total Environment*, *717*, 137042.

Mohan, D., & Pittman Jr, C. U. (2007). Arsenic removal from water/wastewater using adsorbents—a critical review. *Journal of hazardous materials*, *142*(1-2), 1-53.

Mohan, D., Dey, S., Dwivedi, S. B., & Shukla, S. P. (2019, August). Adsorption of arsenic using low cost adsorbents: guava leaf biomass, mango bark and bagasse. Indian Academy of Sciences.

Mohan, D., Sarswat, A., Ok, Y. S., & Pittman Jr, C. U. (2014). Organic and inorganic contaminants removal from water with biochar, a renewable, low cost and sustainable adsorbent–a critical review. *Bioresource technology*, *160*, 191-202.

Mohanty, P., Nanda, S., Pant, K. K., Naik, S., Kozinski, J. A., & Dalai, A. K. (2013). Evaluation of the physiochemical development of biochars obtained from pyrolysis of wheat straw, timothy grass and pinewood: effects of heating rate. *Journal of Analytical and Applied Pyrolysis*, *104*, 485-493.

Mondal, M. K., & Garg, R. (2017). A comprehensive review on removal of arsenic using activated carbon prepared from easily available waste materials. *Environmental Science and Pollution Research, 24*(15), 13295-13306.

Mondal, P., Bhowmick, S., Chatterjee, D., Figoli, A., & Van der Bruggen, B. (2013). Remediation of inorganic Arsenic in groundwater for safe water supply: a critical assessment of technological solutions. *Chemosphere, 92*(2), 157–170.

Mood, B. M., Naseri, K., Tahergorabi, Z., Khazdair, M. R., & Sadeghi, M. (2021). Toxic mechanisms of five heavy metals: mercury, lead, chromium, cadmium, and arsenic. *Frontiers in pharmacology*, *12*.

Moreno, R. K., Loira, G. B., Carrillo, L. L., & Cebrián, M. E. (2022). Prevalence of type 2 diabetes mellitus in relation to arsenic exposure and metabolism in Mexican women. *Environmental Research*, *210*, 112948.

Mou, F., Guan, J., Xiao, Z., Sun, Z., Shi, W., & Fan, X. A. (2011). Solvent-mediated synthesis of magnetic Fe2O3 chestnut-like amorphous-core/γ-phase-shell hierarchical nanostructures with strong As (v) removal capability. *Journal of Materials Chemistry*, *21*(14), 5414-5421.

Mukherjee, A., Sengupta, M. K., Hossain, M. A., Ahamed, S., Das, B., Nayak, B., Lodh, D., Rahman, M. M., & Chakraborti, D. (2006). Arsenic contamination in

groundwater: a global perspective with emphasis on the Asian scenario. *Journal of Health, Population and Nutrition*, 142-163.

Mukherjee, S. C., Rahman, M. M., Chowdhury, U. K., Sengupta, M. K., Lodh, D., Chanda, C. R., Saha, K. C., & Chakraborti, D. (2003). Neuropathy in arsenic toxicity from groundwater arsenic contamination in West Bengal, India. *Journal of Environmental Science and Health, Part A*, *38*(1), 165-183.

Mukhopadhyay, M., Lakhotia, S. R., Ghosh, A. K., & Bindal, R. C. (2019). Removal of arsenic from aqueous media using zeolite/chitosan nanocomposite membrane. *Separation science and technology*, *54*(2), 282-288.

Mundey, M. K., Roy, M., Roy, S., Awasthi, M. K., & Sharma, R. (2013). Antioxidant potential of Ocimum sanctum in arsenic induced nervous tissue damage. *Brazilian Journal of Veterinary Pathology*, *6*(3), 95-101.

Muthumani, M., & Prabu, S. M. (2012). Silibinin potentially protects arsenic-induced oxidative hepatic dysfunction in rats. *Toxicology Mechanisms and Methods*, *22*(4), 277-288.

Nachman, K. E., Baron, P. A., Raber, G., Francesconi, K. A., Navas-Acien, A., & Love, D. C. (2013). Roxarsone, inorganic arsenic, and other arsenic species in chicken: a US-based market basket sample. *Environmental Health Perspectives*, *121*(7), 818-824.

Nath, B. K., Chaliha, C., & Kalita, E. (2019). Iron oxide Permeated Mesoporous rice-husk nanobiochar (IPMN) mediated removal of dissolved arsenic (As): Chemometric modelling and adsorption dynamics. *Journal of Environmental Management*, *246*, 397-409.

Navarathna, C., Alchouron, J., Liyanage, A., Herath, A., Wathudura, P., Nawalage, S., Rodrigo, P., Gunatilake, S., Mohan, D., Jr. Pittman, C., & Mlsna, T. (2020). Recent developments in aqueous Arsenic (III) remediation using biomass-based adsorbents. In *Contaminants in Our Water: Identification and Remediation Methods* (pp. 197-251). American Chemical Society.

Nayak, L., Rahaman, M., & Giri, R. (2019). Surface modification/functionalization of carbon materials by different techniques: An overview. *Carbon-containing Polymer Composites*, 65-98.

Nayak, R. (2017). Practical approach to the patient with acute neuromuscular weakness. *World Journal of Clinical Cases*, *5*(7), 270.

Neumann, R. B., Ashfaque, K. N., Badruzzaman, A. B. M., Ashraf Ali, M., Shoemaker, J. K., & Harvey, C. F. (2010). Anthropogenic influences on groundwater arsenic concentrations in Bangladesh. *Nature geoscience*, *3*(1), 46-52.

Neyaz, N., Siddiqui, W. A., & Nair, K. K. (2014). Application of surface functionalized iron oxide nanomaterials as a nanosorbents in extraction of toxic heavy metals from ground water: a review. *International Journal of Environmental Sciences*, *4*(4), 472.

Nguyen, T. H., Pham, T. H., Nguyen Thi, H. T., Nguyen, T. N., Nguyen, M. V., Tran Dinh, T., Nguyen, M. P., Do, T. Q., Phuong, T., Hoang, T. T, & Thi, V. H. T. (2019). Synthesis of iron-modified biochar derived from rice straw and its application to arsenic removal. *Journal of Chemistry*, *2019*.

Niazi, N. K., Bibi, I., Shahid, M., Ok, Y. S., Burton, E. D., Wang, H., Shaheen, S., Rinklebe, J., & Lüttge, A. (2018). Arsenic removal by perilla leaf biochar in

aqueous solutions and groundwater: an integrated spectroscopic and microscopic examination. *Environmental Pollution*, *232*, 31-41.

Nikić, J., Agbaba, J., Watson, M. A., Tubić, A., Šolić, M., Maletić, S., & Dalmacija, B. (2019). Arsenic adsorption on Fe–Mn modified granular activated carbon (GAC–FeMn): batch and fixed-bed column studies. *Journal of Environmental Science and Health, Part A*, *54*(3), 168-178.

Nizamuddin, S., Baloch, H. A., Griffin, G. J., Mubarak, N. M., Bhutto, A. W., Abro, R., Mazari, S. A., & Ali, B. S. (2017). An overview of effect of process parameters on hydrothermal carbonization of biomass. *Renewable and Sustainable Energy Reviews*, *73*, 1289-1299.

Noraini, M. N., Abdullah, E. C., Othman, R., & Mubarak, N. M. (2016). Single-route synthesis of magnetic biochar from sugarcane bagasse by microwave-assisted pyrolysis. *Material Letter, 184*, 315–319.

Norazlina, A. S., Che, F. I., & Rosenani, A. B. (2014). Characterization of oil palm empty fruit bunch and rice husk biochars and their potential to adsorb arsenic and cadmium. *American Journal of Agricultural and Biological Sciences*, *9*(3), 450-456.

Nwankwo, C. B., Hoque, M. A., Islam, M. A., & Dewan, A. (2020). Groundwater constituents and trace elements in the basement aquifers of Africa and sedimentary aquifers of Asia: medical hydrogeology of drinking water minerals and toxicants. *Earth Systems and Environment*, *4*(2), 369-384.

O'Bryant, S. E., Edwards, M., Menon, C. V., Gong, G., & Barber, R. (2011). Long-term low-level arsenic exposure is associated with poorer neuropsychological

functioning: a Project FRONTIER study. *International Journal of Environmental Research and Public Health, 8*(3), 861-874.

Ochedi, F. O., Liu, Y., & Hussain, A. (2020). A review on coal fly ash-based adsorbents for mercury and arsenic removal. *Journal of cleaner production*, *267*, 122143.

Oki, T., & Kanae, S. (2006). Global hydrological cycles and world water resources. S*cience, 313*(5790), 1068-1072.

Oliveira, F. R., Patel, A. K., Jaisi, D. P., Adhikari, S., Lu, H., & Khanal, S. K. (2017). Environmental application of biochar: Current status and perspectives. *Bioresource Technology*, *246*, 110-122.

Padungthon, S., German, M., Wiriyathamcharoen, S., & SenGupta, A. K. (2015). Polymeric anion exchanger supported hydrated Zr (IV) oxide nanoparticles: a reusable hybrid sorbent for selective trace arsenic removal. *Reactive and Functional Polymers*, *93*, 84-94.

Palaniappan, V., & Karthikeyan, K. (2022). Bowen's disease. *Indian Dermatology Online Journal*, *13*(2), 177.

Pan, W. C., Seow, W. J., Kile, M. L., Hoffman, E. B., Quamruzzaman, Q., Rahman, M., Mahiuddin, G., Mostofa, G., Lu, Q., & Christiani, D. C. (2013). Association of low to moderate levels of arsenic exposure with risk of type 2 diabetes in Bangladesh. *American Journal of Epidemiology*, *178*(10), 1563-1570.

Panel, E. C. (2014). Scientific Opinion on dietary exposure to inorganic arsenic in the European population. *EFSA Journal*, *12*(3), 3597.

Panwar, N. L., & Pawar, A. (2020). Influence of activation conditions on the physicochemical properties of activated biochar: a review. *Biomass Conversion and Biorefinery*, 1-23.

Parvez, F., Chen, Y., Brandt-Rauf, P. W., Slavkovich, V., Islam, T., Ahmed, A., Argos, M., Hassan, R., Yunus, M., & Ahsan, H. (2010). A prospective study of respiratory symptoms associated with chronic arsenic exposure in Bangladesh: findings from the Health Effects of Arsenic Longitudinal Study (HEALS). *Thorax*, *65*(6), 528-533.

Parvez, F., Chen, Y., Yunus, M., Olopade, C., Segers, S., Slavkovich, V., Argos, M., Hasan, R., Ahmed, A., & Ahsan, H. (2013). Arsenic exposure and impaired lung function. Findings from a large population-based prospective cohort study. *American Journal of Respiratory and Critical Care Medicine*, *188*(7), 813-819.

Patel, H. (2019). Fixed-bed column adsorption study: a comprehensive review. *Applied Water Science*, *9*(3), 1-17.

Patra, C., Gupta, R., Bedadeep, D., & Narayanasamy, S. (2020). Surface treated acid-activated carbon for adsorption of anionic azo dyes from single and binary adsorptive systems: a detail insight. *Environmental Pollution*, *266*, 115102.

Peter, A., Chabot, B., & Loranger, E. (2021). Enhanced activation of ultrasonic pre-treated softwood biochar for efficient heavy metal removal from water. *Journal of Environmental Management*, *290*, 112569.

Pintor, A. M., Vieira, B. R., Santos, S. C., Boaventura, R. A., & Botelho, C. M. (2018). Arsenate and arsenite adsorption onto iron-coated cork granulates. *Science of the Total Environment*, *642*, 1075-1089.

Pizarro, C., Escudey, M., Caroca, E., Pavez, C., & Zúñiga, G. E. (2021). Evaluation of zeolite, nanomagnetite, and nanomagnetite-zeolite composite materials as arsenic (V) adsorbents in hydroponic tomato cultures. *Science of the Total Environment*, *751*, 141623.

Polowczyk, I., Bastrzyk, A., Koźlecki, T., Rudnicki, P., Sawiński, W., Sadowski, Z., & Sokołowski, A. (2007). Application of fly ash agglomerates in the sorption of arsenic. *Polish Journal of Chemical Technology*, *9*(2), 37-41.

Pous, N., Casentini, B., Rossetti, S., Fazi, S., Puig, S., & Aulenta, F. (2015). Anaerobic arsenite oxidation with an electrode serving as the sole electron acceptor: a novel approach to the bioremediation of arsenic-polluted groundwater. *Journal of hazardous materials*, *283*, 617-622.

Power, A., Chandra, S., & Chapman, J. (2018). Graphene, electrospun membranes and granular activated carbon for eliminating heavy metals, pesticides and bacteria in water and wastewater treatment processes. *Analyst*, *143*(23), 5629-5645.

Prabhakar, R., & Samadder, S. R. (2020). Use of adsorption-influencing parameters for designing the batch adsorber and neural network–based prediction modelling for the aqueous arsenate removal using combustion synthesised nano-alumina. *Environmental Science and Pollution Research*, *27*(21), 26367-26384.

Pradhan, R. M., Guru, B., Pradhan, B., & Biswal, T. K. (2021). Integrated multi-criteria analysis for groundwater potential mapping in Precambrian hard rock terranes (North Gujarat), India. *Hydrological Sciences Journal*, *66*(6), 961-978.

Premarathna, K. S. D., Rajapaksha, A. U., Sarkar, B., Kwon, E. E., Bhatnagar, A., Ok, Y. S., & Vithanage, M. (2019). Biochar-based engineered composites for sorptive decontamination of water: A review. *Chemical Engineering Journal*, *372*, 536-550.

Premkumar, M. P., Thiruvengadaravi, K. V., Senthil Kumar, P., Nandagopal, J., & Sivanesan, S. (2018). Eco-friendly treatment strategies for wastewater containing dyes and heavy metals. In *Environmental Contaminants* (pp. 317-360). Springer, Singapore.

Priyadarshni, N., Nath, P., & Chanda, N. (2020). Sustainable removal of arsenate, arsenite and bacterial contamination from water using biochar stabilized iron and copper oxide nanoparticles and associated mechanism of the remediation process. *Journal of Water Process Engineering*, *37*, 101495.

Priyan, V. V., Shahnaz, T., Suganya, E., Sivaprakasam, S., & Narayanasamy, S. (2021). Ecotoxicological assessment of micropollutant Diclofenac biosorption on magnetic sawdust: Phyto, Microbial and Fish toxicity studies. *Journal of Hazardous Materials*, *403*, 123532.

Pulido-Novicio, L., Kurimoto, Y., Aoyama, M., Seki, K., Hata, T., Ishihara, S., & Imamura, Y. (2001). Adsorption of mercury by sugi wood carbonized at 1000 C. *Journal of wood science*, *47*(2), 159-162.

Pulka, J., Manczarski, P., Koziel, J. A., & Białowiec, A. (2019). Torrefaction of sewage sludge: Kinetics and fuel properties of biochars. *Energies*, *12*(3), 565.

Raessler, M. (2018). The arsenic contamination of drinking and groundwaters in Bangladesh: featuring biogeochemical aspects and implications on public health. *Archives of Environmental Contamination and Toxicology*, *75*(1), 1-7.

Rahman, H. L., Erdem, H., Sahin, M., & Erdem, M. (2020). Iron-incorporated activated carbon synthesis from biomass mixture for enhanced arsenic adsorption. *Water, Air, & Soil Pollution*, *231*(1), 1-17.

Rahman, M. A., Rahman, A., Khan, M. Z. K., & Renzaho, A. M. (2018). Human health risks and socio-economic perspectives of arsenic exposure in Bangladesh: a scoping review. *Ecotoxicology and Environmental Safety*, *150*, 335-343.

Rahman, Z., & Singh, V. P. (2019). The relative impact of toxic heavy metals (THMs) (arsenic (As), cadmium (Cd), chromium (Cr)(VI), mercury (Hg), and lead (Pb)) on the total environment: an overview. *Environmental Monitoring and Assessment*, *191*(7), 1-21.

Raju, J. N. (2012). Arsenic exposure through groundwater in the middle Ganga plain in the Varanasi environs, India: A future threat. *Journal of the Geological Society of India*, *79*(3), 302-314.

Ran, H., Guo, Z., Yi, L., Xiao, X., Zhang, L., Hu, Z., Li, C., & Zhang, Y. (2021). Pollution characteristics and source identification of soil metal (loid) s at an abandoned arsenic-containing mine, China. *Journal of Hazardous Materials*, *413*, 125382.

Rana, A., Kumari, N., Tyagi, M., & Jagadevan, S. (2018). Leaf-extract mediated zero-valent iron for oxidation of Arsenic (III): Preparation, characterization and kinetics. Chemical Engineering Journal, 347, 91-100.

Ranjan, S., Yadav, B. K., & Joshi, H. (2020). Development of nZVI-pumice/zeolite composites for effective removal of arsenic (III) from aqueous solution. *Journal of Hazardous, Toxic, and Radioactive Waste*, *24*(3), 04020014.

Rao, S. N., Ravindra, B., & Wu, J. (2020). Geochemical and health risk evaluation of fluoride rich groundwater in Sattenapalle Region, Guntur district, Andhra Pradesh, India. *Human and ecological risk assessment: An International Journal*, *26*(9), 2316-2348.

Rashid, R., Shafiq, I., Akhter, P., Iqbal, M. J., & Hussain, M. (2021). A state-of-the-art review on wastewater treatment techniques: the effectiveness of adsorption method. *Environmental Science and Pollution Research*, *28*(8), 9050-9066.

Rasool, A., Xiao, T., Baig, Z. T., Masood, S., Mostofa, K. M., & Iqbal, M. (2015). Co-occurrence of arsenic and fluoride in the groundwater of Punjab, Pakistan: source discrimination and health risk assessment. *Environmental Science and Pollution Research*, *22*(24), 19729-19746.

Rathi, B. S., & Kumar, P. S. (2021). Application of adsorption process for effective removal of emerging contaminants from water and wastewater. *Environmental Pollution*, *280*, 116995.

Rawat, S., & Singh, J. (2021). Green Synthesis of Iron Nanoparticles Using Plumeria and Jatropha: Characterization and Investigation of Their Adsorption, Regeneration and Catalytic Degradation Efficiencies. *BioNanoScience*, *11*(4), 1142-1153.

Rawat, S., Samreen, K., Nayak, A. K., Singh, J., & Koduru, J. R. (2021). Fabrication of iron nanoparticles using Parthenium: A combinatorial eco-innovative approach to eradicate crystal violet dye and phosphate from the aqueous

environment. *Environmental Nanotechnology, Monitoring & Management*, *15*, 100426.

Richards, L. A. (2012). *The removal of inorganic contaminants using nanofiltration and reverse osmosis* (Doctoral dissertation, Heriot-Watt University).

Rosales, M., Coreño, O., & Nava, J. L. (2018). Removal of hydrated silica, fluoride and arsenic from groundwater by electrocoagulation using a continuous reactor with a twelve-cell stack. *Chemosphere*, *211*, 149-155.

Ruthiraan, M., Abdullah, E. C., Mubarak, N. M., & Thines, K. R. (2017). New generation of magnetic microporus material for enhancing route for methylene blue removal from waste water. *Journal of Environment & Biotechnology Research*, *6*(1), 105-116.

Saavedra, R., Muñoz, R., Taboada, M. E., Vega, M., & Bolado, S. (2018). Comparative uptake study of arsenic, boron, copper, manganese and zinc from water by different green microalgae. *Bioresource Technology*, *263*, 49-57.

Sabir, S., Akhtar, M. F., & Saleem, A. (2019). Endocrine disruption as an adverse effect of non-endocrine targeting pharmaceuticals. *Environmental Science and Pollution Research*, *26*(2), 1277-1286.

Saeed, A. A. H., Harun, N. Y., & Nasef, M. M. (2019). Physicochemical characterization of different agricultural residues in malaysia for bio char production. *International Journal of Civil Engineering and Technology*, *10*, 213-225.

Saha, S., Reza, A. H. M., & Roy, M. K. (2021). Arsenic geochemistry of the sediments of the shallow aquifer and its correlation with the groundwater, Rangpur, Bangladesh. *Applied Water Science*, *11*(10), 1-11.

Saikia, R., Goswami, R., Bordoloi, N., Senapati, K. K., Pant, K. K., Kumar, M., & Kataki, R. (2017). Removal of arsenic and fluoride from aqueous solution by biomass based activated biochar: optimization through response surface methodology. *Journal of environmental chemical engineering*, *5*(6), 5528-5539.

Samadzadeh, Y. M. R., & Khodadadi, D. A. (2010). Effect of arsenic speciation on remediation of arsenic-contaminated soils and waters.

Samoraj, M., Mironiuk, M., Witek-Krowiak, A., Izydorczyk, G., Skrzypczak, D., Mikula, K., Basladynska, S., Moustakas, K., & Chojnacka, K. (2022). Biochar in environmental friendly fertilizers-Prospects of development products and technologies. *Chemosphere,* 133975.

Samsuri, A. W., Zadeh, F. S., & Bardan, B. J. S. (2013). Sorption of As(III) and As(V) by Fe coated biochars and biochars produced from empty fruit bunch and rice husk. *Journal of Environmental Chemical Engineering,* 1, 981-988.

Samuel, M. S., Selvarajan, E., Sarswat, A., Muthukumar, H., Jacob, J. M., Mukesh, M., & Pugazhendhi, A. (2022). Nanomaterials as adsorbents for As (III) and As (V) removal from water: A review. *Journal of Hazardous Materials*, *424*, 127572.

Sandoval, M. A., Fuentes, R., Thiam, A., & Salazar, R. (2021). Arsenic and fluoride removal by electrocoagulation process: A general review. *Science of The Total Environment*, *753*, 142108.

Sankar, P., Gopal Telang, A., Kalaivanan, R., Karunakaran, V., Manikam, K., & Sarkar, S. N. (2015). Effects of nanoparticle-encapsulated curcumin on arsenic-induced liver toxicity in rats. *Environmental Toxicology*, *30*(6), 628-637.

Sanyal, T., Bhattacharjee, P., Paul, S., & Bhattacharjee, P. (2020). Recent advances in arsenic research: significance of differential susceptibility and sustainable strategies for mitigation. *Frontiers in Public Health*, *8*, 464.

Saravanan, A., Kumar, P. S., Jeevanantham, S., Karishma, S., Tajsabreen, B., Yaashikaa, P. R., & Reshma, B. (2021). Effective water/wastewater treatment methodologies for toxic pollutants removal: Processes and applications towards sustainable development. *Chemosphere*, *280*, 130595.

Sari, N. A., Ishak, C. F., & Bakar, R. A. (2014). Characterization of oil palm empty fruit bunch and rice husk biochars and their potential to adsorb arsenic and cadmium. *American Journal of Agricultural and Biological Sciences*, *9*(3), 450-456.

Sarkar, S., Greenleaf, J. E., Gupta, A., Uy, D., & SenGupta, A. K. (2012). Sustainable engineered processes to mitigate the global arsenic crisis in drinking water: challenges and progress. *Annual Review of Chemical and Biomolecular Engineering*, *3*, 497-517.

Sarswat, A., & Mohan, D. (2016). Sustainable development of coconut shell activated carbon (CSAC) & a magnetic coconut shell activated carbon (MCSAC) for phenol (2-nitrophenol) removal. *RSC Advances*, *6*(88), 85390-85410.

Sen, M., & Pal, P. (2009). Treatment of arsenic-contaminated groundwater by a low cost activated alumina adsorbent prepared by partial thermal dehydration. *Desalination and Water Treatment*, *11*(1-3), 275-282.

Senn, A. C., Hug, S. J., Kaegi, R., Hering, J. G., & Voegelin, A. (2018). Arsenate co-precipitation with Fe (II) oxidation products and retention or release during precipitate aging. *Water Research*, *131*, 334-345.

Shahnaz, T., Priyan, V. V., Pandian, S., & Narayanasamy, S. (2021). Use of Nanocellulose extracted from grass for adsorption abatement of Ciprofloxacin and Diclofenac removal with phyto, and fish toxicity studies. *Environmental Pollution*, *268*, 115494.

Shaji, E., Santosh, M., Sarath, K. V., Prakash, P., Deepchand, V., & Divya, B. V. (2021). Arsenic contamination of groundwater: A global synopsis with focus on the Indian Peninsula. *Geoscience Frontiers*, *12*(3), 101079.

Shakoor, M. B., Niazi, N. K., Bibi, I., Murtaza, G., Kunhikrishnan, A., Seshadri, B., Shahid, M., Ali, S., Bolan, N.S., Ok, Y.S., Abid, M., & Ali, F. (2016). Remediation of arsenic-contaminated water using agricultural wastes as biosorbents. *Critical Reviews in Environmental Science and Technology*, *46*(5), 467-499.

Shakoor, M. B., Niazi, N. K., Bibi, I., Shahid, M., Saqib, Z. A., Nawaz, M. F., Shaheen, S.M., Wang, H., Tsang, D. C. W., Bundschuh, J., Ok, Y. S., & Rinklebe, J. (2019). Exploring the arsenic removal potential of various biosorbents from water. *Environment International*, *123*, 567-579.

Shakoor, M. B., Niazi, N. K., Bibi, I., Shahid, M., Sharif, F., Bashir, S., Shaheen, S. M., Wang, H., Tsang, D. C. W., Ok, Y. S., & Rinklebe, J. (2018). Arsenic removal by natural and chemically modified water melon rind in aqueous solutions and groundwater. *Science of the Total Environment*, *645*, 1444-1455.

Shakya, A. K., & Ghosh, P. K. (2018). Simultaneous removal of arsenic and nitrate in absence of iron in an attached growth bioreactor to meet drinking water standards: importance of sulphate and empty bed contact time. *Journal of Cleaner Production*, *186*, 304-312.

Shakya, A., Núñez-Delgado, A., & Agarwal, T. (2019). Biochar synthesis from sweet lime peel for hexavalent chromium remediation from aqueous solution. *Journal of environmental management*, *251*, 109570.

Shanmugarajah, B., Chew, I. M., Mubarak, N. M., Choong, T. S., Yoo, C., & Tan, K. (2019). Valorization of palm oil agro-waste into cellulose biosorbents for highly effective textile effluent remediation. *Journal of Cleaner Production*, *210*, 697-709.

Shen, B., Chen, J., Yue, S., & Li, G. (2015). A comparative study of modified cotton biochar and activated carbon based catalysts in low temperature SCR. *Fuel*, *156*, 47-53.

Siddique, T. A., Dutta, N. K., & Roy Choudhury, N. (2020). Nanofiltration for arsenic removal: challenges, recent developments, and perspectives. *Nanomaterials*, *10*(7), 1323.

Siddiqui, S. I., Naushad, M., & Chaudhry, S. A. (2019). Promising prospects of nanomaterials for arsenic water remediation: A comprehensive review. *Process Safety and Environmental Protection*, *126*, 60-97.

Singh, J., Reddy, K. J., Chang, Y. Y., Kang, S. H., & Yang, J. K. (2016). A novel reutilization method for automobile shredder residue as an adsorbent for the removal of methylene blue: Mechanisms and heavy metal recovery using an ultrasonically assisted acid. *Process Safety and Environmental Protection*, *99*, 88-97.

Singh, N., & Singh, O. P. (2020). Sustainable arsenic mitigation: Problems and prospects in India. In *Arsenic Water Resources Contamination* (pp. 131-156). Springer, Cham.

Singh, S., Sharma, P., Mudhulkar, R., Chakravorty, B., & Singh, A. (2022). Assessment of hydrogeochemistry and arsenic contamination in groundwater of Bahraich District, Uttar Pradesh, India. *Arabian Journal of Geosciences*, *15*(1), 1-18.

Sinha, D., & Prasad, P. (2020). Health effects inflicted by chronic low-level arsenic contamination in groundwater: A global public health challenge. *Journal of Applied Toxicology*, *40*(1), 87-131.

Smith, A. H., Marshall, G., Yuan, Y., Ferreccio, C., Liaw, J., Von Ehrenstein, O., Steinmaus, C., Bates, M. N., & Selvin, S. (2006). Increased mortality from lung cancer and bronchiectasis in young adults after exposure to arsenic in utero and in early childhood. *Environmental Health Perspectives, 114(8),* 1293-1296.

Sohi, S. P., Krull, E., Lopez-Capel, E., & Bol, R. (2010). A review of biochar and its use and function in soil. *Advances in agronomy*, *105*, 47-82.

Soni, R., & Shukla, D. P. (2019). Synthesis of fly ash based zeolite-reduced graphene oxide composite and its evaluation as an adsorbent for arsenic removal. *Chemosphere, 219,* 504-509.

Srivastav, A. L., Pham, T. D., Izah, S. C., Singh, N., & Singh, P. K. (2021). Biochar Adsorbents for Arsenic Removal from Water Environment: A Review. *Bulletin of Environmental Contamination and Toxicology,* 1-13.

Srivastava, S., & Flora, S. J. (2020). Arsenicals: toxicity, their use as chemical warfare agents, and possible remedial measures. In *Handbook of Toxicology of Chemical Warfare Agents* (pp. 303-319). Academic Press.

Stummann, M. Z., Elevera, E., Hansen, A. B., Hansen, L. P., Beato, P., Davidsen, B., Wiwel, P., Gabrielsen, J., Jesen, P. A., Jensen, A. D., & Høj, M. (2020). Catalytic hydropyrolysis of biomass using supported CoMo catalysts–Effect of metal loading and support acidity. *Fuel*, *264*, 116807.

Suhag, R. (2019). *Overview of ground water in India*. PRS.

Sullivan, C., Tyrer, M., Cheeseman, C. R., & Graham, N. J. (2010). Disposal of water treatment wastes containing arsenic—a review. *Science of the Total Environment*, *408*(8), 1770-1778.

Sun, Y. P., Li, X. Q., Zhang, W. X., & Wang, H. P. (2007). A method for the preparation of stable dispersion of zero-valent iron nanoparticles. *Colloids and Surfaces A: Physicochemical and Engineering Aspects*, *308*(1-3), 60-66.

Sun, Y., Lei, C., Khan, E., Chen, S. S., Tsang, D. C., Ok, Y. S., Lin, D., Feng, Y., & Li, X. D. (2017). Nanoscale zero-valent iron for metal/metalloid removal from model hydraulic fracturing wastewater. *Chemosphere*, *176*, 315-323.

Szerement, J., Szatanik-Kloc, A., Jarosz, R., Bajda, T., & Mierzwa-Hersztek, M. (2021). Contemporary applications of natural and synthetic zeolites from fly ash in agriculture and environmental protection. *Journal of Cleaner Production*, *311*, 127461.

Taba, L. E., Irfan, M. F., Daud, W. A. M. W., & Chakrabarti, M. H. (2012). The effect of temperature on various parameters in coal, biomass and CO-gasification: a review. *Renewable and Sustainable Energy Reviews*, *16*(8), 5584-5596.

Tabassum, R. A., Shahid, M., Niazi, N. K., Dumat, C., Zhang, Y., Imran, M., *Bakhat, H. F.Hussain, I.,* & Khalid, S. (2019). Arsenic removal from aqueous solutions and groundwater using agricultural biowastes-derived biosorbents and biochar: a column-scale investigation. *International Journal of P hytoremediation*, *21*(6), 509-518.

Tabelin, C. B., Igarashi, T., Villacorte-Tabelin, M., Park, I., Opiso, E. M., Ito, M., & Hiroyoshi, N. (2018). Arsenic, selenium, boron, lead, cadmium, copper, and zinc in naturally contaminated rocks: A review of their sources, modes of enrichment, mechanisms of release, and mitigation strategies. *Science of the Total Environment, 645*, 1522-1553.

Tam, N. T. M., Liu, Y., Bashir, H., Yin, Z., He, Y., & Zhou, X. (2020). Efficient removal of diclofenac from aqueous solution by potassium ferrate-activated porous graphitic biochar: ambient condition influences and adsorption mechanism. *International Journal of Environmental Research and Public Health*, *17*(1), 291.

Tan, G., Mao, Y., Wang, H., & Xu, N. (2020a). A comparative study of arsenic (V), tetracycline and nitrate ions adsorption onto magnetic biochars and activated carbon. *Chemical Engineering Research and Design*, *159*, 582-591.

Tan, X., Wei, W., Xu, C., Meng, Y., Bai, W., Yang, W., & Lin, A. (2020b). Manganese-modified biochar for highly efficient sorption of cadmium. *Environmental Science and Pollution Research*, *27*(9), 9126-9134.

Tang, W., Li, Q., Gao, S., & Shang, J. K. (2011). Arsenic (III, V) removal from aqueous solution by ultrafine α-Fe2O3 nanoparticles synthesized from solvent thermal method. *Journal of hazardous materials*, *192*(1), 131-138.

Tavares, D. S., Lopes, C. B., Coelho, J. P., Sánchez, M. E., Garcia, A. I., Duarte, A. C., Otero, M., & Pereira, E. (2012). Removal of arsenic from aqueous solutions by sorption onto sewage sludge-based sorbent. *Water, Air, & Soil Pollution*, *223*(5), 2311-2321.

Temkin, M. I. (1940). Kinetics of ammonia synthesis on promoted iron catalysts. *Acta physiochim. URSS*, *12*, 327-356.

Thines, K. R., Abdullah, E. C., & Mubarak, N. M. (2017b). Effect of process parameters for production of microporous magnetic biochar derived from agriculture waste biomass. *Microporous and Mesoporous Materials*, *253*, 29-39.

Thines, K. R., Abdullah, E. C., Mubarak, N. M., & Ruthiraan, M. (2017a). Synthesis of magnetic biochar from agricultural waste biomass to enhancing route for waste water and polymer application: a review. *Renewable and Sustainable Energy Reviews*, *67*, 257-276.

Tomczyk, A., Sokołowska, Z., & Boguta, P. (2020). Biochar physicochemical properties: pyrolysis temperature and feedstock kind effects. *Reviews in Environmental Science and Bio/Technology*, *19*(1), 191-215.

Toro, S. J. C., Aguirre, G. J. A., Giraldo, J. A. P., & Alzate, C. A. C. (2021). Thermochemical processing of woody biomass: A review focused on energy-driven applications and catalytic upgrading. *Renewable and Sustainable Energy Reviews*, *136*, 110376.

Uddin, M., & Jeong, Y. K. (2020). Efficiently performing periodic elements with modern adsorption technologies for arsenic removal. *Environmental Science and Pollution Research*, *27*(32), 39888-39912.

Ulatowska, J., Polowczyk, I., Sawiński, W., Bastrzyk, A., Koźlecki, T., & Sadowski, Z. (2014). Use of fly ash and fly ash agglomerates for As (III) adsorption from aqueous solution. *Polish Journal of Chemical Technology*, *16*(1).

Ungureanu, G., Santos, S., Boaventura, R., & Botelho, C. (2015). Arsenic and antimony in water and wastewater: Overview of removal techniques with special reference to latest advances in adsorption. *Journal of environmental management*, *151*, 326-342.

Valdés, M., Hanchey, A., Muñoz, M. P., Baumert, B., & Iglesias, V. (2017). Low-level arsenic exposure during pregnancy and its association with postpartum depression: A cohort study of women from Arica, Chile. *Revue d'Épidémiologie et de Santé Publique*, *65*(6), 427-435.

VanDerwerker, T., Zhang, L., Ling, E., Benham, B., & Schreiber, M. (2018). Evaluating geologic sources of arsenic in well water in Virginia (USA). *International journal of environmental research and public health*, *15*(4), 787.

Velazquez-Peña, G. C., Solache-Ríos, M., Olguin, M. T., & Fall, C. (2019). As (V) sorption by different natural zeolite frameworks modified with Fe, Zr and FeZr. *Microporous and Mesoporous Materials*, *273*, 133-141.

Verma, L., & Singh, J. (2019). Synthesis of novel biochar from waste plant litter biomass for the removal of Arsenic (III and V) from aqueous solution: a mechanism characterization, kinetics and thermodynamics. *Journal of Environmental Management, 248,* 109235.

Verma, L., Azad, A., & Singh, J. (2021). Performance of a novel iron infused biochar developed from Raphanus sativus and Artocarpus heterophyllus refuse for trivalent and pentavalent arsenic adsorption from an aqueous solution: mechanism, isotherm and kinetics study. *International Journal of Phytoremediation,* 1-14.

Verma, L., Siddique, M. A., Singh, J., & Bharagava, R. N. (2019). As (III) and As (V) removal by using iron impregnated biosorbents derived from waste biomass of Citrus limmeta (peel and pulp) from the aqueous solution and ground water. *Journal of Environmental Management*, *250,* 109452.

Verma, S., & Sinha, A. (2022). Appraisal of groundwater arsenic on opposite banks of River Ganges, West Bengal, India, and quantification of cancer risk using Monte Carlo simulations. *Environmental Science and Pollution Research*, 1-21.

Vilvanathan, S., & Shanthakumar, S. (2017). Modeling of fixed-bed column studies for removal of cobalt ions from aqueous solution using Chrysanthemum indicum. *Research on Chemical Intermediates*, *43*(1), 229-243.

Vinayagam, R., Pai, S., Varadavenkatesan, T., Narasimhan, M. K., Narayanasamy, S., & Selvaraj, R. (2020). Structural characterization of green synthesized α-Fe2O3

nanoparticles using the leaf extract of Spondias dulcis. *Surfaces and Interfaces*, *20*, 100618.

Vithanage, M., Herath, I., Joseph, S., Bundschuh, J., Bolan, N., Ok, Y. S., Kirkham, M.B., & Rinklebe, J. (2017). Interaction of arsenic with biochar in soil and water: a critical review. *Carbon*, *113*, 219-230.

Vivekanandhan, S. (2018). Biochar supercapacitors: recent developments in the materials and methods. *Green and Sustainable Advanced Materials: Applications*, *2*, 223-249.

Wan, X., Li, C., & Parikh, S. J. (2020). Simultaneous removal of arsenic, cadmium, and lead from soil by iron-modified magnetic biochar. *Environmental Pollution*, *261*, 114157.

Wang, S., Gao, B., Li, Y., Creamer, A. E., & He, F. (2017). Adsorptive removal of arsenate from aqueous solutions by biochar supported zero-valent iron nanocomposite: batch and continuous flow tests. *Journal of Hazardous Materials*, *322*, 172-181.

Wang, S., Gao, B., Zimmerman, A. R., Li, Y., Ma, L., Harris, W. G., & Migliaccio, K. W. (2015). Removal of arsenic by magnetic biochar prepared from pinewood and natural hematite. *Bioresource Technology*, *175*, 391-395. result 1st

Wang, Y. Y., Chai, L. Y., & Yang, W. C. (2019a). Arsenic distribution and pollution characteristics. In Arsenic Pollution Control in Nonferrous Metallurgy (pp. 1-15). Springer, Singapore.

Wang, W., Ma, X., Sun, J., Chen, J., Zhang, J., Wang, Y., Wang, J., & Zhang, H. (2019b). Adsorption of enrofloxacin on acid/alkali-modified corn stalk biochar. *Spectroscopy Letters*, *52*(7), 367-375.

Wang, L., Wang, Y., Ma, F., Tankpa, V., Bai, S., Guo, X., & Wang, X. (2019c). Mechanisms and reutilization of modified biochar used for removal of heavy metals from wastewater: a review. *Science of the Total Environment*, *668*, 1298-1309.

Wang, Y. Y., Ji, H. Y., Lu, H. H., Liu, Y. X., Yang, R. Q., He, L. L., & Yang, S. M. (2018). Simultaneous removal of Sb (III) and Cd (II) in water by adsorption onto a MnFe 2 O 4–biochar nanocomposite. *RSC Advances*, *8*(6), 3264-3273.

Wang, Y., Liu, H., Wang, S., Li, X., Wang, X., & Jia, Y. (2020). Simultaneous removal and oxidation of arsenic from water by δ-MnO2 modified activated carbon. *Journal of Environmental Sciences*, *94*, 147-160.

Watanabe, T., & Hirano, S. (2013). Metabolism of arsenic and its toxicological relevance. *Archives of toxicology*, *87*(6), 969-979.

Weber Jr, W. J., & Morris, J. C. (1963). Kinetics of adsorption on carbon from solution. *Journal of the sanitary engineering division*, *89*(2), 31-59.

Weerasundara, L., Ok, Y. S., & Bundschuh, J. (2021). Selective removal of arsenic in water: a critical review. *Environmental Pollution*, *268*, 115668.

Wiedner, K., Rumpel, C., Steiner, C., Pozzi, A., Maas, R., & Glaser, B. (2013). Chemical evaluation of chars produced by thermochemical conversion (gasification, pyrolysis and hydrothermal carbonization) of agro-industrial biomass on a commercial scale. *Biomass and Bioenergy*, *59*, 264-278.

Wongrod, S., Simon, S., van Hullebusch, E. D., Lens, P. N., & Guibaud, G. (2018). Changes of sewage sludge digestate-derived biochar properties after chemical treatments and influence on As (III and V) and Cd (II) sorption. *International Biodeterioration & Biodegradation*, *135*, 96-102.

Wu, L., Wei, C., Zhang, S., Wang, Y., Kuzyakov, Y., & Ding, X. (2019). MgO-modified biochar increases phosphate retention and rice yields in saline-alkaline soil. *Journal of Cleaner Production*, *235*, 901-909.

Wu, R., Podgorski, J., Berg, M., & Polya, D. A. (2021). Geostatistical model of the spatial distribution of arsenic in groundwaters in Gujarat State, India. *Environmental geochemistry and health*, *43*(7), 2649-2664.

Wu, X., Burnell, S., Neil, C. W., Kim, D., Zhang, L., Jung, H., & Jun, Y. S. (2020). Effects of phosphate, silicate, and bicarbonate on arsenopyrite dissolution and secondary mineral precipitation. *ACS Earth and Space Chemistry*, *4*(4), 515-525.

Xia, D., Tan, F., Zhang, C., Jiang, X., Chen, Z., Li, H., Zheng, Y., Li, Q., & Wang, Y. (2016). ZnCl2-activated biochar from biogas residue facilitates aqueous As (III) removal. *Applied Surface Science*, *377*, 361-369.

Xiong, H., Tan, Q. G., Zhang, J., Wang, W. X., Yuan, X., Zhang, W., & Yan, B. (2021). Physiologically based pharmacokinetic model revealed the distinct bio-transportation and turnover of arsenobetaine and arsenate in marine fish. *Aquatic Toxicology*, *240*, 105991.

Xiong, Y., Tong, Q., Shan, W., Xing, Z., Wang, Y., Wen, S., & Lou, Z. (2017). Arsenic transformation and adsorption by iron hydroxide/manganese dioxide doped straw activated carbon. *Applied Surface Science*, *416*, 618-627.

Xu, J., Liu, J., Ling, P., Zhang, X., Xu, K., He, L., Wang, Y., Su, S., Hu, S., & Xiang, J. (2020). Raman spectroscopy of biochar from the pyrolysis of three typical Chinese biomasses: A novel method for rapidly evaluating the biochar property. *Energy*, *202*, 117644.

Xu, P., Capito, M., & Cath, T. Y. (2013). Selective removal of arsenic and monovalent ions from brackish water reverse osmosis concentrate. *Journal of Hazardous Materials*, *260*, 885-891.

Xu, X., Cao, X., Zhao, L., Zhou, H., & Luo, Q. (2014). Interaction of organic and inorganic fractions of biochar with Pb (II) ion: further elucidation of mechanisms for Pb (II) removal by biochar. *Rsc Advances*, *4*(85), 44930-44937.

Xu, Y. H., Nakajima, T., & Ohki, A. (2002). Adsorption and removal of arsenic (V) from drinking water by aluminum-loaded Shirasu-zeolite. *Journal of hazardous materials*, *92*(3), 275-287.

Yadav, M. K., Saidulu, D., Gupta, A. K., Ghosal, P. S., & Mukherjee, A. (2021). Status and management of arsenic pollution in groundwater: A comprehensive appraisal of recent global scenario, human health impacts, sustainable field-scale treatment technologies. *Journal of Environmental Chemical Engineering*, *9*(3), 105203.

Yadav, V., Baruah, B. P., & Khare, P. (2013). Comparative study of thermal properties of bio-coal from aromatic spent with low rank sub-bituminous coals. *Bioresource technology*, *137*, 376-385.

Yang, J. C., & Yin, X. B. (2017). CoFe2O4@ MIL-100 (Fe) hybrid magnetic nanoparticles exhibit fast and selective adsorption of arsenic with high adsorption capacity. *Scientific Reports*, *7*(1), 1-15.

Yang, M. H., Zang, Y. S., Huang, H., Chen, K., Li, B., Sun, G. Y., & Zhao, X. W. (2014). Arsenic trioxide exerts anti-lung cancer activity by inhibiting angiogenesis. *Current Cancer Drug Targets*, *14*(6), 557-566.

Yang, X., Luo, Z., Yan, B., Wang, Y., & Yu, C. (2021). Evaluation on nitrogen conversion during biomass torrefaction and its blend co-combustion with coal. *Bioresource Technology*, *336*, 125309.

Yang, X., Yan, B., Liu, Y., Zhou, F., Li, D., & Zhang, Z. (2020). Gamma-FeOOH based hierarchically porous zeolite monoliths for As (V) removal: Characterisation, adsorption and response surface methodology. *Microporous and Mesoporous Materials*, *308*, 110518.

Yin, C. Y., Aroua, M. K., & Daud, W. M. A. W. (2007). Review of modifications of activated carbon for enhancing contaminant uptakes from aqueous solutions. *Separation and Purification Technology*, *52*(3), 403-415.

Yin, H., Kong, M., Gu, X., & Chen, H. (2017). Removal of arsenic from water by porous charred granulated attapulgite-supported hydrated iron oxide in bath and column modes. *Journal of Cleaner Production*, *166*, 88-97.

Yoon, K., Cho, D. W., Tsang, D. C., Bolan, N., Rinklebe, J., & Song, H. (2017). Fabrication of engineered biochar from paper mill sludge and its application into removal of arsenic and cadmium in acidic water. *Bioresource technology*, *246*, 69-75.

Yu, Z., Zhou, L., Huang, Y., Song, Z., & Qiu, W. (2015). Effects of a manganese oxide-modified biochar composite on adsorption of arsenic in red soil. *Journal of Environmental Management*, *163*, 155-162.

Yuan, J. H., Xu, R. K., & Zhang, H. (2011). The forms of alkalis in the biochar produced from crop residues at different temperatures. *Bioresource Technology*, *102*(3), 3488-3497.

Yuan, T., He, W., Yin, G., & Xu, S. (2020). Comparison of bio-chars formation derived from fast and slow pyrolysis of walnut shell. *Fuel*, *261*, 116450.

Zakhar, R., Derco, J., & Cacho, F. (2018). An overview of main arsenic removal technologies. *Acta Chimica Slovaca*, *11*(2), 107-113.

Zazycki, M. A., Godinho, M., Perondi, D., Foletto, E. L., Collazzo, G. C., & Dotto, G. L. (2018). New biochar from pecan nutshells as an alternative adsorbent for removing reactive red 141 from aqueous solutions. *Journal of Cleaner Production*, *171*, 57-65.

Zeng, Z. W., Tan, X. F., Liu, Y. G., Tian, S. R., Zeng, G. M., Jiang, L. H., Liu, S.B., Li, J., Liu, N., & Yin, Z. H. (2018). Comprehensive adsorption studies of doxycycline and ciprofloxacin antibiotics by biochars prepared at different temperatures. *Frontiers in chemistry*, *6*, 80.

Zhang, K., Zhang, D., & Zhang, K. (2016). Arsenic removal from water using a novel amorphous adsorbent developed from coal fly ash. *Water Science and Technology*, *73*(8), 1954-1962.

Zhang, M., Gao, B., Varnoosfaderani, S., Hebard, A., Yao, Y., & Inyang, M. (2013). Preparation and characterization of a novel magnetic biochar for arsenic removal. *Bioresource technology*, *130*, 457-462.

Zhang, W., Zheng, J., Zheng, P., Tsang, D. C., & Qiu, R. (2015). Sludge-derived biochar for arsenic (III) immobilization: effects of solution chemistry on sorption behavior. *Journal of environmental quality*, *44*(4), 1119-1126.

Zheng, S., Yang, Y., Wen, C., Liu, W., Cao, L., Feng, X., Chen, J., Wang, H., Tang, Y., Tian, L., Wang, X., & Yang, F. (2021). Effects of environmental contaminants in

water resources on nonalcoholic fatty liver disease. *Environment International*, *154*, 106555.

Zhong, D., Jiang, Y., Zhao, Z., Wang, L., Chen, J., Ren, S., Liu, Z., Zhang, Y., Tsang, D. C., & Crittenden, J. C. (2019). pH dependence of arsenic oxidation by rice-husk-derived biochar: roles of redox-active moieties. *Environmental Science & Technology*, *53*(15), 9034-9044.

Zhou, Z., Liu, Y. G., Liu, S. B., Liu, H. Y., Zeng, G. M., Tan, X. F., Yang, C. P., Ding, Y., Yan, Z. L., & Cai, X. X. (2017). Sorption performance and mechanisms of arsenic (V) removal by magnetic gelatin-modified biochar. *Chemical Engineering Journal*, *314*, 223-231.

Zhu, J., Pigna, M., Cozzolino, V., Caporale, A. G., & Violante, A. (2013). Higher sorption of arsenate versus arsenite on amorphous Al-oxide, effect of ligands. *Environmental Chemistry Letters*, *11*(3), 289-294.

Zhu, N., Yan, T., Qiao, J., & Cao, H. (2016). Adsorption of arsenic, phosphorus and chromium by bismuth impregnated biochar: Adsorption mechanism and depleted adsorbent utilization. *Chemosphere*, *164*, 32-40.

Zhu, S., Qu, T., Irshad, M. K., & Shang, J. (2020). Simultaneous removal of Cd (II) and As (III) from co-contaminated aqueous solution by a-FeOOH modified biochar. *Biochar*, 1–12.

Zouboulis, A. I., & Katsoyiannis, I. A. (2005). Recent advances in the bioremediation of arsenic-contaminated groundwaters. *Environment International*, *31*(2), 213-219.

# *Appendix*

# Appendix-I List of Publications

1. **Verma, L.,** & Singh, J. (2022). Removal of As (III) and As (V) from aqueous solution using engineered biochar: batch and fixed-bed column study. International Journal of Environmental Science and Technology, 1-20. **(IF. 2.86)**
2. **Verma, L.,** Azad, A., Singh, J., (2021). Performance of a novel iron infused biochar developed from *Raphanus sativus* and *Artocarpus heterophyllus* refuse for trivalent and pentavalent Arsenic adsorption from an aqueous solution: Mechanism, isotherm and kinetics study. International Journal of Phytoremediation. **(IF. 3.212)**.
3. **Verma, L**., & Singh, J. (2019). Synthesis of novel biochar from waste plant litter biomass for the removal of Arsenic (III and V) from aqueous solution: A mechanism characterization, kinetics and thermodynamics. Journal of Environmental Management, 248, 109235**. (IF 6.78)**

Journal of Environmental Management 248 (2019) 109235

Contents lists available at ScienceDirect

Journal of Environmental Management

journal homepage: www.elsevier.com/locate/jenvman

Research article

# Synthesis of novel biochar from waste plant litter biomass for the removal of Arsenic (III and V) from aqueous solution: A mechanism characterization, kinetics and thermodynamics

Lata Verma, Jiwan Singh*

*Department of Environmental Science, Babasaheb Bhimrao Ambedkar University, Lucknow, 226025, India*

ARTICLE INFO

*Keywords:*
Tectona
Lagerstroemia
As(III and V)
Thermodynamics
Regeneration study
Biochar

ABSTRACT

The present study is focusing on utilization of a new feedstock material for the preparation of biochar. The dry waste leaves litter of *Tectona* and *Lagerstroemia speciosa* was used for synthesizing the biochar at 800 °C for 1 h in muffle furnace represents as TB 800 and LB 800 and then used for the removal of As(III) and As(V) from aqueous solution. The prepared biochar materials had a crystalline structure and was characterized by using Scanning electron microscopy (SEM), Energy dispersive X-ray (EDX), Brunaur emmit teller (BET), Fourier transform infrared spectroscopy (FTIR), X-ray diffraction (XRD), Zeta potential, particle size and X-ray photoelectron spectroscopy (XPS). In regeneration study it was observed that prepared biochar material could be used up to four times with good removal percentage of Arsenic (III and V). The experimental data fitted well by Langmuir model for As(V) removal using TB 800 and LB 800, Freundlich model for As(III) removal by LB 800 and Temkin model for As(III) removal by TB 800. Pseudo-second-order kinetics was followed and best fitted with the obtained data of As(III) and (V) removal. Thermodynamics study revealed that the process of adsorption was endothermic for the removal of As(III) and exothermic for the adsorption of As(V) using TB 800 and LB 800. The adsorption capacity obtained for the removal of As(III) was 666.7 μg/g and 454.54 μg/g for TB 800 and LB 800, respectively and adsorption capacity for As(V) was 1250 μg/g for TB 800 and 714.28 μg/g was attained by LB 800.

## 1. Introduction

Arsenic contamination in groundwater affects a large group of population worldwide, particularly in Bangladesh, India, China, United States and Pakistan (Linlin et al., 2018). Arsenic is an metalloid mainly found in two forms Arsenite and Arsenate, both these inorganic species of Arsenic are considered as hazardous toxicants to the environment, but the As(III) in comparison with As(V) is more toxic in nature (Wongrod et al., 2018). Weathering of Arsenic containing rocks, biological accomplishments and volcanic eruptions are the natural source of Arsenic in a drinking water (Omwene et al., 2019). It has been reported that various detrimental health related issues occur in human beings due to intake of As contaminated water, common diseases are pulmonary disease, cardiovascular disease, nervous system dysfunction and also increases the risk of cancer in humans and animals (Rana et al., 2018). According to the World Health Organization (WHO), 10 μg/L is the permissible limit of Arsenic in drinking water i.e. is very low due to its high toxicity (Hu et al., 2012).

Several techniques have already been employed for the arsenic removal from the water like ion exchange, chemical precipitation, adsorption, membrane separation, permeable reactive barriers and coagulation (Bakshi et al., 2018). Among all these techniques, adsorption is one of the most effective techniques as it is low cost and not generates any secondary waste that needs further treatment. It has been found that the adsorption is a procedure that effectively removes Arsenic from the water with vast options of adsorbent materials (Kazi et al., 2018). Biochar is one of the best adsorbent and is an emerging technology effectively used for the removal of contaminants from water in a cost effective way (Liu et al., 2019). Biochar is a carbonaceous compound produced under oxygen deficient condition through the process of slow and fast pyrolysis (Yu et al., 2015). Biochar approaches potentially an innovative technology for As removal from the water or aqueous solution having some unique properties like porosity, large surface area and negative surface charge that makes it an efficient means for decontaminating water (organic and inorganic pollutants) (Agrafioti et al., 2014a). Some of the recent studies focusing on the As(III) and As

* Corresponding author.
*E-mail address:* jiwansingh95@gmail.com (J. Singh).

https://doi.org/10.1016/j.jenvman.2019.07.006
Received 9 April 2019; Received in revised form 10 June 2019; Accepted 4 July 2019

International Journal of Environmental Science and Technology
https://doi.org/10.1007/s13762-022-03920-7

ORIGINAL PAPER

# Removal of As(III) and As(V) from aqueous solution using engineered biochar: batch and fixed-bed column study

**L. Verma**[1] · **J. Singh**[1]

Received: 23 June 2021 / Revised: 20 October 2021 / Accepted: 4 January 2022


## Abstract

Magnetic biochar materials were developed using waste dry leaves of *Tectona species* (Teak) and *Lagerstroemia speciosa* (Banaba plant). The adsorption efficiency of these synthesized biochar was examined for As(III) and As(V) adsorption from an aqueous solution and natural groundwater. The biochar was characterized via point of zero charge ($pH_{ZPC}$), energy dispersive X-ray, scanning electron microscopy, Fourier transform infrared spectroscopy, X-ray diffraction, Raman spectroscopy, zeta potential, and particle size analysis. Both the magnetic biochar were found to be potent in adsorbing As(III and V) from aqueous solution and groundwater samples. The maximum adsorption of As(III) was 92.1% and 97.8%, respectively, by MTB-800 and MLB-800. However, the highest As(V) adsorption was 94.7% and 96.7%, achieved by MTB-800 and MLB-800, respectively, at lower initial As concentrations. The adsorption process was well-fitted to the Langmuir model of isotherm and pseudo-second-order kinetic. The reusability test of the biochar revealed that biochar can be successfully reprocessed up to five cycles. Different models were directed to evaluate the breakthrough curve obtained in column study. As per the available literature, the waste biomass (Teak and Banaba plant) utilized in this study was first time infused with $FeCl_3$ for biochar synthesis development of magnetic properties and applied for As removal. As these magnetic biochar effectively adsorbed arsenic from synthetically prepared As solution as well as from groundwater at laboratory level so, these can be utilized for low-cost filter development to eradicate the problem of arsenic from arsenic-prone areas.

**Keywords** Dry leaves waste biomass · Arsenic (III and V) · Adsorption · Magnetic biochar · Isotherms

## Introduction

In the past few years, the depletion of groundwater has been increased with the increasing population, environmental pollution, poor management of resources due to this the source of clean drinking water diminishing continuously (Siddique et al. 2020). The major source of water pollution is various organic and inorganic pollutants like dyes, phenolic compounds, heavy metals (Cr, Ni, Pb, As, etc.). Among these heavy metals, As is one of the highly toxic metalloids, as it originates from rocks, natural soil due to natural phenomenon as well as anthropogenic activities. Arsenic is the 20$^{th}$ most abundant metalloid naturally existing in the earth's crust (Alka et al. 2021). For medicinal and agricultural uses, arsenic has also been used in antibiotics and pesticides production, consequently, in various ways, it gets into the water bodies especially in aquifers (Zhang et al. 2013). Arsenic contamination leads to numerous health-related issues to humans, and about two hundred million peoples worldwide are at high possibility of arsenic contamination because of consumption of drinking water contaminated with the arsenic, specifically in unindustrialized countries due to its carcinogenic properties (Amen et al. 2020). A 10 µg/L standard arsenic level has been set in the drinking water by US Environmental Protection Agency. Arsenic is noted as the catastrophe of twenty-first century by researchers, globally (Hare et al. 2019).

Biochar is a carbonaceous material, produced through the process of thermal conversion (pyrolysis) of organic biomass for various environmental applications. It is counted as a cost-effective and potential biosorbent because of its porous

Editorial responsibility: Samareh Mirkia.

✉ J. Singh
jiwansingh95@gmail.com

[1] Laboratory of Environmental Nanotechnology and Bioremediation, Department of Environmental Science, Babasaheb Bhimrao Ambedkar University, Lucknow, UP 226025, India

Published online: 18 February 2022

INTERNATIONAL JOURNAL OF PHYTOREMEDIATION
https://doi.org/10.1080/15226514.2021.1985078



# Performance of a novel iron infused biochar developed from *Raphanus sativus* and *Artocarpus heterophyllus* refuse for trivalent and pentavalent arsenic adsorption from an aqueous solution: mechanism, isotherm and kinetics study

Lata Verma, Akanksha Azad, and Jiwan Singh

Department of Environmental Science, Laboratory of Environmental Nanotechnology and Bioremediation, Babasaheb Bhimrao Ambedkar University, Lucknow, India

**ABSTRACT**

Fabrication of magnetic biochar was done by pyrolysis of waste leaves of *Raphanus sativus* (MRB) and *Artocarpus heterophyllus* (MJB) peel pretreated with $FeCl_3$ was examined for As(III and V) adsorption from an aqueous solution. The synthesized bioadsorbents were characterized using X-ray diffraction (XRD), Fourier transform infrared spectroscopy (FTIR), particle size analysis (PSA), scanning electron microscope (SEM), energy dispersive x-ray (EDX), zeta potential, Vibrating sample magnetometer (VSM) and point of zero charge ($pH_{ZPC}$). MRB-800 exhibits greater efficiency toward the removal of both As species with $q_{max}$ value 2.08 mg/g for As(III) and 2.03 mg/g for As(V). Whereas, the $q_{max}$ value was 1.13 mg/g for As (III) and 1.26 mg $g^{-1}$ for As (V) adsorption using MJB-800. Temkin and Freundlich isotherm were best fitted to the adsorption of As(III) and As(V) by MRB-800, respectively. Langmuir isotherm was best followed to the adsorption of As (III and V) by MJB-800. Pseudo-second-order kinetics was well simulated by the experimental data of As adsorption using both the bioadsorbents. Surface complexation and electrostatic attraction was dominant mechanism for As (III) and As (V) adsorption. Thermodynamic study shows that removal of As (III) was exothermic while the As (V) adsorption was endothermic for MRB-800 and MJB-800.

**Novelty statement**

Based on the available literature, it was revealed that no work has been reported yet for the utilization of *Raphanus sativus* (Radish leaves) and *Artocarpus heterophyllus* (Jackfruit peel) waste for the preparation of magnetic biochar and its application for As(III) and As(V) removal for aqueous solution.

**KEYWORDS**

Biochar; adsorption; water treatment; arsenic; mechanism

## Introduction

Arsenic pollution in water arises from anthropogenic and natural sources. Anthropogenic sources include disposal of residual solid by-products derived from combustion (paper mills, coal plants, cement plants), use of arsenic-containing pesticides in the agricultural field. While the natural source of Arsenic in water involves weathering of rocks comprising arsenic minerals (Guo *et al.* 2019). As per several studies, it was suggested that trivalent As is more toxic than the pentavalent As. Exposure of As to the human being for a long term in excess amount (>10 µg/L) can cause several health-related issues such as lung, kidney, skin and bladder cancer etc. (Alchouron *et al.* 2020). Worldwide, it was reported in various countries i.e. the contamination of water by the occurrence of As in groundwater due to natural sources affects a large population. Several chemical and physical techniques like coagulation, filtration, precipitation, membrane separation, etc. have already been used for the treatment of water contaminated with Arsenic (Saranya *et al.* 2020). In contrast to the traditional or common techniques for As removal, sorption has developed as a simple, cost-effective, environmentally friendly and time-saving method that potentially removes water contaminants including As without forming toxic end products (Sun *et al.* 2017; Patra *et al.* 2020). Many sorbents like commercially available activated carbon, fly ash, iron-coated nano-bioadsorbents, natural materials, etc. have been utilized for As sorption from water (Li *et al.* 2020).

Biochar is an efficient and economical adsorbent for organic and inorganic pollutants removal from water. Biochar is a carbonaceous compound synthesized under an inert atmosphere (oxygen-limited conditions) (Zhou *et al.* 2017). It also has many attractive properties like complex surface, large surface area, abundant surface functional groups, etc. that enhance the potential of the bioadsorbent to remove Arsenic from the arsenic-contaminated water (Liu *et al.* 2020). Many studies reported that there is a negative charge on pristine biochar but several modifications of

**CONTACT** Jiwan Singh jiwansingh95@gmail.com Department of Environmental Science, Laboratory of Environmental Nanotechnology and Bioremediation, Babasaheb Bhimrao Ambedkar University, Lucknow, India.

Supplemental data for this article can be accessed at publisher's website.

# Appendix-II Conferences and Workshops attended

## Conferences

- **Lata Verma** and Jiwan Singh, 2021. Poster Presentation on "**Removal of Arsenic from aqueous solution using biochar synthesized from waste biomass**" in AAEBSSD-2021, 5th International Conference on Advances in Agriculture, Environmental and Biosciences for Sustainable Development, from 5th to 7th August 2021.
- **Lata Verma** and Jiwan Singh, 2020. Oral presentation on "**Utilization of Waste plant leaves biomass for the synthesis of iron impregnated biochar and its application for the removal of As(III) from an aqueous solution**" in Recycle 2020, 3rd international conference on waste management held at Indian Institute of Technology Guwahati, from 13th to 14nd Jan, 2020.
- **Lata Verma**, Kshipra Shukla, Alka Verma, Jiwan Singh, 2018. Oral presentation on "**Bioadsorbent synthesis from waste disposal paper cups: An application for removal of Rh-B (Rhodamine-B) and MG (Malachite Green) from aqueous solution**" in International Seminar on Environmental Issues and Challenges in 21st Centuary (EICC-2019) held at Bareilly College, from 20th to 22nd January, 2019.
- Adil Siddique, Ashish Kumar Nayak, **Lata Verma**, and Jiwan Singh, 2018. Oral presentation on "**Development of magnetic activated carbon derived from sweet lime biomass waste for removal of fluoride**" in International Seminar on

Environmental Issues and Challenges in 21st Centuary (EICC-2019) held at Bareilly College, from 20th to 22nd Jan, 2019.

- **Lata Verma**, Mohd. Ibrahim, Jiwan Singh, 2018. Poster presentation on "**Characterization of iron infused activated carbon developed from *Citrus limetta* biomass: an application for the removal of fluoride from aqueous solution**" in International conference on emerging issues in agricultural, environmental & applied sciences for sustainable development (EIAEASSD-2018) held at SHUATS, Allahabad, from 27th to 29th Nov, 2018.
- **Lata Verma,** Shalu Rawat, Jiwan Singh, 2018. Poster presentation on "**Application of biochar for the removal of Arsenic from waste water: A review**" in International conference on Science and Technology for sustainable future (NISC-2018).

## Workshops

- Attended three days workshop on **"Characterization of Nanomaterials"** held at CSIR-Indian Institute of Toxicology Research, Lucknow, during the period of 20th to 22nd February, 2019.
- Participated in one week short term training programme on **"Waste Management Techniques with Special Attentionto COVID-19 Waste"** organized by Environmental Section, Department of Civil Engineering of Sardar Vallabhbhai National Institute of Technology, Surat, Gujrat, India, on 22nd to 26 June, 2020.

Curiginal

## Document Information

| | |
|---|---|
| **Analyzed document** | Synthesis and characterization of biochar from waste biomass An application for the removal of Arsenic from contaminated water.docx (D134972449) |
| **Submitted** | 2022-04-29T09:05:00.0000000 |
| **Submitted by** | O. P. Saini |
| **Submitter email** | gbl.bbau@gmail.com |
| **Similarity** | 1% |
| **Analysis address** | gbl.bbau.bbau@analysis.urkund.com |

## Sources included in the report

| | | |
|---|---|---|
| W | URL: https://www.pubfacts.com/author/Jiwan+Singh<br>Fetched: 2022-04-29T09:05:06.9100000 | 4 |
| W | URL: https://www.x-mol.com/paper/1446907843547295744<br>Fetched: 2022-04-29T09:05:08.2470000 | 3 |
| W | URL: https://pubmed.ncbi.nlm.nih.gov/31310938/<br>Fetched: 2020-12-09T17:24:22.5770000 | 1 |